Abstract of thesis entitled

Technique and Method Development for Intervertebral Disc (IVD) Research

Submitted by

LEE Tsz Yan, Juliana

for the Joint Degree of Doctor of Philosophy

at The University of Hong Kong and The Imperial Collage London

in August, 2015

Intervertebral disc (IVD) degeneration is one of the major causes of low back pain. The direct and indirect cost of managing back pain posts heavy socioeconomic burden to the society. Improved technologies and techniques together with well documented experiments will benefit the research field by saving effort in doing the optimization in every laboratory and avoiding experiment failure due to incomplete understanding of the procedures. These can accelerate scientific discovery, reduce the sacrifice of animals and enable a more effective use of funding.

Nucleus pulposus (NP) is the central part of IVD. Differences in matrix compositions in human NP clinical samples demand different cell isolation protocols for optimal results but there is no clear guide about this to date. Sub-optimal protocols may result in low cell yield, limited reliability of results or even failure of experiments. We experimented different isolation protocols to study different parameters involved and suggested some rules for cell isolation in three main applications: RNA extraction for phenotyping, cell isolation for cell culture, and characterization by flow cytometry.

In addition, instead of extracting RNA from isolated cells, extraction of RNA from tissues directly may avoid the change of RNA levels during the cell isolation process. However, extraction of RNA directly from human and large animal IVD tissue is

technically challenging due to its tough nature, low cell-to-matrix ratio and high proteoglycan content. Thus we developed a method for RNA extraction from bovine disc tissues by integrating the use of cryosectioning, additional phase separation and high salt precipitation into conventional guanidinium thiocyanate based method. With this method, RNA could be extracted from the NP tissue directly but the concentration was low. A shift toward 270 nm was observed in its UV spectrum which was due to phenol contamination. This caused an overestimation of RNA concentration. Hence we developed a computational method based on UV spectra for correcting the overestimated concentrations of RNA contaminated with phenol. The accuracy of concentration increased substantially with the use of the correction formula.

Mesenchymal stem cells (MSCs) have great potential in IVD engineering and hence we studied the isolation and culturing of MSCs from different sources. Effect of cell shape was reported for MSCs but not for NP cells. Micropatterning can be used to pattern cells into different shapes and arrangements. Therefore, we optimized the preparation of bovine NP cell micropatterns and also investigated the preparation of cell micropatterns for confocal microscopy. Besides, we developed methods to study the gene expression of cells on patterns by RT-qPCR with and without prior selection of cells of interest by laser capture microdissection (LCM).

In short, different methods related to IVD research were developed and optimized. With improved methods together with a better understanding of the underlying rationale, researchers can save time and cost in their experiments and reduce experiment failure rate. This will help to accelerate researches. New methods also enable studies which were not feasible in the past.

(484 words)

Technique and Method Development for Intervertebral Disc (IVD) Research

By

LEE Tsz Yan, Juliana

B.Eng. *HKUST*; M.Phil. *HKUST*

A thesis submitted in partial fulfillment of the requirements

for the Joint Degree of Doctor of Philosophy

at The University of Hong Kong and The Imperial Collage London

August, 2015

Copyright Declaration

The copyright of this thesis rests with the author and is made available under a Creative Commons Attribution Non-Commercial No Derivatives licence. Researchers are free to copy, distribute or transmit the thesis on the condition that they attribute it, that they do not use it for commercial purposes and that they do not alter, transform or build upon it. For any reuse or redistribution, researchers must make clear to others the licence terms of this work.

LEE Tsz Yan, Juliana

Declaration

I declare that this thesis represents my own work, except where due acknowledgement is made, and that it has not been previously included in a thesis, dissertation or report submitted to this University or to any other institution for a degree, diploma or other qualifications.

_____

LEE Tsz Yan, Juliana

Acknowledgements

Here, I would like to thank Prof. Kenneth Cheung for giving me the opportunity to work in his group as well as his exceptional willingness and support to accommodate my various special requests in different aspects from joining the Joint program to academic development. His clinical background brought me closer to the clinical application of science research. Thanks Prof. Victor Leung for his guidance in the IVD research and handling different issues from routine lab issues to thesis revisions, as well as his effort in bringing the essential equipments for bio science research into the department. This combination of clinical doctor and bio-science supervisors with a student of bioengineering background shaped the projects into more extraordinary ones. Thanks Prof. Barbara Chan who is always willing to provide support and useful advice in IVD materials and engineering. Thanks Lucia for teaching bovine tissue harvest and the setting up of a "bioreactor". Thanks Cherry, Jacqueline, Fengjuan, Rita, Vivian, Yongcan, Sunyi, Li Xiong, Sarah, Yan, Weiwei, Cora, Karen Wong, Karen Kwan, Ben, Roy, LiTeng, Jason and friends in the spine science research group and groups in O&T for advices and suggestion. Thanks Francis and Kit in help maintaining the lab. Thanks Helen, Tony, Stephen, Henry and Mui for handling issues in the lab. Thanks Prof. William Lu, Regina, Carmen, Sindy, Janet, Vikkie and other academic staff and office staff in handling the administrative issues regarding my study.

Thanks Prof. Molly Stevens for the opportunity of working in her amazing group and her effort in building a wonderful team and excellent research environment, which are always in continuous improvement. Thanks my co-supervisor and mentor Dr. Jean-Philippe St-Pierre for his guidance and encouragement throughout my study in ICL and his advice in thesis revision. He is always there to help. Thanks Sabrina and Eileen for handling different lab issues and maintaining an efficient lab. Thanks Ben for his help in proofreading a manuscript. Thanks Ciro for silicon master fabrication in the micropatterning project. Thanks Joe, Helene, Elena, Christine, Constant, Thomas, Paola, Amanda, Arbel, Livia and Maya for teaching various techniques. Thanks Lesley, Tommy, Muz, Paresh, Alia, Anu, Andrea, Manu, Adam, Rachael, Astrid, Kyasha and Sergio for suggestions in my projects. Thanks Hainan, Rona, Yiyang, Coline, Kharissa, Rob and Jane for other important aspects. There are numerous other members in this extraordinarily large group who have helped me during my study in ICL and each one of them is important in my study. Thanks the members of the polymer subgroup, bio subgroup, osteochondro subgroup and the Stevens group for their constructive advices in my study and establishing a supportive atmosphere without excessive stress but productive.

Thanks Prof. William Lu's group, Prof. Kelvin Yeung's group and other members in the O&T in HKU for their help in setting up and execution of various experiments. Thanks Dino for the opportunity to work on the stem cell review paper. Thanks the members of Prof. Danny Chan's group for their teaching in basic IVD techniques and access to equipments. Thanks Prof. Judy Mak for her help about living in London. Thanks Ben, Cyril, Guo Jing and Cherry

of the Core Facility for technical assistance in flow cytometry and confocal microscopy. Thanks technicians in the Genome Centre for the RNA bioanalysis service. Thanks Ron and others of Rm202 in helping in my work there. Thanks William, Fiona, Eva, Ryan, Patrick, Angel and others of HKU SCRMC for assistance in the work in the interdisciplinary building. Thanks staff in LAU in handling animals related to my projects. Thanks Dr. Mak and staff in the DK hospital for the human bone marrow source for my MSC study.

Thanks Taka and Helder and their supervisor Prof. Rob Kram in ICL for teaching and discussing the use of LCM as well as granting access to the LCM. Thanks Steve and Martin of FILM for their useful advices and teaching in capturing high resolution confocal photos of cell micropatterns. Thanks Russell in the ME workshop to help trying different methods in punching holes in culture plates. Thanks various staff in handling the issues related to this new Joint PhD program.

Thanks my parents and brother for their endless support in my choice. Without their understanding and support, I would not be able to complete the study. Thanks my fiancé for his understanding and full support in my study as well as discussing my projects and research related issues. Also thank my friends and relatives for their company and support.

Thanks King Chow for his advices in handling different issues related to previous publications and research related matters as well as for his unreserved support in my choice. Thanks all my previous supervisors and mentors for their teaching in research and related philosophy.

Thanks Prof. Julian Tanner for chairing my PhD exam and Prof. Yuan Lin, Prof. Charlotte Bevan and Prof. Karin Wüertz-Kozak for being my examiners and for their constructive comments.

Thanks God for guiding me in research and seeing the meaning of it. Thanks many mentors, brothers and sisters in the Life Fellowship for walking with me through the happiness, anger, frustration, disappointment, joy and excitement. Thanks my live-in landlords in London, Russell and Gill, who helped and treated me like a family member rather than a tenant. Their missionary experience and serving hearts made me reflect more about life. Thanks brothers and sisters in the 3G Fellowship, CCiL and Christian groups in ICL for helping and walking with me, which make my stay in London like home in Hong Kong.

There are many extremely important people who have significantly helped me throughout the study but I am not able to name them one by one in this research thesis. I feel blessed to have people who helped me like angels at different times and I hope I can contribute to research which can help others.

Table of Contents

Declaration i
Acknowledgements ii
Table of Contents iv
Table of Figures xi
Table of Tables xix
Abbreviations xxiii
Nomenclature xxvi
List of Publications xxvii
Chapter 1 Scope of Thesis and Introduction 1
1.1 Scope of thesis 1
1.2 Low back pain and IVD 1
1.2.1 Low back pain 1
1.2.2 IVD structure and composition in human 2
1.2.3 Comparison between IVD and articular cartilage (AC) 5
1.2.4 Types of IVD cells (biology) 5
1.2.5 Development of the IVD from the notochord 7
1.2.6 Origin of the NP cells 8
1.2.7 Disc degeneration 9
1.3 Need of IVD engineering and a better understanding of NP cells 13
1.4 Study models in IVD 14
1.4.1 *In vivo* 14
1.4.2 *In vitro* 14
1.5 Common assays in IVD research 15
1.5.1 Composition analysis of ECM of IVD 16
1.5.2 Protein content analysis by the use of antibodies 17
1.5.3 Gene expression at mRNA level 18
1.6 Developing methods in IVD research 19
1.6.1 Need for developing methods in science research 19
1.6.2 Some areas for method improvement in IVD research 20
1.7 Organization of this thesis 22
1.7.1 Optimization of NP cell isolation from tissues 24
1.7.2 Refining disc RNA extraction methodology 24
1.7.3 Concentration correction for RNA contaminated with phenol 24
1.7.4 Isolation and culturing of MSCs for chondrogenic / discogenic studies 24
1.7.5 Method optimization of cell micropatterning and development of a micropatterning method compatible for high resolution imaging 25
1.7.6 Method development in cell micropatterning compatible with laser capture microdissection (LCM) 25
Chapter 2 Bovine NP Cell Isolation 26
2.1 Background 26

2.1.1 Comparison of different species 26
2.1.2 Use of bovine cells 27
2.2 Introduction 28
2.3 Objectives 32
2.4 Materials and Methods 32
2.4.1 LIVE/ DEAD® assay and cell size estimation 32
2.4.2 Water content estimation and DMMB assay of bovine NP and AF tissues 33
2.4.3 Immunohistochemistry and cell density estimation 33
2.4.4 Cell yield, cell viability and attachment of isolated cells 34
2.4.5 Quality of RNA extracted with different digestion conditions 35
2.4.6 RT-qPCR 35
2.4.7 Isolation of cells from NP, AF, CEP, tendon and adipose (AD) tissues in bovine tail 37
2.4.8 Isolation of cells from rat NP tissue 37
2.4.9 Flow cytometry of pronase treated human MSCs 38
2.4.10 Statistical analysis 38
2.5 Results and Discussion 39
2.5.1 Cell distribution, cell densities and tissue compositions of bovine NP and AF 39
2.5.2 Higher NP marker expression in NP compared to AF 41
2.5.3 Cell yield, viability and attachment 42
2.5.4 Morphology of isolated and attached NP, AF and muscle cells 45
2.5.5 Requirement of pronase in rat NP cell isolation 45
2.5.6 Effect of different isolation protocols on RT-qPCR 48
2.5.7 Isolation of cells from different tissues in a bovine tail 50
2.5.8 Suggestions in designing the cell isolation protocols and the corresponding explanations 52
2.5.9 Optimal protocols for different applications 53
2.5.10 Factors affecting yield (theoretical analysis) 55
2.5.11 Factors affecting cell yield (experimental validation) 60
2.6 Conclusions 61
2.7 Appendix 62
2.7.1 The effect of pronase on surface antigens of human MSCs (hMSCs) 62
2.7.2 Protocols for preparing buffer solutions used in Chapter 2 62
Chapter 3 Refining Disc RNA Extraction Methodology 64
3.1 Background 64
3.1.1 Comparison of different RNA extraction methods 64
3.1.2 Components in TRIzol (Home-made recipe) 65
3.1.3 Liquid-liquid extraction 66
3.1.4 Phase separation and precipitation involved in RNA extraction using TRIzol 66
3.2 Introduction 67
3.3 Objectives 69

3.4 Materials and Methods 69
3.4.1 Bovine IVD tissue harvest 69
3.4.2 Tissue homogenization of bovine tissue 69
3.4.3 Comparison of RNA extracted using TRIzol and combined TRIzol-column method 70
3.4.4 Extraction of RNA from bovine IVD tissue 70
3.4.5 Extraction of RNA from mouse and rat tissue 71
3.4.6 Quantification of RNA yield and quality 71
3.4.7 RT-qPCR 71
3.5 Results 72
3.5.1 Homogenization of bovine NP tissue 72
3.5.2 Comparison of RNA from propanol precipitation and column based method 73
3.5.3 Extraction of RNA from bovine NP, AF and muscle 77
3.5.4 Extraction of RNA from mouse and rat IVDs 79
3.6 Discussion 82
3.6.1 Homogenization methods for IVD tissue 82
3.6.2 Glycogen in RNA precipitation 84
3.6.3 Identity of the large precipitate 85
3.6.4 Yield of RNA from rat NP tissue 85
3.6.5 Limitation of the current study 86
3.7 Conclusions 86
3.8 Appendix 87
3.8.1 Use of glycogen in RNA precipitation 87
3.8.2 Preliminary experiment to find out the optimal RNA extraction conditions for bovine NP 88
3.8.3 Suggested experimental flow for RNA extraction from IVD tissues 91
3.8.4 Recommended protocols for extracting RNA from bovine / human IVD tissues (tissues rich in extracellular matrix with low cellularity) 92
3.8.5 Recommended protocols for extracting RNA from murine IVD tissues (tissues rich in extracellular matrix but with relatively high cellularity) 95
3.8.6 Technical notes 98
Chapter 4 Concentration Correction for RNA with TRIzol 101
4.1 Introduction 101
4.2 Materials and methods 102
4.2.1 UV spectra 102
4.2.2 Extraction of RNA 103
4.2.3 RT-qPCR 103
4.3 Results and Discussion 104
4.3.1 Derivation of the concentration correction formula 104
4.3.2 Electrophoregrams of RNA with TRIzol 105
4.3.3 Testing of the concentration correction formula 106
4.3.4 Phenol level index (PLI) 107

4.3.5 Effect of contaminants on RT-qPCR 107
4.3.6 Taqman gene expression assay using RNA extracted with TRIzol 108
4.4 Conclusions 109
Chapter 5 Isolation and Culturing of MSCs for Chondrogenic / Discogenic Studies.....111
5.1 Introduction 111
5.1.1 Use of mesenchymal stem cells (MSCs) in IVD regeneration 111
5.1.2 MSC isolation techniques 112
5.1.3 Validation of MSC properties 112
5.1.4 Culture conditions of MSCs during expansion and differentiation 113
5.2 Objectives 114
5.2.1 The sources of MSCs 114
5.2.2 The culture conditions of MSC 115
5.3 Materials and Methods 115
5.3.1 Rats used in MSC harvest 115
5.3.2 Harvest of rat MSCs from bone marrow 115
5.3.3 Culture of rat MSCs using α-MEM with hFGF-2 116
5.3.4 Harvest of rat MSCs using bone chip method 117
5.3.5 Mouse MSC isolation, culturing and flow cytometry 117
5.3.6 Human MSC isolation and culturing 118
5.3.7 Adipogenic and osteogenic differientiation of human MSCs 120
5.3.8 Oil Red O staining (for adipogenesis) 121
5.3.9 Alizarin Red S staining (for osteogenesis) 121
5.3.10 Pellet formation of MSCs or C3H10T1/2 cells 121
5.3.11 Preparation of pellets for histology 122
5.3.12 FAST staining of the pellets 122
5.3.13 RT-qPCR of the pellets 122
5.3.14 Setting up of hypoxic culture 124
5.4 Results 127
5.4.1 Harvest of rat MSCs from bone marrow 127
5.4.2 Harvest of rat MSCs using bone chip method 128
5.4.3 MSCs from immunodeficient mice did not show CD44 surface marker expression 130
5.4.4 The adipogenic and osteogenic potential of the harvested human MSCs was confirmed 132
5.4.5 Human MSCs from bone marrow clot and transferred medium 132
5.4.6 Source of MSCs had influence in the chondrogenic differentiation and inhibition 135
5.4.7 Culture of rat MSCs using α-MEM with hFGF-2 137
5.4.8 Human bone marrow MSCs can form pellets even in the absence of dexamethasone, sodium ascorbate and TGF-β1 138
5.4.9 Hypoxia 140
5.5 Discussion 141

5.5.1 Chondrogenic potential of rat MSCs 141
5.5.2 Genetic background of MSCs might affect the phenotype of MSCs harvested 142
5.5.3 Exogenous TGF- β1 is required in pellet formation in mouse C3H10T1/2 cells but not in human bone marrow MSCs 143
5.6 Summary and Conclusions 145
5.7 Appendix 147
5.7.1 Hypoxia 147
5.7.2 Influence of ERK on NP cells/ MSCs 151
5.7.3 Influence of p38 on IVD cells/ MSCs/ spine 152
5.7.4 Gene expression markers 153
5.7.5 FAST staining 157
Chapter 6 Optimization and Development of Cell Micropattern Preparation 160
6.1 Background 160
6.1.1 Effect of cell shape or geometry 160
6.1.2 Micropatterning 162
6.1.3 Micropatterning methods 163
6.1.4 General procedures involved in patterning with microcontact printing 165
6.1.5 Cell type specific requirements of micropatterning 168
6.1.6 Requirement of thin substrate for high resolution microscopy using an inverted microscope 170
6.2 Introduction 173
6.3 Objectives 173
6.4 Materials and Methods 174
6.4.1 Cell isolation 175
6.4.2 Cell size estimation of different cell types 175
6.4.3 PDMS stamp preparation 176
6.4.4 Preparation of surfaces for micropatterning 177
6.4.5 Preparation of protein micropatterns by microcontact printing 182
6.4.6 Seeding of cells on the micropatterns 183
6.4.7 Phase contrast microscopy and fluorescent microscopy of cells on micropatterns 183
6.4.8 Statistical analysis 184
6.5 Results and Discussion 184
6.5.1 Different cell types exhibit different sizes and morphologies 184
6.5.2 Pattern and gap size affect the success of single cell micropatterns 187
6.5.3 Quantification of nuclear areas and shapes 192
6.5.4 Fewer cells were observed on protein patterns irradiated with UV 193
6.5.5 Pluronic is required for micropatterning 195
6.5.6 Stability of cell patterns 196
6.5.7 Preparing cell micropatterns for confocal microscopy 197
6.6 Conclusions 206

6.7 Appendix 207
6.7.1 Patterns of cells could be successfully formed when gap size was not larger than 50 μm while pattern size not smaller than 20 μm 207
6.7.2 Cell area evaluation at cell confluence 208
6.7.3 Study of spheroid formation by NP cells 208
Chapter 7 Quantitative Gene Expression Analysis of Micropatterned Cells 211
7.1 Introduction 211
7.1.1 Background about laser capture microdissection (LCM) 211
7.1.2 Motivation for developing methods for preparing micropatterns compatible with LCM 214
7.2 Objectives 216
7.3 Materials and Methods 216
7.3.1 Preparation of micropatterned surfaces in cell culture plates 217
7.3.2 RT-qPCR of micropatterned cells in cell culture plates 217
7.3.3 Surface modifications, contact angle measurement and UV spectrometry 220
7.3.4 Preparation of slides for cell micropatterns for LCM 223
7.3.5 Preparation of protein micropatterns on membrane slides 223
7.3.6 Seeding of cells on membrane slides 224
7.3.7 Dehydration of slides for LCM 224
7.3.8 LCM 225
7.3.9 RT-qPCR of laser captured cells using Cell-to-Ct kit 225
7.3.10 Statistical analysis 225
7.4 Results and Discussion 226
7.4.1 The use of Cell-to-Ct kit for micropatterned cells 226
7.4.2 Laser cutting and catapult of polystyrene (PS) coated glass slide 228
7.4.3 Identifying materials for micropatterning compatible with LCM through understanding the material wettability and UV absorbance 229
7.4.4 Summary of findings of contact angle measurements and UV spectrometry 237
7.4.5 Critical precautions in successful cell micropatterning on membrane slides 238
7.4.6 Specific area of cells on membrane slide could be cut or catapulted precisely 240
7.4.7 Minimum cell number required to perform RT-qPCR 241
7.4.8 Gene expression profile in single-cell patterns versus two-cell patterns 243
7.4.9 LCM to select different cell populations on micropatterns 245
7.5 Conclusions 246
7.6 Appendix 247
7.6.1 Relationship between cell seeding density and number of cells per micropattern 247
Chapter 8 Overall Conclusion and Perspective 251
8.1 Optimization of NP cell isolation from tissues 251
8.2 RNA extraction from IVD tissues 251
8.3 Concentration correction for RNA contaminated with TRIzol 252

8.4 Isolation and culturing of MSCs for chondrogenic / discogenic studies..... 252
8.5 Study of micropatterning methods and imaging 253
8.6 Methods for gene expression study at mRNA levels 253
8.7 Significance..... 253
References 256

Table of Figures

Figure 1-1 Structure of IVD in (A) a saggital view and (B) a transverse view 3

Figure 1-2 Axial sections of IVDs in (A) a 10-month-old girl and (B) a 50-year-old adult. 4

Figure 1-3 A NP cell in proteoglycan aggregate. 7

Figure 1-4 Schematic representation of the main stages in axial skeletogenesis. 8

Figure 1-5 Schematic showing current theories concerning the origin of cells of the NP. 9

Figure 1-6 Schematic diagram of the possible interactions among the changes of cell proliferation, cell senescence, cell phenotype and cell death in the formation of cell cluster during IVD degeneration. 12

Figure 1-7 Schematic showing the need for developing methods in research. 20

Figure 1-8 Schematic showing different studies related to IVD researches described in this thesis. 23

Figure 2-1 Relative sizes of IVDs in different species. 26

Figure 2-2 Isolation of bovine tail disc cells. 39

Figure 2-3 Representative photos of cryosectioned NP and AF tissues immunostained with different NP-specific markers (CDH2, KRT18 and KRT19). 42

Figure 2-4 Effects of different pre-collagenase treatments and different collagenase treatment cocncentrations and duration. 43

Figure 2-5 The difference in cell attachment speed between NP cells isolated from the tissue and NP cells during passaging. 44

Figure 2-6 Morphology of unattached and attached cells. 45

Figure 2-7 The difference in requirement of pronase in different NP tissues. 47

Figure 2-8 The requirement of pronase in rat NP cell isolation. 47

Figure 2-9 Effect of different isolation protocols on the relative mRNA levels in bovine cells detected by RT-qPCR. 50

Figure 2-10 Cells isolated from tissues with photos taken at low cell density at passage 0. ... 51

Figure 2-11 Cells isolated from tissues with photos taken at high cell density at passage 0. .. 51

Figure 2-12 Schematic illustrating enzyme kinetics in a heterogeneous system of tissue digestion. 58

Figure 2-13 The effect of pronase on surface antigens of hMSCs. 62

Figure 3-1 Comparison of different methods for RNA extraction from tissues. 64

Figure 3-2 Chemical structure of glycerol. 65

Figure 3-3 Schematics showing a liquid-liquid extraction process. 66

Figure 3-4 Phase separation involved in RNA extraction using TRIzol. 67

Figure 3-5 RNA precipitation from the aqueous phase using propanol. 67

Figure 3-6 Homogenizer system (pestle and mortar type). 70

Figure 3-7 (A) Representative UV-spectra of RNA extracted from bovine cells measured using Nanodrop and (B) electropherograms of RNA extracted with different methods. 76

Figure 3-8 (A) Representative amplification plot of qPCR with different template concentrations of two-fold dilutions and (B) representative Ct against Log (template concentration) plots for calculating the amplification efficiency. 77

Figure 3-9 (A) UV-spectra of RNA extracted from bovine NP and AF tissues, and from (B) bovine muscle tissue measured using Nanodrop; (C) qPCR amplification curves of RNA extracted from bovine NP and AF tissues using primers for *GAPDH*. 79

Figure 3-10 (A) UV-spectra of RNA extracted from mouse IVD tissue and from (B) rat NP, AF and muscle tissues measured using Nanodrop. 81

Figure 3-11 (A) Electropherograms of RNA extracted from mouse IVD and rat NP and the corresponding spectra (B) and (C). 81

Figure 3-12 (A) qPCR amplification curves of RNA extracted from mouse IVD and (B) from rat NP. 82

Figure 3-13 (A) Omni Tissue Homogenizer (TH), (B) stainless steel generator probes and (C) Omni tip plastic homogenizer probes. 84

Figure 3-14 UV-spectra of RNA extracted from (A) tubes 1-4 and (B) tubes 5-8 as listed in Table 3-12 measured using Nanodrop. 90

Figure 3-15 Suggestion of experimental flow for extraction of RNA from tissues rich in extracellular matrix with low or high cellularity. 91

Figure 3-16 Schematic showing the precautions to prevent the melting of tissue sections because of the body warmth. 92

Figure 3-17 Samples after the first phase separation step. 93

Figure 3-18 Sample after the second phase separation. 93

Figure 3-19 Preparation of aluminum container. 95

Figure 3-20 Schematic showing the flow of embedding small tissue samples in DEPC-treated water prior to cryosectioning. 96

Figure 3-21 Schematic showing that a bubble may be formed after the 75% ethanol addition when the mixture of supernatant with propanol and high salt solution is not sufficiently removed. 99

Figure 3-22 Schematic showing how the microcentrifuge tubes may be oriented during the centrifugation. 100

Figure 4-1 (A) The measured UV spectra of 25 ng/µl total RNA with different concentrations of TRIzol, (B) Concept of absorbance compensation due to TRIzol. 102

Figure 4-2 (A) Plot of A_{260} vs A_{270} of TRIzol solution of different concentrations and (B) Plot of A_{270} vs A_{260} of RNA solution of different concentrations. 105

Figure 4-3 Electropherograms of RNA without and with TRIzol contamination (0.005% and 0.05%) obtained by Agilent 2100 bioanalyzer. 106

Figure 4-4 Amplification plot in RT-qPCR of RNA extracted using TRIzol. 109

Figure 5-1 Intervertebral disc tissue engineering procedures based on mesenchymal stem cells (MSCs). 111

Figure 5-2 Experiments involved in Chapter 5. 114

Figure 5-3 Isolation of rat MSCs from bone marrow with cell separation using Ficoll. 116

Figure 5-4 Procedures of MSC isolation from rats using the bone chip method. 117

Figure 5-5 Schematic showing MSCs obtained from different portions of human bone marrow. 120

Figure 5-6 Hypoxic set up using an incubator with O_2 control and N_2 inlet..... 125

Figure 5-7 Components for setting up hypoxia using a sealed modular incubator chamber. 126

Figure 5-8 Phase contrast photos of cells isolated from rat bone marrow with Ficoll separation cultured with DMEM with 10% FBS. 127

Figure 5-9 Rat MSCs with flat morphology. 128

Figure 5-10 Phase contrast photos of cells isolated from rat cortical bones cultured with DMEM with 10% FBS. 129

Figure 5-11 Rat MSCs from compact bones. 129

Figure 5-12 Phase contrast photos of cells isolated from mouse cortical bones cultured with DMEM with 10% FBS. 130

Figure 5-13 Histogram analysis of cell surface markers by flow cytometry for cells stained with CD44, CD45, CD29, VCAM and CD11b for mouse MSCs isolated with bone chip method from NOD/SCID mice. 131

Figure 5-14 Human MSCs differentiated into adipocytes and osteocytes before and after Oil Red O staining and Alizarin Red S staining respectively. 132

Figure 5-15 (A) Photo of a dish with bone marrow clot showing that the clot has been disintegrated at day 3 and (B) a phase contrast photo of human MSCs from bone marrow clot at day 3 after PBS wash and medium change. 133

Figure 5-16 Phase contrast photos of human MSCs from transferred medium at (A) day 11 and (B) day 17..... 134

Figure 5-17 Photos of human MSCs differentiated into adipocytes and osteocytes with Oil Red O staining or Alizarin Red S staining for cells obtained from Ficoll interface, from transferred medium and from bone marrow clot. 135

Figure 5-18 Photos of paraffin sections of pellets formed from human MSCs from umbilical cord (CMSC) and from bone marrow (BMSC) cultured with different conditions. 136

Figure 5-19 Phase contrast photos of cells isolated from human bone marrow cultured with α-MEM with 15% FBS and 0.5 ng/ml hFGF-2 at passage 9 at (A) a lower density region and (B) a higher density region of the dish. 137

Figure 5-20 Phase contrast photos of cells isolated from rat bone marrow without Ficoll separation cultured with α-MEM with 15% FBS and 0.5 ng/ml hFGF-2. 138

Figure 5-21 Photos of pellets in 96-well polypropylene plates cultured at day 1 in normoxia condition. 138

Figure 5-22 Relative mRNA levels of matrix genes *ACAN* and *COL2A1* in hMSC pellets cultured with different supplements. 139

Figure 5-23 Relative mRNA levels of chondrocyte markers in hMSC pellets cultured with different supplements. 140

Figure 5-24 Photos of pellets in 96-well polypropylene plates cultured after 14 days in hypoxia condition. 141

Figure 5-25 Comparison of hMSC pellets cultured in hypoxia (3% O_2) and normoxia (21% O_2) at day 14. 141

Figure 5-26 Photos of pellets in 96-well polypropylene plates cultured after 14 or 21 days in normoxia condition. 144

Figure 5-27 Some common approaches of achieving hypoxia. 149

Figure 5-28 Relative mRNA levels of matrix genes in hMSC pellets cultured with different conditions (without TGF-β1, with TGF-β1 with and without p38/ MEK inhibitors) under normoxia. 155

Figure 5-29 Relative mRNA levels of chondrogenic genes in hMSC pellets cultured with different conditions (without TGF-β1, with TGF-β1 with and without p38/ MEK inhibitors) under normoxia. 156

Figure 6-1 Schematic showing how cells are maintained in round shape using different methods. 163

Figure 6-2 Simplified schematic showing cell patterning through microcontact printing of proteins. 165

Figure 6-3 Fabrication of silicon master with micropatterns and preparation of PDMS stamps. 166

Figure 6-4 Preparation of protein micropatterns and cell micropatterns. 168

Figure 6-5 Resolution of microscope. 170

Figure 6-6 Schematic showing the working distance of a typical microscope objective. 171

Figure 6-7 Schematic showing (A) a dipping lens in an upright microscope and (B) an immersion lens in an inverted microscope. 172

Figure 6-8 Experimental procedures involved in this Chapter. 174

Figure 6-9 Approaches for preparing substrates for confocal microscopy of cell micropatterns. 178

Figure 6-10 Schematic showing the preparation of polystryene coated cover slips. 179

Figure 6-11 Preparation of a thin bottom container with a silicone ring. 180

Figure 6-12 Preparation of a thin bottom container with a hole drilled at the centre of the culture plate well / dish (only one of the wells was shown for simplicity). 182

Figure 6-13 Phase contrast photos of (A) bovine NP cells, (B) mouse 10T1/2 cells, (C) HUVECs (human cells) and (D) hMSCs at confluence. 186

Figure 6-14 (A) Sample fluorescent photo of bovine NP cells at 4 h after cell plating used for cell area and shape analysis using Fiji; (B) Outline of cells in the particle analysis of Fiji. 187

Figure 6-15 Phase contrast photos of bovine chondrocytes on fibronectin patterns of different circle sizes at 4 h after cell seeding..... 188

Figure 6-16 Schematic of possible explanation for the non-specific patterns. 189

Figure 6-17 The relationship between the change in length and the cross-sectional area. 190

Figure 6-18 Photos of cross-sections of PDMS stamps captured under phase contrast microscopy. 190

Figure 6-19 Phase contrast photos of bovine NP cells on fibronectin patterns of 20 μm circles, 50 μm circles, 20 μm strips, 50 μm strips and fibronectin coating at day 1. 191

Figure 6-20 Fluorescent photos of nuclei of bovine NP cells stained with DAPI at day 1 (scale bar = 25 μm) and the quantification of areas, aspect ratios and roundness descriptors using Fiji. 192

Figure 6-21 The alignment of cells on 20 μm strips compared to 20 μm circles and non-patterns. 193

Figure 6-22 Schematics and phase contrast photos of (A) bovine NP cells on fibronectin patterns on surfaces without UV sterilization, (B) bovine AF cells on fibronectin patterns on UV sterilized surfaces without UV irradiated protein patterns and (C) with UV irradiated protein patterns. 194

Figure 6-23 Phase contrast photos of bovine NP cells with and without surface passivation by pluronic and with and without serum (10% FBS) used during cell seeding..... 196

Figure 6-24 Schematic showing the covering of area without proteins with passivation chemicals to prevent cell attachment. 197

Figure 6-25 The requirement of thin bottom substrate for high resolution confocal microscopy with immersion lens for reliable cell shape or height estimation. 199

Figure 6-26 Fluorescent photos of bovine NP cells on (A) 20 μm strips, (B) 50 μm strips, (C) small circles and (D) large area of fibronectin..... 200

Figure 6-27 Fluorescent photos of bovine NP cells on a circle fibronectin pattern (left) and non-pattern fibronectin (right). 201

Figure 6-28 Fluorescent photos of HUVECs on (A) circle pattern, (B) triangle pattern, (C) rhombus pattern and (D) large area of fibronectin..... 203

Figure 6-29 Orthogonal view of a HUVEC in spread morphology stained blue with DAPI for cell nuclei and green with Phalloidin Alexafluor 488 for actin. 204

Figure 6-30 Orthogonal view of a HUVEC in round morphology stained blue with DAPI for cell nuclei and green with Phalloidin Alexafluor 488 for actin. 205

Figure 6-31 Design of patterns in the software LayoutEditor to mimic the round shape of NP cells and the elongated shape of tendon cells. 207

Figure 6-32 Phase contrast photos of micropatterns formed from cells of different sources. 209

Figure 6-33 Different behavior of cells on micropatterns. 210

Figure 7-1 Schematic representation of the two main LCM systems: the Arcturus PixCell II IR laser system and the PALM Zeiss UV laser system..... 213

Figure 7-2 The laser cutting function and the catapulting function in PALM MicroBeam from Carl Zeiss. 214

Figure 7-3 Experimental procedures involved in this Chapter..... 216

Figure 7-4 Two approaches of RT-qPCR used for micropatterned cells in this study..... 217

Figure 7-5 Materials and types of modifications involved in this study. 220

Figure 7-6 Relative mRNA levels in bovine NP cells on fibronectin micropatterns of 20 μm circles and 20 μm strips at day 3 with RNA extracted using a RNeasy kit and reverse transcribed using a QuantiTect Rev Transcription Kit..... 226

Figure 7-7 Phase contrast photos of NP cells on micropatterns. NP cells on (A) 20 μm circles at day 1, (B) 20 μm strips at day 1, (C) 20 μm circles at day 3 and (E) 20 μm strips at day 3. 227

Figure 7-8 Relative mRNA levels in bovine NP cells on fibronectin micropatterns of 20 μm circles and 20 μm strips detected using a Cell-to-Ct Kit. 228

Figure 7-9 Laser cutting and catapult using Zeiss LCM on PS coated glass slide. 229

Figure 7-10 Photos of water droplets on plastic substrates in contact angle measurements.. 230

Figure 7-11 Photos of water droplets on glass substrates in contact angle measurements. ... 231

Figure 7-12 (A) UV-vis spectra of materials listed in Table 7-6 normalized with material thickness and (B) the corresponding normalized absorbances at 355 nm. 234

Figure 7-13 Absorption spectra of benzene, naphthalene and anthracene in cyclohexane. ... 235

Figure 7-14 Photos of water droplets on glass substrates in contact angle measurements. ... 236

Figure 7-15 Fluorescence images of bovine NP cells cultured on fibronectin patterns on a PEN membrane glass slide and a PEN membrane frame slide with and without polystyrene coating. 239

Figure 7-16 Precise cutting and catapulting. 240

Figure 7-17 Titration of bovine NP cells. Cells were stained with CellTracker green and seeded on polystyrene-coated PEN membrane frame slides. 242

Figure 7-18 *ACAN* and *COL2A1* gene expression of single round cells and double round cells of bovine NP at 4 h after cell seeding. 244

Figure 7-19 Study of two cell types from the same membrane slide. 245

Figure 7-20 Trade off between obtaining single cells and percentage occupancy. 247

Figure 7-21 Relationship between the number of cells seeded and λ. 249

Figure 7-22 Plot of Poisson distribution with different λs. 250

Table of Tables

Table 1-1 Estimates of direct costs of low-back pain in the United States reported in 2001 2

Table 1-2 Structures of the NP, AF and CEP 3

Table 1-3 Percentages of components in IVD 4

Table 1-4 Comparison of NC cell retention in various mammalian species 6

Table 1-5 Summary of characteristics of human IVD cells 6

Table 1-6 Biochemical changes due to altered phenotype and human disc cells during disc aging and degeneration 10

Table 1-7 Some examples of assays used in IVD research. 15

Table 2-1 Comparison of NC cell retention in various mammalian species 27

Table 2-2 Summary of cell isolation conditions and durations for IVD tissues in some reported studies 29

Table 2-3 Sequences of bovine primers used in this study 37

Table 2-4 Water, GAG contents and cell densities in bovine tail IVD 41

Table 2-5 Yield and quality of RNA obtained with different isolation methods. 49

Table 2-6 Suggestions in designing the cell isolation protocols and the corresponding explanations 52

Table 2-7 Digestion of tissues under different conditions for the study of the effects of shaking 60

Table 3-1 A recipe for 1 L of home-made "TRIzol". 65

Table 3-2 Studies that investigated the gene expression in IVD tissues through cell isolation with sequential digestion using pronase and collagenase 68

Table 3-3 Sequences of mouse primers used in this study 72

Table 3-4 Sequences of rat primers used in this study 72

Table 3-5 Concentration, yield and quality of RNA extracted from cultured cells with different methods estimated by Nanodrop 74

Table 3-6 Concentration, yield and quality of RNA extracted from cultured cells with different methods estimated by Bioanalyzer 75

Table 3-7 Ct values and qPCR efficiency estimated from the curves for *GAPDH* amplification 77

Table 3-8 Concentration, yield and quality of RNA extracted from bovine tissues with different methods estimated by Nanodrop. 78

Table 3-9 Concentration, yield and quality of RNA extracted from mouse IVD tissue, rat NP, AF and muscle tissues estimated by Nanodrop. 80

Table 3-10 Studies that investigated the gene expression in IVD tissues through direct RNA extraction from the tissues after pulverization 83

Table 3-11 Pellet formation with and without the use of hight salt (HS) solution. 87

Table 3-12 Experiment conditions to find the conditions for extracting RNA from samples with high proteoglycan content and the corresponding RNA concentrations 89

Table 4-1 The concentration estimated by Nanodrop UV spectrometry before and after correction using the derived formula (6) for RNA solution with different concentrations of TRIzol. 106

Table 4-2 Ct values of RT-qPCR of total RNA with different concentrations of TRIzol 107

Table 4-3 Concentration and quality of RNA from HES2 cells extracted using TRIzol. 108

Table 5-1 List of donors for MSCs involved in this study 119

Table 5-2 List of Taqman Gene Expression Assays used in experiments in this Chapter 124

Table 5-3 Some specifications of the Thermo Scientific Forma Water Jacketed CO_2 Incubator 3131, used as hypoxic incubator 125

Table 5-4 Summary of marker expression for MSC characterization 131

Table 5-5 Relative mRNA levels of pellets formed from CMSCs and BMSCs cultured with different conditions. 136

Table 5-6 Percentages of some major gases in atmosphere and hypoxic conditions used in cell culture 151

Table 6-1 Studies of IVD cells, chondrocytes and hMSCs in chondrogenesis which involved cell micropatterning 169

Table 6-2 Comparison of water dipping objective and water immersion objective for confocal microscopy that are available in Facility for Imaging by Light Microscopy (FILM) of Imperial College London (ICL) 172

Table 6-3 Surfaces used for micropatterning studies in Chapter 6 and Chapter 7. 177

Table 6-4 The cell diameters of cells in cell suspension 185

Table 6-5 Summary of some single cell micropattern studies..... 185

Table 6-6 Areas, aspect ratios and roundnesses of bovine NP and AC cells at 4 h after cell plating. 187

Table 6-7 Fibronectin-binding integrins..... 195

Table 6-8 Excitation (Ex) and emission (Em) wavelengths of the fluorescent probes used in this study. 202

Table 6-9 Estimated resolutions of objectives for confocal microscopy available in Facility for Imaging by Light Microscopy (FILM) of Imperial College London (ICL). 202

Table 6-10 The approximate numbers of cells per mm^2 and areas of cells estimated from photos in Figure 6-13 in the Results and Discussion Section..... 208

Table 7-1 Conditions used in qPCR using Rotor Gene Q (Qiagen)..... 220

Table 7-2 Different types of surface treatments used in samples for contact angle measurements..... 222

Table 7-3 Concentrations, A_{260}/A_{280} and A_{260}/A_{230} of RNA extracted with a RNeasy kit from bovine NP cells on fibronectin micropatterns at day 3. 227

Table 7-4 Contact angles of plastic substrates without and with cleaning with 70% ethanol 230

Table 7-5 Contact angles of glass substrates without and with different treatments 232

Table 7-6 Materials used for UV-vis spectrometry measurements and contact angle measurements..... 233

Table 7-7 Chemical structures of polystyrene (PS), polyethylene naphthalate (PEN) and polyethylene terephthalate (PET) 235

Table 7-8 Contact angles of membrane slides without and with different treatments 237

Table 7-9 The Ct values and frequency of amplification detected for *GAPDH*, *COL2A1*, *ACTB*, *18S rRNA* in samples of 1 cell, 3 cells and 5 cells. 243

Table 7-10 Poisson distribution of numbers of cells per micropattern for different values of λ. 250

Abbreviations

3D	three dimensional
Ab	antibody
AC	defined as articular chondrocytes/ cartilage in this thesis
ACAN/ *Acan*	aggrecan
AD	defined as adipose (fat) tissue in this thesis and used when referring to cells isolated from fat tissue
ADAMTS	a disintegrin and metalloprotease with thrombospondin type 1 motifs
AF	annulus fibrosus
AFM	atomic force microscopy
arb. unit	arbitrary unit
BASP1/ *Basp1*	brain abundant, membrane attached signal protein 1
BCP	bromochlorpropane
bFGF	basic fibroblast growth factor
BMP	bone morphogenetic protein
BMP-R	bone morphogenetic protein receptor
BMSC	human mesenchymal stem cells from bone marrow
BSC	biosafety cabinet; a hood specially designed to provide a sterile working environment for handling cell culture
CD/ Cd	cluster differentiation
CDH2	cadherin-2, also known as neural cadherin (NCAD)
cDNA	complementary DNA
CEP	cartilaginous endplate
cited2	CREB-binding protein/p300-interacting transactivator with ED-rich tail
CLC	chondrocyte-like cells
CMSC	human mesenchymal stem cells from umbilical cord
CO_2	carbon dioxide
COL/ *Col*	collagen
COL1A1	collagen, type I, alpha 1
COL2	denotes type II collagen
COL2A1	collagen, type II, alpha 1
COL3A1	collagen, type III, alpha 1
COMP	cartilage oligomeric matrix protein
COX-2	cyclooxygenase-2/ prostaglandin-endoperoxide synthase 2
CULATR	Committee of the Use of Live Animals in Teaching and Research
DAPI	4',6-diamidino-2-phenylindole; a fluorescent dye for staining cell nuclei
DEPC	diethylpyrocarbonate
DMEM	Dulbecco's Modified Eagle Medium
DMMB assay	colorimetric assay using the dye, 1,9-dimethylmethylene blue, to detect sGAGs content

DMSO	dimethyl sulfoxide
DNA	deoxyribonucleic acid
ECM	extracellular matrix
EDTA	ethylenediaminetetraacetic acid
EGF	epidermal growth factor
ELISA	enzyme-linked immunosorbent assay
EP	end plate
ERK	extracellular-signal-regulated kinase
FACS	fluorescence-activated cell sorting
FAST staining	sequential staining with fast green, Alcian blue, Safranin O, and tartrazine
FBS	fetal bovine serum
FC	flow cytometry
FGF-2	basic fibroblast growth factor
FILM	facility for imaging by light microscopy, in Imperial College London
Foxn1	forkhead transcription factor
GAG	glycosaminoglycan
GAPDH	glyceraldehyde 3-phosphate dehydrogenase
GD2	disialoganglioside
GFP	green fluorescent protein
GITC	guanidine isothiocyanate
HA	hyaluronic acid
HBSS	Hank's balanced salt solution
HEPES	4-(2-hydroxyethyl)-1-piperazineethanesulfonic acid
HES2	human embryonic stem cells
hFGF-2	human basic fibroblast growth factor
HIF	hypoxia-inducible factor
HKU	The University of Hong Kong
hMSC	human mesenchymal stem cells
HS	high salt
HUVEC	human umbilical vein endothelial cell
ICL	Imperial College London
IF	immunofluorescence
IGF	insulin-like growth factor
IHC	immunohistochemistry
IL	interleukin
IR	infrared
ITS	insulin, transferrin and selenite
IVD	intervertebral discs
IVDD	intervertebral disc degeneration
JAK-STAT	Janus kinase/ signal transducers and activators of transcription
KRT	keratin
KRT18	keratin 18, type I

KRT19	keratin 19, type I
LbL	layer by layer
LCM	laser capture microdissection
LVC	large vacuolated cells
MAPK	mitogen-activated protein kinase
MEK	mitogen-activated protein kinase kinase
MIA	melanoma inhibitory activity (a gene or protein)
MMP	matrix metalloproteinase
mRNA	messenger RNA
MSC(s)	mesenchymal stem cell(s)
NA	numerical aperture
NaCl	sodium chloride
NC	notochordal/ notochord
NCDN/ *Ncdn*	neurochondrin
NOD/SCID	Nonobese diabetic/ severe combined immunodeficiency
NP	nucleus pulposus (central part of IVD)
NRP1/ *Nrp1*	neuropilin-1
O/N	overnight
O_2	oxygen
p38	p38 mitogen-activated protein kinases
PBS	phosphate buffered saline
PCR	polymerase chain reaction
PDGF	platelet-derived growth factor
PDMS	polydimethylsiloxane
PEG	polyethylene glycol
PEN	polyethylene naphthalate
PET	polyethylene terephthalate
PFA	paraformaldehyde
PGE-2	prostaglandin E2
PHD-2	prolyl hydroxylase-containing protein 2
pHEMA	poly(2-hydroxyethyl methacrylate)
PI3K-PKB/ Akt	phosphoinositide-3-kinase-protein kinase B/ Akt
PLI	phenol level index
PLL-g-PEG	poly(l-lysine)-graft-poly(ethylene glycol)
PNS	perinotochordal sheath
PS	polystyrene
PTHrP	parathyroid hormone-related protein
PVA	poly vinyl alcohol
PVA/ PVP	PVA/ polyvinyl pyrrolidone
PVDF	polyvinylidene fluoride
qPCR	quantitative polymerase chain reaction

qRT-PCR	same as RT-qPCR
RH	relative humidity
RIN	RNA integrity number
RNA	ribonucleic acid
RPE1	retinal pigment epithelial
RT	reverse transcription
RT-PCR	reverse transcription - polymerase chain reaction
RT-qPCR	reverse transcription - quantitative polymerase chain reaction; used to estimate the gene expression at mRNA level
RUNX1	runt-related transcription factor 1
SAMs	self-assembled monolayers
SCA	Sircol collagen assay
SEM	scanning electron microscopy
sGAGs	sulphated glycosaminoglycans
SOX/ *Sox*	SRY (sex determining region Y)-box
SOX5	SRY (sex determining region Y)-box 5
SOX6	SRY (sex determining region Y)-box 6
SOX9	SRY (sex determining region Y)-box 9
SVP	saturated vapor pressure
TE	Tris-EDTA
TGF	transforming growth factor
TIE2	TEK tyrosine kinase, endothelial
TIMP	tissue inhibitor of metalloproteinase
TNF	tumor necrosis factor
UV	ultraviolet
VEGF	vascular endothelial growth factor
WB	western blot

Nomenclature

- Gene symbol
  - Italicized and all capital letters for human and bovine genes
  - Italicized and first letter capital letter for rat and mouse genes
- Protein symbol
  - All capital letters but not italicized for human, bovine, rat and mouse proteins

List of Publications

Peer-reviewed journals

- **J TY Lee**, J P St-Pierre, T Homma, C Chiappini, V YL Leung, K MC Cheung and M M Stevens. Laser capture microdissection of micropatterned cells (In preparation)

- **J TY Lee**, K MC Cheung, and V YL Leung (2015) Extraction of RNA from tough tissues with high proteoglycan content by cryosection, second phase separation and high salt precipitation. Journal of Biological Methods. Journal of Biological Methods, 2(2):e20

- **J TY Lee**, K MC Cheung, and V YL Leung (2015) Systematic study of cell isolation from bovine nucleus pulposus: Improving cell yield and experiment reliability. Journal of Orthopaedic Research (Accepted)

- **J TY Lee**, K MC Cheung, and V YL Leung (2014) Correction for concentration overestimation of nucleic acids with phenol. Analytical Biochemistry, 465:179 – 186 (Cover art of the issue)

- R LH Yim, **J TY Lee**, C H Bow, B Meij, V Leung, K MC Cheung, P Vavken, D Samartzis (2014) A Systematic Review of the Safety & Efficacy of Mesenchymal Stem Cell for Disc Degeneration: Insights & Future Directions for Regenerative Therapeutics. Stem cells and development, 23(21):2553-67

Conference poster / oral presentation

- **J TY Lee**, V YL Leung, J P St-Pierre, M M Stevens, K MC Cheung (2014) Collagen II in native nucleus pulposus (NP) tissue may suppress COL2A1 expression in NP cells. World Forum for Spine Research and Hong Kong Inter-University Biochemistry Postgraduate Symposium

- **J TY Lee**, V YL Leung, K MC Cheung (2014) Transcriptional changes of bovine nucleus pulposus, annulus fibrosus and muscle cells upon cell isolation and culturing: Implication in cell type specific marker selection. Orthopaedics Research Society Annual Meeting

- R Yim, **J Lee**, P Vavken, D Samartzis (2013) The safety and efficacy of mesenchymal stem cells for prevention or regeneration of intervertebral disc degeneration: a systematic review. Global Spine Congress

- **J TY Lee**, V YL Leung, V Tam, K MC Cheung (2012) A systematic re-evaluation of enzymatic isolation methodology for nucleus pulposus cells. World Forum for Spine Research

Chapter 1 Scope of Thesis and Introduction

1.1 Scope of thesis

This thesis will focus on the methods developed related to intervertebral disc (IVD) research. In my PhD study, researches in different areas in IVD were carried out to study nucleus pulposus (NP) cells, IVD tissues, mesenchymal stem cells (MSCs) and cell shape. Methods were developed and optimized en voyage. Improved technologies and techniques will accelerate scientific discovery. And well documented experiments that lead to each experiment design decision or protocol will benefit the field by saving effort in doing the optimization in every laboratory and avoiding experiment failure due to incomplete understanding of the procedures. Herein I believe it is worthwhile to document the development of methods and techniques in this thesis.

Some brief background about IVD biology and IVD research is given in the following sections and the organization of the thesis is given at the end of this Chapter.

1.2 Low back pain and IVD

1.2.1 Low back pain

Eighty percent of the general population in industrialized countries experience low back pain in their lifetime [1]. Joint and back pain is also among the major causes of disability and morbidity for adult population and causes a considerable burden on public health systems [1-5]. **Table 1-1** shows the direct costs of low back pain in the United States. The total cost was around 20 billion per year. In an estimate in 2005, it was suggested that the total cost of low-back pain including indirect cost such as lost wages could reach $200 billion per year in the United States [6]. This posted heavy socioeconomic burden to the society. Low back pain correlates with IVD degeneration, a major problem with ninety percent of Southern Chinese exhibiting signs of IVD degeneration by age 50 to 55 [7]. Most degenerative disc “abnormalities” were moderately associated with low back pain [8]. IVD degeneration is not

only a problem associated with aging and is also present in one-third of the juvenile population in Southern China [9]. IVD regenerative engineering is a research area that can improve the quality of life of people by alleviating low back pain and improving the mobility of patients with degenerative disc disease.

Table 1-1 Estimates of direct costs of low-back pain in the United States reported in 2001 (Reproduced with permission of Journal of Bone and Joint Surgery from [6] © 2006 JBJS).

Expense Category	Number per year	Medium unit cost (US dollars)	Total cost (US dollars)
Office visits for low-back pain	19 million	150	3 billion
Medical admissions for low-back pain	224,000	9000	2 billion
Laminectomy and discectomy	286,000	14000	4 billion
Lumbar spinal fusion procedures	298,000	37000	11 billion

1.2.2 IVD structure and composition in human

IVDs lie between vertebral bodies and they occupy one-third of height of the spinal column. Human IVDs are around 7 to 10 mm thick and 4 cm in diameter. It is consisted of a more gelatinous nucleus pulposus (NP) core surrounded by a thick outer ring of fibrous annulus fibrosus (AF) and sandwiched inferiorly and superiorly by cartilage endplates (CEP) (**Figure 1-1**) [10]. The CEP anchors the NP and AF to the adjacent vertebral body bones. IVD from people of different ages have slightly different structures as shown in **Figure 1-2**. The structures and components of NP, AF and CEP are summarized in **Table 1-2** and **Table 1-3** respectively.

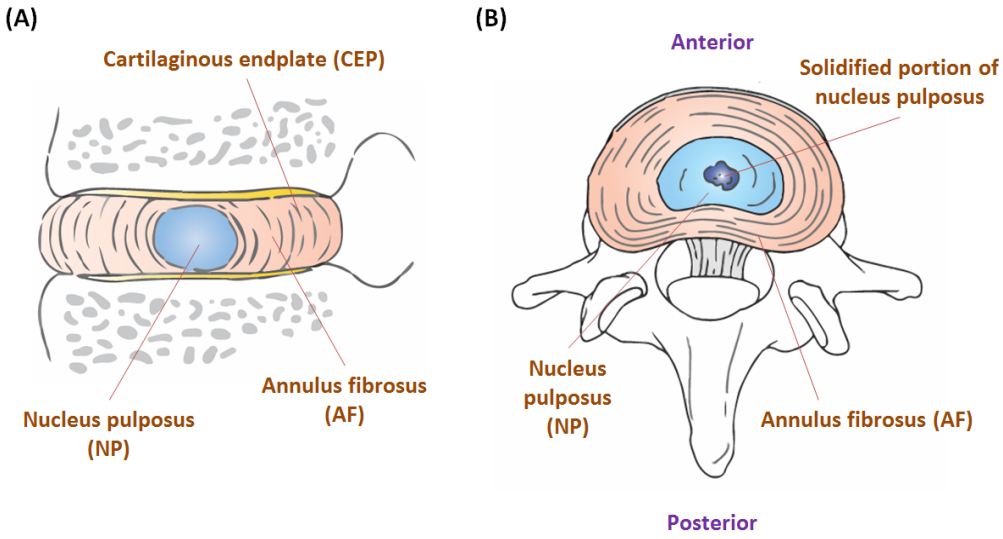


Figure 1-1 Structure of IVD in (A) a saggital view and (B) a transverse view (Reproduced with permission of John Wiley and Sons from [10] © 2008 John Wiley and Sons. The figures were relabelled without changes in the words and color was added).

Table 1-2 Structures of the NP, AF and CEP

NP	*AF*	*CEP*
• NP contains randomly organized collagen fibers and radially arranged elastin fibers, which sometimes are up to 150 µm in length [10]. These fibers are embedded in a highly hydrated aggrecan- containing gel [10]. • Aggrecan is highly anionic and provides the osmotic properties which enable the NP to maintain height and turgor against compressive loads [11].	• AF consists of a series of 15 to 25 concentric rings, or lamellae [12] with the collagen fibers lying parallel within each lamella. • The fibers are oriented at approximately 60° to the vertical axis, alternating to the left and right of it in adjacent lamellae [10]. • Elastin fibers lie between the lamellae, possibly helping the disc to return to its original arrangement following bending, whether it is flexion or extension [10]. • The elastin fibers may also bind the lamellae together as they pass radially from one lamella to the next [13].	• CEP is a thin horizontal layer of hyaline cartilage which is usually less than 1 mm thick. It interfaces the disc and the vertebral body. The collagen fibers within it run horizontal and parallel to the vertebral bodies, with the fibers continuing into the disc [14]. • In young IVDs, there are numerous vascular channels and wide CEPs traversing to the NP and AF (**Figure 1-2A**). In an IVD from a 50-year-old adult, the CEPs are thin and there are fewer vascular channels traversing to less hydrated distinct NP and AF (**Figure 1-2B**) [10].

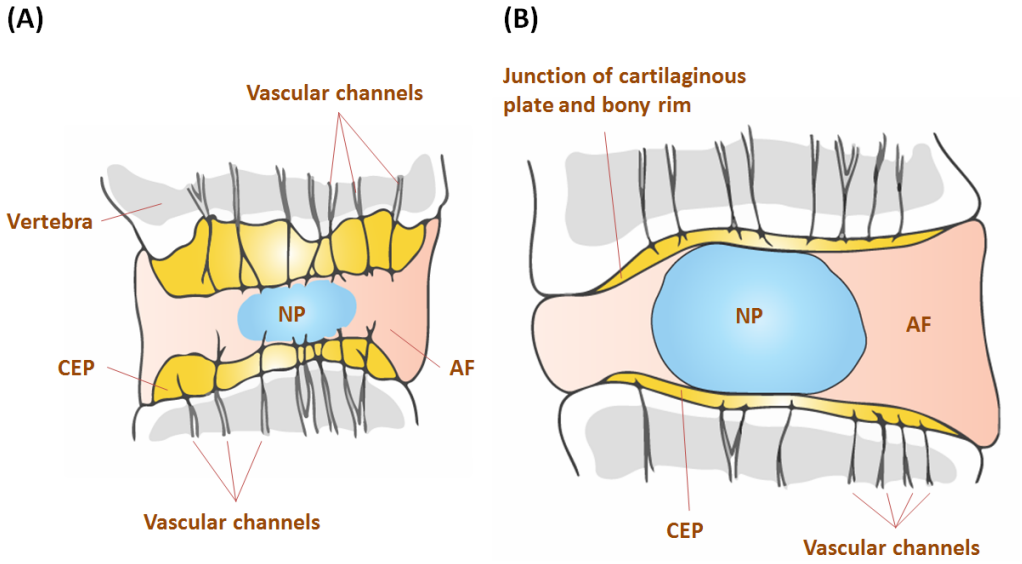


Figure 1-2 Axial sections of IVDs in (A) a 10-month-old girl and (B) a 50-year-old adult. (Reproduced with permission of John Wiley and Sons from [10] © 2008 John Wiley and Sons. The figures were relabelled without changes in the words and color was added).

The proportions of major components in IVD are summarized in **Table 1-3**. NP has a higher proteoglycan content and AF has a higher collagen content.

Table 1-3 Percentages of components in IVD[1, 10]

	NP	*AF*	*CEP*
Water	• Decreases with age (childhood: 90%, young adult: 80%, older adult: 70%) [1]	• No change during life (60-70%) [1]	• 55% [10]
Proteoglycan	• 14% of NP wet weight [10] • 60% of NP dry weight [1]	• 5% of AF wet weight [10] • 30% of AF dry weight [1]	• 8% of CEP wet weight [10]
Collagen	• 4% of NP wet weight [10] • 20% of NP dry weight ▪ Type II collagen: 50% ▪ Type I collagen: 20% [1]	• 15% of AF wet weight [10] • 65-70% of AF dry weight ▪ Type I collagen: 50% ▪ Type II collagen: 30% [1]	• 25% of CEP wet weight [10]

1.2.3 Comparison between IVD and articular cartilage (AC)

The tissue hydration is maintained through the osmotic pressure provided by its constituent chondroitin and keratan sulfate chains [10]. Compared to deep zone articular cartilage (AC), the aggrecan in IVD is more highly substituted with keratan sulfate. The aggrecan molecules in IVD are less aggregated (30%) and more heterogeneous, with smaller, more degraded fragments than in AC (80% aggregated) from the same individual [10, 15]. NP and AF cells can have several long, thin cytoplasmic projections, which may be more than 30 μm long but these are not found for AC cells [10, 16, 17]. The function of these cytoplasmic projections in IVD is not known but their roles as sensors and communicators of mechanical strain within the tissue were suggested [10, 16].

1.2.4 Types of IVD cells (biology)

In IVD, there are different types of cells, namely, the notochordal (NC) cells, the nucleus pulposus (NP) cells, the annulus fibrosus (AF) cells and the cartilaginous endplate (CEP) cells. In NP tissue, there are two distinct cell types: large clusters of NC cells and smaller and more disperse cartilage-like cells [18]. Since the loss of NC cells is linked with the onset of disc degeneration, it has been suggested that these NC cells are required for NP maintenance [11, 19-21]. In some vertebrates such as rats and cats, the NC cells persist through most of adult life, whereas in other species such as humans and cows, the NC cells gradually disappear during maturation and eventually become undetectable in the NP (**Table 1-4**) [21]. **Table 1-5** shows the morphology, density, gene expression and extracellular matrix (ECM) proteins of human IVD cells. In adult animals of some species, it contains chondrocyte-like cells, sometimes sitting in a capsule within the matrix as shown in **Figure 1-3** [10].

Table 1-4 Comparison of NC cell retention in various mammalian species (Reproduced with permission of Mary Ann Liebert, Inc. from [21] © 2003 Mary Ann Liebert, Inc.)

Animal	Age at skeletal maturity	Age at loss of NC cells	Age at onset of disc degeneration	Report of chordoma
Human	20 years	10 years	30-50 years	Yes
Rat	2 months	12 months	12 months	Yes
Chondrodystrophoid dog	12 months	6 months	4 years	None
Nonchondrodystrophoid dog	12 months	5 years	7 years	Yes
Rabbit	6 months	6 months	Not reported	None
Cat	2 years	18 years	Rare	Yes
Cow	3 years	12 months	Not reported	None
Horse	5 years	birth	Not reported	None

Table 1-5 Summary of characteristics of human IVD cells [1, 10, 22]**.** FOX-F1: Forkhead box protein F1, CA12: carbonic anhydrase 12, PAX-1: paired box protein

	NP cells	*AF cells*	*CEP cells*
Morphology	Rounded; chondrocyte-like or vacuolated [22]	Elongated, fibroblast-like; elongated and thin in outer AF and more oval in inner AF [10, 22].	Rounded [22]
Density	3000-5000 cells/ mm^3 [1, 10].	9000 cells/ mm^3 [1]	/
Gene expression	Type II collagen, Cytokeratin-19, FOX-F1, CA12, PAX-1, Brachyury [22]	Type I collagen, type V collagen, tenomodulin [22]	/
ECM proteins	Type II collagen, aggrecan, hyaluronan [22]	Type I collagen, type II collagen, aggrecan, elastin [22]	Type II collagen, aggrecan, hyaluronan [22]

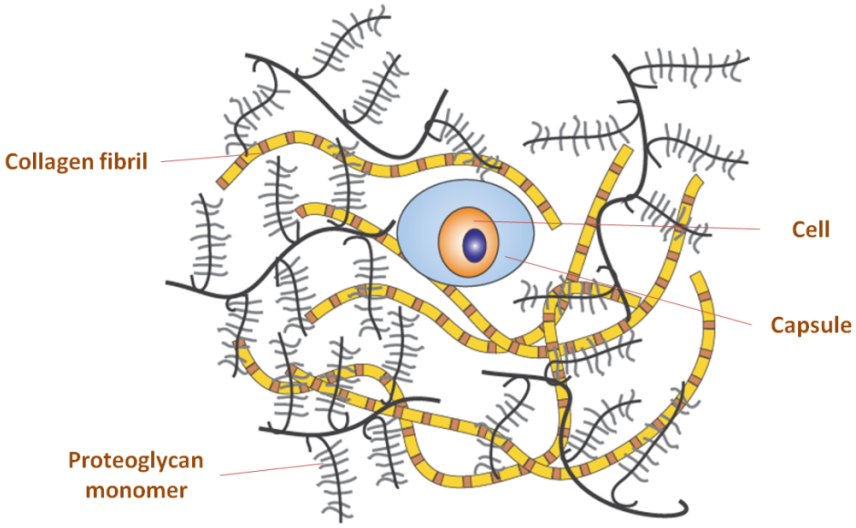


Figure 1-3 A NP cell in proteoglycan aggregate. (Reproduced with permission of John Wiley and Sons from [10] © 2008 John Wiley and Sons. The figure was redrawn based on the figure in [10]).

1.2.5 Development of the IVD from the notochord

The notochord has been well studied for its role during gastrulation [23], but comparatively less studied for its function during IVD formation [11]. Developmental studies have revealed that the notochord plays an essential role in forming the spinal column, including the IVDs [21]. The notochord is derived from gastrulation, the process which the embryo develops into three layers (ectoderm, endoderm and mesoderm) [24]. Noto is a highly conserved homeobox transcription factor whose expression is restricted to the organizer node and the nascent notochord during gastrulation and axis elongation (E7.5-E12.5). It regulates node morphogenesis, notochord ciliogenesis and left-right patterning [11]. At embryonic day 7.5 (E7.5) of mouse, the node is formed and provides cells that will form the rod-like structure of the notochord [11, 25]. Then the somatic mesenchyme aggregates around the notochord and form a continuous perichordal tube (PT) that undergoes segmentation at E13.5. The condensed region gives rise to the vertebrae while the non-condensed regions IVDs [11, 26]. The NC cells in the IVDs proliferate and accumulate proteoglycans that increase the osmotic pressure within their cell vacuoles and the NP becomes surrounded by the mesenchyme-derived AF [11, 27, 28] (**Figure 1-4**) [11].

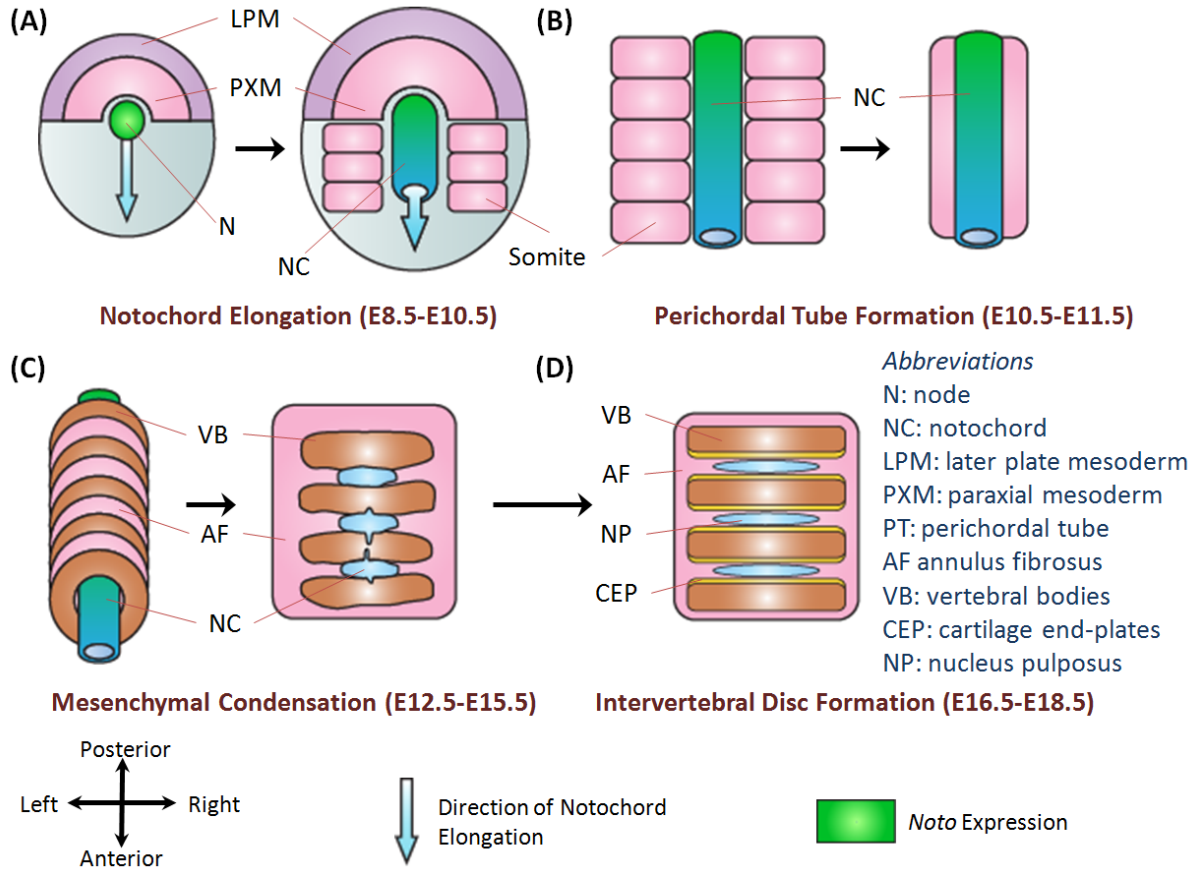


Figure 1-4 Schematic representation of the main stages in axial skeletogenesis. (A) Formation of the node (N) and elongation of the notochord (NC). LPM denotes lateral plate mesoderm and PXM denotes paraxial mesoderm. (B) Aggregation of the somatic mesenchyme around the notochord leads to formation of a continuous perichordal tube (PT). The green area indicates the localization of *Noto* expression at these time points. (C) Condensation of the axial mesenchyme leads to spine segmentation and perichordal disc formation. AF: denotes annulus fibrosis, VB denotes vertebral bodies. (D) Formation of IVDs is linked with the disappearance of the notochord within the vertebral bodies, and its expansion within the IVD. CEP denotes cartilage endplates and NP denotes nucleus pulposus. (Reproduced with permission of The Company of Biologists Ltd. from [11] under a Creative Commons Attribution Non-Commercial Share Alike License. The figure was redrawn with a list of abbreviations added).

1.2.6 Origin of the NP cells

It is well accepted that large NP cells are from the notochord (NC) during embryogenesis but there are controversies about the origin of small chondrocytic cells in the adult. Gegenbauer and Hertig suggested that NP cells were from the NC while Virchove, Heildberg and Weiss believe NP is from tissues surrounding the NP. As the NC contains both small spindle-shaped cells and large vacuolated cells, Risbud *et al.* hypothesized that both the large vacuolated cells

(LVC) and chondrocyte-like cells (CLC) of the NP are derived from the NC (**Figure 1-5**). These cells then undergo self-renewal to maintain cellular homeostasis of the NP tissue. It is possible that LVC may differentiate into CLC. It is known that the perinotochordal sheath (PNS) gives rise to both endplate (EP) chondrocytes and annulus fibrosus (AF) cells. Some workers are of the opinion that, in the adult, endplate chondrocytes and inner AF cells give rise to CLC at the same time replacing LVC. There is debate that loss or replacement of LVC in the nucleus pulposus initiates disc degeneration [29].

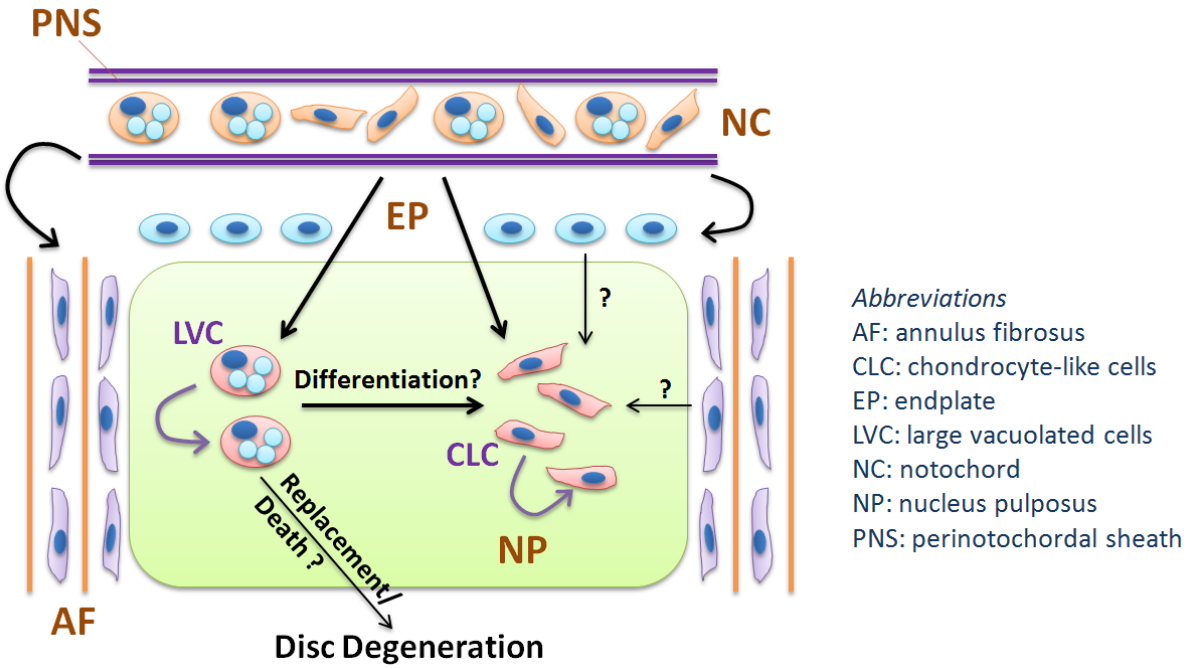


Figure 1-5 Schematic showing current theories concerning the origin of cells of the NP. (Reproduced with permission of John Wiley and Sons from [29] © 2010 John Wiley and Sons. The figure was redrawn and with a list of abbreviations added).

1.2.7 Disc degeneration

During aging and degeneration, numerous changes in the matrix synthesis, catabolic metabolism, growth factors and their receptors, and pro-inflammatory cytokines and their receptors were reviewed and summarized by Zhao *et al.* as listed in **Table 1-6**. The same group also suggested some possible interactions among different changes during IVD degeneration as shown in **Figure 1-6**.

Table 1-6 Biochemical changes due to altered phenotype and human disc cells during disc aging and degeneration (Reproduced with permission of Elsevier from [30] © 2007 Elsevier). ADAMTS: a disintegrin and metalloprotease with thrombospondin type 1 motifs, AF: annulus fibrosus, bFGF: basic fibroblast growth factor, BMP-R: bone morphogenetic protein receptor, CEP: cartilaginous endplate, EGF: epidermal growth factor, IGF: insulin-like growth factor, IL: interleukin, IVD: intervertebral disc, IVDD: intervertebral disc degeneration, MMP: matrix metalloproteinase, NP: nucleus pulposus, PDGF: platelet-derived growth factor, TGF: transforming growth factor, TIMP: tissue inhibitor of metalloproteinase, TNF: tumor necrosis factor.

Change types	*Parameters*	*Major variations*	*Implication*
Matrix synthesis	Collagen I	Occurs and increases in NP	Fibrosis of NP
	Collagen II	Decreases, especially in NP	Fibrosis of NP
	Collagen III	Increases	Repairing tendency
	Collagen IV	Exclusively exists in discs aged 16-30 years	Early stage of IVDD
	Collagen V	Slightly increases in NP and CEP	Probably indicates IVDD
	Collagen VI	Significantly increases	Possible repairing tendency
	Collagen IX	Decreases, similar to collagen II	Fibrosis of NP
	Collagen X	Exists in fetal NP, CEP and severely degenerated IVD	Advanced stage of IVDD
	Elastic fibres	Decreases	Reduced elasticity of IVD
	Total proteoglycans	Significantly decreases, especially in NP	Decreased hydration of IVD
	Aggrecan	Transient increases in AF, then decreases throughout	
	Decorin	Decreases after adolescence	
	Verscian	Transient increases in AF, then decreases throughout	
	Fibromodulin	Contradictory findings	Unclear
	Lumican	Increases	
Catabolic metabolism	MMP-1, 2, 3, 7, 8, 9, 13	Increases	Breakdown of IVD matrix
	MMP-19	Decreases	Reduced IGF-mediated proliferation
	TIMP-1, 2, 3	Contradictory findings	Less importance of MMPs in IVDD?
	ADAMTS-4	Increases	More effectiveness in IVDD?
	Cathepsin D, G, K, L	Exists at degenerated sites within AF Degradation of AF matrix	

Change types	*Parameters*	*Major variations*	*Implication*
Growth factors and their receptors	bFGF	Increases in degenerated and herniated IVD	Probably links to proteolytic activity
	EGF	No expression in herniated IVD	Involving in depletion of matrix
	IGF-1	Increases in degenerated IVD	Possible repairing tendency
	PDGF	Exists in herniated but not degenerated IVD	Neovascularization, cell proliferation?
	TGF-α	Occasionally expresses in herniated IVD	Involving in depletion of matrix
	TGF-β	Contradictory findings	Matrix remodelling?
	BMP-RII, FGF-R3, IGF-RI	Similarly expresses in degenerated or healthy IVD	Matrix remodelling?
	TGF-β-RII	Contradictory findings	Matrix remodelling?
	EGF-R	No expression in herniated IVD	Involving in depletion of matrix
Pro-inflammatory cytokines and their receptors	IL-1α	Increases in degenerated and herniated IVD	Responsible for enhanced catabolic
	IL-1β	Increases in degenerated and herniated IVD metabolism	
	IL-6	Increases in degenerated and herniated IVD	
	IL-1-RI	Increases in degenerated and herniated IVD	
	IL-1-Rα	Decreases in degenerated and herniated IVD	
	IL-6-R	Exists in herniated IVD	
	TNF-α	Increases in degenerated and herniated IVD	

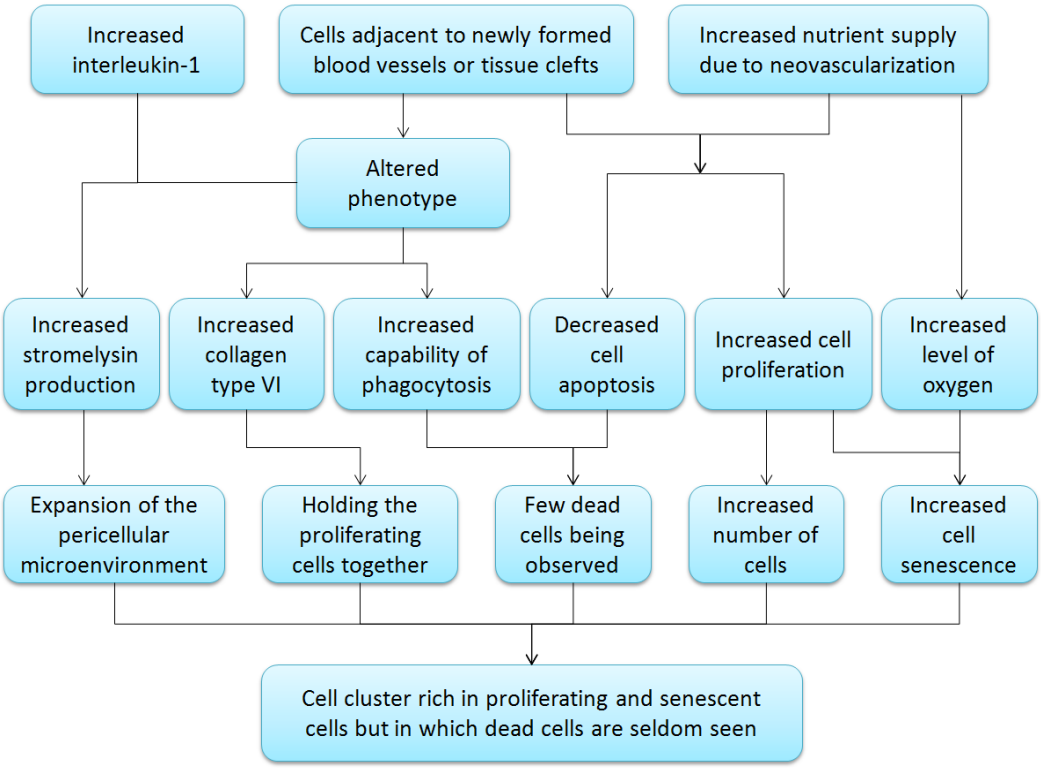


Figure 1-6 Schematic diagram of the possible interactions among the changes of cell proliferation, cell senescence, cell phenotype and cell death in the formation of cell cluster during IVD degeneration. (Reproduced with permission of Elsevier from [30] © 2007 Elsevier. The figure was redrawn).

Other than the synthesis rate, the molecular size and composition of the matrix also change during aging. These include:

- a decrease of molecular size of disc proteoglycans,
- a decrease of the chondroitin sulphate: keratansulphate ratio,
- a decrease of the related glucosamine: galactosamine ratio caused by impaired oxygen supply,
- a decrease in average chondroitin sulphate chain size with changes in the pattern of sulphation implicated in the impairment of biomechanical properties, and
- a progressive degradation of aggrecan and other proteoglycans due to the action of proteolytic enzymes and free oxygen radicals and lead to a large accumulation of proteoglycan-derived degradation products.

[31, 32]

1.3 Need of IVD engineering and a better understanding of NP cells

Low back pain is often related to the herniation, rupture or tears of IVD [33]. The current clinical solution to disc herniation is discectomy of the NP or spinal fusion. It is suggested that the lost NP tissue should be replaced by a scaffold seeded with native cells or stem cells to initiate regeneration [34]. When the IVD degeneration is severe, it may be necessary to replace the entire IVD. Allografts may be used for the replacement [35] but similar to allografts of other body parts, there are drawbacks of donor shortage and possible transmission of diseases. Acellular IVD implants such as metal and polymer prostheses have been developed to restore the range of motion [36] but these designs are mainly focused on replicating the mechanical properties only. There have been efforts in tissue engineering IVD [37, 38] and IVD cell based implants may be possible in the future. While low back pain is not life-threatening, the absence of minimally-invasive treatment approaches may lead patients who suffer from the torturing chronic pain associated with the condition to seek alternate means to alleviate the pain such as seeking advice and treatments from unregistered practitioners. This may make the disease more difficult to treat and exacerbate the pain condition. Gaining a better understanding of NP cells and the environmental cues that control their phenotypes will provide clues to rationally devise better therapeutic approaches as well as design better functional implants. 80% of the general population in industrialized countries experience low back pain in their lifetime and this causes a huge public health burden [1].

Due to the shortage of allografts for IVD replacements, there have been intensive researches in engineering discs using different materials, especially focusing on biologically based implants. Since NP cells from adult human are chondrocyte-like cells, scaffolds or techniques developed in the study of chondrocytes were also used in NP cell studies. When NP cells and articular chondrocytes (AC) are cultured in monolayer culture, they become more spindle-like and express more type I collagen and type III collagen. Pellet culture or alginate bead culture have been used in culturing chondrocytes to maintain their phenotypes and they were then adapted for NP cell cultures. The cells can be embedded into natural hydrogels such as

alginate, collagen and chitosan or synthesis hydrogels such as poly vinyl alcohol (PVA), PVA/ polyvinyl pyrrolidone (PVA/PVP) and polyethylene glycol (PEG) [39].

Although NP cells can produce collagen II and aggrecan for establishing the matrix of the scaffolds, it is often difficult to obtain NP cells of sufficient quantity and the quality of cells from degenerated discs may not be good enough for disc regeneration application. Thus quite a number of researches have been focusing on MSCs for disc engineering.

Regenerative medicine and tissue engineering are closely related fields in terms of definitions [40, 41] and they may bypass the problems of allograft shortage and improve the quality of human life, especially the aged.

1.4 Study models in IVD

1.4.1 *In vivo*

Due to the difficulty of obtaining human samples, especially normal healthy discs for IVD research, different animal species are used. These include mouse, rat, sand rat, chicken, rabbit, dog, sheep, pigs, goats and apes [42]. In IVD research, natural degeneration and induced degeneration have been studied. The degeneration models can be spontaneous in which research did no special treatment to induce disc degeneration to the animals. Or can be induced by treating the animals with chemicals, inducing inflammation by antigen, compressing the discs, forcing the animals to stand with hind limbs, forcing the animals to run, creating fusion, spinal distraction, spinal stability, disc lesion, chronic lesion or pinealectomy. Alini *et al.* [42] give a detailed review of the models used by different groups.

1.4.2 *In vitro*

Cell culture of IVD related cells or MSCs has also been widely used in understanding disc degeneration and regeneration. The cell culture model has the advantage that it is simple, which takes the cell down to literally its bare minimum and various interventions can be made

to the culture. However, it may be regarded as non-physiological [42]. For example, the NP cells are round and surrounded by ECM with negligible cell-cell contact *in vivo* but become spread in monolayer when cultured on culture dishes. It has been demonstrated that the shape of cells have significant influence on cell behavior [43, 44]. Thus, 3D culture systems such as alginate beads, agarose gels, collagen gels, hyaluronan hydrogel, fibrin/ collagen co-polymer gel, *etc.* have also been used [42].

Compared to cell culture, explant cultures of whole discs are considered as more physiologically relevant since the cells are still in the ECM of the tissue [42]. This was used in studying the effects of mechanical loading on IVDs [45, 46].

1.5 Common assays in IVD research

Some common methods used in IVD research are tabulated in **Table 1-7** which will be explained in more details in the sections that follow. They can be classified into three main categories: 1. compositional analysis, 2. protein analysis using antibodies and 3. gene expression analysis at mRNA levels.

Table 1-7 Some examples of assays used in IVD research. (DMMB: dimethylmethylene blue, ELISA: enzyme-linked immunosorbent assay, FC: flow cytometry, IF: immunofluorescence IHC: immunohistochemistry, RT-qPCR: reverse transcription-quantitative polymerase chain reaction, WB: western blot) (ACAN/ *Acan*: aggrecan, BASP1/ *Basp1*: brain abundant, membrane attached signal protein 1, CD/ *Cd*: cluster differentiation, COL/ *Col*: collagen, HIF: hypoxia-inducible factor, KRT: keratin, NCDN/ *Ncdn*: neurochondrin, NRP1/ *Nrp1*: neuropilin-1, SOX/ *Sox*: SRY (sex determining region Y)-box)

Group and year	*ECM*	*Protein (Antibody based)*	*mRNA*
Dai *et al.*, 2014 [47]		WB (COL2)	RT-qPCR (rat; *Col2a1*, *Sox9*, *Acan*)
Feng *et al.*, 2014 [48]	DMMB, Safranin O	IHC (COL2), ELISA (COL2)	RT-qPCR (bovine; *COL2A1*, *ACAN*, *SOX9*, *COL1A1*)
Foss *et al.*, 2014 [49]	DMMB	ELISA (COL2)	
Gupta *et al.*, 2014 [50]	DMMB	IHC (COL2, COL6, COL10), ELISA (COL2)	RT-qPCR (human; *COL2A1*, *COL10A1*, *ACAN*)

Group and year	*ECM*	*Protein (Antibody based)*	*mRNA*
Kim *et al.*, 2014 [51]	DMMB, Safranin O, chloramine-T assay	IHC (COL2)	
Naqvi *et al.*, 2014 [52]	DMMB, chloramine-T assay	IHC (COL1, COL2)	
Tam *et al.*, 2014 [53]	DMMB	IHC (ACAN, COL2)	RT-qPCR (mouse; *Acan*, *Col2a1*)
Bridgen *et al.*, 2013 [54]		FC (integrin subunits), IF (integrin subunits)	
Chen *et al.*, 2013 [55]	DMMB, Sircol collagen assay	IHC (COL2, laminin α5, vimentin, KRT5/8, integrin subunit α6)	
Feng *et al.*, 2013 [56]	DMMB	IF (HIF-1α)	RT-qPCR (human; *COL2A1*, *ACAN*, *SOX9*, *COL1A1*)
Ning *et al.*, 2013 [57]	^{35}S-Proteoglycan	IHC (COL1, COL2), WB (COL2)	
Sakai *et al.*, 2012 [58]	Safranin O, Toluidine blue	IF (NP progenitor markers), FC (NP progenitor markers)	
Tang *et al.*, 2012 [59]	Safranin O	IF (BASP1, NCDN, NRP1, CD221, CD24, CD90, Brachyury)	microarray, RT-qPCR (rat; *Basp1*, *Ncdn*, *Nrp1*, *Cd221*, *Cd155*, *T2*, *Cd24*, *Cd90*)
Minogue *et al.*, 2010 [60]			microarray, RT-qPCR (human NP markers)
Minogue *et al.*, 2010 [61]			microarray, RT-qPCR (bovine and human NP markers)
Fujita *et al.*, 2005 [62]		FC (CD24), IF (CD24)	microarray, RT-qPCR (rat *Cd24* and human *CD24*)

1.5.1 Composition analysis of ECM of IVD

1.5.1.1 Collagen

There are different methods to measure the content of collagen such as high-performance liquid chromatography [63], colorimetric assays involving the oxidation of free hydroxyproline with chloramine-T reagent which is capable of precise collagen quantification down to the nanogram level [64, 65] and a more recently developed method, the Sircol collagen assay (SCA) [66]. The SCA is a more convenient colorimetric assay based on the amino acid binding property of Sirius red with sulphonated acid side-chain groups that react

with the side-chain groups of basic amino acids [66]. Sirius red is used widely as a selective histochemical stain for collagen in normal and pathological tissue. It is also reported to be used to quantify the collagen content by Lareu *et al.* after some essential modifications of the assay [66].

1.5.1.2 Proteoglycan

Glycosaminoglycan (GAG) is one of the major components in the cellular environment and all GAGs have N- and/ or O-sulfate groups on their disaccharide building blocks except for hyaluronic acid. Most sulfated GAG chains are covalently linked to core proteins to form proteoglycans, which are at the cell surface and in the ECM [67]. One of the most common methods to measure the GAG content is by the dye 1,9-dimethylmethylene blue (DMMB) assay. This method is based on the change of absorption spectrum of DMMB when bound to GAGs. Besides DMMB, Alcine blue and Toluidine blue are also used for GAG content estimation.

1.5.2 Protein content analysis by the use of antibodies

1.5.2.1 Western blot (WB)

Western blot (WB) is a common method to detect specific proteins in a sample of tissue homogenate or extract. Gel electrophoresis is used to separate the proteins based on 3D structure (for native proteins) or length of polypeptide (for denatured proteins). The proteins are then transferred to a membrane (typically nitrocellulose or polyvinylidene fluoride, PVDF) and stained with antibodies specific to the target proteins [68, 69].

1.5.2.2 Immunohistochemistry, immunocytochemistry and immunofluorescence

Immunohistochemistry (IHC), immunocytochemistry (ICC) and immunofluorescence (IF) are quite similar staining methods. IHC refers to the staining of tissue sections while ICC refers to the staining of cells. The detection methods can be using fluorescence dyes as in IF or using

enzymes such as peroxidase and alkaline phosphatase. The principles behind the methods on immunostaining are given in details in [70] and [71].

1.5.2.3 Enzyme-linked immunosorbent assay (ELISA)

Enzyme-linked immunosorbent assay (ELISA) provides a sensitive and selective method for detecting a wide range of antigens in diverse matrices. One of the simplest forms of an ELISA involves the immobilization of a target antigen on a plastic substrate by adsorption and its detection with a selective antibody conjugated to a measurable label [72]. ELISA allows the quantitative and semi-quantitative determination of protein concentrations in a multi-well format. In general, the throughput of ELISA is higher than WB but it does not give information about the molecular sizes of the proteins detected.

1.5.2.4 Flow cytometry (FC)

Flow cytometry is a laser-based technology that is used in a wide range of applications such as cell counting, cell sorting, biomarker detection and protein engineering. Normally the cells are stained similarly as in IHC but the cells are in suspension instead of on glass slides. Then the cells will pass through an electronic detection apparatus in a stream of fluid. This technology allows the detection of cells/ particles up to thousands of particles per second.

1.5.3 Gene expression at mRNA level

1.5.3.1 RT-qPCR

Reverse transcription polymerase chain reaction (RT-PCR) is commonly used in molecular biology to detect RNA expression levels [73]. qRT-PCR or RT-qPCR refers to the type of RT-PCR in which real time (quantitative) PCR is used for PCR steps. The use of quantitative PCR allows the RNA levels to be estimated more accurately. In the decade after the first few reports of RT-qPCR in 1988-1990, the use of this technique has grown exponentially [73]. In RT-qPCR, RNA molecules are first converted into complementary DNA (cDNA) molecules using an enzyme, reverse transcriptase. The cDNA molecules are then used as templates in

PCR for exponential amplification. RT-PCR was considered to be more sensitive than other methods based on hybridization such as Northern blotting, solution hybridization and RNase protection assays due to its exponential amplification of small amounts of nucleic acid [74].

1.6 Developing methods in IVD research

1.6.1 Need for developing methods in science research

It is well established that technological innovations are sometimes called forth by the demands of scientific research, and that the technological infrastructure is an enabling factor in the conduct of such research [75]. The same is true for the medicine field. In 2003, Nature medicine published a special issue on "Technology: pushing the boundaries of scientific discovery" [76]. It valued the importance of technologies behind the scientific discovery, especially emerging technologies which are undergoing unusually rapid development and platform technologies that have broad applications.

This thesis focuses on the systematic study of methods. Although similar methods have been used, the technical challenges involved have not been addressed systematically. This resulted in experiment failure or waste of samples due to the suboptimal methods used. The methods developed in our studies enhance the use of samples.

Some of the major motivations behind development of methods in research are depicted in **Figure 1-7**.

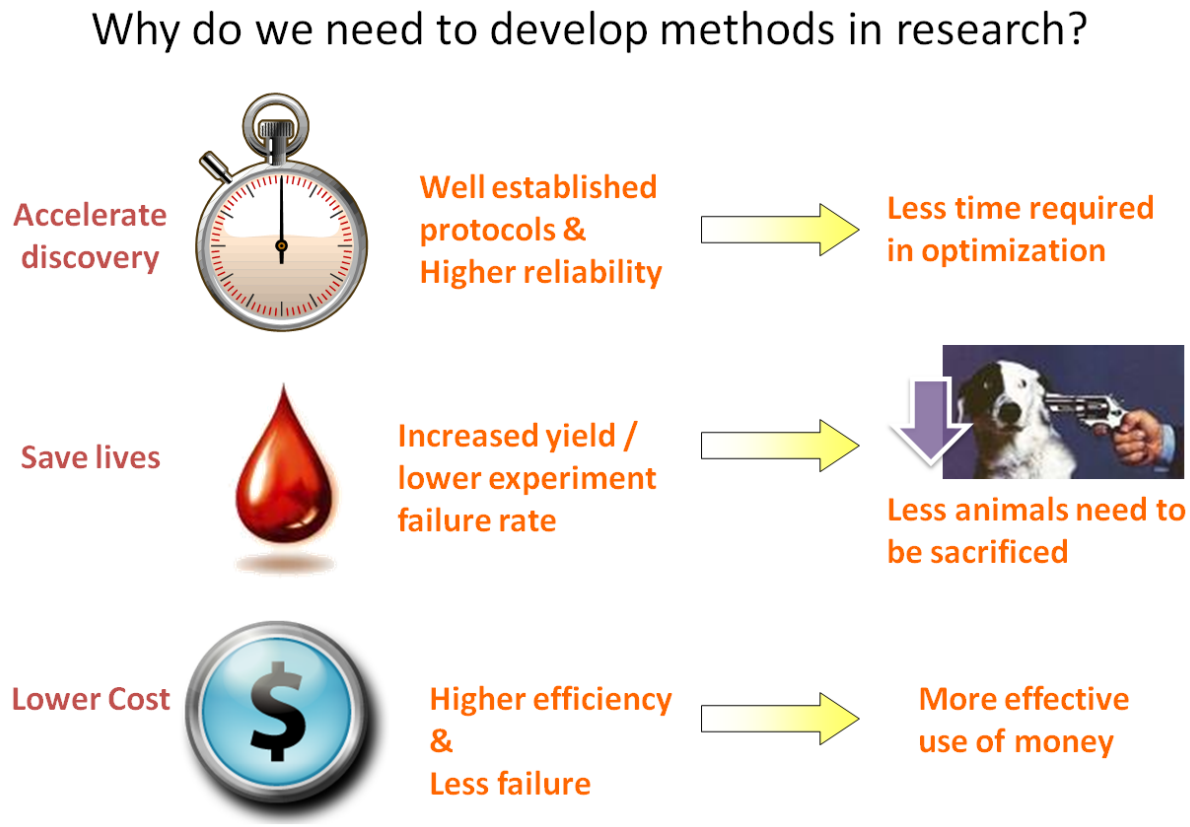


Figure 1-7 Schematic showing the need for developing methods in research.

1.6.2 Some areas for method improvement in IVD research

This thesis focused on several aspects of method development related to IVD research which are described in Chapters 2 to 7 and briefly explained in the following:

1.6.2.1 Isolation of cells from bovine or human IVD tissue

In order to study the behavior of cells, cells are often isolated from the tissues and expanded in culture medium. There are a variety of protocols for cell isolation recorded in literature but there was no systematic study of NP cell isolation to date. Optimal cell yield is critical to the feasibility and success of experiments when the starting materials are limited such as from clinical sources. Thus there is a need to analyze different parameters involved in cell isolation in order to provide a guide in NP cell isolation from tissues.

1.6.2.2 Isolation of RNA from bovine or human IVD tissues

There may be changes of gene expression during cell isolation from tissues. Most studies focus on gene expression of isolated cells rather than tissues directly. This is probably due to the high proteoglycan content and low cellularity of NP tissue which make RNA extraction more difficult. Conventional RNA extraction method cannot be used even with the modification of precipitating the RNA with high salt solution as suggested by the manufacturer. Hence there is a need to develop a method to extract RNA from bovine NP tissue.

1.6.2.3 Understanding MSCs for IVD studies

As the source of NP cells from patients is limited, MSCs were suggested to be a potential source of cells for NP repair or regeneration. There are different sources of MSCs and the properties of these cells may differ greatly. There were studies comparing the osteogenic and adipogenic potential of MSCs but few has addressed the discogenic potential (potential to differentiate into the IVD cell phenotype). Yuan *et al.* have summarized some *in vivo* studies using MSCs in disc regeneration [77]. It was observed that different outcomes can be resulted for MSCs of different sources. Slight differences were also observed for the NP cell marker expression in MSCs upon exposure to different niches. These suggest that the sources of MSCs and the culture conditions may have significant effects on the outcome. This necessitates a better understanding of the MSCs used in our studies.

1.6.2.4 Controlling the shape of cells in cell culture

Although NP cell culture can be used to study NP cell response, *ex vivo* culture often changes the shapes of cells when cultured on planar surfaces. Pellet culture and alginate culture are common methods to maintain the shape of cells. However, diffusion gradient may be built up within the pellets or alginate beads. Besides, these millimeter scale 3D cell culture often requires fixation and sectioning before observation under microscope which can be time consuming and may introduce artifacts. Thus for certain studies, it is necessary to maintain

the shape of cells in an alternative way such as micropatterning. Micropatterning can be used to control the shape of cells.

1.7 Organization of this thesis

The organization of this thesis is depicted in **Figure 1-8**. In my PhD study, researches in different areas in IVD were carried out to study NP cells, IVD tissues, MSCs and cell shape. Different technical aspects were also studied along the way. This thesis focuses on the technical aspects and can be viewed as three main parts:

(1) the isolation of cells and RNA from bovine NP tissue (Chapter 2, Chapter 3 and Chapter 4)
(2) the study of MSC isolation methods, characterization and culturing (Chapter 5)
(3) the techniques associated with maintaining cell shape through micropatterning (Chapter 6 and Chapter 7)

Finally, Chapter 8 gives the overall conclusions and perspective of this thesis.

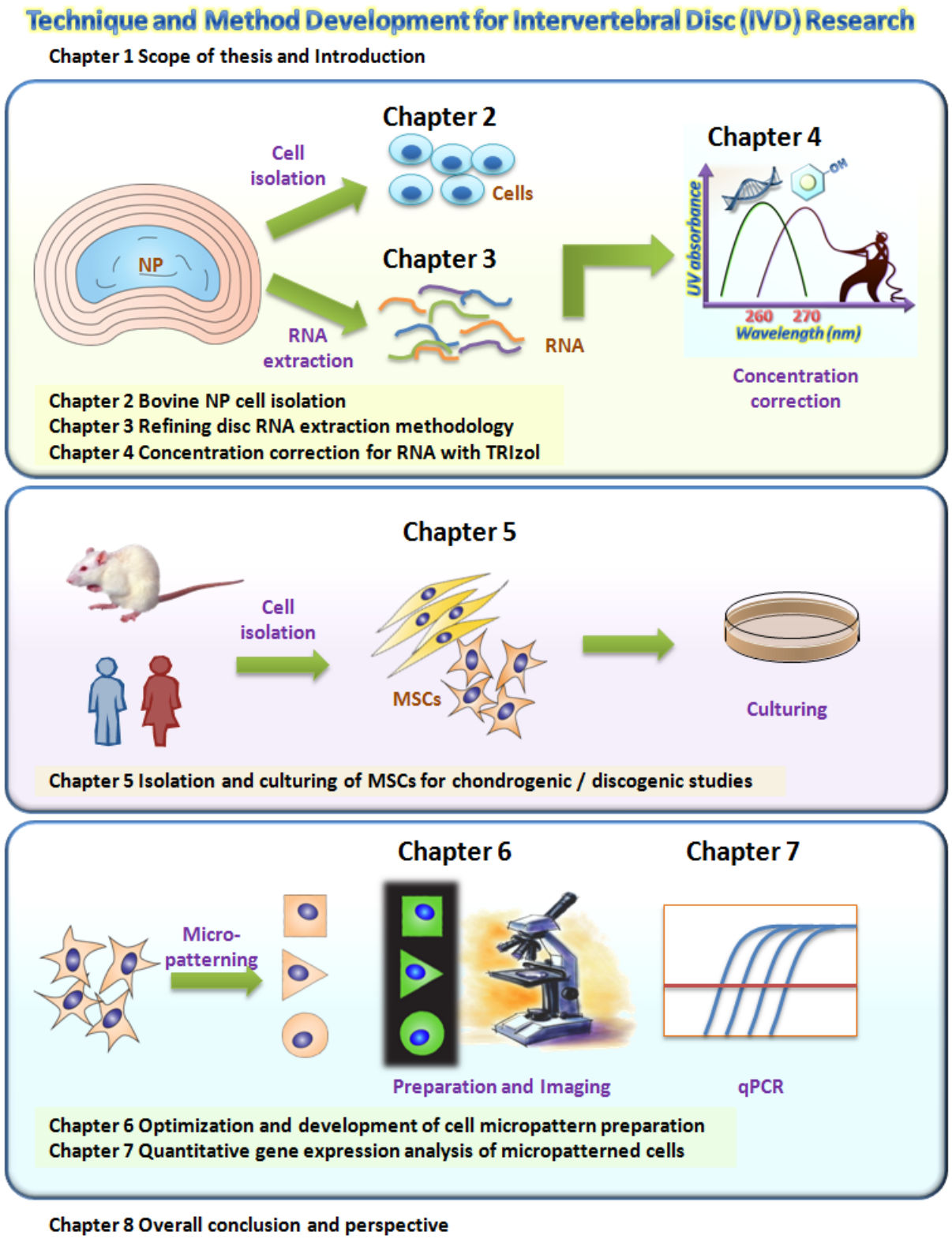


Figure 1-8 Schematic showing different studies related to IVD researches described in this thesis.

The content in Chapter 2 to Chapter 7 is summarized in the following:

1.7.1 Optimization of NP cell isolation from tissues

Numerous studies have used isolated NP cells to study biological phenomenon. Different groups used different protocols and there is no clear guide in the selection of different parameters in the isolation procedures. Suboptimal protocols will reduce the cell yield. In Chapter 2, a systematic experimental study of the cell isolation process from bovine NP tissue is given together with theoretical analysis of the isolation from an engineering point of view.

1.7.2 Refining disc RNA extraction methodology

RT-qPCR is a widely used method in assessing gene expression of cells quantitatively at mRNA level. However, there were limited studies assessing the mRNA levels of cells in IVD tissues, especially for bovine and human IVD tissues due to the low cell density but high proteoglycan content which make RNA extraction difficult. In Chapter 3, RNA extraction from bovine IVD tissues was developed. Methods for RNA extraction from mouse and rat IVD tissues were also described and assessed.

1.7.3 Concentration correction for RNA contaminated with phenol

With the RNA extraction method using TRIzol described in Chapter 3, it was possible to extract RNA from bovine IVD but the concentration of RNA obtained was very low and the peak of UV spectra of the RNA was shifted from 260 nm to 270 nm which was due to contamination with phenol. The absorbance at 270 nm contributed by phenol causes over-estimation of RNA concentrations. In Chapter 4, a computational method to correct the concentration over-estimation based on subtraction was developed and verified.

1.7.4 Isolation and culturing of MSCs for chondrogenic / discogenic studies

MSCs have been implicated in tissue engineering and regenerative medicine for disc degeneration therapy in the future. Different aspects of MSCs were investigated for the setting

up of study for MSC differentiation into NP-like cells through signaling pathway inhibition and were described in Chapter 5.

1.7.5 Method optimization of cell micropatterning and development of a micropatterning method compatible for high resolution imaging

In Chapter 6, micropatterning was studied to maintain the round shape of cells at single cell level, which will reduce the effect due to diffusion limitation. Various parameters such as pattern sizes, use of pluronic, use of serum in cell culture medium, *etc.* were investigated for the study of shape in bovine NP cells. To enable the capture of high resolution images and 3D image reconstruction of cells on micropatterns, different methods to prepare cell micropatterns compatible for high resolution microscopy were explored.

1.7.6 Method development in cell micropatterning compatible with laser capture microdissection (LCM)

Many micropatterning studies focus on immunostaining to assess the gene expression of cells. RT-qPCR can be a powerful way to assess the gene expression quantitatively with multiple genes. In Chapter 7, we modified the protocol of a commercial kit to study gene expression of micropatterned cells using RT-qPCR. In addition, a method to patterns cells compatible with laser capture microdissection (LCM) was developed to enable the selection of cells of interest from the micropatterns.

Chapter 2 Bovine NP Cell Isolation

2.1 Background

2.1.1 Comparison of different species

The IVDs from different species have different sizes as shown in **Figure 2-1**. The diameters measured from **Figure 2-1** are around 60 mm (human lumbar disc), 30 mm (bovine tail disc), 25 mm (sheep thoracic disc), 5 mm (rat lumbar disc) and 3.5 mm (rat tail disc). Compared to rat, bovine discs are closer in size to human discs.

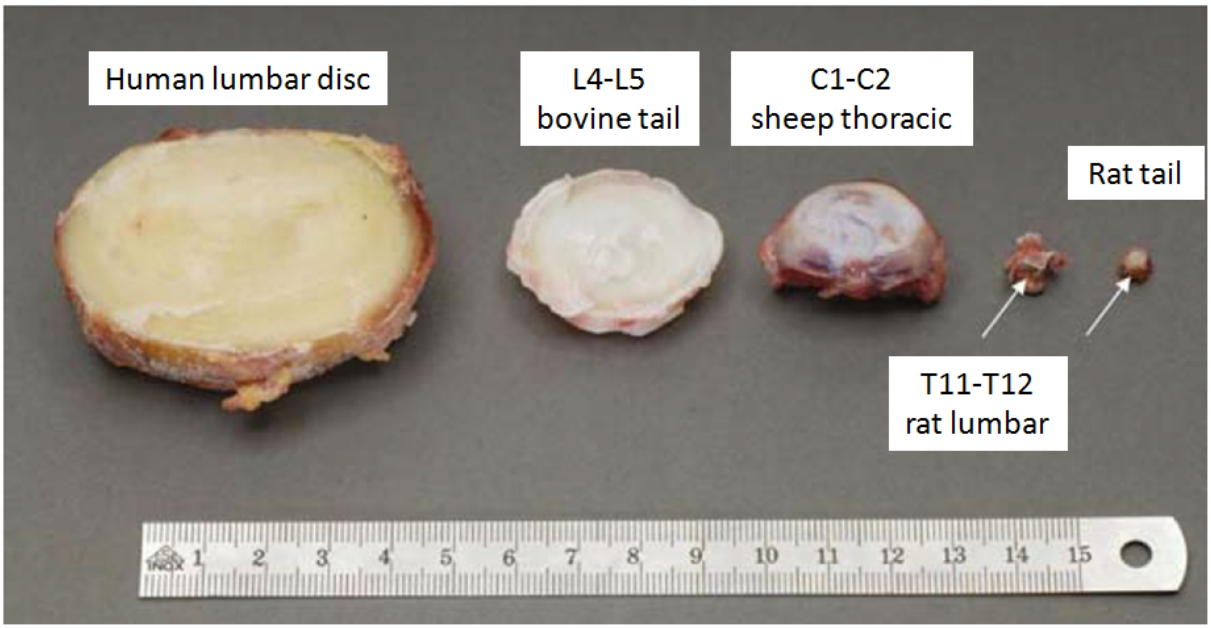


Figure 2-1 Relative sizes of IVDs in different species. (Reproduced with permission of Springer from [42] © 2007 Springer. Labels were added to the photo).

Other than disc sizes, the difference in the presence of notochordal (NC) cells in NP is also one of the special differences in different species. The diameters of the large NC cells are 25 – 85 μm. They are highly vacuolated which may be due to unsecreted proteoglycan and contain glycogen stores. The Golgi of these cells is well-demarcated and the mitochondria is considered ‘‘immature’’ with generous association endoplasmic reticulum, and forms fasciculi

with neighboring cells [29]. Morphology of NC cells in different species using the same staining method was studied by Hunter *et al.* [78] and this gave a better idea about the variability of NC cells in the IVDs of different species.

Animals of different species retain their NC cells up to different stages of lives as summarized in **Table 2-1** by *Hunter et al.* [21]. Similar to cow, horse and chondrodystrophoid dog, human loses NC cells before skeletal maturity.

Table 2-1 Comparison of NC cell retention in various mammalian species (Reproduced with permission of Mary Ann, Inc. from [21] © 2003 Mary Ann, Inc. The order of rows was re-arranged with human, cow, rabbit and rat put on the top of the list. These animal species were used in experiments in our laboratory.)

Animal	Age at skeletal maturity	Age at loss of notochordal cells	Age at onset of disc degeneration	Report of chordoma
Human	20 years	10 years	30-50 years	Yes
Cow	3 years	12 months	Not reported	None
Rabbit	6 months	6 months	Not reported	None
Rat	2 months	12 months	12 months	Yes
Horse	5 years	Birth	Not reported	None
Chondrodystrophoid dog	12 months	6 months	4 years	None
Nonchondrodystrophoid dog	12 months	5 years	7 years	Yes
Cat	2 years	18 years	Rare	Yes

2.1.2 Use of bovine cells

Mature bovine NP tissue has higher similarity to mature human NP tissue [79]. For instance, the swelling pressure of bovine tail discs is similar to that of human lumbar discs [80] and the loading in bovine discs is similar to that of human [81, 82]. Besides, bovine tail discs are also less gel-like compared to immature porcine discs which resemble discs in developed human more closely. The major cell population in immature porcine discs is NC cells as contrasted with chondrocyte-like cells in aged human discs and bovine discs [83]. These differences suggest that NP cells from bovine or human source will be more relevant in studying IVD aging and degeneration in human.

2.2 Introduction

Intervertebral disc (IVD) is an important part of the spine and its degeneration is highly associated with back pain, which is one of the major health problems in many developed countries. The major components of IVD are nucleus pulposus (NP), annulus fibrosis (AF) and cartilaginous endplates (CEP). To elucidate the mechanism related to disc degeneration, primary NP cells were isolated from the NP tissue of different animal species for different *in vitro* studies. The cell isolation from tissues is often achieved by enzymatic digestion using collagenase. As summarized in **Table 2-2**, there are various protocols for NP cell isolation and they vary greatly in terms of enzyme concentrations (0.01% to 0.5%), digestion duration (30 min to overnight) and type of pre-collagenase treatments such as digestion by pronase, which is a mixture of different proteases. To date, there is no systematic study about the cell isolation protocols for NP tissues and sub-optimal protocols may result in a lower cell yield, which can be a critical problem for human IVD samples as their availability is usually more limited. Human NP was suggested to have most dramatic changes with age of any cartilaginous tissue [26] and variability was observed in clinical samples obtained from patients of different ages with discs of different degrees of degeneration. Theoretically in scientific studies, same protocol should be used throughout the same set of experiments but for clinical NP samples, using the same protocol does not guarantee similar isolation efficiency as the samples themselves can be quite different. Interestingly, the digestion duration of human NP in reported studies can be as short as 1 h [84] but also as long as overnight [85]. When the tissues are insufficiently digested, the cells in the tissues cannot be released and sufficient RNA cannot be extracted for reliable gene expression studies. This necessitates a better understanding of the cell isolation process.

Table 2-2 Summary of cell isolation conditions and durations for IVD tissues in some reported studies (Reproduced with permission of John Wiley and Sons from [86] © 2015 John Wiley and Sons).

Reference	*Pre-collagenase treatment*	*Collagenase treatment* [a]	*Tissue* [b]	*Species*	*Notes*
Minogue *et al.* 2010 [61]	0.5% protease for 1 h	0.5% collagenase II + 0.1% hyaluronidase for 2-3 h	NP, AF	bovine	serum free medium
Bron *et al.* 2011 [34]	2.5% protnase E for 1 h	0.125% collagenase for 16 h	NP, AF	goat	1%, 25% FBS
Gilbertson *et al.* 2008 [87]	0.2% pronase for 90 min	0.02% collagenase II for O/N	NP, AF	human	with gentle agitation
Risbud *et al.* 2006 [88]		0.1% collagenase + 10 U/ml hyaluronidase for 4-6 h	NP, AF	rat	
GantenbeinRitter *et al.* 2012 [89]	0.19% pronase for 1 h	collagenase II for 14 h	NP	bovine	1-year-old
GantenbeinRitter *et al.* 2011 [90]	0.19% pronase for 1 h	0.4% collagenase II for O/N	NP	bovine	6- to 12-month-old
Arana *et al.* 2010 [91]	0.5% protease for 1 h	0.1% collagenase A for O/N	NP	bovine	
Gilson *et al.* 2010 [92]		0.05% type I collagenase for O/N	NP	bovine	
Halloran *et al.* 2008 [93]	0.2% pronase + 0.004% DNase II for 90 min	0.05% collagenase II + 0.01% hyaluronidase + 0.004% DNase II for O/N	NP	bovine	
Jones *et al.* 2008 [94]		0.8 mg/ml crude type XI collagenase + 1.67 U/ml DNase for O/N	NP	bovine	18- to 32-month-old
Korecki *et al.* 2009 [95]	0.2% pronase for 1 h	0.125% collagenase type IV for 8-10 h	NP	bovine	constant agitation
Zeiter *et al.* 2009 [96]	0.19% pronase for 1 h	32 IU/ml collagenase II for 10 h	NP	bovine	
Watanabe *et al.* 2010 [97]	0.27% pronase for 1 h	0.025% collagenase for 2 h	NP	human	
Yang *et al.* 2010 [85]		0.2% collagenase for O/N	NP	human	
Purmessur *et al.* 2008 [98]	2 U/ml protease for 30 min	0.4 mg/ml collagenase I for 4h	NP	human	
Studer *et al.* 2007 [99]	0.2% pronase for 90 min	0.02% collagenase type II for O/N	NP	human	
LeMaitre *et al.* 2005 [100]	2 U/ml protease for 30 min	0.4 mg/ml collagenase I for 4 h	NP	human	
Fernando *et al.* 2011 [101]		0.75 mg/ml collagenase type II + 0.6 mg/ml protease for O/N	NP	pig	
Guehring *et al.* 2009 [102]	0.2% protease for 1 h	0.2% collagenase for 18 h	NP	pig	

Reference	*Pre-collagenase treatment*	*Collagenase treatment* [a]	*Tissue* [b]	*Species*	*Notes*
Cheng *et al.* 2011 [103]		0.2% collagenase for 18 h	NP	rabbit	10% FBS
Yuan *et al.* 2011 [104]	0.2% pronase for 1.5 h	0.05% collagenase IA for 16 h	NP	rabbit	
Su *et al.* 2010 [105]		0.01% collagenase for 16 h	NP	rabbit	
Hiyama *et al.* 2011 [106]	0.01% trypsin for 15 min		NP	rat	
Hiyama *et al.* 2010 [107]		0.0125% collagenase P + 0.4% pronase for 30 min	NP	rat	
Kakutani K 2006 [84]		0.25% collagenase for 1 h	NP	rat, human	
GantenbeinRitter *et al.* 2012 [89]	0.19% pronase for 1 h	collagenase type 2 for 14 h	NC	pig	4- to 5-month-old
Guehring *et al.* 2009 [102]	0.2% protease for 1 h	0.025% collagenase for 18 h	NC	pig	Additional 2 h digestion in nonenzymatic cell dissociation solution
Gilson *et al.* 2010 [92]		0.075% type I collagenase for O/N	AF	bovine	
Korecki *et al.* 2009 [95]	0.2% pronase for 1 h	0.2% collagenase type IV for 8-10 h	AF	bovine	with constant agitation
Gilbert *et al.* 2010 [108]	300-350 PUK/ml pronase for 1 h	0.25% collagenase II + 0.01% hyaluronidase for 4 h	AF	human	
LeMaitre *et al.* 2005 [100]	2 U/ml protease for 30 min	2 mg/ml collagenase I for 4 h	AF	human	
Fernando *et al.* 2011 [101]		1.5 mg/ml collagenase type II + 0.6 mg/ml protease for O/N	AF	pig	
Guehring *et al.* 2009 [102]	0.2% protease for 1 h	0.6% collagenase for 18 h	AF	pig	
Hiyama *et al.* 2010, 2011 [106, 107]	0.4% pronase for 1 h	0.025% collagenase P for 3 h	AF	rat	
Wan *et al.* 2007 [109]		0.1% collagenase II for 3-6 h	AF	rat	

[a] Collagenase preparation from different companies may have different classifications of collagenase types

[b] NP: nucleus pulposus; AF: annulus fibrosus; NC: immature nucleus pulposus with notochordal cells

Among different species, we chose bovine NP tissue for studying various factors affecting the cell isolation procedures since bovine IVD has higher similarity to human IVD in terms of cell distribution, cell phenotypes, disc compositions, disc sizes and mechanical loadings. Unlike rodent NP cells which are in direct cell-cell contact, cells in bovine caudal NP tissues are at low cell density and are separated by extracellular matrix. Cows and sheep resembles human in that they may have some NC cells at birth but the numbers of cells decrease rapidly with age, while most other species such as mouse, rat, cat, mink, dog, pig and rabbit all have NC cells in the NP at birth and retain them throughout much of their adult life [42]. Besides, bovine coccygeal discs have similar NP compositions compared with human 40 to 80 years of age in terms of water content (77%), proteoglycan content (bovine, 166-341 mg/ g dry weight; human 188-356 mg/ g dry weight) and type II collagen content (bovine, 269-333 mg/ g dry weight; human, 224-367 mg/ g dry weight) [110]. Bovine caudal discs (14-22 mm in diameter and 5-10 mm thick) are comparatively close in size to the human lumbar disc and the musculature of the bovine tail maintains an *in vivo* pressure on the discs that is approximately the same as in the human lumbar disc in the prone position (0.1-0.3 MPa) [42]. Besides, Oshima *et al.* reported that the swelling pressure in bovine tail discs is similar to that in human lumbar discs, indicating that the prevailing compressive stress of the tail discs is probably of similar magnitude to lumbar discs [42, 111]. Thus bovine disc cells may be more clinically relevant to the study of IVD degeneration.

In this optimization study, we started with characterizing the bovine tissues to provide information in designing our experiments. We focused on three main applications of the isolated NP cells, namely for cell culturing, for RT-qPCR and for flow cytometry. For cell culturing, we tested different types of pre-collagenase treatments, different collagenase concentrations and different digestion durations to assess the cell yield obtained. For RT-qPCR, we extracted RNA from cells isolated from bovine NP, AF and muscle with different protocols and assessed the relative mRNA levels of chondrocyte markers and NP markers. The effect of cell isolation was also assessed by comparing with the mRNA levels in

cells in tissues without cell isolation. For flow cytometry, different studies have already been performed by different groups to assess the effect of pronase on cell surface proteins of different cells. Thus this study makes suggestions based on these literatures. In addition, due to the infinite possible combinations of parameters in the cell isolation protocol design, we also aim to provide suggestions in the cell isolation protocols through theoretical analysis based on enzyme kinetics and results in this study.

We hypothesize the cell yield can be increased through modifying the cell isolation conditions.

2.3 Objectives

The objectives of experiments in this Chapter are:

- To characterize bovine NP and AF tissues
- To study different parameters involved in cell isolation and suggest optimal protocols for different applications (cell culturing, RNA extraction, characterization by flow cytometry)
- To analyze different factors involved in cell isolation theoretically followed by experimental validation

2.4 Materials and Methods

2.4.1 LIVE/ DEAD® assay and cell size estimation

Bovine IVD tissues were obtained from bovine tails of young adult animals (18 - 36 month old) purchased from a local market in Hong Kong. The discs were excised with NP and AF tissues separated manually. For LIVE/ DEAD® assays, the NP and AF tissues were stained in 2 μg/ml calcein and 4 μg/ml ethidium homodimer-1 (Invitrogen, catalog # L3224) for 1 h. Fluorescence photos were taken using an upright microscope (Nikon, Eclipse 80i).

Bovine NP and AF cells were isolated with collagenase type 2 (Worthington) from bovine caudal IVD tissues. Photos of isolated cells were taken using an inverted microscope (Leica) using a 10× objective and the diameters of cells were measured using rulers in Adobe Photoshop CS4. The scale was calibrated by the use of a photo of a hemocytometer with known grid sizes and with the same microscope magnification (10×).

2.4.2 Water content estimation and DMMB assay of bovine NP and AF tissues

NP and AF tissues of about 1 mm thick were cut with a 4 mm biosy punch without immersing the tissues in saline to avoid absorption of water and swelling of tissues. The weights of the tissues were measured before and after freeze drying for estimating the water content. The freeze dried tissues were then digested using 50 μg/ml proteinase K (Roche, catalog # 03 115 801 001) in TE buffer at 60 °C overnight. The digested samples were diluted using TE buffer and mixed with DMMB reagent to estimate the GAG amount with the standard curve prepared using chondronitin sulphate A (Sigma, catalog # C9819) in the range of 0-128 μg/ml. The protocols for preparing the TE buffer and the DMMB reagent in formate buffer are described in **Section 2.7.2** in the Appendix of this Chapter.

2.4.3 Immunohistochemistry and cell density estimation

Immediately after harvest, the NP, AF and muscle tissues were quickly frozen in liquid nitrogen and stored in a -80 °C freezer. The frozen tissue was cryosectioned using a cryostat (Leica, CM 1900 UV) into 10 μm sections. The sections were allowed to dry for at least an hour at room temperature and then stored in a -20 °C freezer. Prior to staining, the sections was allowed to dry at room temperature and fixed with acetone. The sections were stained with antibodies to GAPDH (Aviva Systems Biology; ARP40175_P050; 1:200), CDH2 (Santa Cruz Biotechnology; sc-7939; 1:200), KRT18 (Aviva Systems Biology; ARP40206_T100; 1:200) and KRT19 (Aviva Systems Biology; ARP47463_P050; 1:200) diluted in 5% (v/v) goat serum. Samples treated with 5% (v/v) goat serum without primary antibodies added were used as negative controls. Primary antibodies were detected using a Vectastain ABC-AP kit

(VECTOR, catalog # AK-5000) for signal amplification and Liquid Permanent Red reagents (Dako, catalog # K0640). The slides were counterstained using Harris hematoxylin (Sigma) to visualize the cell nuclei. Samples were viewed under an upright microscope (Nikon, Eclipse 80i).

2.4.4 Cell yield, cell viability and attachment of isolated cells

2% (w/v) pronase stock solution and 5% (w/v) collagenase stock solution were prepared by dissolving the lyophilized pronase (Roche, catalog # 11 459 643 001) and type 2 collagenase (Worthington) respectively in water and filtered using 0.22 μm syringe filters (Millipore). The enzyme stocks were diluted to the desired concentration using high glucose Dulbecco's Modified Eagle Medium (DMEM, Gibco, catalog # 12100-046) with N-2-Hydroxyethylpipcrazine- N'-2-ethanesulfonic acid (HEPES, Sigma, catalog # H4034) added. Fetal bovine serum (FBS, Biosera, catalog # FB-1001/500) was added to a final concentration of 10% (v/v). Antibiotics (penicillin and streptomycin, Gibco, catalog # 15140) and fungizone amphotencin B (Gibco, catalog # 15290-018) were added to the medium to final concentrations of 100 U/ml, 100 μg/ml and 1 μg/ml respectively. Prior to cell isolation, NP tissues were cut into 2 mm pieces using a scalpel. The pieces of NP were mixed and distributed evenly into plastic tubes and different enzymes were added and incubated as shown in **Figure 2-4**. After the digestion, the cell suspensions with undigested tissues were filtered through tailor made metal strainers with pores of 23 μm to remove undigested tissues. The cell suspension was centrifuged and most supernatant was removed leaving 100 μl of medium behind. The cell pellets were resuspended in the supernatant and counted using a hemacytometer after mixing with 0.4% (w/v) Trypan blue (Sigma, catalog # T8154) in 1:1 ratio. For cell attachment assessment, the cells without being stained with Trypan blue were washed with phosphate buffered saline (PBS) for three times and re-suspended in DMEM without HEPES. The cells were plated in a 48-well plate and photos were taken at 0, 1, 2, 3, 4 and 7 days after the harvest of tissues.

2.4.5 Quality of RNA extracted with different digestion conditions

In this set of experiments, higher concentrations of collagenase were used and hence the collagenase stock solution was prepared in DMEM instead of water to avoid a significant dilution to the salts present in the DMEM due to stock solution addition. 2% (w/v) collagenase solution was prepared by dissolving type 2 collagenase (Worthington) in DMEM with HEPES and filtered using 0.22 μm syringe filters (Millipore). The required concentrations of the enzyme solutions were prepared by diluting the stock solutions with DMEM with HEPES. Prior to cell isolation, NP, AF and muscle tissues were cut into 2 mm pieces using a scalpel and digested in different conditions as shown in **Table 2-5**. Then the digested samples were centrifuged and washed with PBS. The cell suspension was centrifuged again and the supernatant was then removed. TRIzol (Invitrogen, catalog # 15596-018) was added to the cell pellets to lyse the cells and the lysates were stored in a -80°C freezer prior to RNA extraction. RNA extraction was performed with the addition of high salt precipitation solution as recommended by the manufacturer and also the following modifications: Bromochlorpropane (BCP) was used instead of chloroform as it has been suggested that it is a safer yet equally effective phase separation reagent in RNA extraction [112] and an additional 75% (v/v) ethanol wash step was added to remove the salt more completely. The RNA solution was quantified using a Nanodrop 2000c spectrophotometer (Thermo Scientific).

2.4.6 RT-qPCR

RT-qPCR was performed to further evaluate the effect of different digestion protocols on relative mRNA levels. In previous trials, total RNA cannot be obtained after overnight digestion, probably due to the degradation of RNA prior to RNA extraction (data not shown). Thus there is possibility that relative mRNA levels may change with different duration of collagenase digestion. Longer digestion yields a higher cell number while this may also result in more RNA degradation. In view of this, we performed RT-qPCR using RNA obtained with different protocols to assess the relative mRNA levels of some IVD or NP markers.

Six different genes were chosen in the RT-qPCR. *GAPDH* serves as a housekeeping gene which is used as a base of normalization. *ACAN* and *COL2A1* are typical chondrocyte markers and they are highly expressed in bovine articular chondrocytes (AC), NP and AF cells without much difference in mRNA levels detected among these three tissues [113]. *CDH2*, *KRT18* and *KRT19* are suggested to be NP-specific markers in bovine samples [113]. *CDH2* is a cadherin protein which has been shown to be important in mesenchymal condensation and chondrogenesis. *KRT18* is a type I cytokeratin which dimerises with *KRT8* to form intermediate filament in the cytoplasm of cells. *KRT19* is also a type I cytokeratin but does not pair with a basic cytokeratin.

Total RNA was reverse transcribed into cDNA using PrimeScript RT Master Mix (Takara, catalog # HRR036A) in a 10 µl reaction volume using a thermocycler (Applied Biosystems, Veriti 96 well thermocycler). The cDNA was diluted five times by adding 40 µl of autoclaved water. qPCR was performed with a total reaction volume of 10 µl, containing 1 µl of single stranded cDNA, 5 µl of SYBR Green PCR Master Mix (Applied Biosystems, part # 4309155) and 500 nM each of forward primer and reverse primer (*GAPDH*, *ACAN*, *COL2A1*, *CDH2*, *KRT18* and *KRT19* from [113] with sequences given in **Table 2-3**), in 96 well reaction plates using a standard PCR protocol for SYBR green reactions (Applied Biosystems, StepOnePlus) with a melt curve analysis. Primers were ordered from Tech Dragon Limited. Autoclaved water was used as a negative control and RNA before reverse transcription was used to estimate the level of genomic DNA contamination. DNase1 treatment by Amplification Grade DNase1 (Invitrogen, catalog # 18068-015) was also included when necessary. The relative gene expression was calculated based on comparative Ct method.

Table 2-3 Sequences of bovine primers used in this study (Sequences were from [113]; the sequences were written in 5' to 3' for both forward and reverse primers) (Reproduced under a Creative Commons Attribution License).

Primer	Sequence (forward)	Sequence (reverse)
Bovine *GAPDH*	TGCCGCCTGGAGAAACC	CGCCTGCTTCACCACCTT
Bovine *ACAN*	GGGAGGAGACGACTGCAATC	CCCATTCCGTCTTGTTTTCTG
Bovine *COL2A1*	CGGGCTGAGGGCAACA	CGTGCAGCCATCCTTCAGA
Bovine *CDH2*	GCCATCAAGCCAGTTGGAA	TGCAGATCGAACCGGGTACT
Bovine *KRT18*	TTGAGCTGCTCCATCTGCAT	AAGGCCAGCTTGGAGAACAG
Bovine *KRT19*	CGGTGCCACCATTGAGAACT	CAAACTTGGTGCGGAAGTCA

2.4.7 Isolation of cells from NP, AF, CEP, tendon and adipose (AD) tissues in bovine tail

Adult cow tails were purchased from a local butcher in Brixton of London, United Kingdom. NP, AF, CEP, tendon and adipose (AD) tissues were dissected from bovine tail and digested in collagenase solution (0.05% w/v for NP tissue; 0.2% w/v for AF, CEP, tendon and AD). Collagenase, Type II (Gibco, catalog # 17101-015) was dissolved in DMEM (Gibco) with 10% (v/v) FBS with 1% (v/v) antibiotics/ antimycotics (Invitrogen, catalog # 15240-062) and filtered through 0.22 μm syringe filters. Prior to cell isolation, the tissues were cut into 1-2 mm pieces using a scalpel and digested in the collagenase solution overnight at 37 °C with shaking. For NP, AF and AD tissues, the cell suspensions with undigested tissues were filtered through 70 μm cell strainers to remove undigested tissues. The cells were washed with full DMEM and seeded in plastic culture flasks. For CEP and tendon tissues, similar procedures were performed but without using the cell strainers and the undigested tissues together with the cells were transferred to plastic culture flasks.

2.4.8 Isolation of cells from rat NP tissue

Rat NP tissue was obtained from the dead bodies of Lewis rats maintained by the Laboratory Animal Unit of the University of Hong Kong for MSC harvest. The experimental protocol of harvesting the MSCs was approved by the Committee of the Use of Live Animals in Teaching and Research, the University of Hong Kong (CULATR Ref. No.: 2202-10). The rat NP was digested with 0.2% (w/v) pronase for 1 h with subsequent collagenase (0.05% or 0.2% w/v)

treatment for 2 h or 3 h collagenase (0.05% or 0.2% w/v) treatment without pronase pre-treatment. The digestion was carried out at 37 °C. Shorter digestion time in collagenase was used for rat NP compared to bovine NP as the rat NP tissue is smaller and the digestion time used in literatures is in general shorter for rat NP than bovine NP (ranges from 30 min to 6 h for rat NP and 2 h to overnight for bovine NP) (**Table 2-2**).

2.4.9 Flow cytometry of pronase treated human MSCs

Human MSCs were harvested and cultured as described in Section 5.3.6 in Chapter 5. The MSCs on plastic culture surface were detached using accutase (Gibco, catalog # A11105-01) with incubation at 37 °C for 5-10 min. 1 ml of DMEM with 10% (v/v) FBS was then added to the cell suspension and the cell suspension was centrifuged at 500 × g for 4 min. The cells were washed twice with 1% (w/v) bovine serum albumin (BSA, Sigma-Aldich, catalog # A7906) in PBS with 0.1% (w/v) sodium azide (Sigma-Aldich, catalog # S2002). For the tube for pronase treatment, 100 µl of 2% (w/v) pronase was added to 0.5 ml of cell suspension and incubated at room temperature for 5 min. The tubes without pronase treatment were incubated at room temperature for 5 min without pronase added. The cells was centrifuged and re-suspended in 100 µl of 1% (w/v) of BSA in PBS with 0.1% (w/v) sodium azide. 5 µl of CD90 antibodies (BD Pharmingen, catalog # 555595) was added to each tube except the tube of negative control. The tubes were put on ice in dark for 30 min and the cells were centrifuged and washed with 1% (w/v) BSA in PBS with 0.1% (w/v) sodium azide. The cells were centrifuged and re-suspended in 0.3 ml of 1% (w/v) BSA in PBS with 0.1% (w/v) sodium azide. Immediately before the measurements, the cells were filtered using 70 µm cell strainers into FACS tubes and flow cytometry was performed using BD LSR Fortessa analyzer.

2.4.10 Statistical analysis

P-values were calculated using Student's two-tailed t-test of unequal variance.

2.5 Results and Discussion

2.5.1 Cell distribution, cell densities and tissue compositions of bovine NP and AF

The cells in the bovine IVD are separated by the extracellular matrix and a higher percentage of dead cells is present in AF than NP after tissue harvest. **Figure 2-2A**, **B**, **C** and **D** shows the distribution of cells on NP and AF tissues stained with Invitrogen LIVE/ DEAD® stain, which stains living cells green and dead cells red. Most cells in the NP and AF tissues are not in direct cell-cell contact and there are more dead cells in AF compared with NP in general. One of the reasons may be the cells are dying after the animal is killed and the cells in AF, which in general have more access to nutrient, die more easily. In contrast, the NP cells which originally are in tissue with low nutrient supply and hence are able to survive for a longer time after the animal is killed. Another reason for this phenomenon is that antiseptic was used to sterilize the tail surface before the tissue harvest and the antiseptic might diffuse into the AF more easily and killed the cells, causing the relatively high dead cell percentage in the AF tissue. **Figure 2-2E** and **F** shows cryosectioned tissues stained with hematoxylin and the cell nuclei are in purple. From the figure, we can see that there are more cells in AF than in NP, which is consistent with the staining of tissues with LIVE/ DEAD® stain.

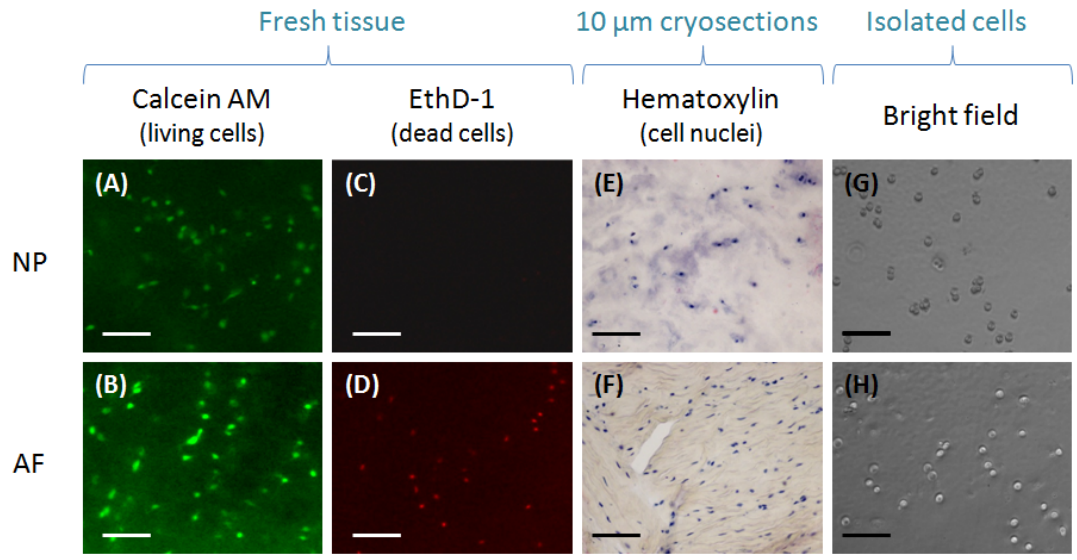


Figure 2-2 Isolation of bovine tail disc cells. (A-D) Representative micrographs indicating cell distribution and viability in NP and AF tail tissues revealed by LIVE/ DEAD® cell viability assays, where calcein AM signals indicate live cells (green) and ethidium homodimer-1 (EthD-1) signals indicate dead

cells (red); (E, F) Cryosections of NP and AF tissues stained with hematoxylin for visualization of cell nuclei; (G, H) NP and AF cells isolated by collagenase digestion (scale bar = 100 μm). (Reproduced with permission of John Wiley and Sons from [86] © 2015 John Wiley and Sons).

Similar to human IVD, cells only constitute a small volume in the bovine IVD tissues. The cell densities estimated from these cryosection photos are 124 cells per mm^2 (1530 cells per mm^3) and 483 cells per mm^2 (11724 cells per mm^3) for NP and AF respectively (**Table 2-4**). **Figure 2-2G** and **H** shows the cells isolated from bovine NP and AF with the collagenase treatment. The cells are round in shape and from the photos, we quantify the cell size by measuring the diameters of cells. On average, the cell diameter of NP is 13.3 μm and that of AF is 13.0 μm (**Table 2-4**). By using this information, the percentage volume occupied by cells can be calculated. NP cells occupies about 0.19% of NP tissue by volume while AF cells occupies a much larger volume of 1.35%.

The water content of NP and AF are 76.9% and 65.4% respectively (**Table 2-4**), which is similar to that of human samples [10, 110]. Similar to the phenomenon in human, the bovine NP tissue has a higher GAG content (7.1% of wet weight and 29.6% of dry weight) compared to AF tissue (2.6% of wet weight and 7.8% of dry weight) but the content is lower than the human samples.

Table 2-4 Water, GAG contents and cell densities in bovine tail IVD (Some of the data was published in [86]. Reproduced with permission of John Wiley and Sons © 2015 John Wiley and Sons) (mean ± SD; [a.] n = 9, 3 batches of tails and 3 samples per batch. [b.] n = 50 cells. [c.] n = 24, 3 slides and 8 sections per slide. [d.] The % volume of cells in tissues in this table was estimated based on cell volume estimates from the cell diameters of isolated cells while that in [86] was estimated based on cell volume estimates from the cryosection micrographs. [e.] n = 10 cell counts from 4 independent batches of experiments)

	NP	*AF*
1. Water content (%) [a]	76.9% ± 3.2%	65.4% ± 8.7%
2a. Proteoglycan content (% wet weight) [a]	7.7% ± 1.0%	2.9% ± 1.8%
2b. Proteoglycan content (% dry weight) [a]	33.9% ± 5.2%	9.7% ± 7.4%
3. Cell diameter (μm) [b]	13.3 ± 2.3	13 ± 2.1
4a. Planar cell density (per mm^2) (from micrographs) [c]	124.2 ± 70.4	483.2 ± 260.9
4b. Volumetric cell density (per mm^3) (based on micrographs) [c]	1530 ± 1385	11724 ± 9038
4c. % volume of cells in tissues (based on micrographs) [d]	0.19% ± 0.17%	1.35% ± 1.04%
5a. Cell density (per mm^3) (from cell isolation) [e]	868.7 ± 117.5	N/A
5b. % volume of cells in tissues (based on cell isolation) [e]	0.11% ± 0.01%	N/A

2.5.2 Higher NP marker expression in NP compared to AF

In this study, the markers for bovine NP used in qPCR were chosen based on a microarray analysis confirmed by RT-qPCR by Minogue *et al.* [2] but there may be difference between the expression at protein levels and the expression detected at mRNA levels. Thus immunostaining was performed to confirm the presence of the proteins in bovine NP tissues. The proteins for the chosen bovine NP markers (CDH2, KRT18 and KRT19) were detected at comparatively high levels in NP tissue compared to AF tissue (**Figure 2-3**), confirming that CDH2, KRT18 and KRT19 are relatively highly expressed in NP compared with AF at both mRNA and protein levels. Thus we used *CDH2*, *KRT18* and *KRT19* together with other chondrocyte markers (*ACAN* and *COL2A1*) in the following RT-qPCR experiments.

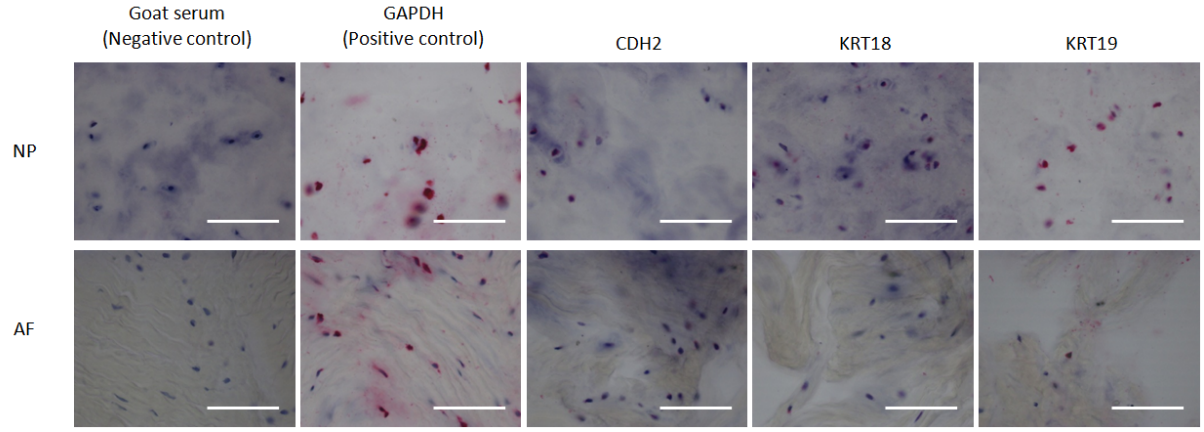


Figure 2-3 Representative photos of cryosectioned NP and AF tissues immunostained with different NP-specific markers (CDH2, KRT18 and KRT19). Goat serum was used as the negative control and GAPDH as the positive control. The nuclei of cells were stained purple by hematoxylin and the proteins under study were stained red. (Scale bar = 100 μm) (n ≥ 4 cryosections for each protein and 1-2 fields of view per cryosection).

2.5.3 Cell yield, viability and attachment

As the degeneration of IVD is often accompanied by changes in the NP tissue, NP cells have been one of the major focuses in understanding the IVD degeneration mechanism. Thus we focused on the isolation of cells from NP in this study. Among the protocols tested, 0.2% collagenase treatment overnight gave the highest yield but also resulted in a higher percentage of cell death. On average, each gram of NP tissue yielded 7.2×10^5 cells after complete digestion of the tissue. **Figure 2-4A** and **Figure 2-4B** show the relative cell yield obtained from NP tissues after different enzyme digestion protocols. For the low collagenase concentration (0.05%) treatment, a pronase incubation step prior to collagenase treatment gave a much higher yield for 6 h of digestion duration. More cells could be released after a longer time of collagenase digestion. A higher concentration (0.2%) of collagenase yielded a larger cell number when compared with a lower concentration (0.05%) after 6 h of digestion (**Figure 2-4B**). After overnight digestion, the tissues disappeared for both 0.05% and 0.2% collagenase concentrations and this gave the highest possible yields available from the tissues.

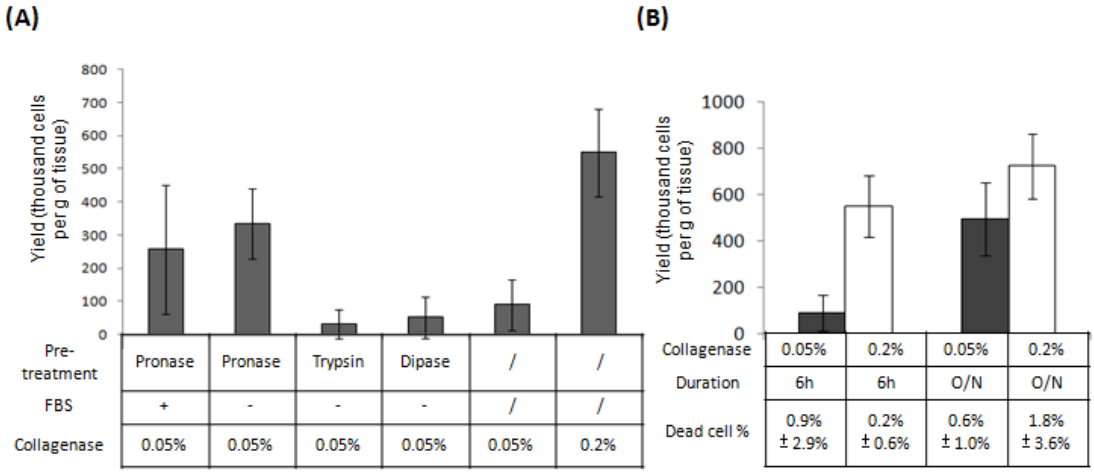


Figure 2-4 Effects of different pre-collagenase treatments and different collagenase treatment cocncentrations and duration. (A) Effect of different pre-collagenase treatments on cell yield in bovine NP cell isolation with 6 h of digestion; (B) Effect of different collagenase concentrations and reaction duration on cell yield. (n=10; from three batches of bovine tails; biological duplicates in batch 1, biological duplicates and counting duplicates in batches 2 and 3; mean ± SD). (Reproduced with permission of John Wiley and Sons from [86] © 2015 John Wiley and Sons).

Most cells remained alive even after the digestion with a high collagenase concentration (0.2%) overnight. In the Trypan blue exclusion staining, only less than 5% of cells were stained blue, indicating most cells were living and the average % of dead cells was lower for a shorter digestion duration or a lower collagenase concentration (**Figure 2-4B**). Besides, majority of cells were able to attach to the plastic culture plate upon plating after a week (**Figure 2-5**) and this confirms the high viability of cells from Trypan blue staining.

The isolated NP cells attached to plastic culture surface and spread like fibroblasts though the speed of attachment was slower than established cultures. From **Figure 2-5A**, the NP cells started to attach on the culture surface at around day 4 and the cells spread more on the culture plate at day 7. This phenomenon is similar to the attachment of trypsinzed cells during cell culture passaging but is slower than trypsinzed cells which may attach to the culture surface again within a day (**Figure 2-5B**). Besides, heterogeneity in attachment time was observed for the isolated cells.

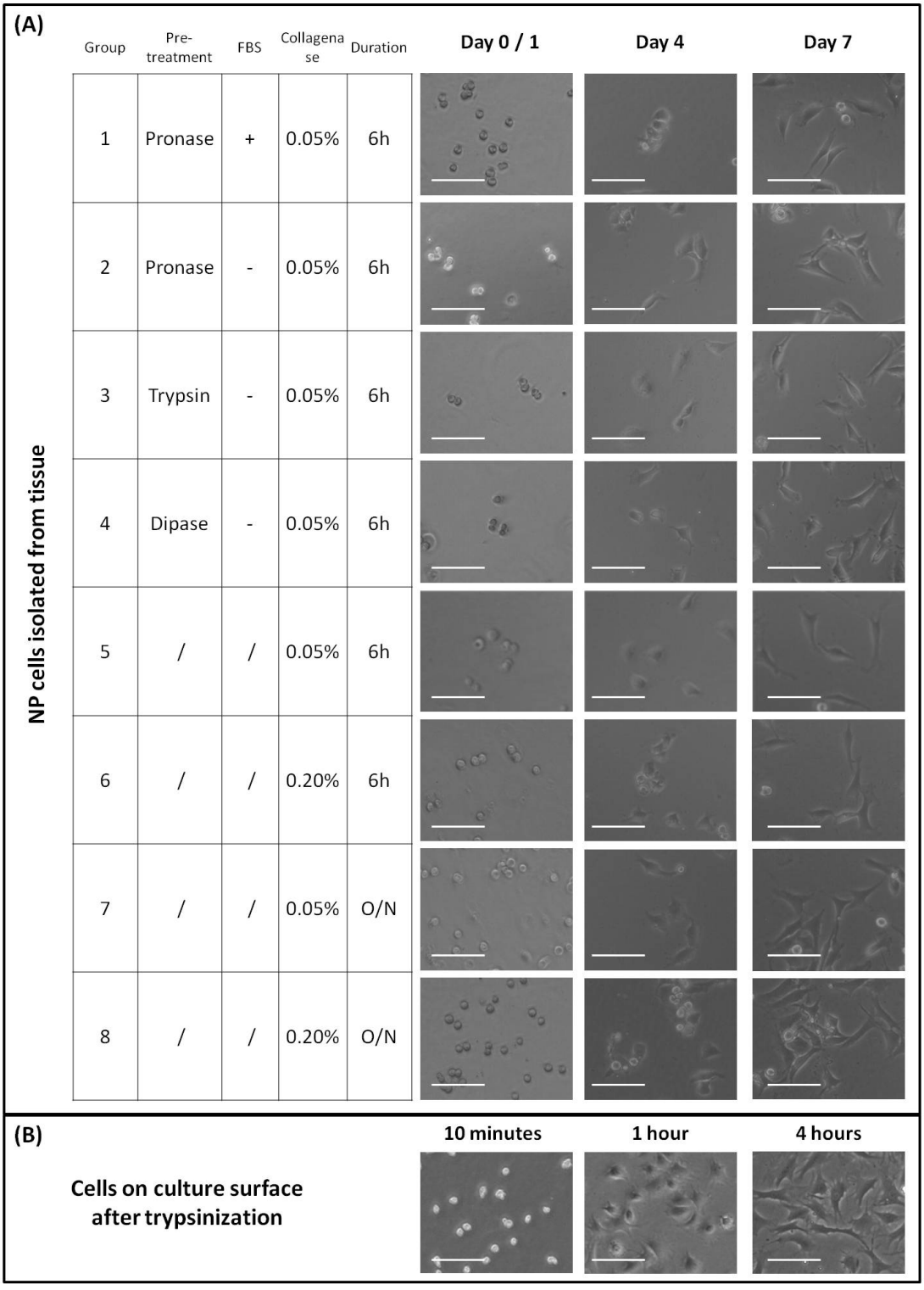


Figure 2-5 The difference in cell attachment speed between NP cells isolated from the tissue and NP cells during passaging. (A) Representative micrographs showing NP cells isolated with different conditions and cultured in monolayer at day 0 (day 1 for the samples with overnight digestion), day 4 and day 7 from the day of tissue harvest. (B) Representative micrographs showing cells cultured for 10 min, 1 h and 4 h after trypsinization and re-plating in passaging (scale bar = 100 μm). (Reproduced with permission of John Wiley and Sons from [86] © 2015 John Wiley and Sons).

2.5.4 Morphology of isolated and attached NP, AF and muscle cells

As shown in **Figure 2-6**, the sizes and shapes of the NP and AF attached cells were similar. There was much debris in the suspension of isolated muscle cells but was removed by medium change. The morphology of attached muscle cells were different from NP and AF with slightly more spread morphology.

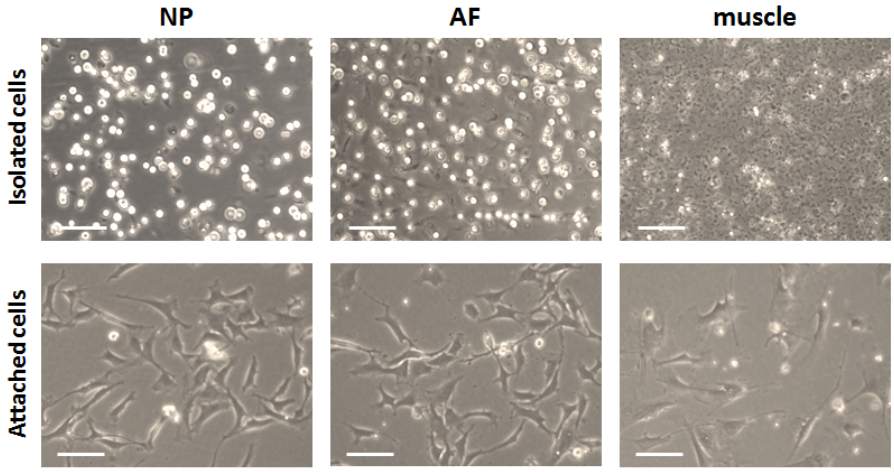


Figure 2-6 Morphology of unattached and attached cells. Upper row: Representative micrographs of cells isolated from NP, AF and muscle tissues captured at day 2 after cell isolation, showing the morphology of cells before attachment to the plastic culture surface; Lower row: Representative micrographs of cells attached to the plastic culture surface (captured at day 4 of passage 3 cells; the morphology of cells were similar at different passages from passage 1 to passage 7, data not shown) (scale bar = 100 μm). (Reproduced with permission of John Wiley and Sons from [86] © 2015 John Wiley and Sons).

Due to the similarity of the morphology of NP cells and AF cells and their close proximity in the tissues, further characterization of the isolated cells may be necessary in some studies.

2.5.5 Requirement of pronase in rat NP cell isolation

Flow cytometry is widely used to confirm the identity of mesenchymal stem cells (MSCs) isolated from various sources but few NP cell surface markers is available for characterization to date. Fujita *et al.* has identified a surface protein CD24 that is specifically expressed in rat

nucleus pulposus cells [62] but the use of surface proteins as NP markers is relatively rare compared to markers at transcriptional level. We have noticed that a number of studies suggested that pronase may damage surface proteins [114-117] and in our studies, cells can be isolated from bovine NP tissue even without the use of pronase (**Figure 2-4** and **Figure 2-5**). The difference in cellular arrangements (as shown in **Figure 2-7**) prompted us to investigate the requirement of pronase in rat NP cell isolation. As shown in **Figure 2-8**, pronase is required for isolation of NP cells from rat. In contrast, cells can be isolated from bovine NP tissue even without the use of pronase (**Figure 2-8**).

Since proteases have been shown to affect the membrane architecture and/ or surface proteins of different cell types such as lymnaea neurons [114], chondrocytes [115], Kupffer cells [116] and lymphocytes [117], we have also tested the effect of pronase on surface antigens using human MSCs from bone marrow. The treatment of cells with pronase for 5 min decreased the CD90 antigen by 10% (**Figure 2-13** in the Appendix). In our study, human MSCs were used to demonstrate the effect of pronase instead of bovine NP cells due to the lack of verified NP surface antigens for bovine NP cells. The reduction in surface antigens for MSCs after pronase treatment suggested that caution should be made when interpreting the flow cytometry results for cells isolated with the use of pronase.

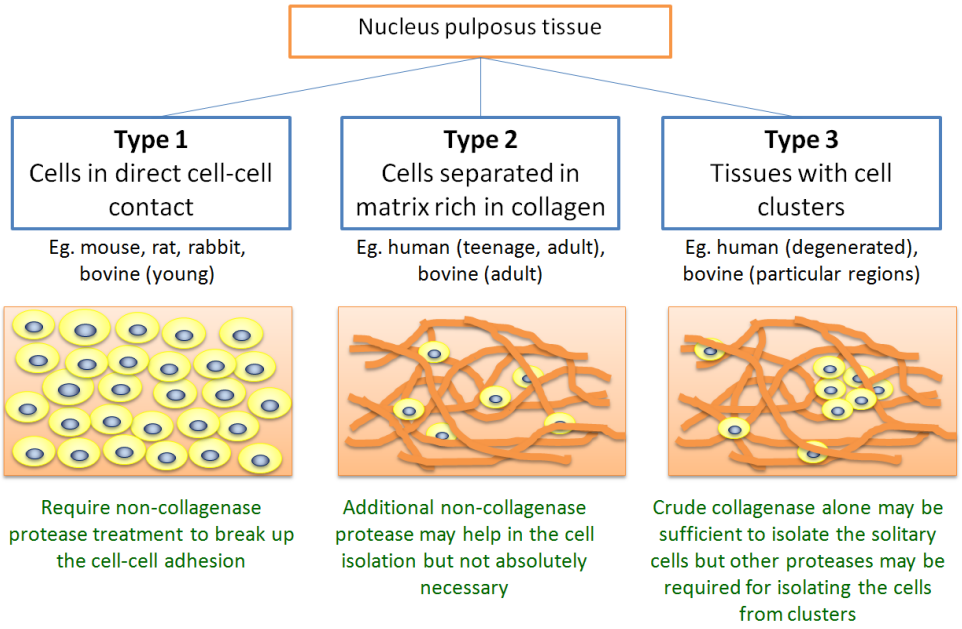


Figure 2-7 The difference in requirement of pronase in different NP tissues. For NP tissues with cells in direct cell-cell contact (type 1), digestion by pronase is required to break the adhesion among cells. For NP tissues with cells separated by matrix rich in collagen (type 2), the use pronase may not be absolutely required for cell isolation. For NP tissues with cell clusters (type 3), crude collagenase alone may be sufficient to isolate the solitary cells but pronase may be required to effectively isolate the cells in clusters. (Reproduced with permission of John Wiley and Sons from [86] © 2015 John Wiley and Sons).

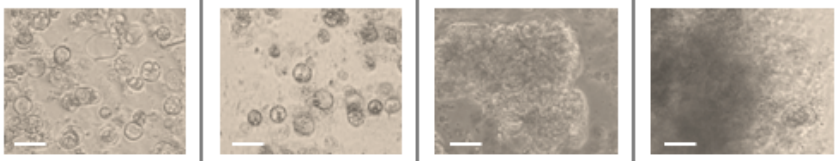
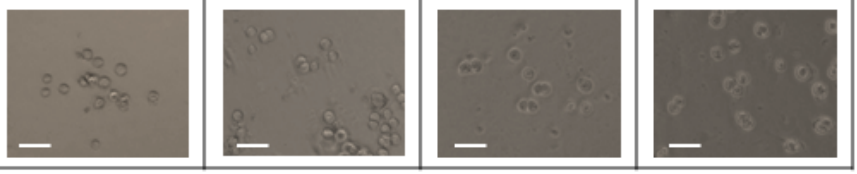
	Pronase	0.2% (w FBS)	0.2% (w/o FBS)	-	-
	Collagenase	0.05%	0.05 %	0.05%	0.2%
Rat (Type 1)	Observation	Tissue was broken down into pieces		Tissue remained in a large piece	
	Under microscope				
Bovine (Type 2)	Observation	Tissue was digested		Tissue was digested	
	Under microscope				

Figure 2-8 The requirement of pronase in rat NP cell isolation. For bovine NP, 1 h of pronase digestion followed by 5 h of collagenase digestion or 6 h of collagenase digestion. For rat NP, 1 h of pronase digestion followed by 2 h of collagenase digestion or 3 h of collagenase digestion. Shorter digestion time was used for rat NP due to its smaller disc size and the general shorter digestion used in reported studies (**Table**

2-2). (Scale bar = 50 μm) (Reproduced with permission of John Wiley and Sons from [86] © 2015 John Wiley and Sons).

2.5.6 Effect of different isolation protocols on RT-qPCR

RT-qPCR was widely used to characterize NP cells at the mRNA level. Compared to proteins, mRNA is more susceptible to degradation and different isolation protocols may affect the relative mRNA levels. Hence the quality of the mRNA extracted from cells isolated with different protocols was assessed using UV spectrometry and the relative mRNA levels were compared using RT-qPCR.

All of the chosen protocols yielded cells of quality suitable for RT-qPCR (260/280 > 1.8 and 260/230 > 1). In these sets of experiments, higher collagenase concentrations (1% or 2%) were used to release the cells in a shorter time. Among the chosen conditions, RNA extracted from cells with simultaneous collagenase (1%) and pronase (0.1%) digestion for 3 h had the highest RNA yield of about 5.81 μg RNA per g of NP tissue (**Table 2-5**). However, the difference was not statistically significant and different protocols under test could provide RNA of a reasonable yield. As bovine AF has higher collagen content than NP, the digestion of AF tissues for 3 h with collagenase and pronase was not sufficient to release enough cells for RNA extraction using TRIzol and a large proportion of tissues have remained undigested. Thus the digestion was extended to 6 h for AF tissues. Even with longer digestion duration, the yield of RNA from AF tissues was still lower than NP.

Table 2-5 Yield and quality of RNA obtained with different isolation methods. The quantity of RNA was calculated using the absorbance at 260 nm and the quality was assessed by determining the ratio of absorbance at 260 to 280 nm and 260 to 230 nm. [a.] "col" denotes "collagenase", "pro" denotes "pronase". [b.] 6 h of digestion of AF was used instead of 3 h since the numbers of collected cells with 3 h of digestion were not enough for RNA extraction and a large proportion of AF tissue was not completely digested. [c.] The yield of RNA was calculated based on concentrations corrected with a mathematical formula [118]. (Mean ± SD; n=6; from two batches of bovine tails). (Reproduced with permission of John Wiley and Sons from [86] © 2015 John Wiley and Sons).

Cells [a]	Yield (µg RNA per g tissue) [c]	A_{260}/A_{280}	A_{260}/A_{230}
NP col 1% 2h	4.00 ± 1.38	2.00 ± 0.05	1.32 ± 0.22
NP col 1% 3h	4.96 ± 1.08	2.00 ± 0.05	1.15 ± 0.23
NP col 2% 2h	5.41 ± 2.20	2.02 ± 0.04	1.27 ± 0.28
NP col 1% pro 0.1% 3h	5.81 ± 1.76	2.01 ± 0.04	1.28 ± 0.21
AF col 1% pro 0.1% 6h [b]	2.78 ± 0.88	2.02 ± 0.06	1.35 ± 0.22
muscle col 1% pro 0.1% 3h	5.41 ± 3.00	2.06 ± 0.09	1.66 ± 0.30

As shown in **Figure 2-9**, there were slight changes in relative gene expression for cells isolated with different protocols but NP cells still had higher chondrocyte and NP marker expression compared with AF and muscle. **Figure 2-9** shows the relative mRNA levels detected for RNA extracted from cells isolated with different protocols. With longer digestion time (3 h instead of 2 h with 1% collagenase), there were lower relative mRNA levels of *CDH2* ($p = 0.24$) and *KRT18* ($p = 0.08$). Digestion with a higher collagenase concentration (2% instead of 1%) may reduce the mRNA levels of *ACAN* ($p = 0.11$) and *COL2* ($p = 0.29$). There was not much difference in relative mRNA levels for NP cells isolated with or without the use of pronase. Despite the variations in relative mRNA levels in cells isolated with different isolation methods, the *ACAN* and *COL2A1* mRNA levels were higher in NP and AF cells compared with muscle cells. And NP cells obtained from different protocols had higher *CDH2*, *KRT18* and *KRT19* expressions than AF cells.

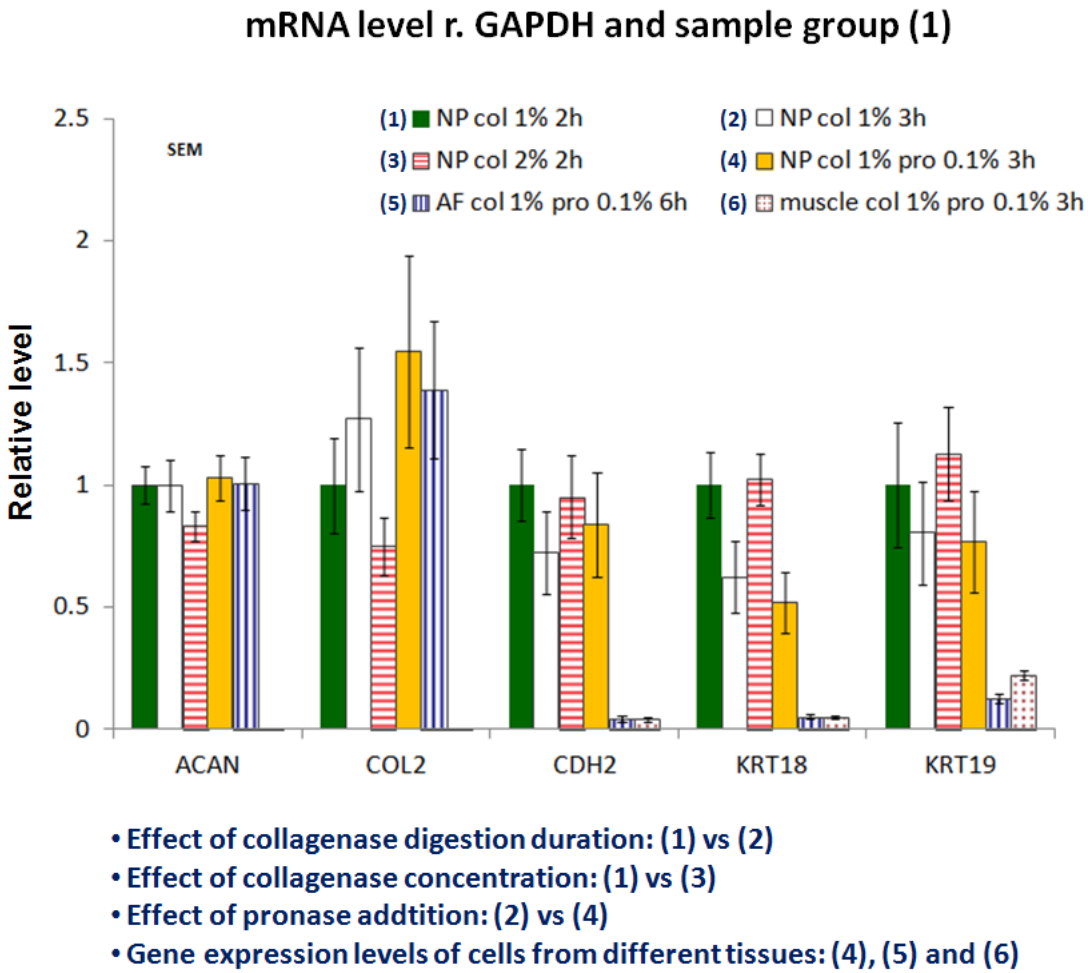


Figure 2-9 Effect of different isolation protocols on the relative mRNA levels in bovine cells detected by RT-qPCR. (Mean ± SEM; n=12; 2 batches of cell isolation; biological triplicates and technical duplicates in each batch except for AF where n=10). Note: Unlike the previous conditions used for cell isolation for cell culture, the concentration of collagenase for isolating cells for RNA extraction was higher (1% and 2% as contrasted to 0.05% and 0.20%) as short isolation duration can be more critical for RNA extraction. (Reproduced with permission of John Wiley and Sons from [86] © 2015 John Wiley and Sons).

2.5.7 Isolation of cells from different tissues in a bovine tail

Cells could also be obtained from NP, AF, EP, tendon and AD using a similar method with collagenase digestion. At day 5, attached cells were observed for cells from different tissues (**Figure 2-10**). The initial cell densities were low but all cultures could reach confluence with further culturing (**Figure 2-11**).

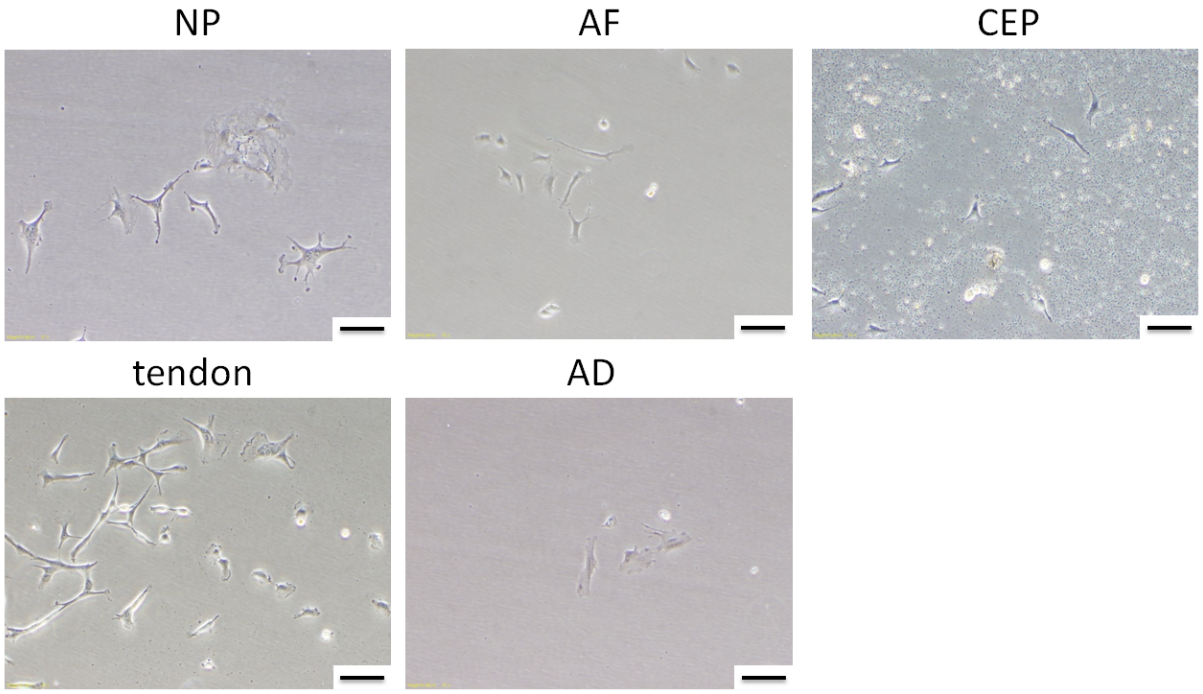


Figure 2-10 Cells isolated from tissues with photos taken at low cell density at passage 0. (NP at day 5, AF at day 4, CEP at day 8, tendon at day 4, AD at day 5; scale bar = 100 μm).

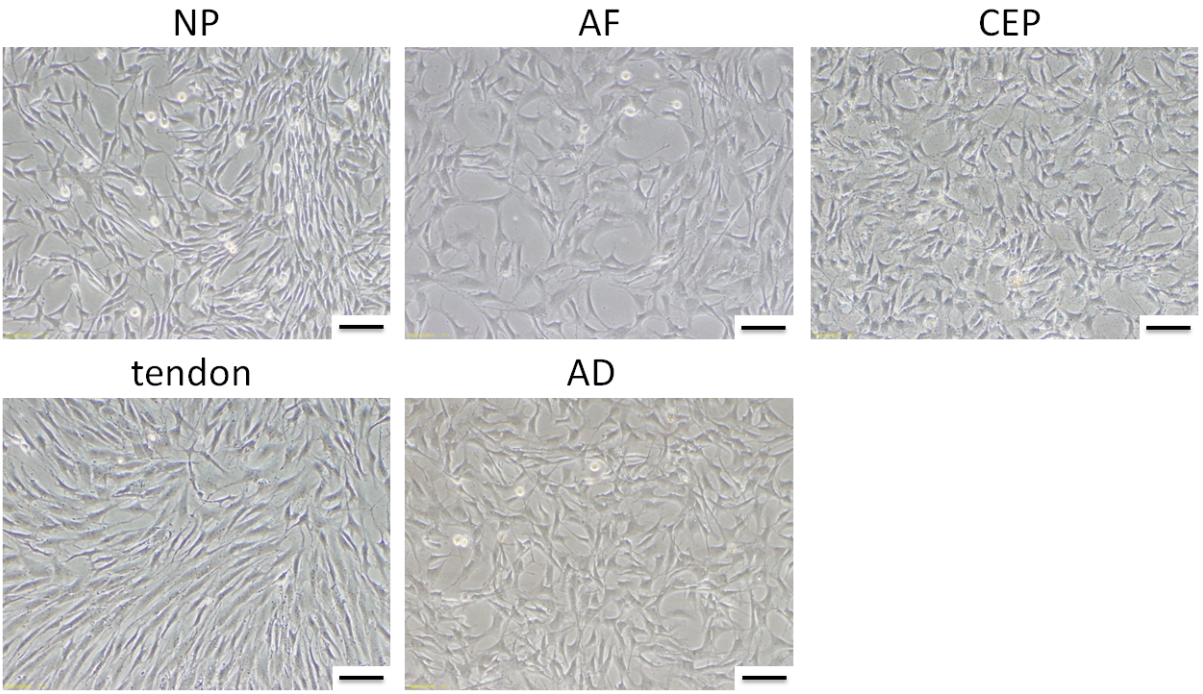


Figure 2-11 Cells isolated from tissues with photos taken at high cell density at passage 0. (NP at day 11, AF at day 11, CEP at day 15, tendon at day 8, AD at day 8; scale bar = 100 μm).

2.5.8 Suggestions in designing the cell isolation protocols and the corresponding explanations

The suggestions in deciding the isolation protocols were summarized in **Table 2-6** and explained in more details in **Sections 2.5.10** with associated experimental data given in **Section 2.5.11** that follows.

Table 2-6 Suggestions in designing the cell isolation protocols and the corresponding explanations

Parameters	*Suggestions*	*Explanations*
Enzyme type	○ May use collagenase alone to isolate cells from bovine NP tissues ○ May pre-treat the tissues with pronase before the collagenase digestion to increase the yield ○ Precaution should be taken when analyzing cell characterization results using pronase	○ Cells can be isolated from bovine NP even when pronase was not used ○ Pre-treatment with pronase increases the cell yield when a low concentration of collagenase was used. ○ Pronase may damage the surface proteins on the cell surfaces
Enzyme concentration and digestion duration	○ Decide the digestion duration based on the rate of disappearance of the tissues in the first digestion instead of following protocols defined by other groups ○ For cell culturing, use longer digestion duration at a lower collagenase concentration or shorter digestion duration at a higher collagenase concentration ○ For RNA extraction and flow cytometry, use short digestion duration	○ The digestion duration required depends much on the actual setting which varies from lab to lab but the cell yield is generally correlated with the disappearance of tissues ○ Both approaches can result in a reasonably good cell yield ○ Short digestion duration is preferred so that the characteristics of the cells may be better preserved
Volume of enzyme	○ Use a volume larger than the volume of tissues	○ When the NP tissues are placed in the medium, they may swell to double in size. The NP tissues may absorb all the enzyme solution if the volume used is too small.

Parameters	*Suggestions*	*Explanations*
Size of tissues	○ about 1 – 2 mm	○ Cutting into small pieces increases the surface area to volume ratio which speeds up the digestion but mincing into too small pieces may damage the cells by excessive mechanical forces
pH and temperature	○ pH of about 7.4 and temperature of 37 °C	○ Physiological pH and temperature normally used for cell culture and thus easily available
Shaking	○ Shake the tissues during the digestion if possible	○ Shaking maintains the high local enzyme concentration at the tissue surface and hence facilitates the digestion

2.5.9 Optimal protocols for different applications

Among the factors affecting cell yield, enzyme type and activity, enzyme concentration, enzyme solution volume and digestion duration should be decided for procedures aimed at different applications. We focus on three common purposes of cell isolation in this study, namely, for primary cell culture, for RNA extraction and for flow cytometry.

2.5.9.1 Isolation of cells for primary cell culture

A comparatively wide range of protocols can be used for isolating cells for cell culturing purpose. High cell viability was obtained even after 0.2% collagenase treatment overnight for bovine NP tissue digestion (**Figure 2-4B**). In other words, 0.2% collagenase did not cause serious cell damages. However, the cell yields were both high for 0.2% collgenase digestion of 6 h or 0.05% overnight. Thus we may use a high collagenase concentration with shorter time or a low collagenase concentration for longer time to suit our other experimental schedule or cost consideration. As each batch of enzyme preparation may not be the same and there are many other factors which vary from laboratory to laboratory that may influence the actual tissue digestion rate, it is desirable to monitor the disappearance of the tissues rather than simply follow a fixed protocol optimized by others. In general, the cell yield is closely related to the disappearance of tissues.

2.5.9.2 Isolation of cells for RNA extraction for phenotyping

For isolation of cells for RNA extraction, it is preferred to use shorter time for digestion as RNA may start to degrade when the animal is sacrificed. Sharova *et al.* have shown that the average half life for mRNA is about 7.1 h in mouse embryonic cells and the half life is longer for genes related to metabolism and structure such as extracellular matrix and cytoskeleton while genes with regulatory functions such as transcription factors may have half-lives less than 1 h [119]. Among our chosen markers, *ACAN* and *COL2A1* are genes for extracellular matrix while *KRT18* and *KRT19* are related to intermediate filament which is a type of cytoskeleton. Thus these makers are comparatively less affected by the possible degradation process during the digestion.

2.5.9.3 Isolation of cells for characterization by flow cytometry

In cell characterization by surface markers, the use of pronase seems not preferred as it may damage the surface proteins due to its relatively low substrate specificity. A number of studies have been performed to investigate the effect of pronase in different applications. Hermann *et al.* have shown that proteases may affect the architecture of membrane and acutely modifies high voltage-activated calcium currents and cell properties of Lymnaea neurons [120]. By comparing freshly isolated chondrons with cryostat sections of cartilage, Lee *et al.* revealed that type VI collagen, type II collagen and aggrecan were retained in chondrons isolated by dispase and collagenase digestion, but fibronectin and a unique chondroitin sulfate epitope recognized by the antibody, 7D4, were lost [121]. Ikejima *et al.* have shown that pronase can destroy the lipopolysaccharide receptor CD14 on Kupffer cells [122]. Lobo *et al.* have used pronase to remove Fc IgG receptors, CD16 and CD32, on lymphocytes while retaining the antigenicity of HLA and CD3 receptors [117, 123]. In addition, some collagenase preparation may also contain some other proteases. Thus cautions are required when analyzing data about cell characterization using surface markers when proteases are involved in the cell preparation. On the other hand, some intra-cellular markers may be used in cell characterization using flow cytometry after fixation and cell permeabilization.

2.5.10 Factors affecting yield (theoretical analysis)

From the cell yield as shown in **Figure 2-4**, it seems that the optimal protocol for the best yield will be the combination of pronase pretreatment, a high collagenase concentration and long digestion duration. However, it is not always desirable to use these conditions when considerations in quality, time and cost are also taken into account. In addition to yield, the quality of the cells isolated is also of critical importance. Long digestion duration may affect the quality of RNA extracted from the isolated cells. Too high collagenase concentrations may damage cells and can be costly as enzyme is a comparatively expensive component in the digestion procedures. Hence, instead of blindly using high collagenase concentrations overnight with pronase pre-treatment, it is recommended to decide the protocol for each application. The most straightforward method of optimization is to test the outcome empirically. Nevertheless, in the cell isolation using enzymatic methods, there are a number of parameters which can be altered, which in other words, nearly an infinite number of combinations are possible. Thus it can be time-consuming and costly to find the optimum through experiments and this is also impractical due to the limited availability of samples as in the case of human IVD. In contrast, an understanding of the isolation procedures will allow the conditions to be strategically decided with a minimum number of experiments for optimization. This section focuses on the factors that should be modified based on applications (enzyme type and activity, enzyme concentration, enzyme solution volume and digestion duration) and factors that are less dependent on applications (size of tissue, pH, temperature and agitation).

2.5.10.1 Enzyme type and activity

As collagen is one of the major extracellular matrix components in bovine or human IVDs, collagenase is usually involved in the cell isolation from these tissues. Collagenase can break the peptide bonds in collagen. Prior to collagenase treatment, some treatments by other proteases may be included. In this study, we have chosen pronase, trypsin and dipase as they are commonly involved in either cell isolation or cell passaging. Pronase is a mixture of

proteinases, which lead to complete or nearly complete digestion into individual amino acids. Trypsin cleaves peptide chains mainly at the carboxyl side of the amino acids lysine or arginine, except when either is followed by proline. Dipase cleaves fibronectin, collagen IV, and to a lesser extent collagen I. It is a gentler enzyme compared with pronase. Though trypsin and dipase are more specific in substrates, treatments of tissues with these two enzymes do not increase the cell yield obtained (**Figure 2-4**). Hence, it is not recommended to use these enzymes in isolation of cells from bovine or human NP which cells are not in contact with each other. Pronase is preferred for a higher cell yield in shorter time but not an absolute need for bovine NP. In contrast to NP from other species, the cells in bovine or human mature NP have fewer cell-cell contacts and are surrounded by less gel-like matrix rich in proteoglycan and collagen. Pronase may destroy the surface proteins on cells.

On the other hand, the collagenase solution used in tissue isolation may also contain other enzymes. For example, collagenase type 2 from Worthington (catalog # LS004177) has clostripain activity. Collagenase from Clostridium histolyticum from Sigma (catalog # C5894) contains clostripain, nonspecific neutral protease and tryptic activities. And collagenase from Gibco (catalog # 17101-015) contains clostripiopeptidase A and a number of other proteases, polysaccharidases, and lipases.

2.5.10.2 Enzyme concentration

Unlike the most typical enzyme kinetics models with homogeneous systems, the digestion of tissue is heterogeneous which the enzyme is soluble in the medium while the substrate is insoluble. Therefore, the access to the reaction site on the tissue by enzymes is often limited by enzyme diffusion. The reaction rate in this heterogeneous system can be modeled by the following equation [124]:

$$\nu = \frac{k_2[S_o][E]}{K_{eq}+[E]} \quad (1)$$

where v is the reaction rate, k_2 is a constant, $[S_o]$ is the number of substrate bonds available initially for breakage, $[E]$ is the enzyme concentration and K_{eq} is dependent on the rates of enzyme desorption and adsorption onto the insoluble matrix. **Figure 2-12** shows the reaction rate plotted from the above equation. With a larger number of substrate bonds available initially for breakage, the reaction rate increases. With higher enzyme concentrations, the reaction rate increases to a certain point but levels off for even higher concentrations. In other words, above a certain enzyme concentration, more enzymes do not increase the reaction rate. This occurs when all the surfaces of the tissues have been saturated with the enzyme. Thus further increasing the enzyme concentration may not increase the reaction rate. In general, the high concentrations at which higher concentrations cause no increase in reaction rate are not used in cell isolation for cell culturing purpose as too high enzyme concentrations may damage the cells. Other than collagenase, there are also other enzymes present in the collagenase isolated from bacteria sources and some of them are proteases which have less substrate specificity. These proteases may digest other proteins on cells and damage them.

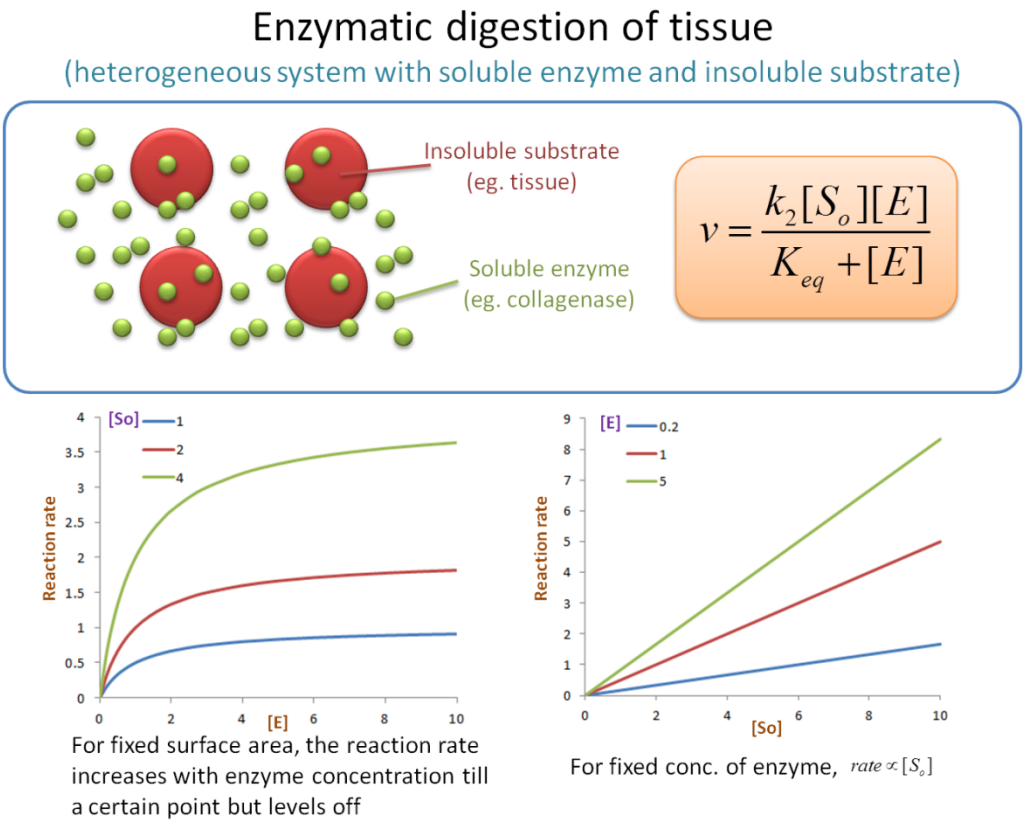


Figure 2-12 Schematic illustrating enzyme kinetics in a heterogeneous system of tissue digestion.

2.5.10.3 Volume of enzyme

In the equation, the rate of reaction is dependent on the enzyme concentration but not affected by the volume of enzyme used. However, the volume of enzyme used has an indirect effect on the concentration of enzyme during the tissue digestion process. When the tissues are digested, they are "liquefied" and the volume of liquid will increase. If the volume of enzyme was too small compared with the initial tissue amount, the enzyme concentration would be significantly reduced when the tissues were being digested. Besides, when we used closed containers for the cell isolation, the volume of enzyme used would affect the volume of air that could be dissolved in the medium. If the tube was completely filled with solution, there would be less air to be dissolved into the tube and may not be desirable for prolonged digestion. The enzyme solution volume to tissue volume ratio will affect the local enzyme concentration when the tissues are being digested, especially when there is no shaking or

agitation of the reaction mixture. When the NP tissue is digested, the swelling of tissue should also be taken into account when deciding the enzyme solution volume as the tissue may swell for more than two times by volume when immersed in aqueous solution.

2.5.10.4 Digestion duration

When we digest the tissue for longer time, the cell yield will increase until all the tissues have been digested. However, when the cells are used for RNA extraction, it may be better to avoid prolonged digestion as the RNA levels may change during the digestion.

2.5.10.5 Size of tissue

In cell isolation from IVD tissues, the tissues are usually cut into smaller pieces of about 1 to 2 mm and this will increase the surface area for the enzyme to work on. Theoretically, the smaller the tissues are cut into, the higher overall reaction rate. However, mincing the tissues is not recommended as it may result in damages of cells due to excessive mechanical forces.

2.5.10.6 pH and temperature

Different enzymes may have different ranges of optimum or workable pH and temperature for the reactions they catalyze. For collagenase isolated from bacteria sources, the physiological pH and temperature for mammalian cells of pH 7.4 – 7.6 and 37 °C are compatible with the enzyme reactions. Thus we normally use the cell culture medium of about pH 7.4 at 37 °C for the digestion.

2.5.10.7 Agitation

As the digestion of tissue using enzyme is a heterogeneous system that the insoluble solid tissues are digested with soluble enzymes, the reaction rate is limited by diffusion. Shaking or agitation will enhance the diffusion. In addition, the local enzyme concentration decreases when the surface layer of tissues is being digested. Thus with shaking or agitation, the reaction rate may be higher as the local enzyme concentration on the tissue surface is similar

to the bulk enzyme concentration instead of being diluted when the solid tissues are digested into soluble forms.

2.5.11 Factors affecting cell yield (experimental validation)

In order to test the effects of different digestion parameters on tissue digestion rates, bovine NP tissues were digested in different conditions. About 50 µl of tissues were digested with different conditions as shown below (Groups A-G).

Table 2-7 Digestion of tissues under different conditions for the study of the effects of shaking (B vs E), temperature (E-G), tissue size (B vs D) and enzyme solution volume (A-C) (The amount of tissue remained were estimated semi-quantitatively averaging between two samples per group.) [a.] N denotes nearly all or all of the tissue has been digested.

Group	A	B	C	D	E	F	G
Parameter							
Shaking	Yes	Yes	Yes	Yes	No	No	No
Enzyme volume	100 µl	300 µl	500 µl	300 µl	300 µl	300 µl	300 µl
Tissue dimensions	2 mm	2 mm	2 mm	5 mm	2 mm	2 mm	2 mm
Temperature	37 °C	37 °C	37 °C	37 °C	37 °C	21 °C	60 °C
Proportion of tissues remained [a]							
At 0 h	1.0	1.0	1.0	1.0	1.0	1.0	1.0
At 2.5 h	0.4	0.5	0.6	0.8	0.5	0.8	0.5
At 4.5 h	0.4	N	N	N	0.4	0.7	0.4
At 7.5 h	N	N	N	N	N	0.7	0.4

Based on **Table 2-7**, the findings are summarized as follow:

- ✧ Effect of shaking (shake vs not shake) (group B vs group E)
  - Shaking facilitated the digestion of tissue after the initial stage (after 2.5 h in this set up)
- ✧ Effect of temperature (25 °C, 37 °C, 60 °C) (groups E-G)
  - Initially, digestion rate was higher at temperature higher than room temperature (21 °C)
  - Digestion at 60 °C was less complete after 7 h compared to 37 °C, and it is likely that the enzyme may be denatured at 60 °C compared to 37 °C

✧ Effect of tissue size (2 mm vs 5 mm) (group B vs group D)

- Cutting the tissue into smaller pieces speeded up the digestion, particularly at the initial stage

✧ Effect of enzyme solution volume (100 µl, 200 µl, 500 µl) (groups A-C)

- Nearly all the tissues have been digested in the first 4.5 h for the 300 µl and 500 µl enzyme volume while some undigested tissue was still remained for the 100 µl enzyme solution. This may be due to the dilution effect of the enzyme solution by the digested tissue and the comparatively higher digestion product concentration for the smaller volume. However, nearly all or all tissues were digested for all the volume under tested after 7.5 h of digestion.

2.6 Conclusions

In summary, the cell yield from bovine NP tissue can be increased by using a high collagenase concentration, long digestion time or with a pronase pre-treatment in general. Depending on different purposes, the procedures should be fine tuned with a good understanding of the various factors involved in the isolation. For cell culturing, we can obtain a reasonably good yield with a wide range of protocols. In other words, either using a higher collagenase concentration for shorter time or a lower collagenase concentration for longer time may achieve a similar yield. The use of pronase prior to collagenase treatment may facilitate the isolation but it is not absolutely necessary for bovine NP tissue. For RNA extraction, shorter isolation duration is preferable. And for flow cytometry characterization, cautions are required for cells with pronase treatment for reliable interpretation. Based on this information, researchers can devise their own cell isolation protocols for their applications based on a clear rationale and enhance the efficiency and reliability of the associated experiments.

2.7 Appendix

2.7.1 The effect of pronase on surface antigens of human MSCs (hMSCs)

Human MSCs (hMSCs) were used to demonstrate the effect of pronase instead of bovine NP cells due to the lack of verified NP surface antigens for bovine NP cells. With just 5 min of pronase treatment, the proportion of CD90 positive cells decreased by 10%, indicating the use of pronase may change the surface antigen profile of cells and this is consistent with the studies from other groups [114-117].

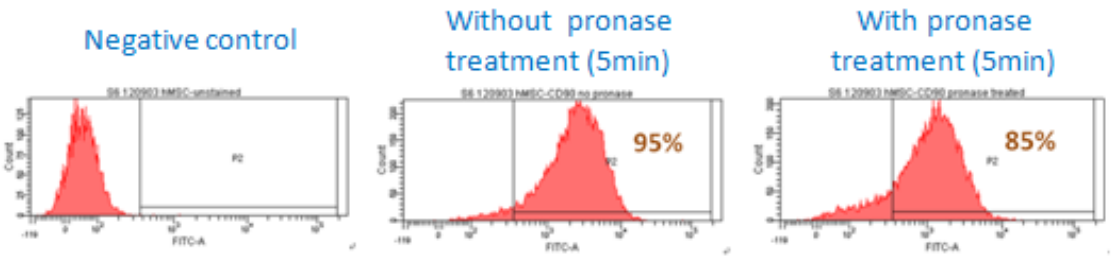


Figure 2-13 The effect of pronase on surface antigens of hMSCs. (Reproduced with permission of John Wiley and Sons from [86] © 2015 John Wiley and Sons).

2.7.2 Protocols for preparing buffer solutions used in Chapter 2

TE buffer (100 mM NaCl, 10 mM TRIS, 1 mM EDTA, pH 8.0)

1. Dissolve the following components in nanopure water

   0.58 g NaCl (sodium chloride, catalog # S3014)

   0.121 g Tris (Tris base, Sigma, catalog # T1378)

   37 mg EDTA (ethylenediaminetetraacetic acid, Sigma, catalog # E6635)

2. Adjust the pH to 8.0 by adding diluted hydrochloric acid (HCl)
3. Sterilize by autoclave

DMMB reagent in formate buffer (16 mg/l, pH 2.5)

1. Dissolve the following components in 700 ml of nanopure water

   21 mg DMMB (Sigma, catalog # 341088, dye content 80 %)
   1.72 g sodium hydroxide

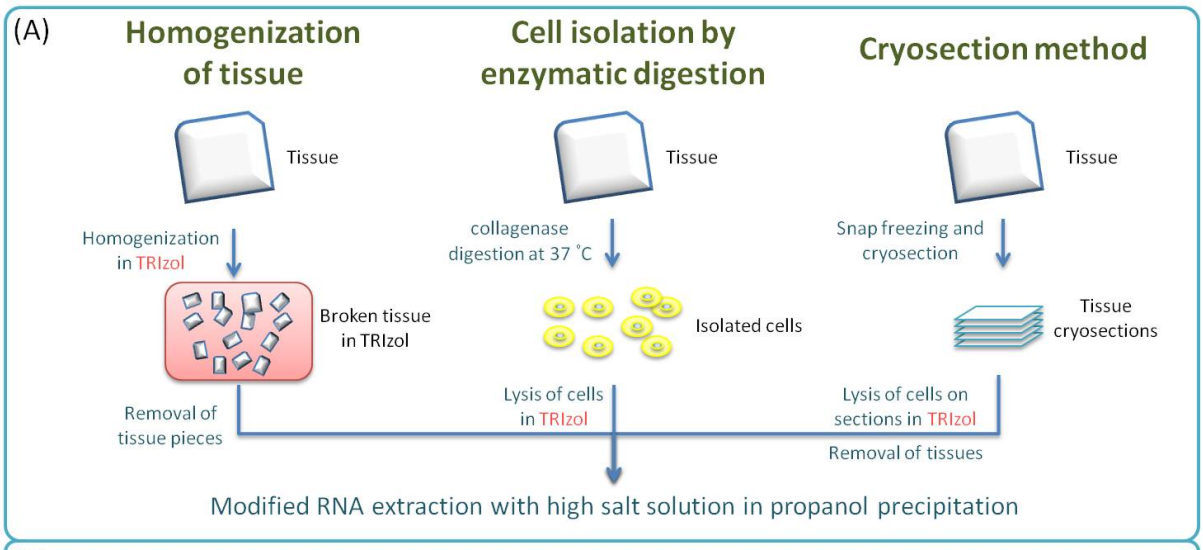
2. Add 5 ml of ethanol
3. Adjust the pH to 2.5 using 10% (v/v) formic acid (EMD Millipore, catalog # 1.00264.2500)
4. Add nanopure water to a final volume of 1 l

Chapter 3 Refining Disc RNA Extraction Methodology

3.1 Background

3.1.1 Comparison of different RNA extraction methods

The comparison of different RNA extraction methods for bovine NP tissue is summarized in **Figure 3-1**. Compared to the other two methods, the cryosection method allows simultaneous preparation of cryosections for histological study and RNA for RT-qPCR. Besides, it may require minimal time of tissue kept at room temperature or elevated temperature after its removal from animals.



(B)

	Homogenization method	Enzymatic method	Cryosection method
✓	•No cell isolation procedure	•Can concentrate the cells and remove the extracellular matrix •Can also obtain cells for culturing	•Can prepare cryosections for histological study at the same time •Minimal time of cells at room temperature or elevated temperature •No cell isolation is required
×	•Heat may be generated, resulting in RNA degradation •May be difficult to break down the tough IVD tissues •Require a homogenizer	•Relative mRNA levels may change during the cell isolation •Extra time is required to isolate cells before RNA extraction	•Require a cryostat

Figure 3-1 Comparison of different methods for RNA extraction from tissues. (A) The flow of different methods and (B) the advantages and disadvantages of the methods. (A similar figure is published in [125]. Reproduced under a Creative Commons Attribution License.)

3.1.2 Components in TRIzol (Home-made recipe)

In order to modify the extraction protocol more strategically, the information about TRIzol was obtained. TRIzol is a commercial product of Invitrogen and its composition is not disclosed. However, a recipe for "home-made" TRIzol was available in the following link from the Academia Sinica: http://ipmb.sinica.edu.tw/microarray/newprotocol/TRI.pdf and given in **Table 3-1**. Phenol is one of the major components in TRIzol. It is partially miscible with water. Guanidine thiocyanate is a strong protein denaturant [126] and can denature the RNases that are present in the cell lysates. Ammonium thiocyanate dissociates into ammonium ions and thiocyanate ions in water. The ammonium ions can assist in the RNA precipitation using propanol while the thiocyanate ions serve as protein denaturants. Sodium acetate of pH 5.0 provides the acidic environment for the phase separation so that DNA partitions into the organic phase while RNA remains in the aqueous phase. The sodium ions also assist RNA precipitation using propanol. The exact function of glycerol is not explicitly mentioned. Glycerol has solvent properties similar to those of water and simple aliphatic alcohols due to its three hydroxyl groups (**Figure 3-2**) and is a solvent for many solids, both organic and inorganic. Besides, glycerol has a density of 1.26 g/cm^3 and increases the density of mixture. DEPC-treated water is RNase1-free and does not introduce active RNase into the mixture.

Table 3-1 A recipe for 1 L of home-made "TRIzol". (http://ipmb.sinica.edu.tw/microarray/newprotocol/TRI.pdf)

Reagent	Quantity	Final concentration
Phenol in saturated buffer	380 ml	38 %
Guanidine thiocyanate	94.53 g	0.8 M
Ammonium thiocyanate	76.12 g	0.4 M
Sodium acetate, pH 5.0	33.4 ml of 3 M stock	0.1 M
Glycerol	50 ml	5 %
DEPC-Water	Adjust the final volume to 1 L	/

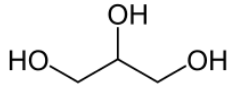


Figure 3-2 Chemical structure of glycerol.

3.1.3 Liquid-liquid extraction

The extraction of RNA using TRIzol is based on a liquid-liquid extraction. **Figure 3-3** shows a simplified diagram of a liquid-liquid extraction. Initially, the solutes are only present in liquid phase B. When liquid A is added and mixed thoroughly with phase B, the solutes may partition into the two phases unequally. For example, there can be more solutes 2 (red circles) in liquid phase A and more solutes 1 (blue circles) in phase B. After phase separation, majority of solutes 1 are present in the heavy phase and solutes 2 in the light phase. Overall, solutes 2 "get separated" from solutes 1 by being extracted into a new liquid phase.

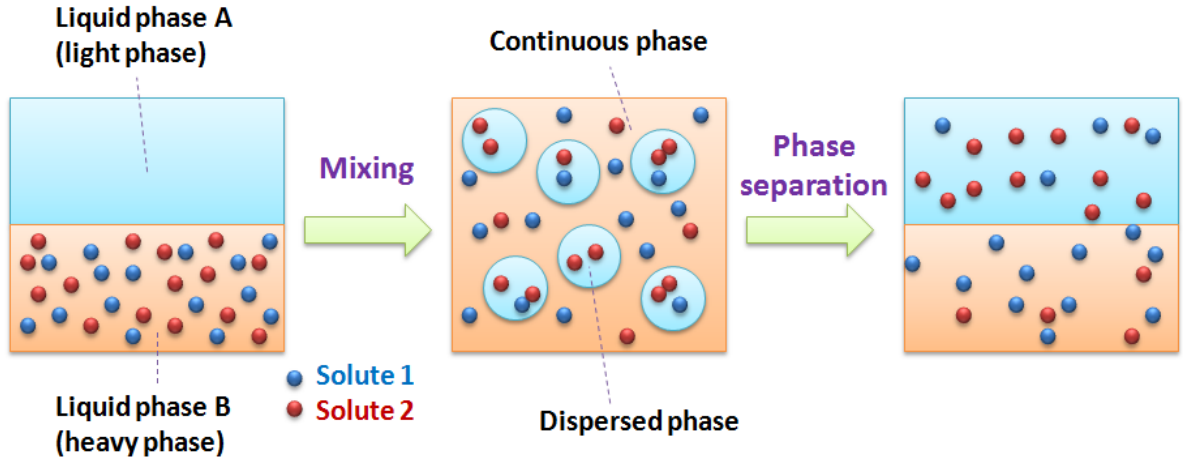


Figure 3-3 Schematics showing a liquid-liquid extraction process. (Modified from HKUST CENG3210 lecture notes).

3.1.4 Phase separation and precipitation involved in RNA extraction using TRIzol

Figure 3-4 shows the phase separation involved in TRIzol RNA extraction. When the cells are lysed in TRIzol, the contents in the cells are released into and dispersed in TRIzol. The TRIzol then contains DNA, RNA, proteins and salts. When chloroform/ bromochloropropane (BCP) is added and mixed thoroughly with the lysate, RNA and salts partition into the aqueous phase while proteins and DNA into the organic phase. After centrifugation, the two phases separate into two layers. The upper layer is the aqueous phase which contains the RNA and salts and the lower layer is the organic phase which contains DNA and proteins with phenol and chloroform/ BCP. The aqueous phase is then further processed to recover the RNA

in a process called precipitation as shown in **Figure 3-5**. When the aqueous phase is mixed with propanol, the RNA in the mixture precipitates since the solubility of RNA is lower in a solution of lower dielectric constant such as a propanol solution. After centrifugation, the precipitated RNA gets to the bottom of the tube. The solution phase is then removed and the precipitated RNA is dissolved in RNase-free water or buffer.

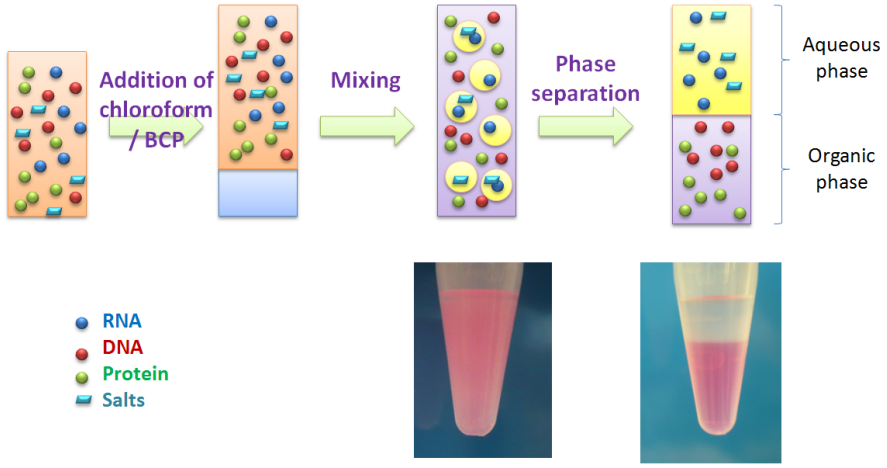


Figure 3-4 Phase separation involved in RNA extraction using TRIzol.

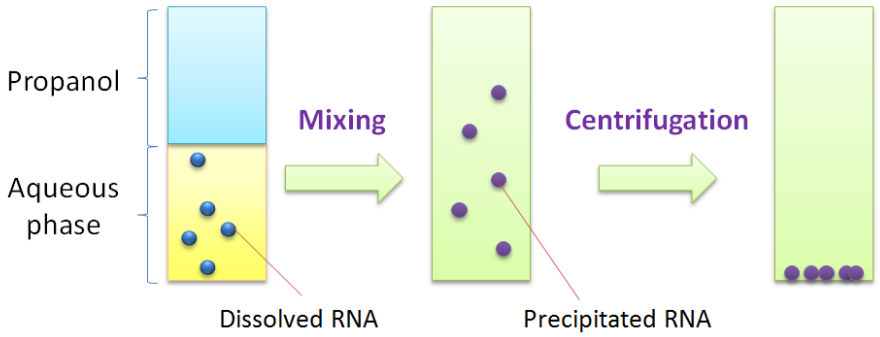


Figure 3-5 RNA precipitation from the aqueous phase using propanol.

3.2 Introduction

Reverse transcription – quantitative polymerase chain reaction (RT-qPCR) is a powerful method to assess the gene expression at transcriptional level. In many applications, especially for cells in tissues, it requires the extraction of RNA of high quality. Extraction of RNA

directly from IVD tissues or cartilage has been difficult due to its low cell density and high proteoglycan content. As estimated in Chapter 2, cells in bovine NP tissue and AF tissue only occupy around 0.19% and 1.35% volume of the tissues respectively while there is 33.9% dry weight of proteoglycan in bovine NP and 9.7% in AF. There are studies assessing the relative mRNA levels of IVD tissue using cells isolated from these tissues by collagenase treatment (**Table 3-2**). The enzymatic cell isolation method requires the dicing of tissues into small pieces and enzymatic digestion for at least two hours normally. This may result in changes in relative mRNA levels, especially for those of short half-lives, due to RNA degradation. Sharova *et al.* have shown that mRNA in mice has a median half-life of 7.1 h and the half-life for mRNA for some genes (< 100 genes) may be less than 1 h [119]. This suggests the possible necessity of quenching RNA degradation before RNA extraction for some short lived genes in some studies.

Table 3-2 Studies that investigated the gene expression in IVD tissues through cell isolation with sequential digestion using pronase and collagenase

Tissue	*Extraction*	*Reference*
Human NP and AF	TRIzol extraction	Minogue *et al.* [60]
Human NP and AF	TRIspin method	Grad *et al.* [127]
Bovine NP and AF	TRIzol extraction (with the addition of high salt precipitation solution)	Minogue *et al.* [61]
Rat NP, AF and AC tissues	Modified TRIspin method	Lee *et al.* [128]

In this study, we chose to use TRIzol for the RNA extraction as some studies have suggested the yield of RNA obtained using the guanidine isothiocyanate (GITC) based method can be higher than the column based method for some samples [129-132]. The studies in **Table 3-2** either used TRIzol extraction or TRIspin method for RNA isolation. TRIspin is a method that combines the one-step TRIzol method with the column fractionation step of the RNeasy kit [133]. We compared the TRIzol method and the combined TRIzol-column based (TRIspin) method in our study. In order to extract RNA from bovine IVD tissue directly, we

experimented with different modifications to the conventional extraction protocols. We hypothesize that the TRIzol method can give a higher RNA yield than the TRIspin method.

3.3 Objectives

The objectives of this Chapter are:

- To find out a method to effectively homogenize bovine NP tissue for RNA extraction
- To compare the efficiency of TRIzol method and combined TRIzol-column method with cultured cells
- To modify the RNA extraction protocols for bovine NP tissues and provide a guide, and
- To extend the guide to rat NP tissue and mouse IVD tissue

3.4 Materials and Methods

3.4.1 Bovine IVD tissue harvest

In our study, bovine NP, AF and muscle tissues were harvested from bovine tails of young adult animals (18 - 36 month old) as described in Chapter 2 and snap frozen in liquid nitrogen to quench RNA degradation as early as possible. Before further processing, the harvested tissue was kept at -80 °C, which most enzymatic reactions are very slow.

3.4.2 Tissue homogenization of bovine tissue

3.4.2.1 By pestle and mortar type homogenizer

Before using the ceramic pestle and mortar as shown in **Figure 3-6**, the bovine NP tissue was frozen in liquid nitrogen. The tissue was transferred to the mortar and I attempted to homogenize the tissue using the pestle connected to an electric motor. However, the bovine NP tissue was very hard when frozen and not brittle even when snap frozen by liquid nitrogen. The tissue could not be homogenized with this set up and we moved on to using the cryosection method.

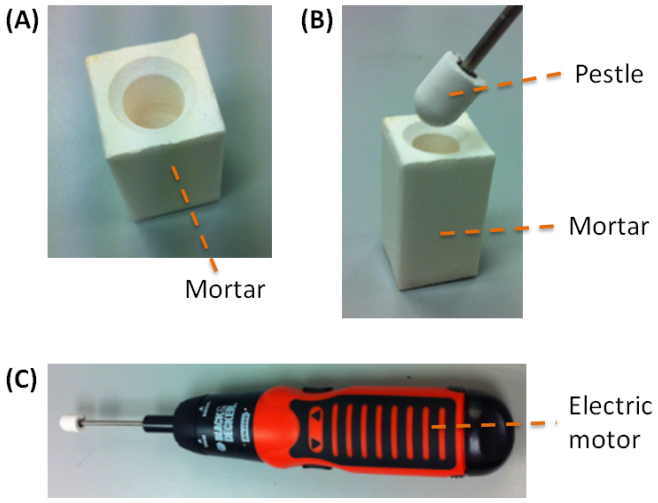


Figure 3-6 Homogenizer system (pestle and mortar type).

3.4.2.2 By cryosectioning

The bovine NP, AF and muscle tissues were put in a cryostat set at around -20 °C before cryosectioning into 30 µm sections. The details of the procedures are given in **Section 3.8.4.1** in the Appendix of this Chapter. The tissue sections were kept frozen in the cryostat or liquid nitrogen during transfer before the addition of TRIzol to avoid RNA degradation.

3.4.3 Comparison of RNA extracted using TRIzol and combined TRIzol-column method

The extraction of RNA using TRIzol was performed according to the manufacturer's instruction and with a high salt solution when proteoglycan was involved according to the manufacturer's recommendation. For the combined TRIzol-column based method, the protocol in a published paper was used [134]. In brief, the aqueous phase after phase separation of the TRIzol protocol was mixed with 0.5 volume of 100% ethanol. The mixture was then applied to the RNeasy spin columns followed by purification according to the manufacturer's instruction.

3.4.4 Extraction of RNA from bovine IVD tissue

When RNA was extracted according to the manufacturer’s instruction without any modification, a large white precipitate of proteoglycan was resulted. Based on manufacturer’s

instruction, high salt solution was added during the RNA precipitation step but this modification is not sufficient for bovine NP tissue which has a very high proteoglycan content. After different trials, the following modifications were made: (i) additional centrifugation of the initial homogenate to remove the residual tissue; (ii) an extra phase separation step when necessary; (iii) use of high salt solution (0.8 M sodium citrate and 1.2 M sodium chloride) in the RNA precipitation step and (iv) an extra RNA wash using 75% (v/v) ethanol to remove salts more completely. The details are given in Section 3.8.4 in the Appendix of this Chapter.

3.4.5 Extraction of RNA from mouse and rat tissue

In addition to bovine NP and AF tissues, RNA from cryosectioned mouse IVD and rat NP tissues were also extracted using slightly different methods (details given in the Appendix).

3.4.6 Quantification of RNA yield and quality

RNA concentration and quality was estimated by Nanodrop 2000c (Thermo Scientific). The integrity of RNA was assessed using an Agilent 2100 Bioanalyzer in the Centre for Genomic Sciences in the University of Hong Kong.

3.4.7 RT-qPCR

RT-qPCR was performed as in Chapter 2 with the bovine *GAPDH* primers (forward 5'-TGCCGCCTGGAGAAACC-3', reverse: 5'-CGCCTGCTTCACCACCTT-3' [61]), mouse primers listed in **Table 3-3** and rat primers listed in **Table 3-4**.

Table 3-3 Sequences of mouse primers used in this study (Sequences of mouse *Gapdh* and *Sox9* are from [135]. Reproduced with permission of Elsevier © 2006 Elsevier. The sequences of mouse *Gapdh*, *Sox9*, *Mia1*, *Runx1*, *Acan*, *Col2a*, *Cdh2* and *Krt19* primers are published in [125]. Reproduced under a Creative Commons Attribution License. The sequences are written in 5' to 3' for both forward and reverse primers.)

Primer	Sequence (forward)	Sequence (reverse)
Mouse *Gapdh*	GCACAGTCAAGGCCGAGAAT	GCCTTCTCCATGGTGGTGAA
Mouse *Sox9*	TGGCAGACCAGTACCCGCATCT	TCTTTCTTGTGCTGCACGCGC
Mouse *Mia1*	GACCGATCAATGGGATTTCT	CATAGAGCCGGAAGGGTAAC
Mouse *Runx1*	GGAGCGGTAGAGGCAAGA	ATGGTAGGTGGCAACTTGTG
Mouse *Acan*	GCAATTACCAGCTGCCCTTC	TCTTCTGCCCGAGGGTTCTA
Mouse *Col2a1*	AGAAGGCCTTGCTCATCCAG	GACGGTCTTGCCCCACTTAC
Mouse *Cdh2*	GACGAGAGGCCTATCCATGC	GGGTCGTTGTCAGCAGCTTT
Mouse *Krt19*	AGGGCCTTGAGATTGAGCTG	GCTCAGCTGGGCTTCAAAAC
Mouse *Galnt3*	TCGCCCCTGGAGAACAGATA	TGTTGCGTCACATGGCACTA
Mouse *Car3*	GTGTGGCTGCTGCTCAAAGA	CTGCCCTTGACAGGCTGAG

Table 3-4 Sequences of rat primers used in this study (Sequences are by design; the sequences are written in 5' to 3' for both forward and reverse primers) (The sequences of rat *Gapdh*, *Sox9*, *Acan*, *Col2a*, *Cdh2* and *Krt19* primers are also published in [125]. Reproduced under a Creative Commons Attribution License.)

Primer	Sequence (forward)	Sequence (reverse)
Rat *Gapdh*	GTGAAGCTCATTTCCTGGTATG	AACTGAGGGCCTCTCTCTTG
Rat *Sox9*	AGGAAGTCGGTGAAGAATGG	TGGCGTTAGGAGAGATGTGA
Rat *Acan*	GGGCGTGAGAACTGTCTACC	ACTGACACACCTCGGAAGC
Rat *Col2a1*	GATGGCTGCACGAAACAC	GCCCTATGTCCACACCAAAT
Rat *Cdh2*	TTAATGAGGGCCTTAAAGCTG	GCTGGAGGAGTTGAGAGAGC
Rat *Krt19*	TCTCAGCTCAGCATGAAAGC	ACTGCTGATCACACCTTGGA
Rat *Car3*	AGACTAAGGGCAAGGAGGCT	GTGAAGGAGCCATGGTAGGT
Rat *Galnt3*	TCGGAAGGACCAACTTCTCT	AGATCTGTTGTGTCGCATGG
Rat *Hopx*	ATCCTTAGCCAGACGCTCAC	GGTGCTTGTTGACCTTGTTG

3.5 Results

3.5.1 Homogenization of bovine NP tissue

With the use of the pestle and mortar type of homogenizer, we could not break the tissue as the frozen bovine NP tissue was rather hard but not brittle even when the tissue was frozen in liquid nitrogen. Thus we moved on to using cryosection to cut the tissues into very thin

sections (30 μm thick). Compared to the ceramic homogenizer, the cutting using the sharp blade was more effective.

3.5.2 Comparison of RNA from propanol precipitation and column based method

The GITC-based method (eg. TRIzol) and the column based method (eg. RNeasy) are two commonly used methods for RNA extraction. Some studies have suggested the yield of RNA obtained using the GITC-based method can be higher than the column based method for some samples [129-132]. Thus we used GITC based TRIzol to lyse the cells. A number of studies used TRIzol followed by RNeasy kit for extracting RNA [133, 136-138] but have not been compared with the TRIzol method. Hence, we compared the extraction of RNA from a small number of cells using the traditional TRIzol method and the combined TRIzol-column method. In the TRIzol protocol, it was suggested that the use of glycogen often improves yield for samples with a small number of cells. Therefore the use of glycogen was also tested.

In order to simulate the extraction of RNA from cells with high proteoglycan content, we also prepared cells in TRIzol with high proteoglycan content by adding IVD tissue to cell lysate in TRIzol. Some components such as proteoglycan dissolved from the IVD tissue into the TRIzol and increased the proteoglycan content in it. The presence of lysates from cultured cells ensured that there was some undegraded RNA present in the lysate. This may not be guaranteed for IVD tissue alone as the quality of RNA is dependent on the freshness of the bovine tail which is more difficult to control. On the other hand, we did not use glycogen for the cells with high proteoglycan content as the proteoglycan co-precipiated with RNA.

Table 3-5 shows the Nanodrop measurements of RNA extracted with the TRIzol method and the combined TRIzol-column method. For the cells without extra proteoglycan added, the concentration of RNA extracted using the TRIzol method (101.6 or 125.9 ng/μl) was more than four times that of using the combined TRIzol-column method (23.3 ng/μl). The use of glycogen increased the yield of RNA obtained but not statistically significant. For the cells

with higher proteoglycan content, the extraction of RNA using TRIzol procedures were also more than four times (171.7 ng/µl) more than the combined TRIzol-column method (38.8 ng/µl). There was no significant difference in the A260/A280 values of RNA obtained. The RNA from the TRIzol method had a larger A260/A230 ratio but not statistically significant.

Table 3-5 Concentration, yield and quality of RNA extracted from cultured cells with different methods estimated by Nanodrop. [a.] The yield is based on the cells which are approximately equivalent to 2 wells of bovine cells in a 96 well plate. (Mean ± SD; 3 samples per group; single measurement per sample for cells and double measurements per sample for cells with tissue) (Reproduced from [125] under a Creative Commons Attribution License).

Samples By Instrument	Concentration (ng/µl) Nanodrop	Yield (µg) [a] Nanodrop	A_{260}/A_{280} Nanodrop	A_{260}/A_{230} Nanodrop
Cells				
TRIzol, w/o glycogen	101.6 ± 24.6	1.22 ± 0.29	1.84 ± 0.05	2.10 ± 0.04
TRIzol, w glycogen	125.9 ± 6.2	1.51 ± 0.07	1.80 ± 0.01	1.96 ± 0.12
TRIzol + Column	23.3 ± 4.1	0.56 ± 0.10	1.87 ± 0.05	0.88 ± 0.39
Cells with tissue (high proteoglycan)				
TRIzol	171.7 ± 5.9	2.06 ± 0.07	1.99 ± 0.02	1.28 ± 0.23
TRIzol + Column	38.8.± 6.1	0.93 ± 0.15	1.92 ± 0.02	0.84 ± 0.46

Table 3-6 shows the Bioanalyzer results of RNA extracted with the TRIzol method and the combined TRIzol-column method. Consistent with the data from Nanodrop, RNA samples extracted with the TRIzol method were of higher concentrations compared with the combined TRIzol-column method. RNA extracted using different methods under test yielded RNA of RNA integrity number (RIN) > 5, indicating their suitability for RT-qPCR.

Table 3-6 Concentration, yield and quality of RNA extracted from cultured cells with different methods estimated by Bioanalyzer (mean ± SD; 3 samples per group) (Reproduced from [125] under a Creative Commons Attribution License).

Samples By Instrument	Conc. (ng/µl) Bioanalyzer	RIN Bioanalyzer	28s/18s Bioanalyzer
Cells			
TRIzol, w/o glycogen	91.0 ± 33.1	9.67 ± 0.25	1.87 ± 0.15
TRIzol, w glycogen	105.0 ± 23.8	9.90 ± 0.10	1.97 ± 0.12
TRIzol + Column	15.7 ± 2.3	8.33 ± 0.45	2.43 ± 0.93
Cells with tissue (high proteoglycan)			
TRIzol	192.0 ± 10.8	6.93 ± 0.81	1.60 ± 0.44
TRIzol + Column	51.0 ± 7.9	9.07 ± 0.15	1.83 ± 0.12

All the samples under test showed peak absorption at 260 nm in Nanodrop measurements and the peaks for TRIzol extracted RNA were sharper due to the higher concentrations of RNA compared to the ones from the combined method (**Figure 3-7A**). The 28S and 18S bands were observed in the electrophoregrams of the samples (**Figure 3-7B**). Bands of light intensity were observed for RNA extracted from cells with the TRIzol methods (CT, CTG) but not for the combined method (CC). This may be due to the low affinity of low molecular weight RNA to the column silica membrane which get discarded during the isolation process. Stronger bands were observed for RNA extracted from cells with proteoglycan using the TRIzol method (HPT) than that using combined method (HPC). The smear present in the HPT sample may be the mRNA of different molecular weights or partially degraded RNA.

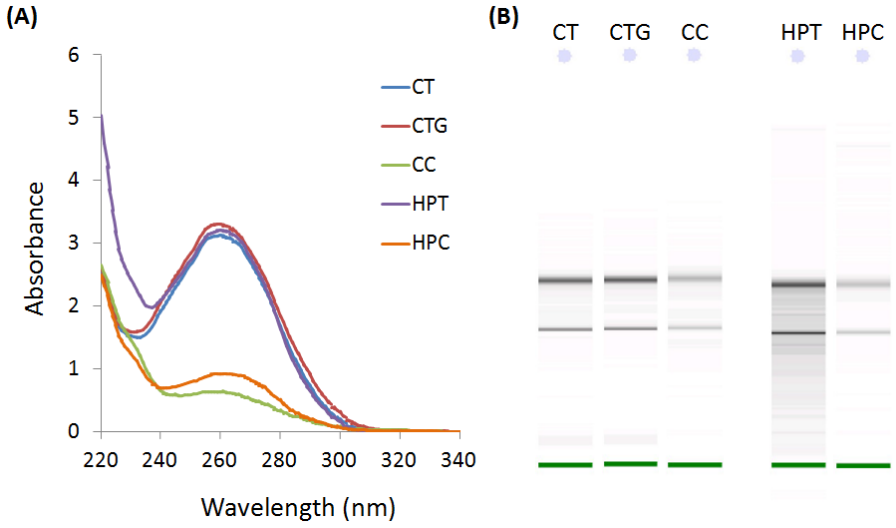


Figure 3-7 (A) Representative UV-spectra of RNA extracted from bovine cells measured using Nanodrop and (B) electropherograms of RNA extracted with different methods. (CT: from cells using TRIzol without the use of glycogen; CTG: from cells using TRIzol with the use of glycogen; CC: from cells using combined TRIzol-column based method; HPT: from cells and high proteoglycan content using TRIzol; HPC: from cells and high proteoglycan content using combined TRIzol-column based method) (3 samples per group). (Reproduced from [125] under a Creative Commons Attribution License).

We tested the RT-qPCR with the RNA extracted with different methods and the representative amplification plot was shown in **Figure 3-8A**. The qPCR amplification efficiency was calculated based on the Ct vs log (template concentration) plots as shown in **Figure 3-8B**.

Table 3-7 shows the Ct values and qPCR efficiency of the cDNA from RNA extracted with different methods. The Ct values within each sample group (cells or cells with tissue) had only difference of less than 0.5 cycles, indicating that the RNA extracted with different methods did not affect the RT-qPCR seriously. Yet the same extraction method is recommended for each batch of samples to avoid any potential difference caused by differences in extraction methods. All samples have amplification efficiency within 90-110% in qPCR calibration curves, which is a criterion for reliable qPCR. These indicate the RNA extracted with these methods was compatible with the qPCR system used.

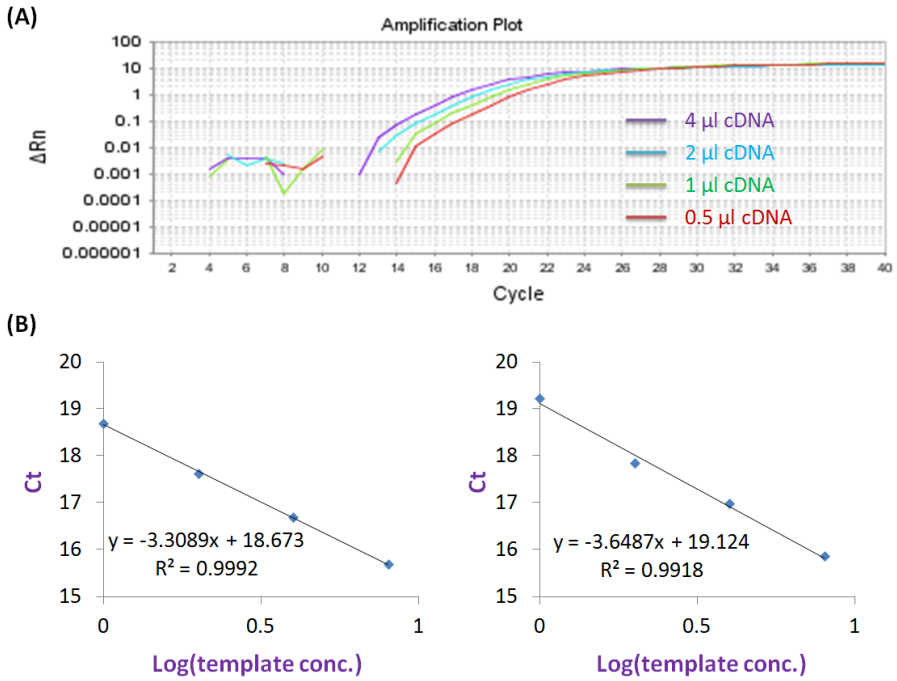


Figure 3-8 (A) Representative amplification plot of qPCR with different template concentrations of two-fold dilutions and (B) representative Ct against Log (template concentration) plots for calculating the amplification efficiency. (Biological duplicates and technical duplicates).

Table 3-7 Ct values and qPCR efficiency estimated from the curves for *GAPDH* amplification (mean ± SD; biological duplicates and technical duplicates) (Ct values shown were obtained with threshold of 0.3 and 1 µl of cDNA in 10 µl reactions) (The qPCR efficiency data is published in [125]. Reproduced under a Creative Commons Attribution License).

Samples	Ct	qPCR efficiency
Cells		
TRIzol, w/o glycogen	17.60 ± 0.08	99% ± 3%
TRIzol, w glycogen	17.96 ± 0.06	107% ± 10%
Column	17.65 ± 0.02	97% ± 11%
Cells with tissue (high proteoglycan)		
TRIzol	17.76 ± 0.13	95% ± 6%
Column	18.15 ± 0.07	101% ± 5%

3.5.3 Extraction of RNA from bovine NP, AF and muscle

As shown in **Table 3-8**, the concentrations and yields of RNA from muscle were much higher than NP and AF, probably due to the higher density of cells. Muscle was included as a non-IVD control. It has a high cell density with low proteoglycan content, to which typical extraction should be applicable. The RNA isolated directly from NP tissue and AF tissue has

lower A260/280 ratios compared to muscle, which was probably due to the contamination by phenol. This was suggested by the UV absorption spectra that there was a shift of peak towards 270 nm for the RNA isolated from NP or AF tissue (**Figure 3-9A**). The RNA from bovine muscle using the same extraction method yielded a sharp peak at 260 nm (**Figure 3-9B**). The presence of phenol from TRIzol in the samples can cause over-estimations of RNA concentrations due to the absorbance contributed by phenol at 260 nm. Therefore, concentration correction for RNA was developed and is described in the next Chapter.

Table 3-8 Concentration, yield and quality of RNA extracted from bovine tissues with different methods estimated by Nanodrop. [a.] The yield of RNA expressed as amount of RNA from each 1.5 ml tube of cryosectioned tissue. The RNA concentrations of bovine NP and AF were below the qualitative range of RNA 6000 Nano total RNA suggested by the Centre for Genomic Sciences of HKU which is 50 - 500 ng/µl. (Mean ± SD; n = 3 for bovine tissues). (Reproduced from [125] under a Creative Commons Attribution License).

Samples By Instrument	Concentration (ng/µl) Nanodrop	Yield (µg) [a] Nanodrop	A_{260}/A_{280} Nanodrop	A_{260}/A_{230} Nanodrop
Bovine NP	30.2 ± 1.5	0.33 ± 0.02	1.76 ± 0.04	0.74 ± 0.10
Bovine AF	42.8 ± 5.5	0.47 ± 0.06	1.81 ± 0.05	0.50 ± 0.28
Bovine muscle	372.1 ± 33.0	4.09 ± 0.36	2.07 ± 0.01	1.55 ± 0.19

Schoor *et al.* found that partially degraded RNA samples with still visible ribosomal bands gave gene expression profiles highly similar to those of intact samples, suggesting RNA samples of suboptimal quality might still lead to meaningful results when used cautiously [139]. Besides, in the study by Fleige and Pfaffl on RNA integrity of its effect on RT-qPCR performance, they pointed out that amplification with large amplicon (> 400 bp) was strongly dependent on a good RNA quality (with RIN > 5 from Bioanalyzer). However, RT-qPCR with small amplicons (70-250 bp), were more or less ‘‘independent’’ of the RNA quality [140]. In Chapter 2, the *GAPDH* primer pair used was with corresponding amplicon size of 54bp while the amplicon sizes of *ACAN*, *COL2A1*, *CDH2*, *KRT18* and *KRT19* were also less than 100bp. The amplifications of cDNA from bovine NP and AF samples were tested and the

amplification curves were shown in **Figure 3-9C**. The effect of different levels of contamination were also tested and discussed in the next Chapter.

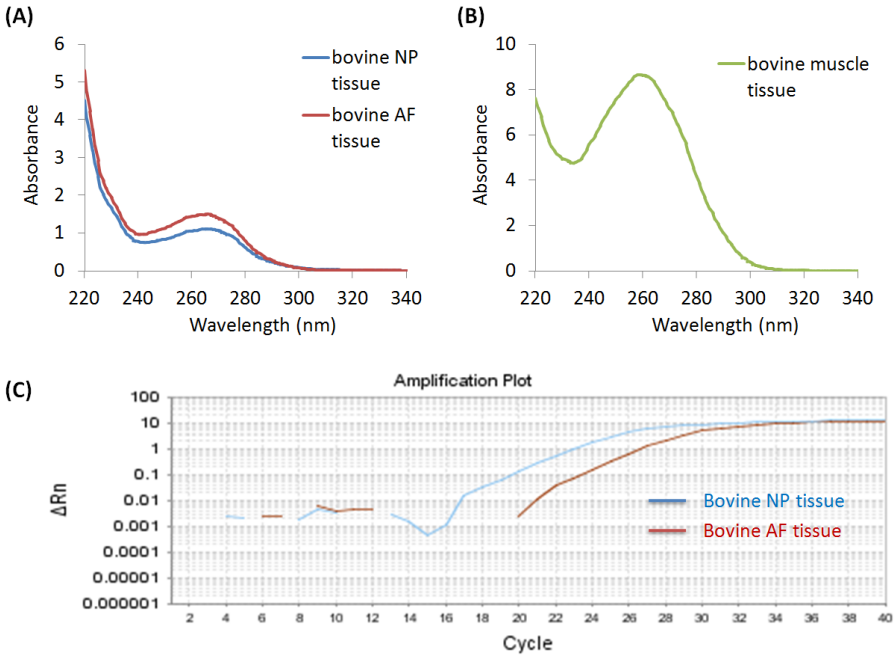


Figure 3-9 (A) UV-spectra of RNA extracted from bovine NP and AF tissues, and from (B) bovine muscle tissue measured using Nanodrop; (C) qPCR amplification curves of RNA extracted from bovine NP and AF tissues using primers for *GAPDH*. (A and B are published in [125]. Reproduced under a Creative Commons Attribution License).

3.5.4 Extraction of RNA from mouse and rat IVDs

In order to extend the RNA extraction guide to other species, we also tested the extraction of RNA from mouse and rat IVDs. The details of the procedures were given in **Section 3.8.5** of the Appendix. Unlike bovine NP and AF tissue, the tissues obtained from mouse and rat IVDs were rather small. It was difficult to mount the mouse or rat tissue directly for cryosection. Thus a method to embed the disc in DEPC-treated water, which was used by Prof. Danny Chan's group, was used. In brief, small aluminum containers were made to hold DEPC-treated water. Then the containers were dipped into liquid nitrogen to partially freeze the water, leaving the central top part of the water unfrozen. The pre-frozen mouse or rat disc tissues were then put in the top part of the unfrozen water and fixed quickly by freezing the

remaining unfrozen water. Afterwards, the procedures of cryosection and RNA extraction were similar to bovine tissues.

The measurements of the extracted RNA by Nanodrop are shown in **Table 3-9**. The A_{260}/A_{280} ratios for rat NP and AF tissues were lower than those of mouse IVD and rat muscle tissue, which were due to the shifts of the peaks from 260 nm to 270 nm (**Figure 3-10**). The shifts were more serious for RNA of low concentrations. **Figure 3-11** shows the electrophoregrams of RNA extracted from mouse IVD and rat NP. The 28S and 18S bands were visible and the RINs were 6.9 and 7.5 for mouse IVD and rat NP respectively.

Table 3-9 Concentration, yield and quality of RNA extracted from mouse IVD tissue, rat NP, AF and muscle tissues estimated by Nanodrop. (mean ± SD; n=7 for mouse IVDs and n =2 for rat tissues) [a.] Concentrations of rat NP and AF were corrected with a mathematical formula [118]. [b.] The yield is based on one mouse disc or rat NP/ AF tissue from half a rat tail. (Data of mouse IVD and rat NP tissues are published in [125]. Reproduced under a Creative Commons Attribution License).

Samples	Concentration (ng/µl)	Yield (µg) [b]	A_{260}/A_{280}	A_{260}/A_{230}
By Instrument	Nanodrop [a]	Nanodrop	Nanodrop	Nanodrop
mouse IVD	325.5 ± 110.4	3.25 ± 1.10	1.88 ± 0.03	1.48 ± 0.34
rat NP tissue	107.6 ± 15.7	1.35 ± 0.20	1.78 ± 0.01	0.97 ± 0.01
rat AF tissue	36.2 ± 13.5	0.45 ± 0.17	1.76 ± 0.03	0.92 ± 0.68
rat muscle tissue	689.1 ± 47.6	8.61 ± 0.59	1.99 ± 0.03	2.22 ± 0.05

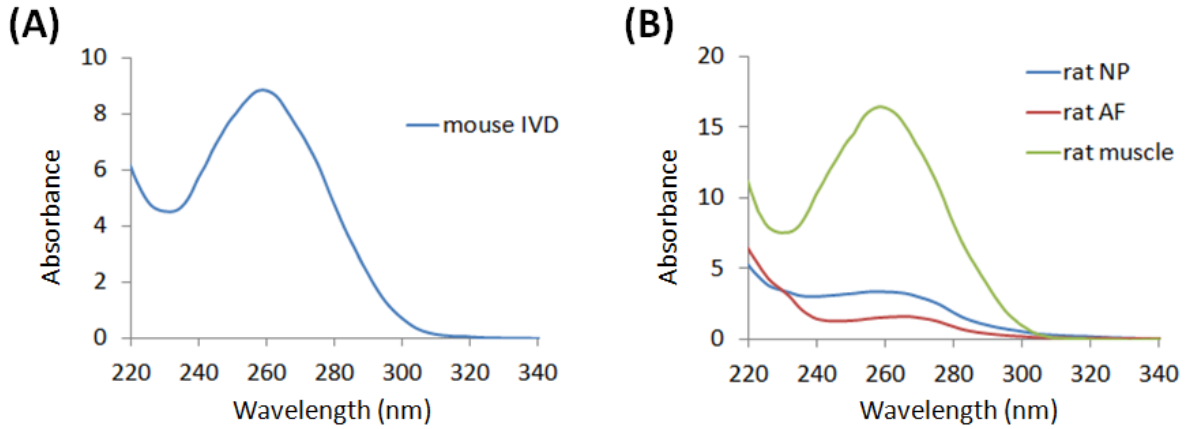


Figure 3-10 (A) UV-spectra of RNA extracted from mouse IVD tissue and from (B) rat NP, AF and muscle tissues measured using Nanodrop. (UV Spectra of mouse IVD and rat NP tissues are published in [125]. Reproduced under a Creative Commons Attribution License).

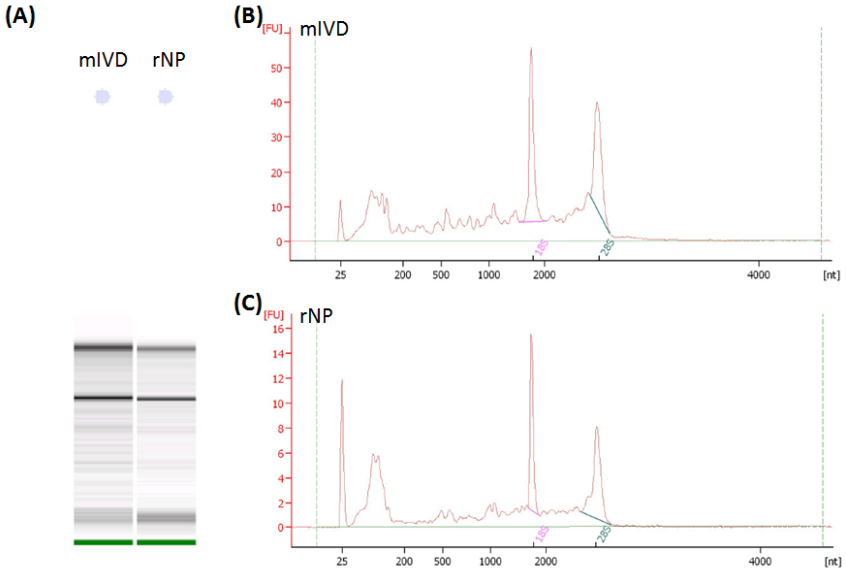


Figure 3-11 (A) Electropherograms of RNA extracted from mouse IVD and rat NP and the corresponding spectra (B) and (C). (The electropherograms are published in [125]. Reproduced under a Creative Commons Attribution License).

The RNA samples from mouse IVD and from rat NP were further tested with RT-qPCR of potential NP markers. Amplifications were detected as shown in **Figure 3-12**.

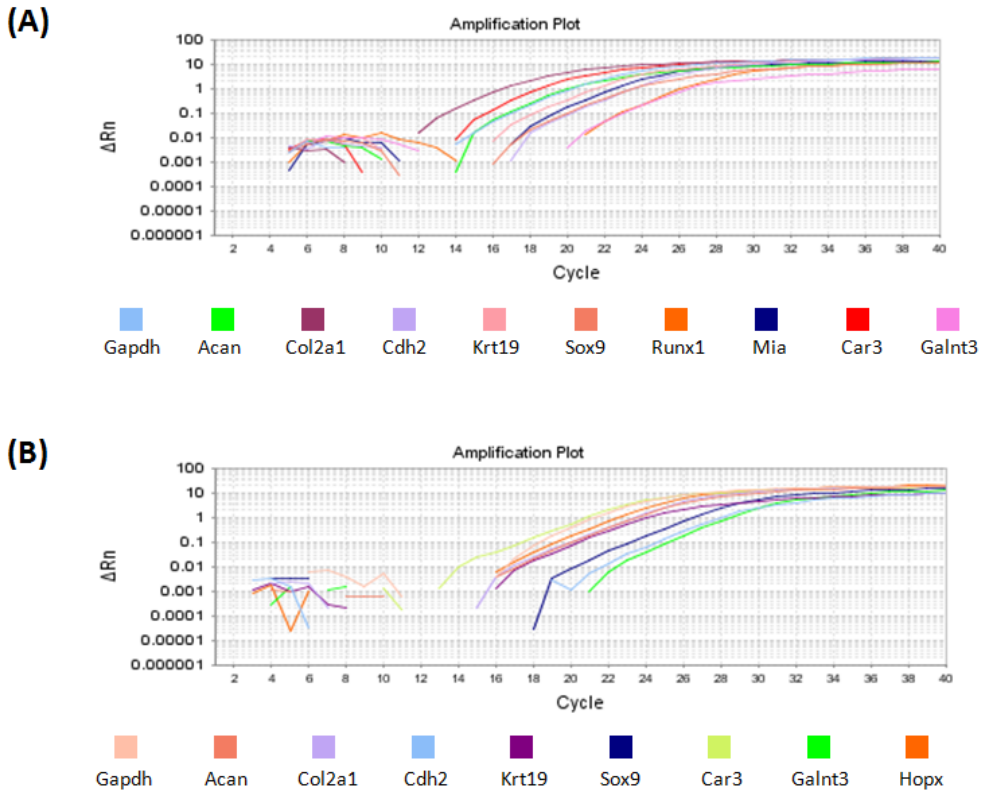


Figure 3-12 (A) qPCR amplification curves of RNA extracted from mouse IVD and (B) from rat NP. (Reproduced under a Creative Commons Attribution License from [125]).

3.6 Discussion

3.6.1 Homogenization methods for IVD tissue

Homogenization is a general term to describe the dispersion of minute fragments of tissue evenly throughout a mixture by mechanical action such as macerations or crushing or by chemicals such as detergents or organic solvents. There are a wide variety of homogenizers available to achieve such a purpose. In our study, bovine NP tissue could not be homogenized by the ceramic pestle and mortar system. However, there were some studies who reported the use of homogenizer for extraction of RNA from NP tissues which are summarized in **Table 3-10**. Only two out of the five studies have mentioned the types of homogenizers used. Wang *et al.* used an Omni TH homogenizer (**Figure 3-13A**) [141] which used vibration to break the tissues. There are two different types of probes for Omni tissue homogenizers: the stainless steel type (**Figure 3-13B**) and the plastic disposable type (**Figure 3-13C**). The plastic disposable type is designed to reduce cross-contamination and the stainless steel type is for

larger and tougher samples. The type of probes used was not specified in their study. The use of Omni tissue homogenizer may be a viable option for bovine NP tissue but this requires the purchase of a specialized equipment. Simple pestle and mortar systems may be a less expensive option. Capossela *et al.* used a stainless steel mortar to pulverize human NP and AF tissue on dry ice [142] but the size and type of mortar was not mentioned precisely. In our experience, the frozen NP tissue is rather hard and tough, which is difficult to be broken by brutal force. Thus we have the concern about the throughput and efficiency of using the stainless steel mortar system to homogenize the bovine NP tissue.

Table 3-10 Studies that investigated the gene expression in IVD tissues through direct RNA extraction from the tissues after pulverization (Reproduced under a Creative Commons Attribution License from [125]).

Tissue	*Tissue processing*	*Homogenizer used*	*Extraction*	*Reference*
Human NP tissue (100-300 mg)	homogenized in TRIzol on ice	Omni TH Homogenizer	TRIzol extraction followed by RNeasy mini clean up	Wang *et al.* [141]
Human NP and AF tissue	frozen at -80 °C and pulverised on dry ice	stainless steel mortar	Aurum Total Mini Kit	Capossela *et al.* [142]
Rat NP tissue	pulverized under liquid nitrogen	not specified	RNeasy mini kit	Yurube *et al.* [143]
Rabbit NP and AF tissue	pulverized after freezing in liquid nitrogen	not specified	not specified	Mwale *et al.* [144]
Rat NP and AF	flash-frozen in liquid nitrogen, pulverized and homogenized in TRIzol	not specified	RNeasy mini kit	Tang *et al.* [59]

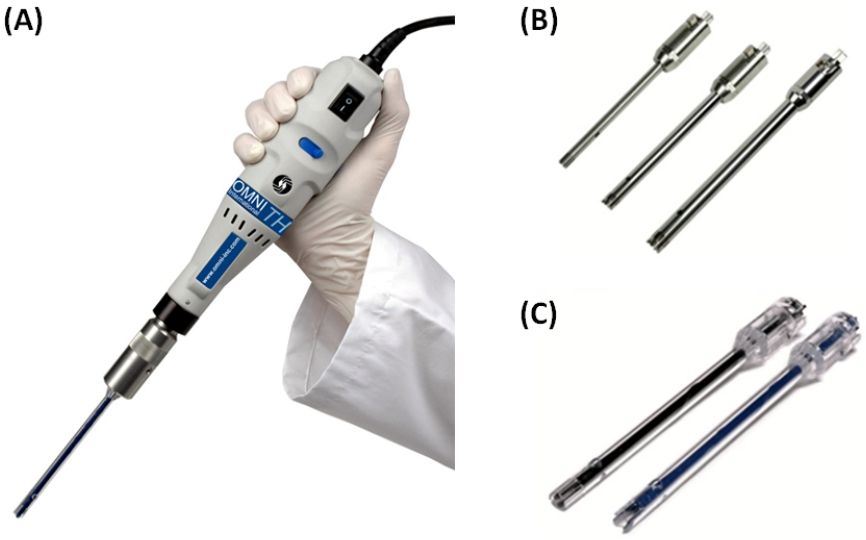


Figure 3-13 (A) Omni Tissue Homogenizer (TH), (B) stainless steel generator probes and (C) Omni tip plastic homogenizer probes. (Photos were obtained from the official web of Omni International).

In addition, the studies listed in **Table 3-10** used column based kits for RNA extraction. In our study, RNA precipitation method using propanol and a high salt solution was used. This may be the first study using TRIzol to extract RNA from bovine NP tissue without the use of columns.

3.6.2 Glycogen in RNA precipitation

According to the protocol of TRIzol, 200 µg glycogen should be added per ml of TRIzol before the phase separation step. However, the purpose of glycogen was to co-precipitate with the RNA. A smaller amount of glycogen may actually be required. Hence we investigated the amount of glycogen required to be added to the samples and the experiment was shown in **Section 3.8.1** in the Appendix. As little as 2 µl of glycogen at 20 µg/µl already gave a visible pellet when high salt solution was not used. The use of high salt solution reduced the size of glycogen precipitated but 5 µl was sufficiently to give visible pellet when high salt solution was used. Therefore we decided to use glycogen amount less than recommended by the manufacturer's protocol in order to reduce the glycogen concentration in our sample and reduce the cost.

3.6.3 Identity of the large precipitate

For bovine NP tissue, a large white precipitate was observed when the aqueous supernatant after phase separation was precipitated without the use of a high salt solution. Such kind of precipitation was not observed for passaged NP cells harvested from culture surfaces. Hence it is likely that the precipitate was from the components dissolved from the tissues. Contamination with polysaccharides and proteoglycans is a common problem in some RNA extraction methods [145-148]. Besides, NP tissue is rich in proteoglycan and collagen. Therefore, we speculate the precipitate has proteoglycan in it. However, without further characterization, we did not rule out the possibility that other components are also present in the precipitate.

3.6.4 Yield of RNA from rat NP tissue

Tang *et al.* extracted RNA from rat NP and AF for cDNA microarray analysis and RT-qPCR. After harvesting the tissue, they immediately flash-freezed the tissues in liquid nitrogen, then pulverized and homogenized in TRIzol reagent, followed by total RNA extraction using a RNeasy mini kit. For each sample in microarray, tissue was pooled from all discs across four rats to collect sufficient RNA for one sample [59]. The amount and quality of RNA used was not mentioned in their study. For Affymetrix GeneChip Expression analysis service provided by the Centre for Genomic Sciences of the University of Hong Kong, 2.5 μg total RNA of RIN > 8 is recommended. In our study, 1.35 μg of total RNA was obtained from NP tissue from half a rat tail. In other words, RNA from one tail (~2.7 μg) was sufficient for microarray analysis. However, the RIN was 7.5 which was lower than 8, indicating that the procedures may need to be improved for better RNA quality. However, in an article about quality control of RNA for microarray, RIN of 7.0 was used as a cut-off value for deciding whether the RNA is suitable for microarray analysis [149]. The authors selected this value because Thompson *et al.* showed that there was a substantial increase in the rate of false positives on the microarray when the starting RNA had a RIN value of < 7.0 [150]. This may suggest the RNA obtained in our study which has RIN value of 7.5 may also be suitable for microarray analysis. Only one

rat is sufficient to obtain RNA from rat NP tissue for microarray analysis using our modified protocol compared to four rats required in the study by Tang *et al.* Fewer animals may be needed to be sacrificed for each microarray analysis.

3.6.5 Limitation of the current study

The concentration of RNA extracted from bovine NP tissue is below the sensitivity limit for the Bioanalyzer for RIN values. Besides, one of the limitations in giving meaningful RIN values for bovine tissue is that we do not have access to fresh tissue. The bovine tail was bought from the butcher but not directly from the slaughter house. There may be degradation of RNA before the tissue can be obtained. Thus the freshness of bovine tail can be one of the determining factors of the RIN values.

3.7 Conclusions

In summary, RNA extraction using the TRIzol method gave RNA of higher concentrations compared to the combined TRIzol-column based method for samples of small numbers of cells with or without high proteoglycan content. We have developed a method to isolate RNA from bovine IVD tissue directly by combining cryosection and high salt precipitation into conventional TRIzol method. Compared with other methods for RNA extraction from tissues, our method allows the pre-RNA extraction processing to be kept at a low temperature which may help to maintain the integrity of RNA and also better preserve the relative mRNA levels. This method may be applied to RNA extraction from cells in tissues which are high in extracellular matrix content and low in cell density. The suggested protocols on extracting RNA from bovine, rat and mouse IVDs are given in details in the Appendix.

3.8 Appendix

3.8.1 Use of glycogen in RNA precipitation

In order to investigate the effect of high salt solution on the precipitation of glycogen. 2 µl or 5 µl of glycogen (20 µg/µl) was added to 0.5 ml of TRIzol. 50 µl of BCP was then added to the TRIzol with glycogen and the samples were shaken vigorously and stood at room temperature for 3 min. The samples were centrifuged at high speed (> 12, 000 ×g) and the supernatant was transferred to new tubes with propanol with or without high salt solution as listed in **Table 3-11**.

As shown in **Table 3-11**, addition of high salt solution inhibited the precipitation of glycogen. The 2 µl addition of glycogen (20 µg/ml) to 0.5ml TRIzol seems sufficient to give a small pellet to avoid the loss of pellet during the supernatant removal and ethanol wash steps) and the pellet from 2 µl of glycogen addition to 0.5 ml of TRIzol probably be even larger when all the supernatant was precipitated instead of 100 µl in each tube only.

Table 3-11 Pellet formation with and without the use of hight salt (HS) solution. ([a] HS solution refers to 1.2 M NaCl and 0.8 M sodium citrate in DEPC-treated water)

	Glycogen	*Propanol precipitation*	*Observation (volume in brackets indicates sizes of pellets)*
Tube 1a	2 µl to 0.5 ml TRIzol	100 µl propanol + 100 µl supernatant	Small pellet (~1 µl)
Tube 1b	2 µl to 0.5 ml TRIzol	50 µl HS solution [a] + 50 µl propanol + 100 µl supernatant	No pellet at all
Tube 2a	5 µl to 0.5 ml TRIzol	100 µl propanol + 100 µl supernatant	Larger pellet (~3 µl)
Tube 2b	5 µl to 0.5 ml TRIzol	50 µl HS solution [a] + 50 µl propanol + 100 µl supernatant	Small pellet (~1 µl)

3.8.2 Preliminary experiment to find out the optimal RNA extraction conditions for bovine NP

Different approaches to extract RNA from bovine NP tissue were attempted and the key decisions which lead to our suggested protocol were summarized below:

Due to the very high proteoglycan content of bovine NP tissue, the supernatant for samples of NP tissues was always milky (as shown in **Figure 3-17** in **Section 3.8.4.2**), which resulted in large precipitates trapping RNA and prevented subsequent dissolution. Different methods were tested to solve this problem. As recommended in the detailed protocol of TRIzol from the manufacturer Invitrogen, high salt solution may be used for samples with high proteoglycans and/ or polysaccharides content. According to the protocol, 0.25 ml of isopropanol should be added to the aqueous phase after the first separation followed by 0.25 ml of a high salt precipitation solution (0.8 M sodium citrate and 1.2 M NaCl) per 1 ml of TRIzol used for homogenization. However, the use of high salt solution was not sufficient for bovine NP samples where proteoglycan content was even higher than cartilage (NP has GAG/ COL2 ratio of 27:1 while cartilage of 2:1). Thus other methods were also explored.

Combined TRIzol-column method was suggested to give RNA of high quality compared to conventional TRIzol method for some samples. Hence it was tested. However, the yield of RNA using combined TRIzol-column method was not as high as TRIzol method (**Table 3-5** in **Section 3.5.2**).

After many failed experiments, it was noticed that not only the supernatant (aqueous portion) after first phase separation was milky, the organic phase was also milky for the portion near the aqueous-organic interface. This indicates that the milky component (probably the proteoglycan) also partitioned into the organic phase. In chemical engineering, multiple stage phase separations can be used to increase the purity of a particular component in a mixture

[151]. Hence we speculated that a second phase separation may help to reduce the proteoglycan content in the aqueous phase of the sample after first phase separation.

The following three parameters were tested: (i) the use of high salt solution and (ii) the precipitation (conventional TRIzol) extraction or the combined TRIzol-column based method and (iii) the extra/ second phase separation. All samples were tested in the same batch of experiment as listed in **Table 3-12** for a better comparison. Among the samples, tube 1 represents typical TRIzol extraction without the use of high salt precipitation, tube 2 represents typical TRIzol extraction with the use of high salt precipitation recommended for high proteoglycan content samples, and tube 5 represents typical combined TRIzol-column based RNA extractions. The others are variations of the protocols being investigated.

Table 3-12 Experiment conditions to find the conditions for extracting RNA from samples with high proteoglycan content and the corresponding RNA concentrations. A260/A280 and A260/A230 were estimated by Nanodrop. (PrOH: 2-propanol, EtOH: ethanol).

Tube	*1*	*2*	*3*	*4*	*5*	*6*	*7*	*8*
1st phase separation	+	+	+	+	+	+	+	+
2nd phase separation	/	/	+	+	/	/	+	+
Salt addition	/	+	/	+	/	+	/	+
Extraction (P: precipitation, C: column)	P	P	P	P	C	C	C	C
Volume of propanol/ ethanol (µl)	150 PrOH	75 PrOH	550 PrOH	275 PrOH	75 EtOH	37.5 EtOH	275 EtOH	137.5 EtOH
Volume of salt solution (µl)	/	75	/	275	/	37.5	/	137.5
RNA concentration (ng/µl)	185.3	158.4	110.2	204.8	26.3	9.2	12.6	13.1
A_{260}/A_{280}	1.59	1.98	1.87	2.02	1.98	1.61	1.74	1.54
A_{260}/A_{230}	0.62	1.26	1.2	1.41	1.33	0.64	0.5	0.2

Figure 3-14 shows the UV spectra of RNA extracted using different methods listed in **Table 3-12**. Peak absorption is observed at 260 nm for all samples extracted using the TRIzol methods (Tubes 1-4). There were peak shifts towards 270 nm for some of the RNA extracted

using the combined method (Tubes 6-8) which was probably due to the low concentrations of RNA obtained.

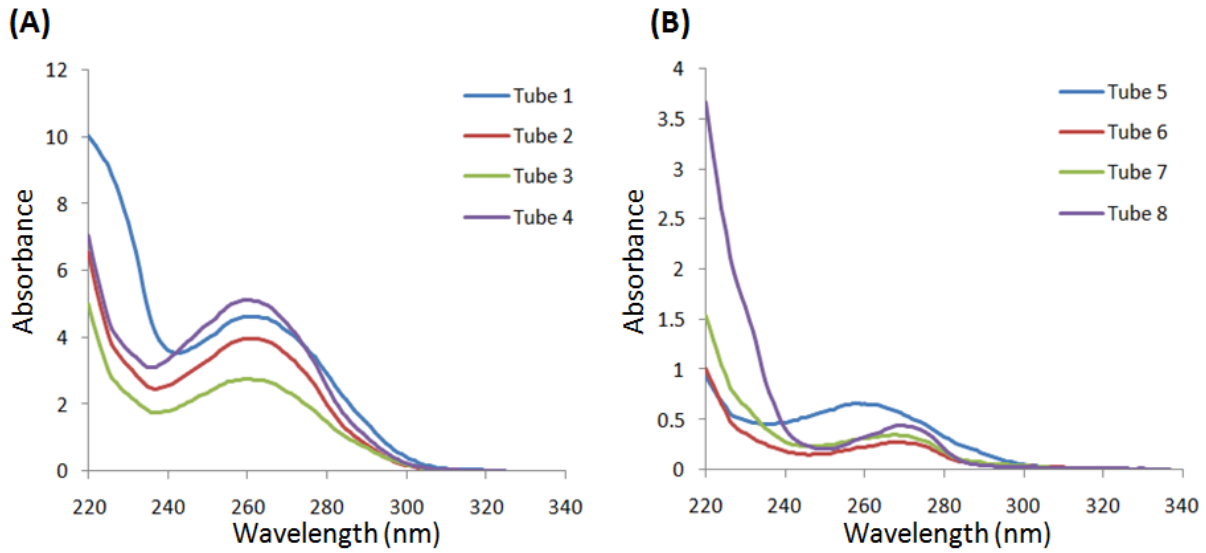


Figure 3-14 UV-spectra of RNA extracted from (A) tubes 1-4 and (B) tubes 5-8 as listed in Table 3-12 measured using Nanodrop.

3.8.3 Suggested experimental flow for RNA extraction from IVD tissues

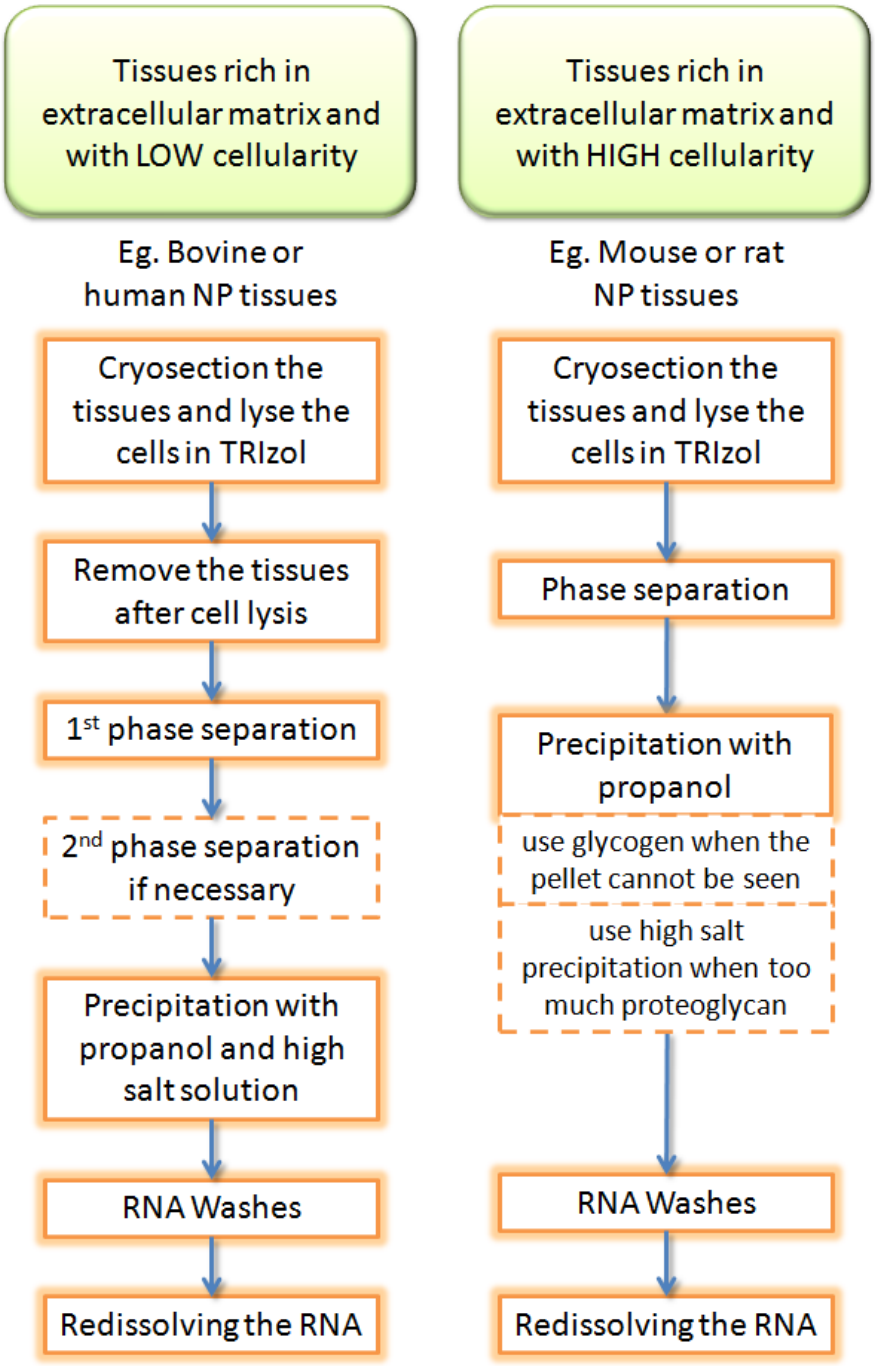


Figure 3-15 Suggestion of experimental flow for extraction of RNA from tissues rich in extracellular matrix with low or high cellularity. (Reproduced under a Creative Commons Attribution License from the supplementary information in [125]).

3.8.4 Recommended protocols for extracting RNA from bovine / human IVD tissues (tissues rich in extracellular matrix with low cellularity)

3.8.4.1 Cryosection the tissues and lyse the cells in TRIzol

1. Cryosection the tissues using a cryostat (10-30 μm)
2. Transfer the sections to 1.5 ml tubes (for a larger amount of tissue, the volume may be scaled up) using forceps pre-cooled in the cryostat chamber

   Note: As the thin sections melt and stick to surfaces at room temperature readily, it is important to pre-cool the tubes in the cryostat chamber. When holding the tubes, hold the cap edge to avoid warming up the tube body.

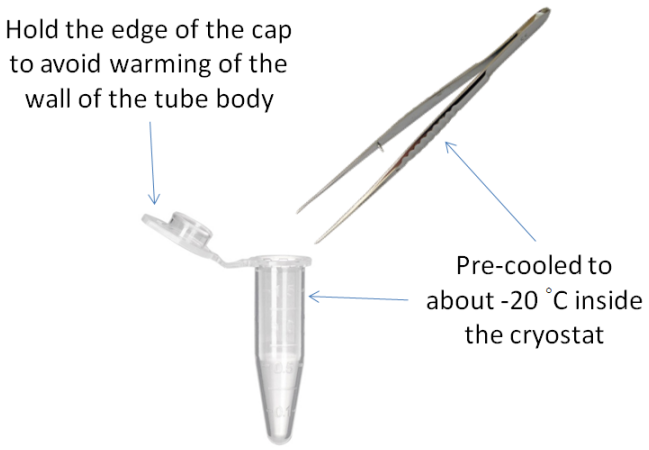


Figure 3-16 Schematic showing the precautions to prevent the melting of tissue sections because of the body warmth.

3. Transfer the tubes of cryosectioned tissues to a chemical fume hood using dry ice or Mr. Frosty pre-cooled to -80°C (or any method that can avoid the thawing of the sections inside the tubes)
4. Add 0.5 ml of TRIzol to the tubes with samples, mix well, store at -80 °C before RNA extraction

3.8.4.2 1st phase separation

1. Centrifuge the samples and transfer the supernatant to new tubes so as to remove the tissues
2. Add 50 µl of bromochloropropane (BCP) to each tube with clear TRIzol lysate, shake vigorously for 15 s and stand at room temperature for 15 min
3. Centrifuge at 12,000 × g at 4 °C for 15 min

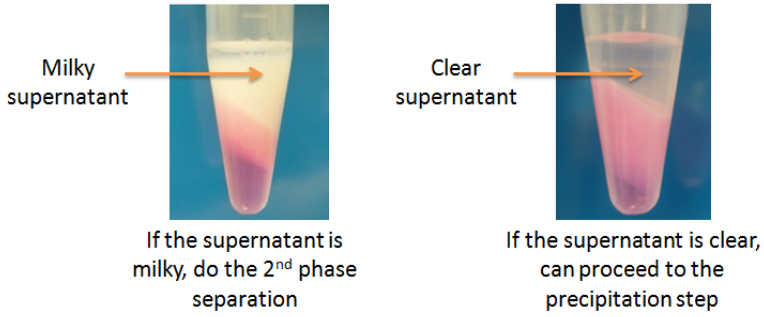


Figure 3-17 Samples after the first phase separation step. If the supernatant phase is milky, there is probably a high concentration of proteoglycan in it and it may be better to perform a second phase separation. If the supernatant phase is clear, it is better to avoid a second phase separation to avoid loss of RNA during the process. (Reproduced under a Creative Commons Attribution License from [125]).

3.8.4.3 2nd phase separation (if necessary)

1. Transfer the supernatant to new tubes
2. Add 1 ml of TRIzol and 150 µl of BCP. Shake vigorously for 15 s and stand at room temperature for 3 min
3. Centrifuge at 12,000 × g at 4 °C for 15 min

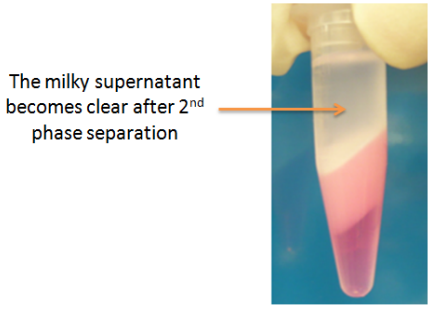


Figure 3-18 Sample after the second phase separation. The supernatant becomes clear after the second phase separation. (Reproduced under a Creative Commons Attribution License from [125]).

3.8.4.4 Precipitation with propanol and high salt solution

1. Transfer the supernatant to new tubes and mix the supernatant with 0.3 ml of high salt solution (0.8 M sodium citrate and 1.2 M NaCl) and 0.3 ml of propanol (or 125 µl of high salt solution and 125 µl of propanol if no 2nd phase separation was performed)
2. Stand at room temperature for 10 min and centrifuge at 15000 × g for 10 min

   Observation: pellets may not be easily observable at this step when the RNA quantity is low
3. Remove most of the supernatant using 1 ml pipet tips and spin down the remaining supernatant again using a mini-centrifuge, then remove the supernatant using 200 µl pipet tips as much as possible

   Note: This is to remove the proteoglycan that is present in the supernatant which will precipitate later when 75% ethanol is added, resulting in large pellets rich in proteoglycan that entrap RNA

3.8.4.5 RNA wash

1. Wash with 0.5 ml of 75% ethanol

   Observation: pellets (even though may be small) should appear at this step
2. Centrifuge at 8,000 × g at 4 °C for 3 min and remove the supernatant
3. Wash the pellets again with 0.5 ml of 75% ethanol
4. Spin and remove the supernatant
5. Dry at room temperature for 10 min

3.8.4.6 Re-dissolving the RNA

1. Add 12.5 µl of DEPC-treated water and heat at 60 °C for 10 min
2. Cool on ice. Spin down, vortex briefly and spin down
3. Measure the absorbance using Nanodrop or assess the quality through Bioanalyzer

3.8.5 Recommended protocols for extracting RNA from murine IVD tissues (tissues rich in extracellular matrix but with relatively high cellularity)

3.8.5.1 Embed the tissue in DEPC treated water

1. Prepare small aluminum containers of about 6 mm in diameter by using aluminum foil (cut it into appropriate size and form the container by wrapping around a pencil or the end of a 2 ml serological pipet)

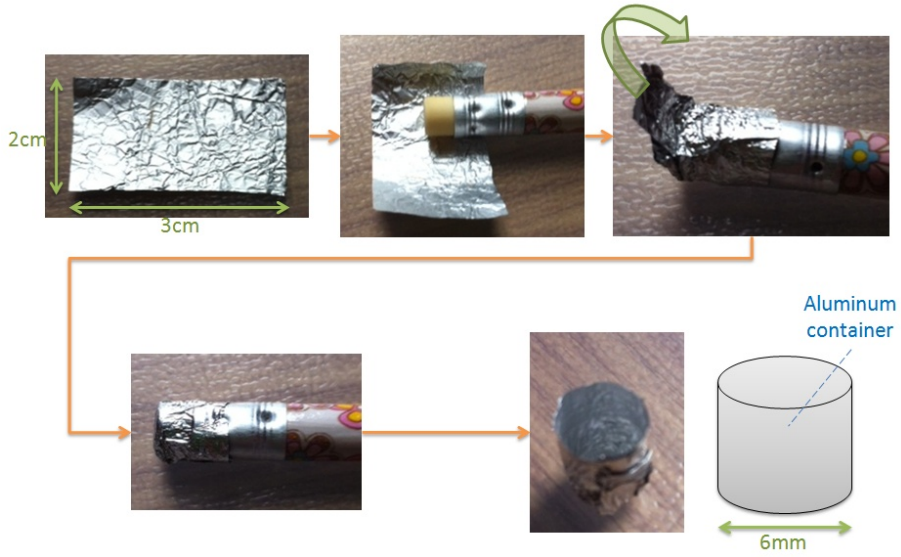


Figure 3-19 Preparation of aluminum container.

2. Add DEPC-treated water to the container
3. Dip the container with water into liquid nitrogen using forceps so that the periphery of the water is frozen while the centre remains in liquid state

   Note: Handle with care when using liquid nitrogen
4. Put the tissue in the top layer of water
5. Freeze the water with tissue completely by dipping it into liquid nitrogen using forceps
6. Remove the aluminum foil before mounting the ice block with tissue
7. Mount the ice block with tissue on the cryostat holder through the attachment of the surface opposite to the tissue

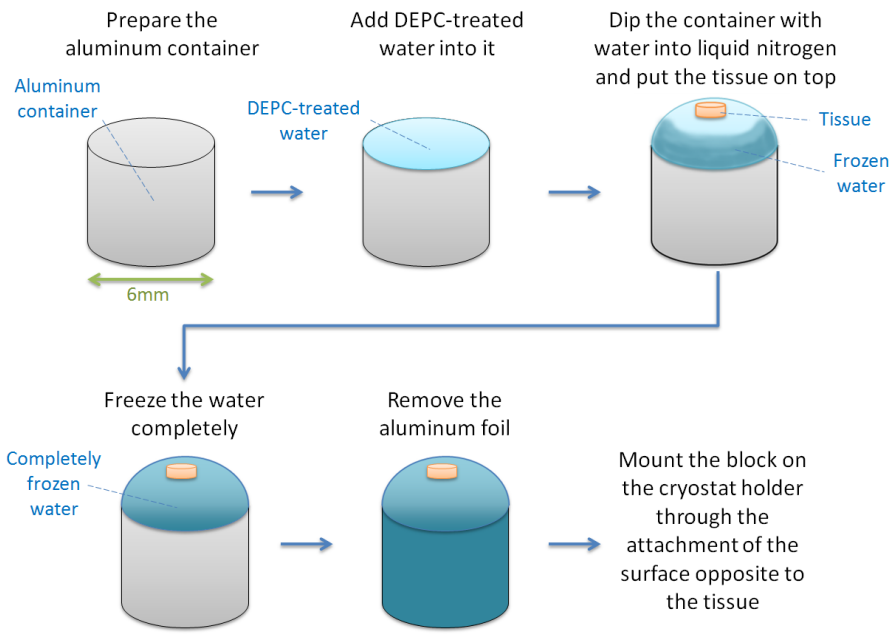


Figure 3-20 Schematic showing the flow of embedding small tissue samples in DEPC-treated water prior to cryosectioning. (Reproduced under a Creative Commons Attribution License from the supplementary information of [125]).

3.8.5.2 Cryosection the tissues and lyse the cells in TRIzol

1. Cryosection the tissues using a cryostat (10-30 µm)
2. Transfer the sections to 1.5 ml tubes (for a larger amount of tissue, the volume may be scaled up) using forceps pre-cooled in the cryostat chamber

   Note: As the thin sections melt and stick to surfaces at room temperature readily, it is important to pre-cool the tubes in the cryostat chamber. When holding the tubes, hold the cap edge to avoid warming up the tube body (Please refer to **Figure 3-16**).

3. Transfer the tubes of cryosectioned tissues to a chemical fume hood using dry ice or Mr. Frosty pre-cooled to -80 °C (or any method that can avoid the thawing of the sections inside the tubes)
4. Add 0.5 ml of TRIzol to the tubes with samples, mix well, store at -80 °C before RNA extraction

3.8.5.3 Phase separation

1. Add 50 µl of BCP to each tube with clear TRIzol lysate, shake vigorously for 15 s and stand at room temperature for 15 min
2. Centrifuge at 12000 × g for 15 min

3.8.5.4 Precipitation with propanol (and high salt solution)

1. Transfer the supernatant to new tubes. Mix with equal volume of propanol (about 200-300 µl)

   Note

   - ✧ If there were very large precipitates (>5 µl) at the end, do the precipitation step with 125 µl of propanol and 125 µl of high salt solution (0.8 M sodium citrate and 1.2 M NaCl).
   - ✧ If the RNA could hardly be seen after the precipitation and centrifugation, add 2 µl of 5 mg/ml glycogen to the sample, mix well and repeat the precipitation step.
2. Stand at room temperature for 10 min and centrifuge at 15000 × g for 10 min

3.8.5.5 RNA wash

1. Wash with 0.5 ml of 75% ethanol
2. Centrifuge at 8,000 × g at 4 °C for 3 min and remove the supernatant
3. Wash the pellets again with 0.5 ml of 75% ethanol
4. Spin and remove the supernatant
5. Dry at room temperature for 10 min

3.8.5.6 Re-dissolving the RNA

1. Add 12.5 µl of DEPC-treated and heat at 60 °C for 10 min
2. Cool on ice. Spin down, vortex briefly and spin down

3. Measure the absorbance using Nanodrop or assess the quality through Bioanalyzer

3.8.6 Technical notes

3.8.6.1 When using high salt solution

✧ When we precipitate RNA without the use of high salt solution, it is not important to remove the supernatant after the RNA precipitation step as much as possible. The supernatant remained will be miscible with the 75% ethanol to be added. However, when high salt solution is added, the miscibility with the 75% ethanol is changed. If too much supernatant (> 50 µl) is left behind, there will be two different liquid phases after mixing with 75% ethanol in the form of a bubble in the liquid. The RNA will be on the surface of the bubble and the RNA cannot be easily washed as we need to get rid of the bubble with probably salts in it but avoid removing the RNA pellet. Thus the following precautions are required:

- Remove as much supernatant as possible after the RNA precipitation step when high salt solution is used. After removing the majority of supernatant using 1 ml pipet tips, use a second quick spin with a bench top mini-centrifuge to bring all the liquid to the bottom and then remove the remaining liquid using 20 µl or 200 µl pipet tips.
- When bubbles of immiscible phase were already formed, try to remove the bubbles using pipet tips with small openings such as 20 µl of 10 µl pipet tips to minimize the chance of sucking the RNA pellets into the pipet tips.

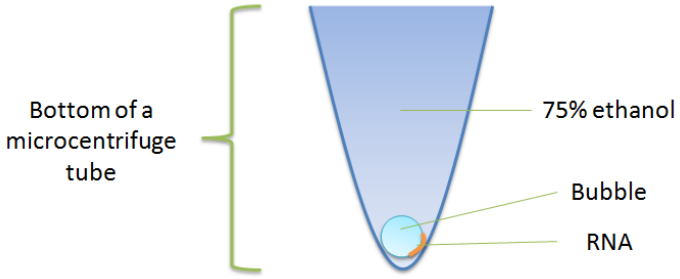


Figure 3-21 Schematic showing that a bubble may be formed after the 75% ethanol addition when the mixture of supernatant with propanol and high salt solution is not sufficiently removed. (Reproduced under a Creative Commons Attribution License from the supplementary information of [125]).

3.8.6.2 When handling small pellets

- ✧ Always make sure you can see the pellets and avoid discarding them during changes of solution. If not, add glycogen during the precipitation step so that the RNA are co-precipitated with the glycogen, making the pellets large enough to be observable
- ✧ During the 75% ethanol wash, vortexing may be required for large pellets but not desirable for small pellets as this may break the pellets into smaller pieces which increases the risk of discarding the RNA pellets during the 75% ethanol wash. Instead of vortexing, the RNA can be washed more effectively by changing the orientation of tubes which can flip the RNA during the centrifugation as illustrated in **Figure 3-22**.

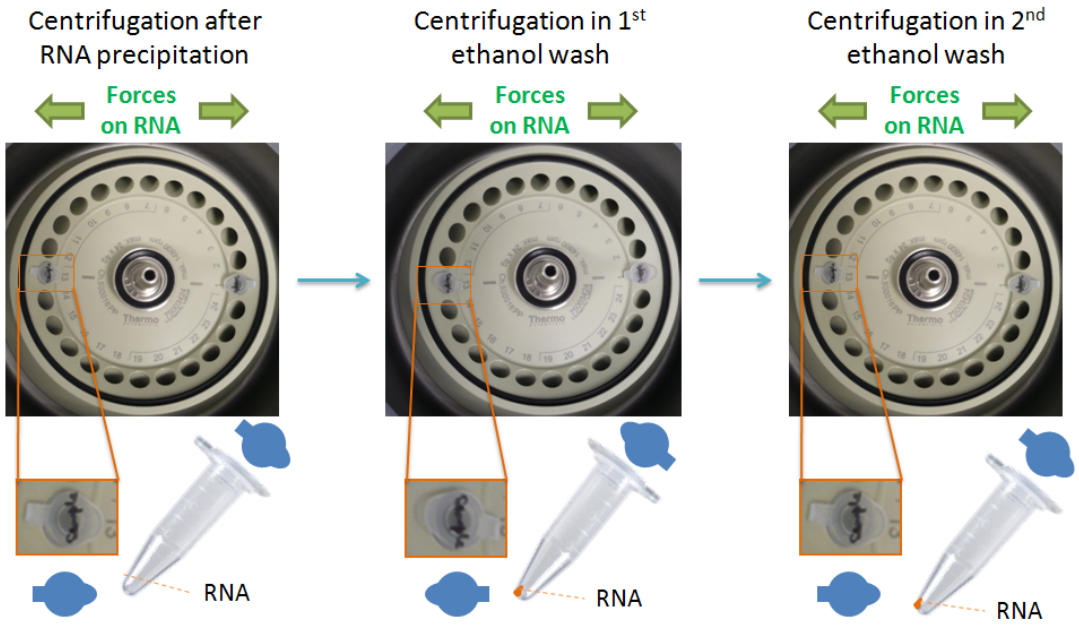


Figure 3-22 Schematic showing how the microcentrifuge tubes may be oriented during the centrifugation. (1. The orientation of the tubes is oriented that it is possible to know the position of pellets. 2. The orientation of the tubes is changed between successive centrifugation so that the pellet is flipped on to the opposite side for more effective washing.) (Reproduced under a Creative Commons Attribution License from the supplementary information of [125]).

Chapter 4 Concentration Correction for RNA with TRIzol

4.1 Introduction

Advances in the Reverse Transcription - quantitative Polymerase Chain Reaction (RT-qPCR) allowed the study of gene expression from a minute amount of RNA. In some situations, only a small number of cells is available for obtaining RNA such as cells sorted using fluorescent assisted cell sorting (FACS) [152], from tissues with a low cell density such as cartilage [153] and intervertebral disc [26] and when numerous cell culture conditions are tested with limited cell source. Some studies have suggested the yield of RNA obtained using the guanidine isothiocyanate (GITC) based method is higher than the column based method for some samples [129-132]. Besides, TRIzol (a GITC based reagent) allows the simultaneous extraction of RNA, DNA and protein from the same sample [154]. Thus sometimes GITC based method is preferred despite various RNA extraction methods available nowadays.

However, when working with samples with a small number of cells, the ultraviolet (UV) spectra of the extracted RNA showed a shift of peak absorption from 260 nm to 270 nm (**Figure 4-1A** and [152]). The peak at 270 nm was due to the trace amount of phenol remained, which became conspicuous in the spectra when the absorption contributed by the RNA was less for low concentrations. The absorption of phenol at 260 nm also caused the overestimation of RNA concentrations as the RNA concentrations are usually estimated as the absorbances at 260 nm × 40 (with units of ng/μl). In flow cytometry, the contribution of the effect of a component was subtracted from the curve in the process of compensation adjustment. By employing a similar concept, we have derived a formula to correct the overestimation of RNA concentrations due to phenol contamination. As shown in **Figure 4-1B**, TRIzol has a peak absorption at 270 nm (the green curve, iii) and thus RNA with TRIzol has a peak shift to 270 nm (the red curve, ii) when the concentration of RNA is low (the blue curve, i). By subtracting the UV absorption contributed by TRIzol, the RNA concentration without contamination can be estimated (the purple broken line curve, iv). The

corrected RNA amount provides more reliable information for the researchers to decide whether to further purify or directly use the RNA.

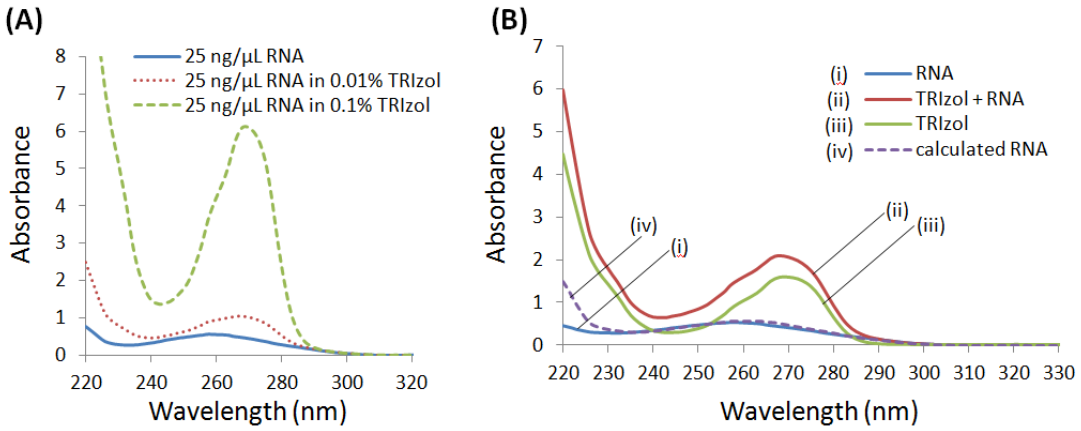


Figure 4-1 (A) The measured UV spectra of 25 ng/µl total RNA with different concentrations of TRIzol, (B) Concept of absorbance compensation due to TRIzol. The measured UV spectra of (i) RNA only, (ii) RNA with TRIzol, (iii) TRIzol only and (d) the calculated UV spectrum of RNA based on spectral data of (ii) and (iii). When RNA is contaminated with pheonol/ TRIzol, the peak of absorption is shifted from 260 nm to 270 nm (from curve i to curve ii). Curve iii shows the absorption spectrum of diluted TRIzol. By subtracting the absorption contributed by the TRIzol from the absorption spectrum of RNA contaminated with TRIzol (curve ii – curve iii), the absorption spectrum close to the spectrum without TRIzol contamination can be obtained (curve iv). (Reproduced with permission of Elsevier from [118] © 2014 Elsevier).

We hypothesize the use of the concentration correction formula can improve the accuracy of the concentration estimations.

4.2 Materials and methods

4.2.1 UV spectra

With an aim to find out the unknown parameters in the derived formula, we obtained the UV spectra of pure RNA and TRIzol of different concentrations using a Nanodrop 2000c spectrophotometer (Thermo Scientific). The data for RNA with A_{260}/A_{280} ratio within 1.85 and 2.15 were selected for the calculations and UV spectral data of 71 RNA samples ranging from 64 ng/µl to 1604 ng/µl were further computed. The UV spectral data of TRIzol solution with concentrations ranging from 0.01% to 1% (v/v) were obtained. The absorbance at 260

nm and 270 nm was extracted from the exported spectrum data and plotted as in **Figure 4-2A** and **B** to find out the values of the unknown parameters in equation (5) in **Section 4.3.1** of the Results and Discussion Section.

4.2.2 Extraction of RNA

In order to verify the formula, RNA was extracted from bovine NP cells cultured in a plastic culture dish at passage 2 as described in Chapter 2. Nanodrop was used to assess the quantity and quality of RNA. The UV spectrum showed peak absorbance at 260 nm with $A_{260}/A_{280} > 1.8$ and $A_{260}/A_{230} > 2$ (data not shown).

For RNA from human embryonic stem cells (HES2) used for Taqman gene expression assays, it was extracted using TRIzol according to the manufacturer's instruction. UV absorbance was measured using a Nanodrop 2000c spectrophotometer (Thermo Scientific).

4.2.3 RT-qPCR

Total RNA was reverse transcribed into cDNA using PrimeScript RT Master Mix (Takara, catalog # HRR036A) using a thermocycler (Applied Biosystems, Veriti 96 well thermocycler). The cDNA was diluted five times by adding ultraPure distilled water (Invitrogen, catalog # 10977-023).

For qPCR using SYBR green, it was performed with a total reaction volume of 10 µl per reaction, containing 1 µl of single stranded cDNA, 5 µl of SYBR Green PCR Master Mix (Applied Biosystems, part # 4309155) and 500 nM each of forward primer and reverse primer (*GAPDH* and *ACAN* from [113]), in 96 well reaction plates using a standard PCR protocol for SYBR green reactions (Applied Biosystems, StepOnePlus) with a melt curve analysis. The relative gene expression was calculated based on comparative Ct method.

For qPCR using Taqman gene expression assays, it was performed with a total reaction volume of 10 µl using Taqman Gene expression Master Mix (Applied Biosystems, part # 4369016) and Taqman Gene Expression Assays (assay ID: Hs02758991_g1 for *GAPDH*, Hs00164004_m1 for *COL1A1*, Hs00264051_m1 for *COL2A1*, Hs00983056_m1 for *CDH2*), in 96 well reaction plates using standard PCR protocol for Taqman assays. The relative gene expression was calculated based on comparative Ct method. The relative gene expression was calculated based on comparative Ct method.

4.3 Results and Discussion

4.3.1 Derivation of the concentration correction formula

The correction formula of concentration for RNA contaminated with TRIzol was derived as follows:

Let A be the measured absorbance in Nanodrop at 260 nm

Let B be the measured absorbance in Nanodrop at 270 nm

Let a be the absorbance at 260 nm contributed by RNA

Let b be the absorbance at 270 nm contributed by phenol/ TRIzol

Let x be the ratio of absorbance at 270 nm/ absorbance at 260 nm for RNA

Let y be the ratio of absorbance at 260 nm/ absorbance at 270 nm for phenol/ TRIzol

$$a + by = A \quad (1)$$

$$ax + b = B \quad (2)$$

By solving the above equations, then

$$a = (A - By) / (1 - xy) \quad (3)$$

$$\text{Phenol level index (PLI)} = b = (Ax - B)/ (xy - 1) \quad (4)$$

$$\text{Corrected RNA concentration} = a \times 40 \text{ (ng/µl)}$$

$$= (A - By) / (1 - xy) \times 40 \text{ (ng/µl)} \quad (5)$$

A and B can be obtained from the spectral data of the samples while x and y can be found by obtaining the spectral data of RNA and phenol/ TRIzol. From **Figure 4-2**, x and y in equation (5) were found to be 0.814 and 0.670 respectively. Thus the derived formula became:

Corrected concentration (ng/ µl) = (A260 – 0.670 × A270) / 0.455 × 40 (6)

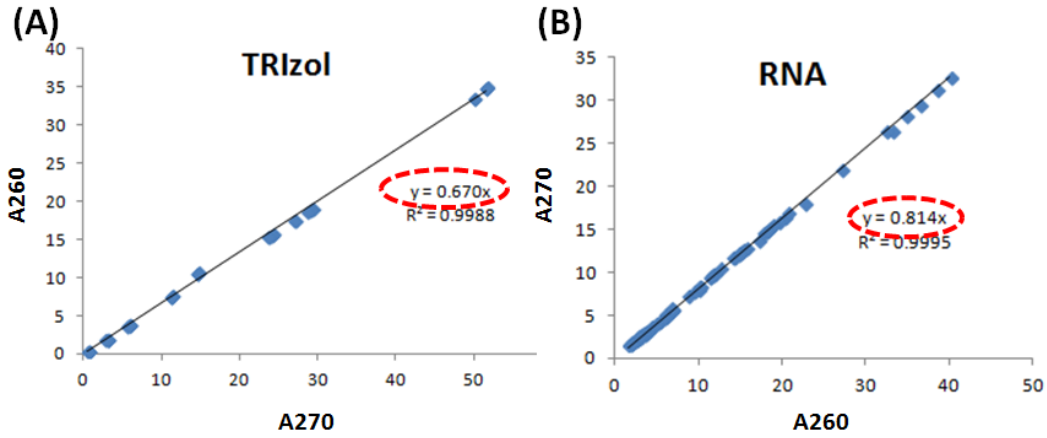


Figure 4-2 (A) Plot of A_{260} vs A_{270} of TRIzol solution of different concentrations and (B) Plot of A_{270} vs A_{260} of RNA solution of different concentrations. The parameter "y" in equation (5) was found to be 0.670. The parameter "x" in equation (5) was found to be 0.814. (71 RNA samples ranging from 64 to 1604 ng/µl were used in plot (A) and 42 TRIzol samples with concentrations ranging from 0.01 to 1% were used in plot (B))(Reproduced with permission of Elsevier from [118] © 2014 Elsevier).

4.3.2 Electrophoregrams of RNA with TRIzol

When TRIzol was added to the RNA solution, there was a shift in the peak towards 270 nm in the UV spectrum as shown in **Figure 4-1A**. In contrast, the electrophoregrams obtained using an Agilent 2100 bioanalyzer did not change much with the addition of TRIzol (**Figure 4-3**), indicating the presence of the RNA in all the samples.

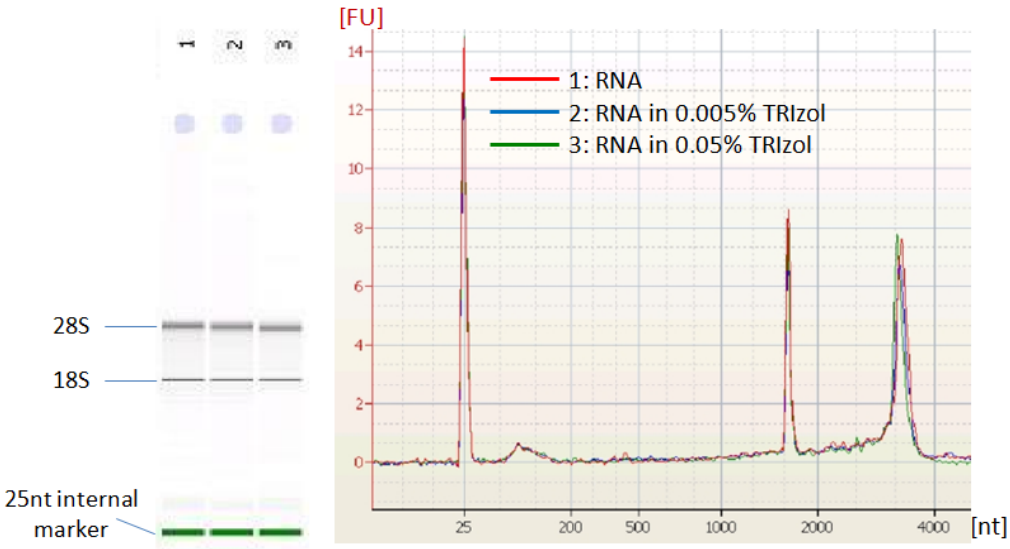


Figure 4-3 Electropherograms of RNA without and with TRIzol contamination (0.005% and 0.05%) obtained by Agilent 2100 bioanalyzer. With 0.05% TRIzol contamination in RNA solution at 25 ng/µl, the electropherogram was not significantly altered. (Reproduced with permission of Elsevier from [118] © 2014 Elsevier).

4.3.3 Testing of the concentration correction formula

The correction formula (6) derived in Section 4.3.1 was tested with 25 ng/µl and 50 ng/µl RNA in 0%, 0.01%, 0.1% and 1% TRIzol. The % derivation of RNA concentration was greatly reduced after the correction (**Table 4-1**).

Table 4-1 The concentration estimated by Nanodrop UV spectrometry before and after correction using the derived formula (6) for RNA solution with different concentrations of TRIzol. The phenol level index (PLI) was also computed based on the formula (7) with details given in the next Section. (n=3 measurements) (Reproduced with permission of Elsevier from [118] © 2014 Elsevier).

	measured conc. (ng/uL)	corrected conc. (ng/uL)	% deviation before corr.	% deviation after corr.	PLI
25ng/µl, 0% TRIzol	22.8 ± 0.5	22.5 ± 0.6	/	-1% ± 3%	0.01 ± 0.01
25ng/µl, 0.01% TRIzol	37.4 ± 0.5	22.8 ± 0.3	64% ± 2%	0% ± 1%	0.55 ± 0.01
25ng/µl, 0.1% TRIzol	169.0 ± 0.3	11.3 ± 0.3	642% ± 1%	-50% ± 2%	5.88 ± 0.01
25ng/µl, 1% TRIzol	1392.7 ± 2.1	43.9 ± 5.9	6015% ± 9%	93% ± 26%	50.33 ± 0.16
50ng/µl, 0% TRIzol	45.8 ± 0.2	45.4 ± 0.3	/	-1% ± 1%	0.02 ± 0.01
50ng/µl, 0.01% TRIzol	62.5 ± 0.3	46.4 ± 0.3	36% ± 1%	1% ± 1%	0.60 ± 0.00
50ng/µl, 0.1% TRIzol	188.7 ± 0.5	32.6 ± 0.3	312% ± 1%	-29% ± 1%	5.82 ± 0.01
50ng/µl, 1% TRIzol	1432.8 ± 4.1	73.6 ± 3.9	3026% ± 9%	61% ± 8%	50.72 ± 0.02

4.3.4 Phenol level index (PLI)

An index, phenol level index (PLI) was introduced to indicate the level of phenol contamination and computed using the following formula:

$$PLI = b = - (0.814 \times A_{260} - A_{270}) / 0.455 \quad (7)$$

RNA solution with 0.1% TRIzol contamination has PLI of about 5.8 (**Table 4-1**). The PLI increased with the concentrations of TRIzol independent of the RNA concentrations (**Table 4-1**). This index can be calculated based on sample spectral data and provides information about the level of contamination as it is unknown in the samples of most studies.

4.3.5 Effect of contaminants on RT-qPCR

Though phenol was suggested to reduce the efficiency of PCR, a very low concentration of contamination may be tolerated in some applications. Some relatively new kit such as the Ambion® Cell-to-CT kit allows the reverse transcription of RNA and the subsequent amplification of cDNA without the RNA purification step, implying it is not an absolute necessity to obtain pure RNA for the downstream enzymatic reactions. Hence, we also assessed the level of contamination which can be tolerated for the RT-qPCR application. In this study, the effect of different degrees of contaminants was assessed using SYBR green PCR. There is no significant difference in the Ct values obtained for TRIzol contamination up to 0.1% for *GAPDH* and *ACAN* ($p > 0.10$) (**Table 4-2**). For 1% TRIzol, there is an increase of 2.1 cycles for *GAPDH* and 2.7 cycles for *ACAN* compared to RNA without contamination.

Table 4-2 Ct values of RT-qPCR of total RNA with different concentrations of TRIzol (mean ± SD, 5 samples per group with technical duplicates from 3 independent experiments, RT was performed with reagents from Takara and qPCR was performed with SYBR green reagents from Applied Biosystems using StepOnePlus). (Reproduced with permission of Elsevier from [118] © 2014 Elsevier).

	GAPDH	*ACAN*
0% TRIzol	18.8 ± 0.2	22.7 ± 0.4
0.01% TRIzol	18.8 ± 0.2	22.8 ± 0.5
0.1% TRIzol	18.8 ± 0.2	22.9 ± 0.4
1% TRIzol	20.9 ± 1.5	25.4 ± 1.2

4.3.6 Taqman gene expression assay using RNA extracted with TRIzol

Taqman based assays may have different tolerance to contaminants compared to SYBR green. Parissenti *et al.* could detect amplifications using SYBR green assay with TRIzol RNA extraction method but inconsistent or no amplification was detected for Taqman assays using TRIzol extracted RNA [155]. In our lab, amplifications were detected for TRIzol extracted RNA using our RT-qPCR system except for RNA of very low concentrations or poor quality. Amplification was detected for the HES2 cell sample of good RNA quality as shown in **Table 4-3** and **Figure 4-4**. There were also a number of studies by other groups using Taqman based gene expression analysis with RNA extracted with TRIzol reagent [156-162] or TRIzol LS reagent [162]. These indicate Taqman assays can be compatible with TRIzol extracted RNA for our systems and the systems used by some other groups. Nevertheless, it may be inappropriate to generalize this for all systems based on the study by Parissenti *et al.* and it is recommended to have a preliminary test about the compatibility before large scale experiments.

Table 4-3 Concentration and quality of RNA from HES2 cells extracted using TRIzol. The RNA was of rather high concentration (> 1 μg/μl) with A_{260}/A_{280} close to 2 and A_{260}/A_{230} > 2, indicating the quality of RNA was good. (Reproduced with permission of Elsevier from the supplementary data of [118] © 2014 Elsevier).

	ng/μl	A_{260}/A_{280}	A_{260}/A_{230}
HES2	1334.5	1.95	2.22

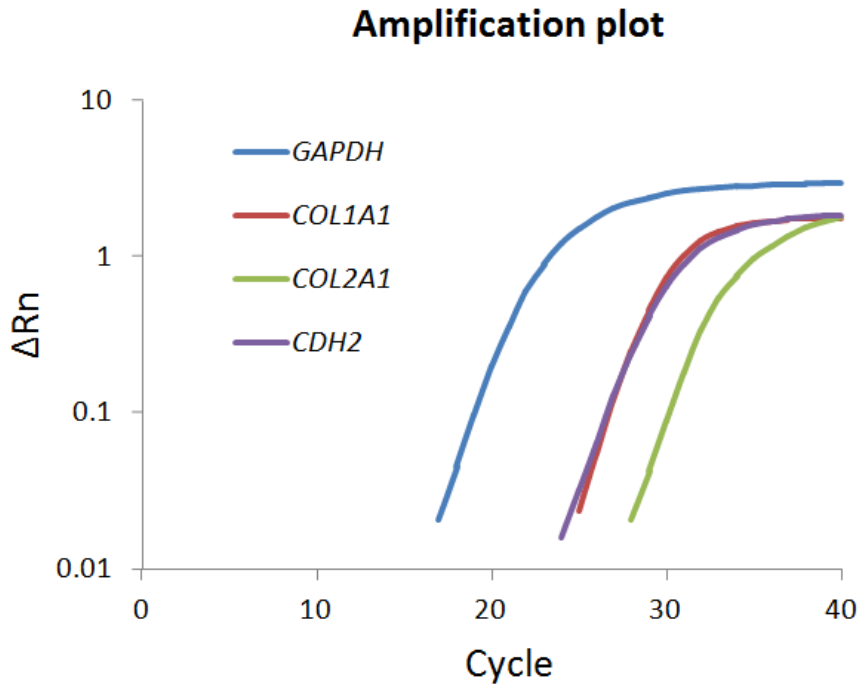


Figure 4-4 Amplification plot in RT-qPCR of RNA extracted using TRIzol. (Cells: HES2; qPCR system: Taqman gene expression assays from Life Technologies, assay ID: Hs02758991_g1 for *GAPDH*, Hs00164004_m1 for *COL1A1*, Hs00264051_m1 for *COL2A1*, Hs00983056_m1 for *CDH2*; ΔR values smaller than 0.01 were not shown in the plot). (Reproduced with permission of Elsevier from the supplementary data of [118] © 2014 Elsevier).

4.4 Conclusions

The proposed method enhanced the accuracy of the estimated RNA concentrations from UV spectrometry (from 64% and 642% deviation to 0% to -50% deviation for 25 ng/µl RNA in 0.01% and 0.1% TRIzol respectively). We recommend this method to be used when determining the concentrations and quality of RNA to decide whether further purification is worthwhile or whether the RNA can be used directly. It is best to obtain high quality RNA for reliable result but there is need to make the best use of RNA of slightly poorer quality in certain instances when other limitations have restricted the availability of high quality RNA at a sufficient yield. Real time-PCR with SYBR green was performed to assess the level of TRIzol contamination that can be tolerated for gene expression quantification. There is no significant difference in the Ct values obtained for RNA contaminated with up to 0.1% TRIzol

(phenol level index, PLI ~5.6) for *GAPDH* and *ACAN* genes under test. We introduced an index for phenol contamination (the phenol level index, PLI). This allows a better assessment of the suitability of RNA for RT-qPCR application when a very minute contamination with phenol can be tolerated. From our data, it is justified to use RNA with PLI < 0.5 for RT-qPCR application but it is advisable to test the performance in individual systems for reliable conclusions.

Chapter 5 Isolation and Culturing of MSCs for Chondrogenic / Discogenic Studies

5.1 Introduction

5.1.1 Use of mesenchymal stem cells (MSCs) in IVD regeneration

One of the regenerative strategies in IVD under research is injection of mesenchymal stem cells (MSCs) into the discs in order to restore disc height and disc function [163-165]. In mild degenerated discs, chemicals or growth factors may be applied to stimulate the matrix production by the native NP cells to restore the disc function. However, in more degenerated discs, the health status of native NP cells may not be good and autogenic or allogenic sources of NP cells are not readily available and this makes MSCs an attractive candidate in IVD regeneration due to their proliferative and differentiation potential and comparative ease of availability in a sufficient number.

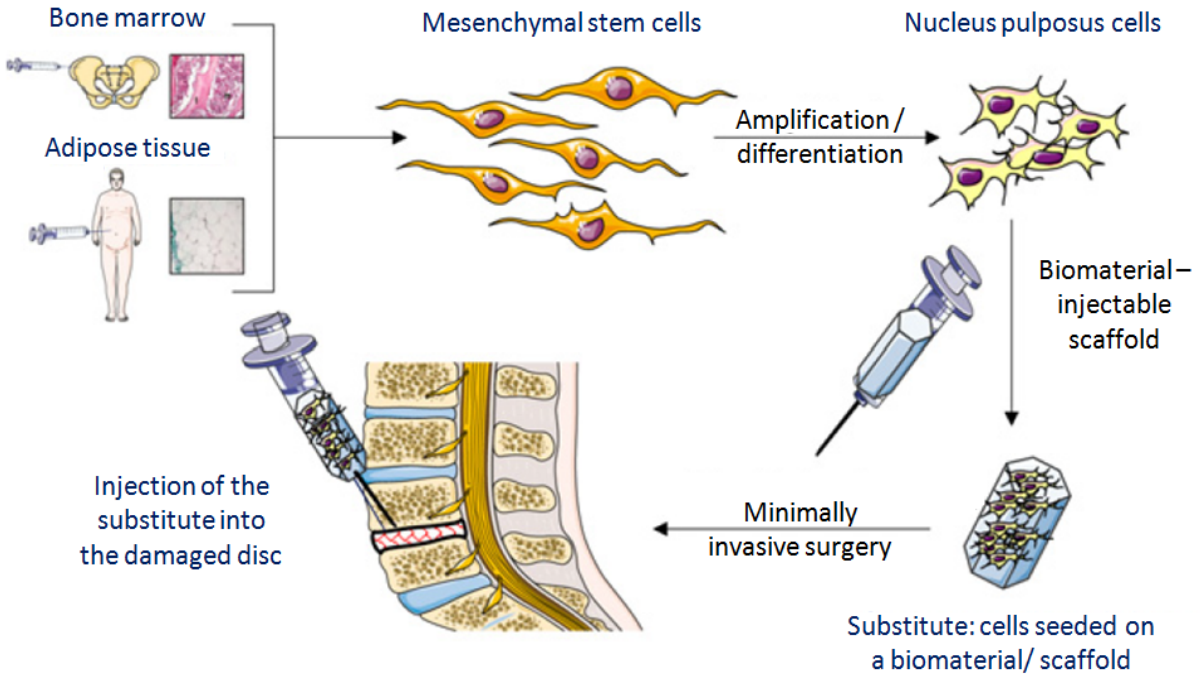


Figure 5-1 Intervertebral disc tissue engineering procedures based on mesenchymal stem cells (MSCs). MSCs are collected from the bone marrow or adipose tissue, amplified *in vitro*, and cultured with various factors to produce cells of NP phenotype. The cells are then seeded on a biomaterial, and the

substitute thus obtained is implanted into the damaged disc. (Reproduced from [1] Copyright © 2009 Elsevier Masson SAS. All rights reserved).

5.1.2 MSC isolation techniques

In research, MSCs from different species were used. The commonly used sources are from human [60, 90, 166, 167], rabbit [168], rat [169] and mouse [170, 171]. There are a number of MSC isolation methods and the method based on the ability of the MSCs to selectively adhere to plastic surfaces is the most common one.

A variety of sources have been explored for the isolation of MSCs from human. Bone marrow is one of the most widely used sources used in IVD studies [60, 90, 166]. Mesenchymal progenitor cells were also identified from other sources [172] such as muscle [173], bone [174-178], tendon [179, 180], adipose tissue [181-186], blood vessels [187], umbilical cord [188, 189] and umbilical cord blood/ stroma [190, 191].

For harvesting MSCs from other species such as rabbit, rat and mouse, the animals were killed and the tibia and/ or femurs were obtained [168-170]. Then the marrow inside these bones was flushed out. MSCs were further cultured based on their plastic adherence properties. Sometimes, the harvesting of the MSCs from large animals is similar to that of human if sufficient bone marrow can be harvested without killing the animals.

5.1.3 Validation of MSC properties

The identification of MSCs is achieved through their ability to adhere to plastic *in vitro*, through a combination of positive expression or distinct lack of defined cell surface markers and also through their multilineage differentiation potential *in vitro* [192]. MSCs were often characterized phenotypically by flow cytometry and suggested to be positive for CD29, CD44, CD105, CD73, CD166, and Sca-1, and negative for CD11b, CD14, CD31 and CD45 [193]. Nevertheless, the lack of specific markers renders the characterization of MSCs difficult and sometimes ambiguous [193]. Besides flow cytometry, the multipotent property of MSCs was

also used to give information about the identity of the harvested cells. MSCs differ from other differentiated cells that they can be differentiated into different cell types of the mesenchyme origin. Osteogenesis, adipogenesis and chondrogenesis assays are the widely used differentiation assays to test the multipotent properties of MSCs [170, 171, 176, 177, 187, 190].

5.1.4 Culture conditions of MSCs during expansion and differentiation

Different culture conditions were tested in this Chapter. These conditions have been used in studies by other groups. Hypoxia promoted chondrogenesis in rat MSCs [194] and human MSCs [195]. Treatment with basic fibroblast growth factor (FGF-2) during MSC expansion could inhibit the differentiation of MSCs [196, 197]. FGF-2 used in cell expansion enhanced the chondrogenic differentiation of MSCs in low glucose DMEM [198]. FGF-2 and parathyroid hormone-related protein (PTHrP) were also reported to be potent inhibitors for early and late chondrogenic differentiation in contrast to bone morphogenetic proteins (BMPs) [199].

For pathway inhibition, inhibiting p38 mitogen-activated protein kinase (MAPK) in rabbit NP cells increased mRNA for matrix proteins (aggrecan, collagen II, versican, collagen I) and anabolic factors (IGF-1, TGF, and SOX9) while decreased basal prostaglandin E2 (PGE-2) accumulation, but had no effect on message for TIMP-1, MMP-3, or cycloxygenase-2 (COX-2) [200]. Expression of collagen II and aggrecan was elevated when rat MSCs were inhibited by PD98059, an extracellular-signal-regulated kinase (ERK) inhibitor, during stimulation with TGF-β1 [201]. Further information about hypoxia and MAPK pathway was described in the **Sections 5.7.1** to **5.7.3** in the Appendix of this Chapter.

We hypothesize that the chondrogenic potential is influenced by cell sources and culturing conditions.

5.2 Objectives

The objectives of experiments in this Chapter is to understand the platform with associated techniques for the study of MSC differentiation into chondrocytes. Experiments were performed and can be categorized into two major categories: (1) the sources of MSCs and (2) the culture conditions of MSCs as represented and explained in **Figure 5-2**.

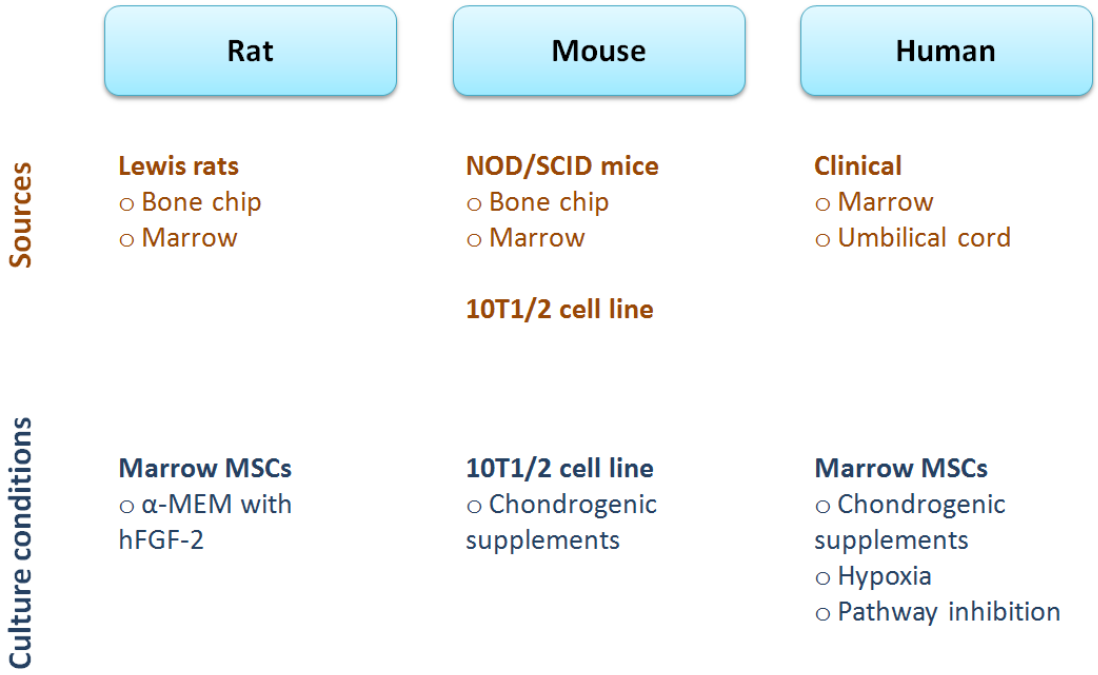


Figure 5-2 Experiments involved in Chapter 5. The choices of MSC sources under test were mainly based on availability in our laboratory. Lewis rats were initially used for isolating MSCs due to its relative easy availability as laboratory animals in many institutes. However, the MSCs isolated from Lewis rats did not show strong chondrogenic potential. Thus we tested the MSCs from NOD/SCID mice which were also readily available in our laboratory. The mouse 10T1/2 cell line was used as it was reported to have MSC properties. In our department, MSCs from patients were also possible. Hence we also tested human MSCs.

5.2.1 The sources of MSCs

Different sources of MSCs which were available in our group were investigated and listed below:

- Bone marrow and cortical bones of Lewis rats
- Bone marrow and cortical bones of NOD/SCID immunodeficient mice
- Bone marrow and umbilical cord of human

- Mouse cell line C3H/10T1/2

Since NP cells in adult human are chondrocyte like, the chondrogenic potential was focused in the characterization of the MSCs. Due to the availability of mouse MSC markers, flow cytometry was also done for the MSCs from the immunodeficient NOD/SCID mice.

5.2.2 The culture conditions of MSC

The following culture conditions were tested:

- the use of α-MEM with human FGF-2 (hFGF-2) in culturing rat MSCs
- the effect of dexamethasone, sodium ascorbate and TGF-β1 on human MSCs and C3H10T1/2 cells
- the effect of hypoxia on human MSC pellets
- the effect of p38 and MEK inhibition on MSC chondrogenic differentiation

5.3 Materials and Methods

5.3.1 Rats used in MSC harvest

Rat MSCs were harvested from Lewis rats maintained by the Laboratory Animal Unit of the University of Hong Kong. The experimental protocol was approved by the Committee of the Use of Live Animals in Teaching and Research, the University of Hong Kong (CULATR Ref. No.: 2202-10). Additional rats were also kindly provided by Dr. Jacqueline Lim or Miss Karen Kwan after being sacrificed for collections of other tissues. The MSCs were harvested within 1-2 h after the killing of the animals.

5.3.2 Harvest of rat MSCs from bone marrow

The Lewis rats were euthanized through intraperitoneal injection of sodium pentobarbitone. Tibia and femur were collected and placed in a 50 ml tube with DMEM (Gibco, catalog # 12100-046) with 10% (v/v) FBS (Biosera, catalog # FB-1001/500) kept on ice (the condyli was kept intact). Then the bones were transferred to a biosafety cabinet (BSC) for cell harvest. Briefly, the condyli was cut away and bone marrow was flushed from femurs and tibias with 5

ml of DMEM with 10% (v/v) FBS using a 5 ml syringe with a 19G needle into 10 cm dishes. The bone was flushed until marrow became white. The clumps were dispersed by drawing the marrow in and out of the syringe through needle. The cell suspension was collected into a 15 ml tube. It was centrifuged at 600 × g for 5 min to collect cells. The cells were resuspended in 5 ml of DMEM with 10% (v/v) FBS, 1% (v/v) Penicillin-Streptomycin (Gibco, catalog # 15140) and 0.4% (v/v) Fungizone Antimycotic (Gibco, catalog # 15290-018).

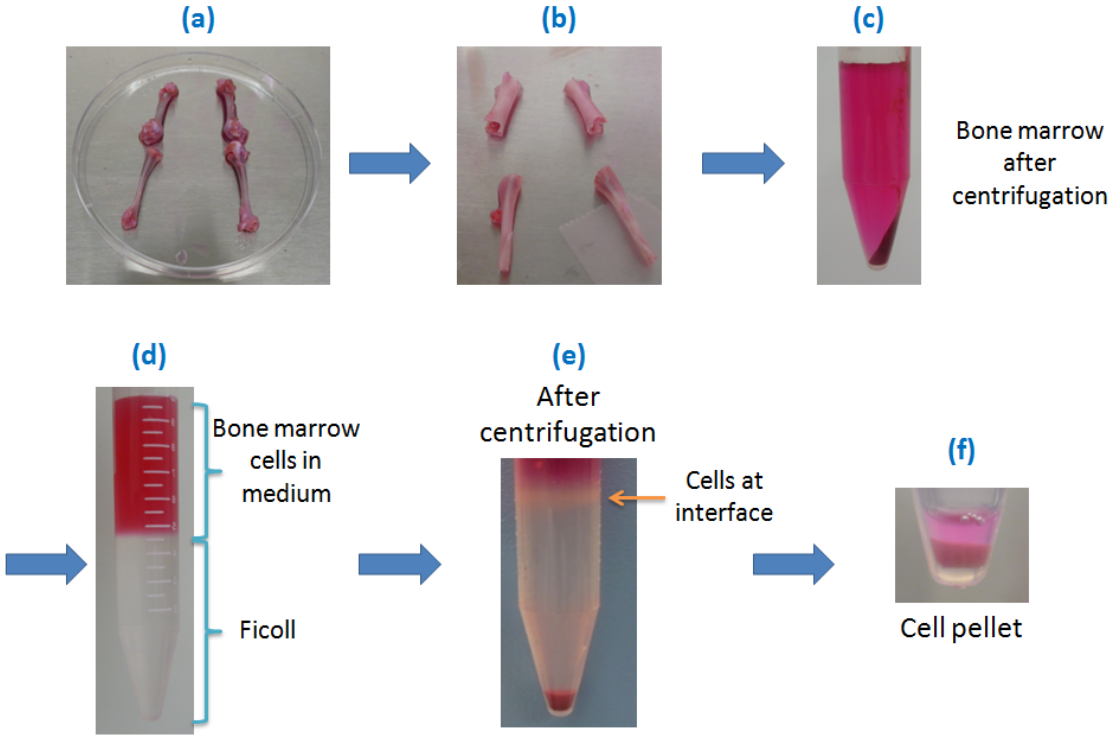


Figure 5-3 Isolation of rat MSCs from bone marrow with cell separation using Ficoll. (a) Femurs and tibias were collected from rats. (b) The condyli was cut away and bone marrow was flushed from femurs and tibias using a syringe and culture medium. (c) The collected bone marrow was centrifuged to collect the cell pellets. (d) The re-suspended bone marrow was overlaid on a Ficoll solution. (e) The mononuclear cells were at the interface of the medium and the Ficoll solution after centrifugation without using brake for deceleration. (f) The cell pellet collected after collecting the cells at the interface with subsequent re-suspension and centrifugation.

5.3.3 Culture of rat MSCs using α-MEM with hFGF-2

In our study, we used α-MEM with hFGF-2 for the culturing of human MSCs and did not observe flattening of cells. We speculated that α-MEM with hFGF-2 may maintain the differentiation potentials of MSCs, thus we tried to culture rat MSCs in α-MEM (Gibco,

catalog # 11900-024) with 15% (v/v) FBS, 1% (v/v) Penicillin-Streptomycin, 0.1% (v/v) Fungizone Antimycotic and 0.5 ng/ml hFGF-2 recombinant protein (eBioscience, catalog # 14-8986-62). Photos of cells were captured using a phase contrast microscope (Leica DM IL).

5.3.4 Harvest of rat MSCs using bone chip method

MSCs were harvested using the bone chip method adapted from the isolation of MSCs from mouse [170] within 1-2 h after the killing of the rats. In brief, the tibias and femurs were collected from the rats and placed in a 50 ml tube with full DMEM kept on ice (the condyli was kept intact). Then the bones were transferred to a biosafety cabinet for cell harvest. Briefly, the condyli was cut away and bone marrow was flushed from femurs and tibias with 5 ml of DMEM with 10% (v/v) FBS using a 5 ml syringe with a 19G needle into 10 cm dishes. The bone was flushed until marrow became white. The bone was cut into pieces and digested with 0.1% (w/v) collagenase type 2 (Worthington) at 37 ˚C with shaking for 1 h. The bone chips were then washed three times with PBS and the bone chips were then placed in a 10 cm cell culture dish with 10 ml of DMEM with 10% (v/v) FBS.

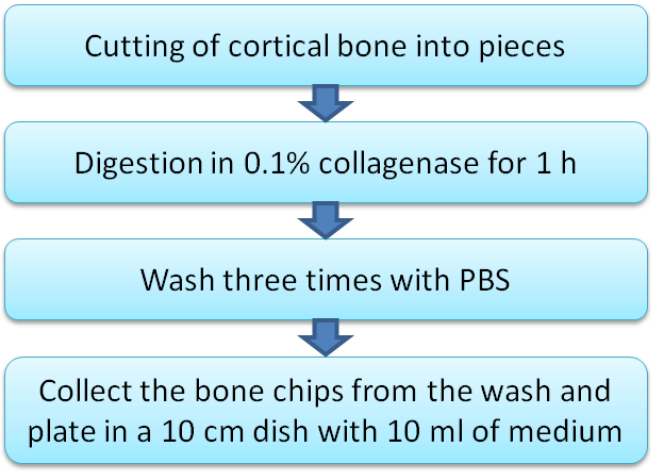


Figure 5-4 Procedures of MSC isolation from rats using the bone chip method.

5.3.5 Mouse MSC isolation, culturing and flow cytometry

Some dead immunodeficient mice (NOD/SCID mice, nude mice) were kindly provided by Dr.

Vivian Tam after sacrifice of her mice and collections of the IVD samples (with the associated experimental protocol approved by the Committee of the Use of Live Animals in Teaching and Research, the University of Hong Kong). MSCs from NOD/SCID mice were harvested within 1-2 h after the killing of the animals. MSCs were harvested from the bone marrow [171] and the bone [170]. The harvested cells were cultured in DMEM with 10% (v/v) FBS, 1% (v/v) Penicillin-Streptomycin and 0.4% (v/v) Fungizone Antimycotic. At passage 4, the cells were detached using 1.5 ml of accutase (Gibco, catalog # A11105-01) with incubation at 37 °C for 5-10 min. 1 ml of DMEM with 10% (v/v) FBS was then added to the cell suspension and the cell suspension was centrifuged at 500 × g for 4 min. The cells were washed twice with 1% (w/v) bovine serum albumin (BSA, Sigma-Aldich, catalog # A7906) in PBS with 0.1% (w/v) sodium azide (Sigma-Aldich, catalog # S2002) and then re-suspended in 1% (w/v) BSA in PBS with 0.1% (w/v) sodium azide. Antibodies were added to the cell suspension in 1:200 dilution (CD44, abcam catalog # ab25064; VCAM/ CD106, abcam catalog # ab25452; CD11b, abcam catalog # ab25507; CD45, abcam catalog # ab82408; CD29, eBioscience catalog # 17-0291). Immediately before the measurements, the cells were filtered using 70 μm cell strainers into FACS tubes and flow cytometry was performed using a BD LSR Fortessa analyzer.

5.3.6 Human MSC isolation and culturing

Human bone marrow samples were obtained from patients undergoing spinal fusion and transferred in ice. The study was carried out with the approval from the Institutional Review Board of the University of Hong Kong/ Hospital Authority Hong Kong West Cluster (IRB # UW12-346) with consents from the patients. Information about the donors was given in **Table 5-1**. The marrow was diluted 5 times with 1× Hank's Balanced Salt Solution (HBSS) which was then laid on top of Ficoll (Ficoll-Paque PLUS, GE Healthcare Life Sciences, product code 17-1440-02) with minimal perturbation. The tubes were centrifuged at 500 × g for 30 min at 4 °C without using a brake during deceleration. The upper layer was removed and the

interface was collected and transferred into another tube. The cells in the interface was then diluted with medium and centrifuged at 500 × g for 5 min at room temperature. The supernatant was removed and the pellet was re-suspended in 10 ml of α-MEM. The centrifugation and re-suspension steps were repeated once and the cell suspension was transferred to plastic culture dishes and incubated at 37 ˚C with 5% CO_2. Cells were cultured with α-MEM with 15% (v/v) FBS, 1% (v/v) Penicillin-Streptomycin, 0.1% (v/v) Fungizone Antimycotic and 0.5 ng/ml hFGF-2 recombinant protein. The use of FGF-2 during MSC expansion improves the chondrogenic potential in the study by Hagmann *et al.* [198]. They used 10 ng/ml of FGF-2. In our group, a lower concentration of 0.5 ng/ml has maintained the chondrogenic potential of hMSC. Thus we used 0.5 ng/ml instead.

Human umbilical cord MSCs were kindly given by Dr. Fengjuan Lv in the form a tube of frozen stock at passage 4.

Table 5-1 List of donors for MSCs involved in this study

Donor	Gender	Age	Medical conditions
1	F	12	Adolescent idiopathic scoliosis
2	F	49	L4/5 degenerative spondylolisthesis
3	M	16	Adolescent idiopathic scoliosis
4	F	12	Adolescent idiopathic scoliosis
5	F	15	Adolescent idiopathic scoliosis
6	M	19	Adolescent idiopathic scoliosis
7	F	22	Adolescent idiopathic scoliosis
8	F	14	Adolescent idiopathic scoliosis

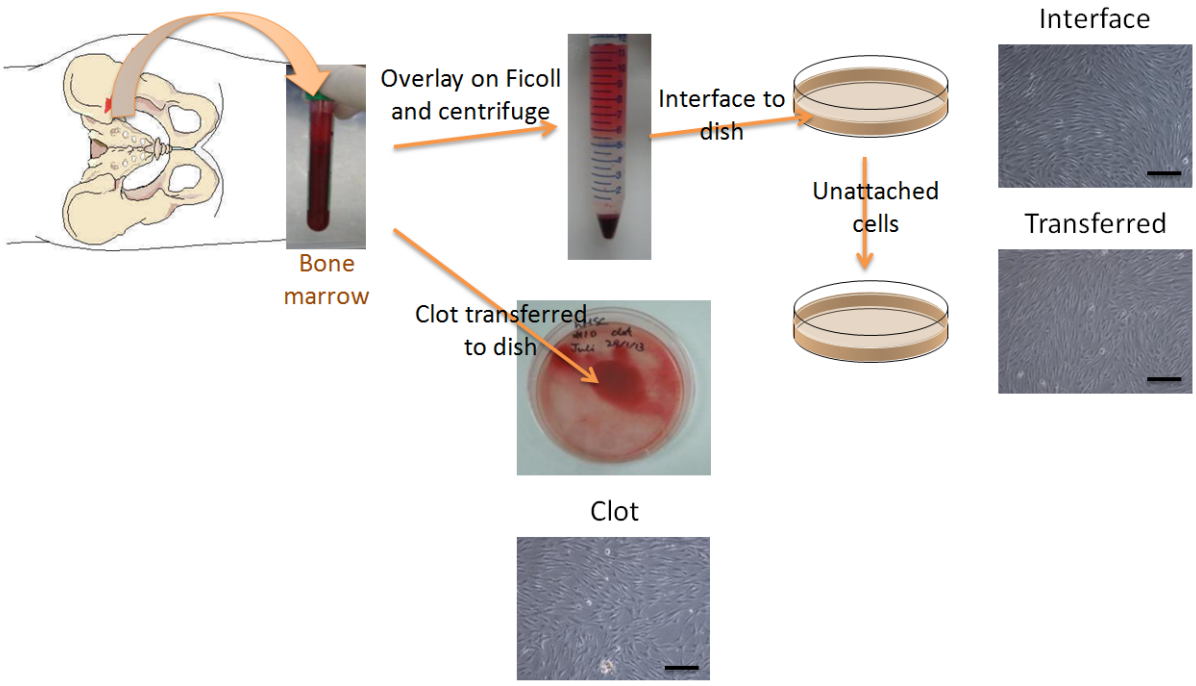


Figure 5-5 Schematic showing MSCs obtained from different portions of human bone marrow. Human bone marrow was collected from iliac crest of patients undergoing spinal fusion. The bone marrow was diluted with 1× HBSS solution and then overlaid on Ficoll. The tube of cells was centrifuged and the interface cells were washed and transferred to a cell culture dish. After 2-3 days, the medium was transferred to a new dish (labeled as "Transferred") and fresh medium was added to the original dish. The clot (if any) in the collected bone marrow was transferred to a dish with cell culture medium (labeled as "Clot"). The dishes of cells were put in a 37 °C incubator with 5% CO_2. (Scale bar = 200 μm).

5.3.7 Adipogenic and osteogenic differientiation of human MSCs

The adipogenic and osteogenic potential of human MSCs were checked using StemPro® Adipogenesis Differentiation Kit (Gibco, catalog # A10070-01) and StemPro® Osteogenesis Differentiation Kit (Gibco, catalog # A10072-01) respectively according to the manufacturer's instruction. In brief, MSCs were plated at 1×10^4 cells or 2×10^4 cells per well of a 24 well plate for differentiation check in 0.5 ml of DMEM of low glucose with 10% (v/v) FBS or adipogenic/ osteogenic differentiation medium prepared with the kits. The cells were incubated at 37 °C and 5% CO_2 for two to three weeks before staining.

5.3.8 Oil Red O staining (for adipogenesis)

Oil Red O powder was purchased from Sigma-Aldich (catalog # O0625). Oil Red O working solution was prepared by diluting the stock solution (0.25 g of Oil Red O powder in 100 ml of isopropanol) by mixing 3 parts of stock solution to 2 parts of nanopure water, followed by filtering after 10 min. Cells were fixed using 4% (w/v) paraformaldehyde (PFA, Sigma, catalog # P6148) and then washed with PBS. The fixed cells were washed twice with 60% (v/v) propanol at room temperature. 0.5 ml of Oil Red O working solution was added to each well of a 24 well plate. The cells were washed with nanopure water after 10 min. Photos were taken using an inverted microscope with phase contrast setting (Leica DM IL).

5.3.9 Alizarin Red S staining (for osteogenesis)

Alizarin Red S powder was purchased from Sigma-Aldich (catalog # A5533). Cells were fixed using 4% (w/v) PFA and then washed twice with nanopure water. The fixed cells were stained with 2% (w/v) Alizarin Red S solution (pH 4.2) for 2 to 3 min. The wells were rinsed three times with distilled water and photos were taken using an inverted microscope with phase contrast setting (Leica DM IL).

5.3.10 Pellet formation of MSCs or C3H10T1/2 cells

Pellets were prepared in 96 well plates using a method similar to the method described by Penick *et al.* [202]. In brief, cells were detached from culture surfaces using TrypLE Express (Gibco, catalog # 12604021) on the day of cell seeding. Cell suspensions of 1×10^6 cells/ml were prepared in low glucose DMEM (Gibco, catalog # 11054) with 1X ITS (Sigma, catalog # I2771), 0.25 µg/ml fungizone amphotencin B (Invitrogen, product # 15290-018), 5 µg/ml gentamycin (Gibco, catalog # 15750-060), L-glutamine and 40 µg/ml L-proline (Sigma, catalog # P5607). Dexamethasone (Sigma, catalog # D4902), sodium ascorbate (Sigma, catalog # A4034) and TGF-β1 (Peprotech, catalog # 100-21) were used at final concentrations of 39 µg/ml, 50 µg/ml and 10 ng/ml respectively. SKF-86002 (Sigma, catalog # S0193) and PD98059 (Sigma, catalog # P215) were used as inhibitors of p38 and MEK respectively.

These two pathway inhibitors were added to a final concentration of 10 μM. 200 μl of cell suspension were aliquoted into wells of an autoclaved-sterilized 96-well V-bottom polypropylene plate (greiner bio-one, item # 651201) and covered with a sterile polystyrene lid (greiner bio-one, item # 656171). The plate was centrifuged at 500 ×g for 2-5 min. The plates with cells were incubated in a humidified 37°C incubator with 5% CO_2 for normoxia or in a modular incubator chamber filled with premixed gas (3% O_2, 5% CO_2 in N_2) placed inside a 37°C incubator for hypoxia.

5.3.11 Preparation of pellets for histology

The pellets were fixed with 4% (w/v) PFA, washed with PBS and dehydrated stepwise in 70% (v/v) ethanol, 100% ethanol, 1:1 ethanol/ xylene, xylene, then wax. The embedded pellets were cut with a Leica microtome into 6 μm sections.

5.3.12 FAST staining of the pellets

Selected slides were dewaxed in xylene and stepwise rehydrated in 100% ethanol, 70% (v/v) ethanol, 30% (v/v) ethanol, tap water. FAST staining (a staining method using Fast Green, Alcian Blue, Safranin O, and Tartrazine) was performed according a published method in our group [203] and the detailed protocol is attached to the Appendix of this Chapter. In brief, the sections were immersed in different solutions in the following sequence: 1% (w/v) Alcian Blue solution, 0.1% (w/v) Safranin O solution, 50% (v/v) ethanol, 0.1% (w/v) Tartrazine solution, 0.01% (w/v) Fast Green solution with a brief rinse with tap water in between successive solutions. The stained sections were then dried and mounted with DePex. Photos were taken using an upright microscope (Nikon, Eclipse 80i).

5.3.13 RT-qPCR of the pellets

On the day of harvest, the pellets were transferred to new 1.5 ml tubes and homogenized with disposable pellet pestles (Kimble® Kontes) in TRIzol (Invitrogen, catalog # 15596-018). The lysates were stored in a -80 °C freezer prior to RNA extraction. RNA extraction was

performed according to the manufacturer's instruction but with the following modifications: Bromochlorpropane (BCP) was used instead of chloroform as it has been suggested that it is a safer yet equally effective phase separation reagent in RNA extraction [112]; 2 µl of glycogen (Invitrogen, catalog # AM9510) was added to each sample during the RNA precipitation step using propanol to better visualize the RNA pellet; and an additional 75% (v/v) ethanol wash step was includeed to remove the salts more completely. The RNA solution was quantified using a Nanodrop 2000c spectrophotometer (Thermo Scientific). DNase1 treatment and reverse transcription were performed as described in Chapter 2.

The cDNA was diluted five times by adding 40 µl of autoclaved water. For rat *Gapdh*, *Acan* and *Col2A1* genes, qPCR was performed as described in Chapter 2 using the rat primer sequences in Chapter 3. For human *COMP* gene, qPCR was performed as described in Chapter 2 using the following primer sequences (*COMP* forward primer: 5'-GCTCTG TGGCATACAGGAGA-3' and reverse primer: 5'- CATAGAATCGCACCCTGATG-3'). For other human genes, qPCR was performed with a total reaction volume of 10 µl using Taqman Gene expression Master Mix (Applied Biosystems, part # 4369016) and Taqman Gene Expression Assays (Applied Biosystems) listed in **Table 5-2**, in 96 well reaction plates using standard PCR protocol (Applied Biosystems, StepOnePlus). Primers were ordered from Tech Dragon Limited. Autoclaved water was used as a negative control and RNA before reverse transcription was used to estimate the level of genomic DNA contamination. DNase1 treatment by Amplification Grade DNase1 (Invitrogen, catalog # 18068-015) was also included when necessary. The relative gene expression was calculated based on comparative Ct method.

Table 5-2 List of Taqman Gene Expression Assays used in experiments in this Chapter

Gene	Taqman Gene Expression Assay ID
GAPDH	*Hs02758991_g1*
ACAN	*Hs00153936_m1*
COL1A1	*Hs00164004_m1*
COL2A1	*Hs00264051_m1*
COL3A1	*Hs00943809_m1*
SOX5	*Hs00753050_s1*
SOX6	*Hs00264525_m1*
SOX9	*Hs00165814_m1*
MIA	*Hs00197954_m1*
RUNX1	*Hs00231079_m1*

5.3.14 Setting up of hypoxic culture

5.3.14.1 Hypoxia using a hypoxic incubator with nitrogen

Initially, cells were cultured in hypoxia using the hypoxic incubator with nitrogen input in the Department of Biochemistry in the University of Hong Kong (**Figure 5-6**). The specifications of the incubator are shown in **Table 5-3**. There are a CO_2 sensor and a O_2 sensor in the incubator, allowing a CO_2 concentration range of 0% to 20% and a O_2 concentration range of 1% to 21%. The nitrogen gas was supplied from a R size cylinder (from Linde HKO Limited) connected to the incubator. The volume of gas in the cylinder was equivalent to about 6 m^3 (6000 L) of gas under atmospheric pressure. Theoretically, it seemed that one cylinder of gas (~6000 L) was sufficient to maintain the low oxygen concentration of the incubator (184 L, **Table 5-3**) even after several openings of the incubator door which increase the oxygen level. However, even with only 2 to 3 openings of the incubator door, the cylinder of compressed nitrogen was consumed completely in about 3 days. It was noted that even when the door of incubator was kept closed, the nitrogen gas was intermittently injected into the incubator in the gas composition regulation process. Using much larger tanks of compressed nitrogen can be a possible solution but not practical due to the space limitation where the incubator was situated in. Having considered the large scale of experiments involved in our study, we thought it might not be feasible to use this hypoxic incubator for our study. Thus we moved

on to using modular incubator chambers with premixed gas to create hypoxic culture conditions.

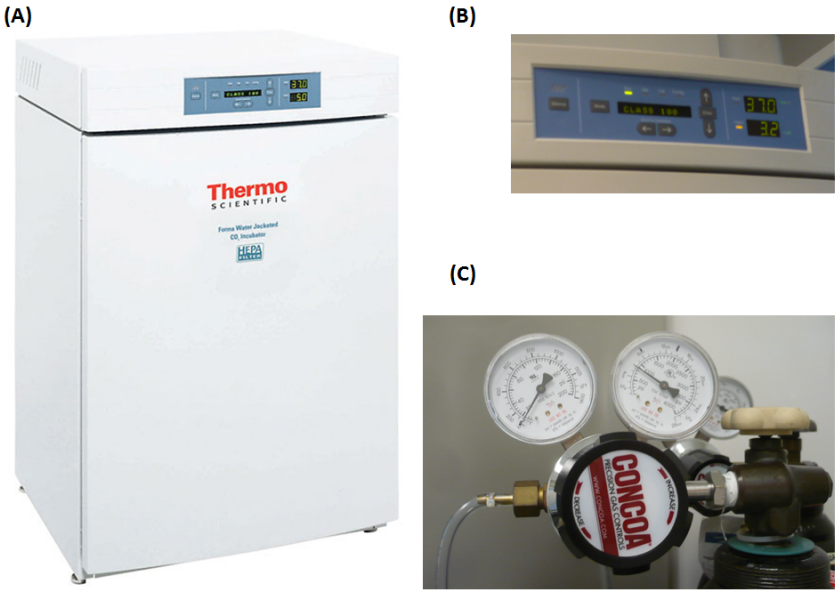


Figure 5-6 Hypoxic set up using an incubator with O_2 control and N_2 inlet. (A) Thermo Scientific Forma Water Jacketed CO_2 Incubator (photo from http://www.coleparmer.com/Product/Thermo_Scientific_Forma_Water_Jacketed_CO2_Incubator_TC_230/EW-39320-06), (B) the display of the incubator and (C) the gas regulator of nitrogen gas for the hypoxic incubator used in the Department of Biochemistry, HKU (Model number 3131 of Forma™ Series II 3110 Water-Jacketed CO_2 Incubators).

Table 5-3 Some specifications of the Thermo Scientific Forma Water Jacketed CO_2 Incubator 3131, used as hypoxic incubator (information from http://www.thermoscientific.com/en/product/forma-series-i-3110 -water-jacketed-co-sub-2-sub-incubators.html)

Specifications	
Brand	Thermo Scientific™
Model number	3131
CO_2 Concentration Range	0 to 20%
CO_2 Sensor Technology	TC
Oxygen Control	1 to 21%
O_2 Sensor Technology	galvanic
Humidity Delivery	Water Pan
Relative Humidity	Ambient to 95% at 37 °C
Temperature range	Ambient + 5 °C to 55 °C
Capacity	184 L

5.3.14.2 Setting up hypoxia using a modular incubator chamber

Sealed Modular Incubator Chambers (Thermo Scientific, catalog # 190043) were purchased as accessory units of the Steri-Cycle® CO_2 Incubators (**Figure 5-7A**). Before the first time use, the incubator chamber were dissembled and cleaned with 70% (v/v) ethanol followed by UV sterilization inside a biosafety cabinet for at least half an hour. The cylinder of premixed gas (3% O_2, 5% CO_2, 92% N_2) (**Figure 5-7B**), the 2-stage gas regulator and the flashback arrester (**Figure 5-7C**) were purchased from the Linde HKO Limited. Flashback arrester was included in the set up as recommended by the company for gas having O_2 in it. The connection of the gas cylinder to the incubator chamber was set up with the help of Mr. Henry Yip with his expertise from the mechanical workshop.

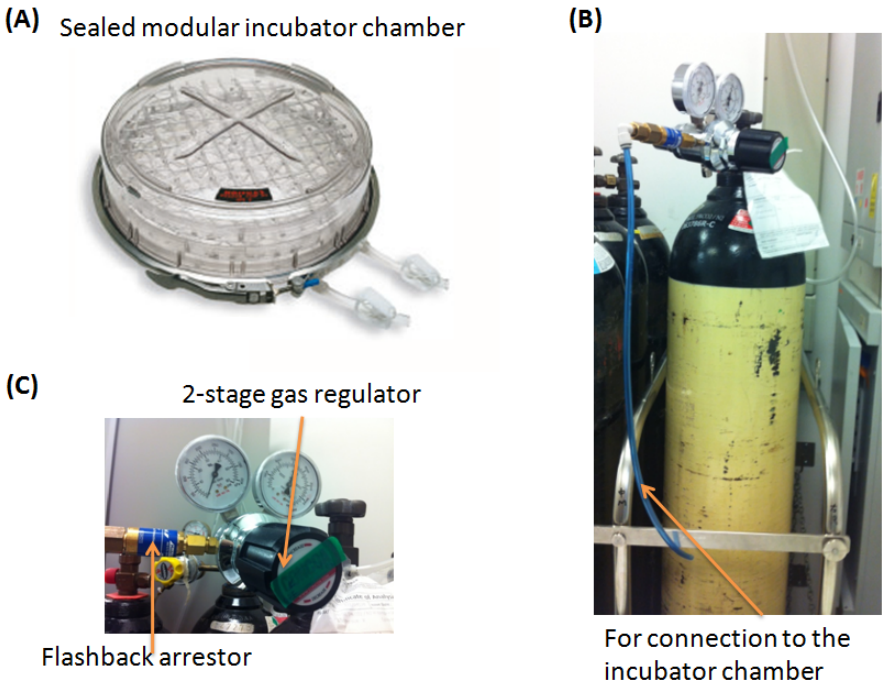


Figure 5-7 Components for setting up hypoxia using a sealed modular incubator chamber. (A) Sealed modular incubator chamber, (B) the cylinder of premixed gas with an arrow showing the tubing for connection to the incubator chamber, and (C) the 2-stage gas regulator connected to the gas cylinder for control of gas release to the incubator chamber and the flashback arrestor connected to it for gas involving oxygen.

5.4 Results

5.4.1 Harvest of rat MSCs from bone marrow

Figure 5-8 shows the cells harvested from rat bone marrow. At day 1 and day 4, there were many floating cells (**Figure 5-8A** and **B**). After medium change, attached cells were observed at day 7 (**Figure 5-8C**). The cells at day 4 of passage 1 were not flat in morphology (**Figure 5-8D**) but became flat when the cells were cultured further (**Figure 5-8E**). The cells remained flat when passaged (**Figure 5-8F**).

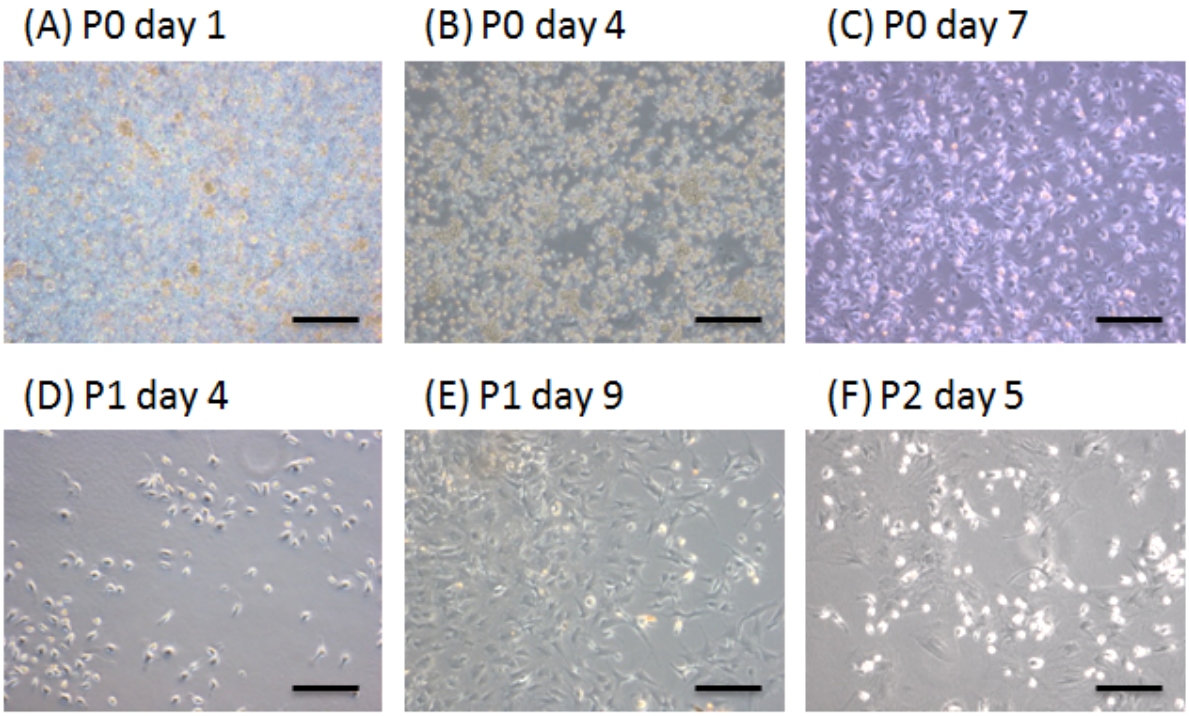


Figure 5-8 Phase contrast photos of cells isolated from rat bone marrow with Ficoll separation cultured with DMEM with 10% FBS. (A) Passage 0 cells at day 1, (B) passage 0 cells at day 4, (C) passage 0 cells at day 7 with medium changed at day 4, (D) passage 1 cells at day 4, (E) passage 1 cells at day 9, and (F) passage 2 cells at day 5 (scale bar = 200 μm).

To obtain enough cells for the studies using pellet culture, we cultured the rat MSCs and performed pellet culture at passage 4. At passage 4, the rat MSCs were flat in morphology (**Figure 5-9A**) and these cells did not form pellets well (the pellets were easy to break during cryosection preparation) (**Figure 5-9B**). Pellets from bovine NP cells were stained blue while the pellets from rat MSCs were more greenish, indicating less amount of glycosaminoglycan

(GAG) in the pellets formed from rat MSCs. The *Acan* and *Col2a1* expression did not increase significantly when the cells were cultured with the addition of TGF-β1 (**Figure 5-9C**) which was not expected for typical MSCs. Neuhuber *et al.* reported that flat subpopulation of rat MSCs have lost adipogenic and chondrogenic potential [204]. In our study, the rat MSCs harvested had flat morphology and they have lost the chondrogenic potential which was consistent with the conclusion by Neuhuber *et al.*

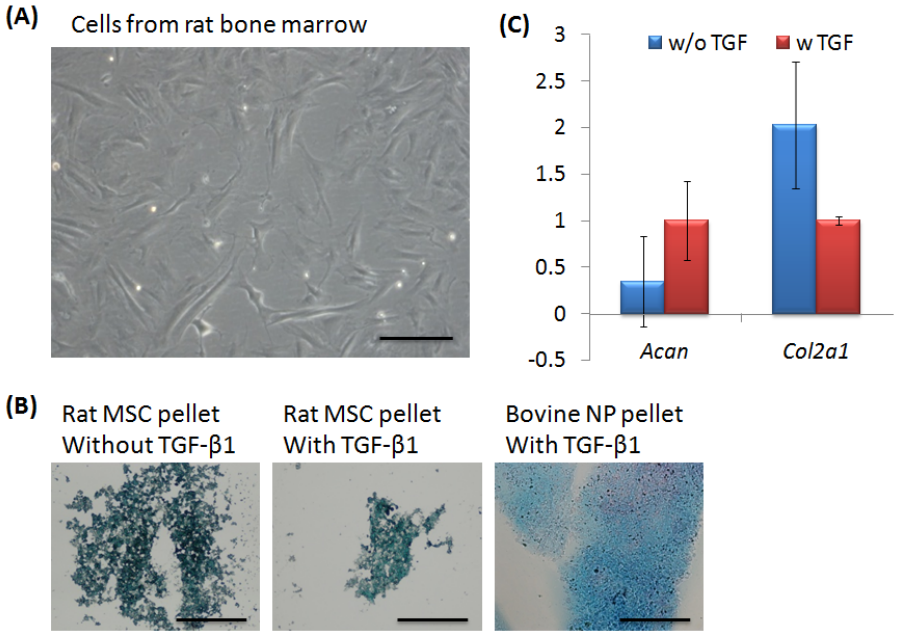


Figure 5-9 Rat MSCs with flat morphology. (A) Cells at passage 4 isolated from rat bone marrow (scale bar = 200 μm), (B) cryosections of pellets cultured with dexamethasone, ascorbic acid, with or without TGF-β1 for 20 days and stained by FAST staining (scale bar = 500 μm) and (C) relative mRNA levels of matrix genes *Acan* and *Col2a1* in rat MSC pellets cultured with dexamethasone and sodium ascorbate but with and without TGF-β1 (relative to G*apdh* and the sample group with TGF-β1 added; mean ± SD, biological duplicates).

5.4.2 Harvest of rat MSCs using bone chip method

The percentage of MSCs in bone marrow is low and the volume of bone marrow available from each rat is rather limited due to the small size of the animal. MSCs has been reported to be present in human trabecular bones and Zhu *et al.* has demonstrated that MSCs could be isolated from the compact bone of mice [170]. They showed that the number of MSCs that could be obtained from the mouse compact bones was significantly higher than that from

mouse bone marrow. Thus we attempted to isolate MSCs from rat bones. Consistent to the report by Zhu *et al.*, we found cells to migrate from the bone chips to the plastic culture surfaces (**Figure 5-10A** and **B**). The cells were spindle-like or polygonal in shape at passage 1 (**Figure 5-10C** and **D**) but became flat in passages 2 and 3 already (**Figure 5-10E** and **F**). Similar to the rat MSCs harvested from the bone marrow in the previous Section, pellets from rat MSCs were greenish after FAST staining (**Figure 5-11**) which indicated the GAG content in these pellets was not high. This implies the cells may have already lost the chondrogenic potential. Therefore, we did not use the data from these MSCs.

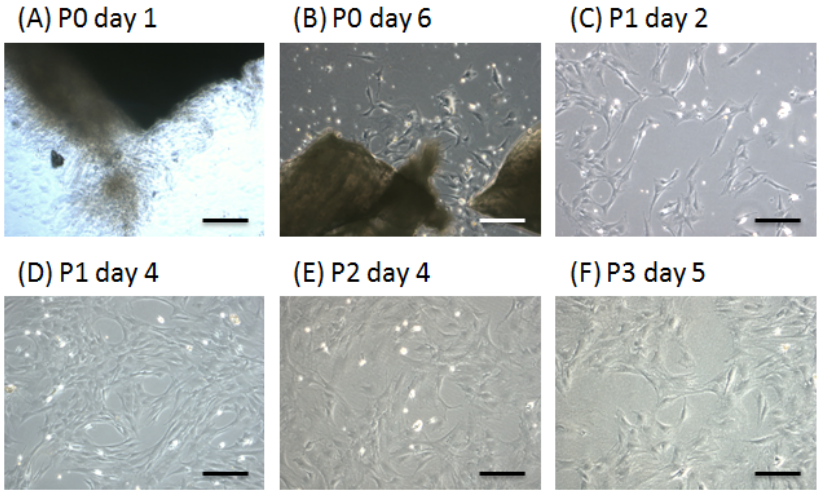


Figure 5-10 Phase contrast photos of cells isolated from rat cortical bones cultured with DMEM with 10% FBS. (A) Passage 0 cells at day 1, (B) passage 0 cells at day 6, (C) passage 1 cells at day 2, (D) passage 1 cells at day 4, (E) passage 2 cells at day 4, and (F) passage 3 cells at day 5 (scale bar = 200 μm).

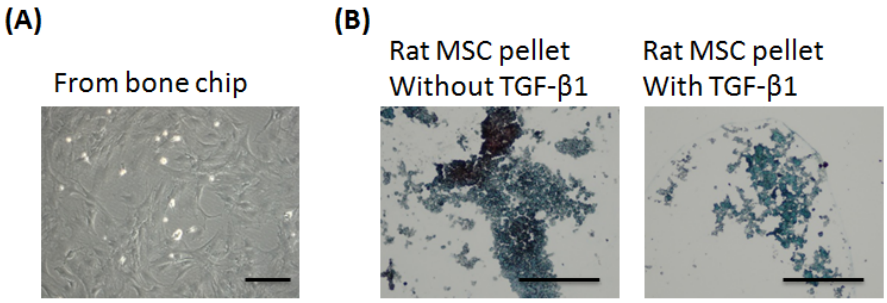


Figure 5-11 Rat MSCs from compact bones. (A) Cells at passage 2 isolated from rat compact bones (scale bar = 200 μm), and (B) cryosections of pellets from rat compact bone MSCs cultured with dexamethasone, ascorbic acid, with or without TGF-β1 for 20 days and stained by FAST staining (scale bar = 500 μm).

5.4.3 MSCs from immunodeficient mice did not show CD44 surface marker expression

Using the method developed by Zhu *et al.*, cells were obtained from the cortical bones of NOD/SCID mice. The cells were polygonal in shape and remained polygonal without becoming flattened as observed for the rat MSCs for the first four passages (**Figure 5-12**). This indicates the chondrogenic potential of these cells may be retained.

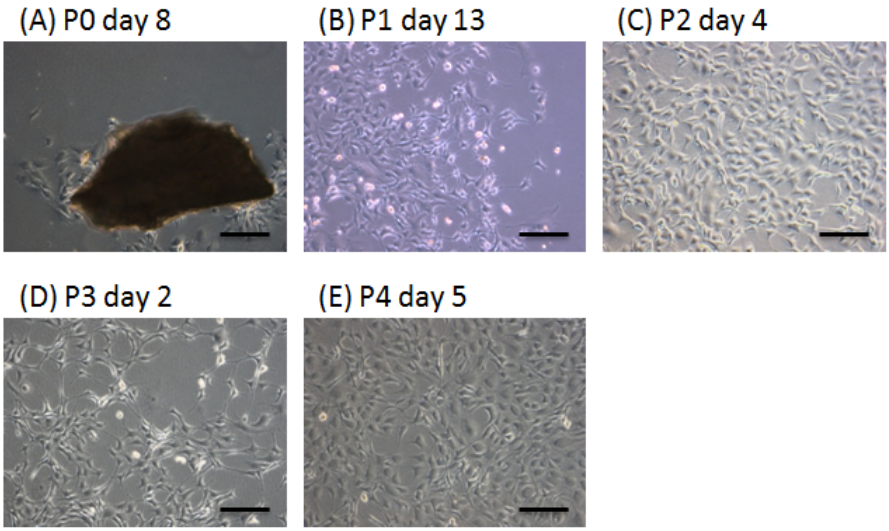


Figure 5-12 Phase contrast photos of cells isolated from mouse cortical bones cultured with DMEM with 10% FBS. (A) Passage 0 cells at day 8, (B) passage 1 cells at day 13, (C) passage 2 cells at day 4, (D) passage 3 cells at day 2, and (E) passage 4 cells at day 5 (scale bar = 200 μm).

Due to the availability of antibodies for mouse MSC markers in our lab, flow cytometry was used to assess the surface marker expression of the isolated mouse MSCs. In this study, the mesenchymal markers CD29, CD44, hematopoietic markers CD11b, CD45 and CD106 used by other groups [170, 171, 205] were chosen to characterize the isolated mouse MSCs. **Figure 5-13** shows the histograms of fluorescence for these markers. The cells isolated from the cortical bones of immunodeficient NOD/SCID mice were negative for CD11b, CD45 and CD44 while positive for CD106 and CD29. It was expected that the MSCs will be positive for the mesenchymal markers CD29, CD44 but negative for the hematopoietic markers CD11b, CD45 and CD106. However, no expression of CD44 was observed in these isolated cells while the cells were also positive for CD106. Thus we further searched from literature about

the MSC markers and summarized some of them in **Table 5-4**. Interestingly, the CD106 which was considered as a hematopoietic marker was also detected in the MSCs from human bone marrow, human chorionic villi and human umbilical cord while CD11b and CD45 were not detected [206]. This shows that there can be considerable variations in surface markers for MSCs obtained from different sources.

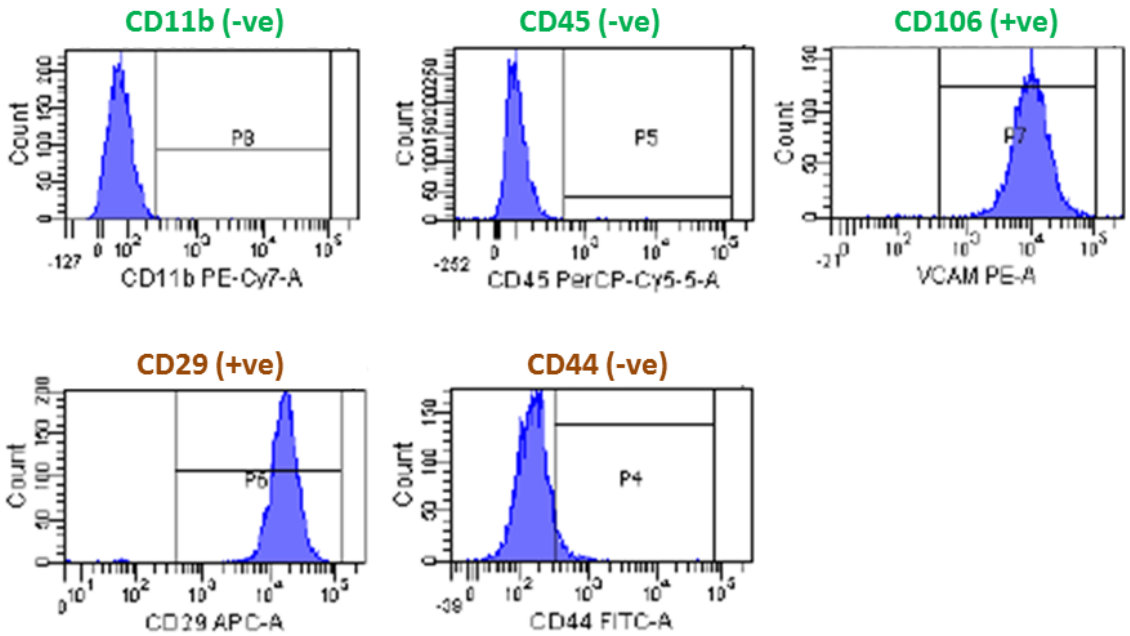


Figure 5-13 Histogram analysis of cell surface markers by flow cytometry for cells stained with CD44, CD45, CD29, VCAM and CD11b for mouse MSCs isolated with bone chip method from NOD/SCID mice.

Table 5-4 Summary of marker expression for MSC characterization

Group	*Source*	*CD11b*	*CD45*	*CD106*	*CD29*	*CD44*
Nadri *et al.* 2007 [205]	Bone marrow of Balb/c mice	-	-	-	/	+
Soleimaini *et al.* 2009 [171]	Bone marrow of Balb/c mice	-	-	-	/	+
Zhu *et al.* 2010 [170]	Bone of mice	-	-	/	+	+
Yang *et al.* 2013 [206]	Human bone marrow	-	-	+	+	+
Yang *et al.* 2013 [206]	Human adipose tissue	-	-	-	+	+
Yang *et al.* 2013 [206]	Human chorionic villi	-	-	+	+	+
Yang *et al.* 2013 [206]	Human umbilical cord	-	-	+	+	+
This study	Bone of nude mice	-	-	+	+	-

5.4.4 The adipogenic and osteogenic potential of the harvested human MSCs was confirmed

As shown in **Figure 5-14**, oil droplets and minerals were observed in human MSCs underwent adipogenesis and osteogenesis respectively. In the differentiation assays, the cells cultured with DMEM with 10% FBS have grown to confluence at higher cell density compared to those cultured in adipogenic medium. The oil droplets were stained red by Oil Red O staining and the minerals stained red by Alizarin S staining. The adipogenic potential and osteogenic potential of the harvested human MSCs were confirmed.

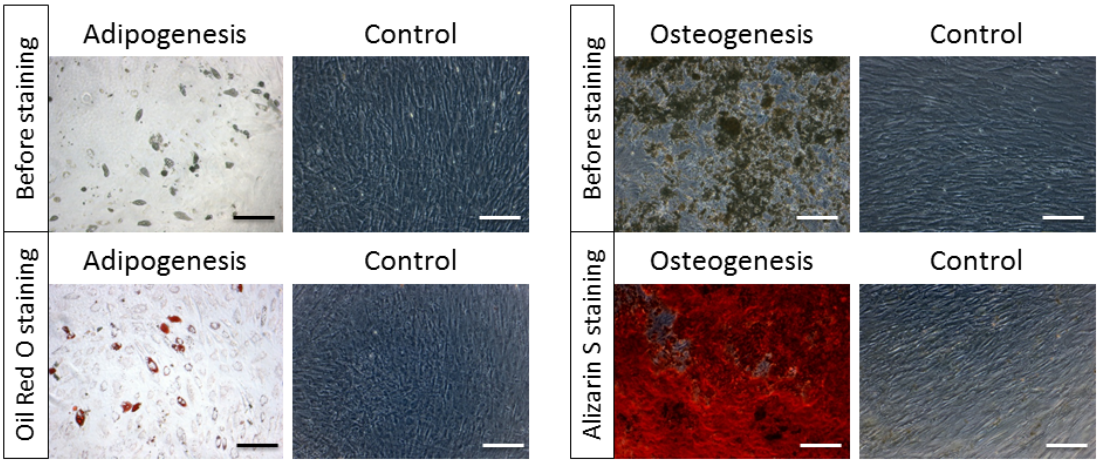


Figure 5-14 Human MSCs differentiated into adipocytes and osteocytes before and after Oil Red O staining and Alizarin Red S staining respectively. Controls were cells cultured using DMEM with 10% FBS. Oil Red O stains lipid droplets while Alizarin Red S was used to identify calcium present in the samples. (Scale bar = 200 μm).

5.4.5 Human MSCs from bone marrow clot and transferred medium

The yield of MSCs from the bone marrow of each donor may vary from batch to batch due to a variety of factors such as age of donor, volume of bone marrow obtained, isolation procedures, *etc.* During MSC isolation, it was noticed that there were clots in some bone marrow samples and some cells remain unattached at the time of first medium change of the culture which were then discarded. Thus we investigated whether MSCs can be utilized from these two sources as well.

When collecting bone marrow from the iliac crest of donors, the bone marrow was placed in tubes with ethylenediaminetetraacetic acid (EDTA) or heparin, which acts as an anti-clotting agent to prevent the clotting of marrows. However, clots were still observed. This may be due to the clotting of marrow before the marrow was transferred to the tubes or insufficient mixing of the marrow with the anti-clotting agent. MSCs may be trapped within the clots and got discarded during the separation with Ficoll as the clot may get to the bottom of the tube which will reduce the numbers of cells obtained from the samples. Instead of discarding the clot or breaking the clots with brutal force, we cultured the clot in a 10 cm cell culture dish with medium. We speculated that MSCs may migrate from the clot into the culture dish like the MSCs migrate from the cortical bone in the bone chip method. Interestingly, when we cultured the clot in human MSC growth medium, the clots disintegrated at day 3 (**Figure 5-15A**). In addition, attached cells were observed after washing the cells with PBS and then replacing the PBS with cell growth medium (**Figure 5-15B**).

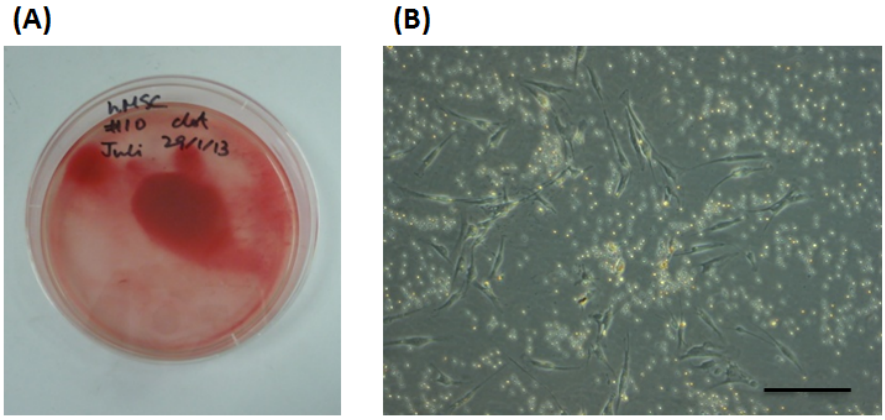


Figure 5-15 (A) Photo of a dish with bone marrow clot showing that the clot has been disintegrated at day 3 and (B) a phase contrast photo of human MSCs from bone marrow clot at day 3 after PBS wash and medium change. (Scale bar = 200 μm).

Normally when changing cell culture medium, we discard the medium in the dish with cells and replace it with fresh medium. For human MSCs from bone marrow, it was noticed that there were still quite a lot of cells not attached to the cell culture surface when we changed the medium at day 3. Thus instead of discarding the medium, we transferred them to a new dish

to observe whether these cells would attach to the culture surface at a later time. As shown in **Figure 5-16A**, attached cells were observed from the transferred medium. Cells of different morphologies such as spindle-like and polygonal were observed. When the cells were cultured further, majority of the cell population was spindle-like (**Figure 5-16B**), which may be due to the higher proliferation rate of these spindle-like cells.

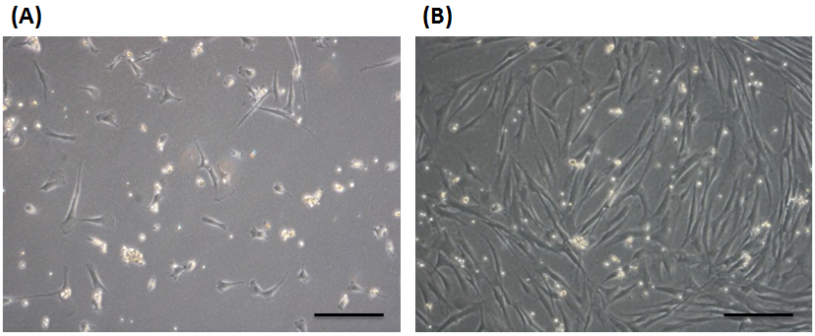


Figure 5-16 Phase contrast photos of human MSCs from transferred medium at (A) day 11 and (B) day 17. (Scale bar = 200 μm).

In order to assess the adipogenic and osteogenic potentials of the MSCs from the clot and from the transferred medium, differentiation assays were performed. Oil droplets and minerals were observed for MSCs from the marrow clot and from the transferred medium (**Figure 5-17**). This indicates the MSCs from these sources may be used when there is a need to maximize the cell yield.

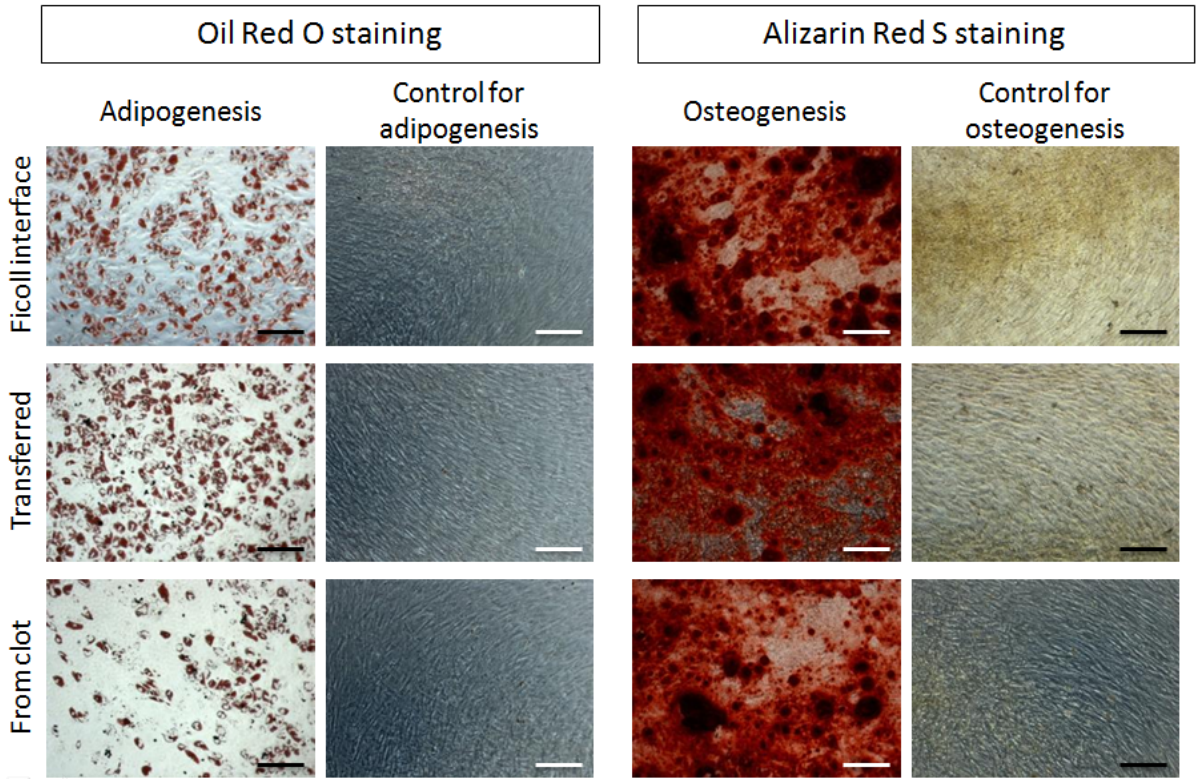


Figure 5-17 Photos of human MSCs differentiated into adipocytes and osteocytes with Oil Red O staining or Alizarin Red S staining for cells obtained from Ficoll interface, from transferred medium and from bone marrow clot. Controls were cells cultured using DMEM with 10% FBS. (Scale bar = 200 μm).

There have been difficulty in obtaining MSCs from our rats that would not become flattened in morphology after several passages but spindle-like cells could be obtained from human bone marrow with relative ease (The eight MSC lines from all bone marrow samples I isolated showed spindle-like morphology). These spindle-like cells are likely to have retained their differentiation potential compared to flattened cells. In our group, we have good access to clinical bone marrow samples. Therefore, the project focused on using human bone marrow MSCs due to better clinical relevance and ease of maintenance.

5.4.6 Source of MSCs had influence in the chondrogenic differentiation and inhibition

Sections from all pellets showed staining by Alcine blue, indicating the presence of glycosaminoglycans (GAGs) (**Figure 5-18**). Compared to pellets from bone marrow MSCs, the pellets from umbilical cord were easier to be fractured during sectioning for the pellets

without TGF-β1 added or with TGF-β1 added but also with p38 inhibitor. This may be due to the lower extracellular matrix (ECM) content as shown by the lower expression of *ACAN* and *COL2A1* for pellets formed from umbilical cord MSCs in general (**Table 5-5**). The cells from the umbilical cord underwent less cell divisions and may be at a more primitive stage compared to cells from bone marrow of adolescents, requiring longer time for differentiation. Yet further experiment is required to confirm this.

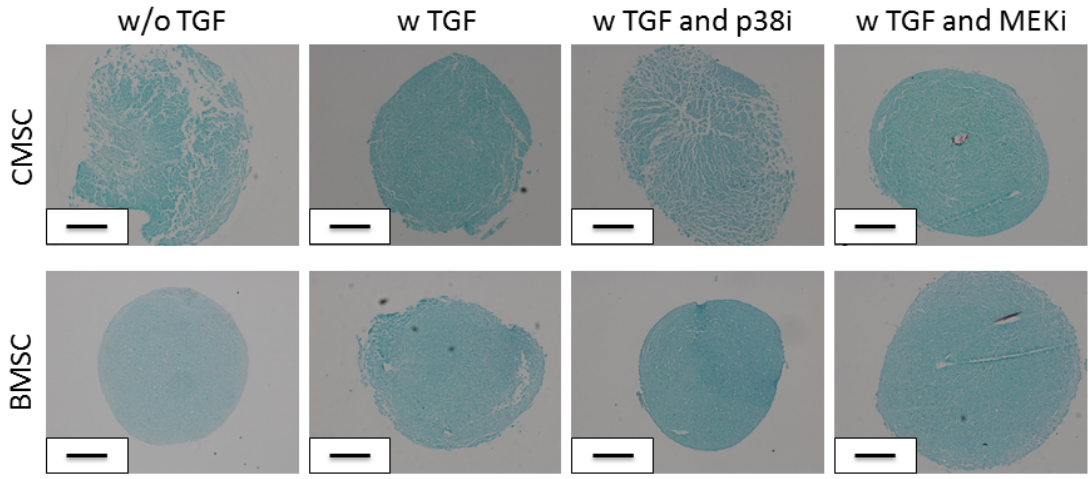


Figure 5-18 Photos of paraffin sections of pellets formed from human MSCs from umbilical cord (CMSC) and from bone marrow (BMSC) cultured with different conditions. (Without TGF-β1, with TGF-β1 with and without p38/ MEK inhibitors) for 14 days under normoxia and stained with FAST staining (scale bar = 200 μm).

Table 5-5 Relative mRNA levels of pellets formed from CMSCs and BMSCs cultured with different conditions. (Without TGF-β1, with TGF-β1 with and without p38/ MEK inhibitors) for 14 days (normalized to *GAPDH* and relative to the sample of BMSC with TGF-β1 without inhibitors) (ND denotes "not detected" in the qPCR)

	w/o TGF		w TGF		w TGF & p38i		wTGF&MEKi	
	CMSC	BMSC	CMSC	BMSC	CMSC	BMSC	CMSC	BMSC
ACAN	ND	0.07	ND	1	ND	0.29	0.00	1.57
COL2A1	0.00	ND	ND	1	ND	0.00	ND	0.71
SOX9	0.09	1.01	0.27	1	0.31	0.79	0.07	1.02
MIA	0.00	0.06	0.01	1	0.01	0.04	0.01	1.55
RUNX1	0.51	1.18	0.49	1	0.92	2.11	0.86	1.32

5.4.7 Culture of rat MSCs using α-MEM with hFGF-2

In culturing human MSCs, we used α-MEM with 15% FBS and 0.5 ng/ml hFGF-2 and the cells remained spindle-shape even until passage 9 (**Figure 5-19**). Thus we speculated that that α-MEM with 15% FBS and 0.5 ng/ml hFGF-2 may be better in maintaining the shape of cells during culturing. However, the use of hFGF-2 in medium to culture the rat MSCs we harvested did not help in maintaining the shape of the cells. The cells became rather flat and large in morphology even at passage 1 (**Figure 5-20**). The use of the culture medium for culturing human MSCs did not help in maintaining the morphology of rat MSCs we harvested.

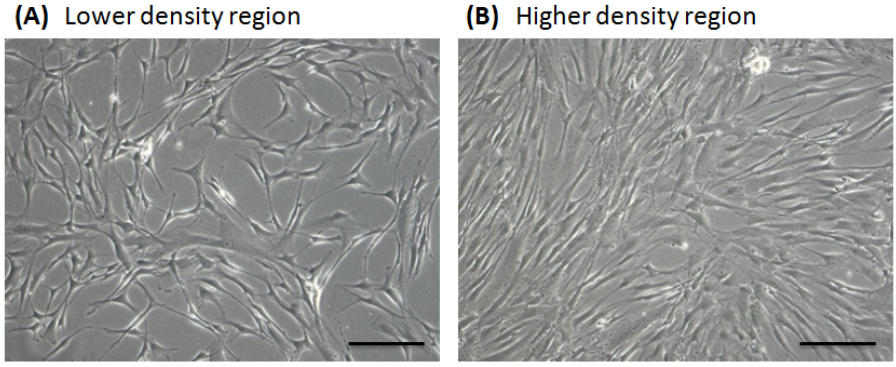


Figure 5-19 Phase contrast photos of cells isolated from human bone marrow cultured with α-MEM with 15% FBS and 0.5 ng/ml hFGF-2 at passage 9 at (A) a lower density region and (B) a higher density region of the dish. (Scale bar = 200μm).

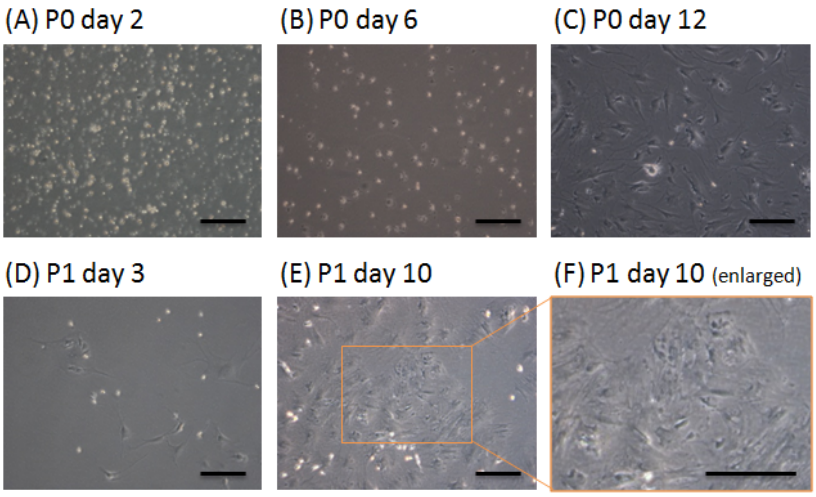


Figure 5-20 Phase contrast photos of cells isolated from rat bone marrow without Ficoll separation cultured with α-MEM with 15% FBS and 0.5 ng/ml hFGF-2. (A) Passage 0 cells at day 2, (B) passage 0 cells at day 6, (C) passage 0 cells at day 12, (D) passage 1 cells at day 3, (E) passage 1 cells at day 10, and (F) enlarged photo of (E) (scale bar = 200 μm).

5.4.8 Human bone marrow MSCs can form pellets even in the absence of dexamethasone, sodium ascorbate and TGF-β1

In this project, experiments were set up with an aim to study the formation of NP-like cells through pathway inhibition as described in the Appendix. It was observed that pellets could be formed from human bone marrow MSCs even in the absence of TGF-β1. Hence we investigated the requirement of different chondrogenic supplements, namely dexamethasone, ascorbic acid/ ascorbate and TGF-β1, in differentiating human bone marrow MSCs along chondrogenesis. Data showed that pellets could be formed even in the absence of any chondrogenic supplement (**Figure 5-21**).

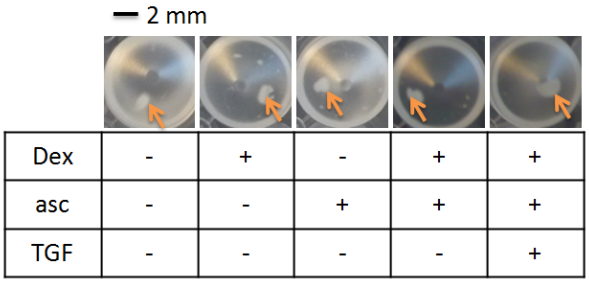


Figure 5-21 Photos of pellets in 96-well polypropylene plates cultured at day 1 in normoxia condition. (Arrows indicate the pellets formed) (Dex: dexamethasone, asc: sodium ascorbate, TGF: TGF-β1).

Pellets could be formed with or without different supplements added for human MSCs (**Figure 5-21**) and therefore RT-qPCR was performed to study the gene expressions in these pellets. *ACAN* and *COL2A1* expression was significantly enhanced when MSC pellets were cultured with dexamethasone, ascorbic acid and TGF-β1 (**Figure 5-22**). The addition of dexamethasone and/ or ascorbic acid did not have significant effect on *ACAN* expression. The *COL2A1* expression was not detected when either dexamethasone or ascorbic acid was added alone. The *COL2A1* was greatly enhanced when the three supplements were added together.

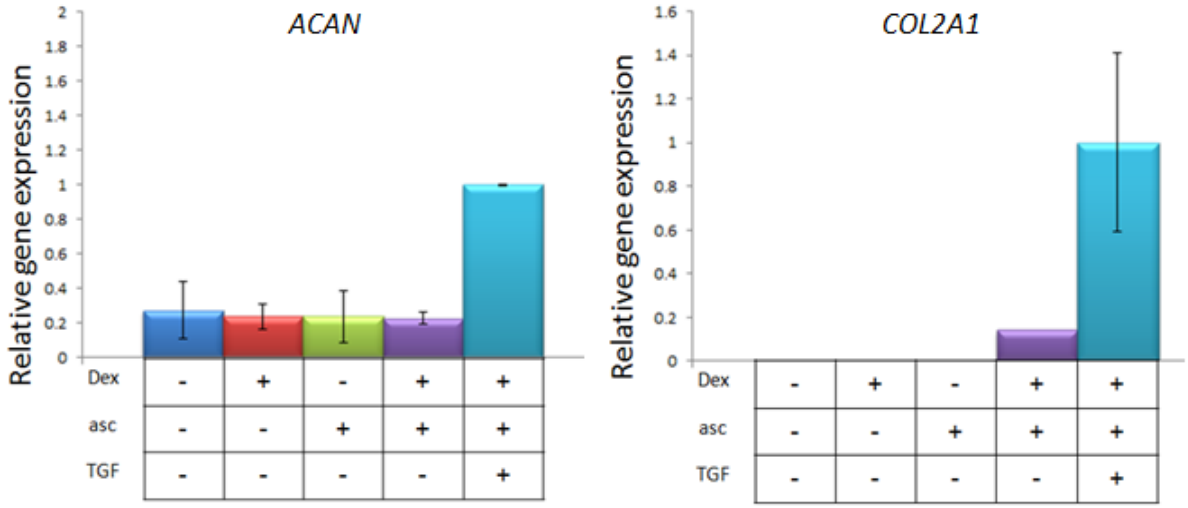


Figure 5-22 Relative mRNA levels of matrix genes *ACAN* and *COL2A1* in hMSC pellets cultured with different supplements. (Dex: dexamethasone, asc: sodium ascorbate, TGF: TGF-β1) (relative to *GAPDH* and the sample group treated with Dex, asc and TGF; mean ± SD, biological duplicates).

Unlike *ACAN* and *COL2A1*, the expression of *SOX9* and *RUNX1* was not greatly enhanced when the three supplements were added (**Figure 5-23**). The *MIA* expression seems to be enhanced but with difference of less than twofold. Thus further experiment will be required for reliable statistics.

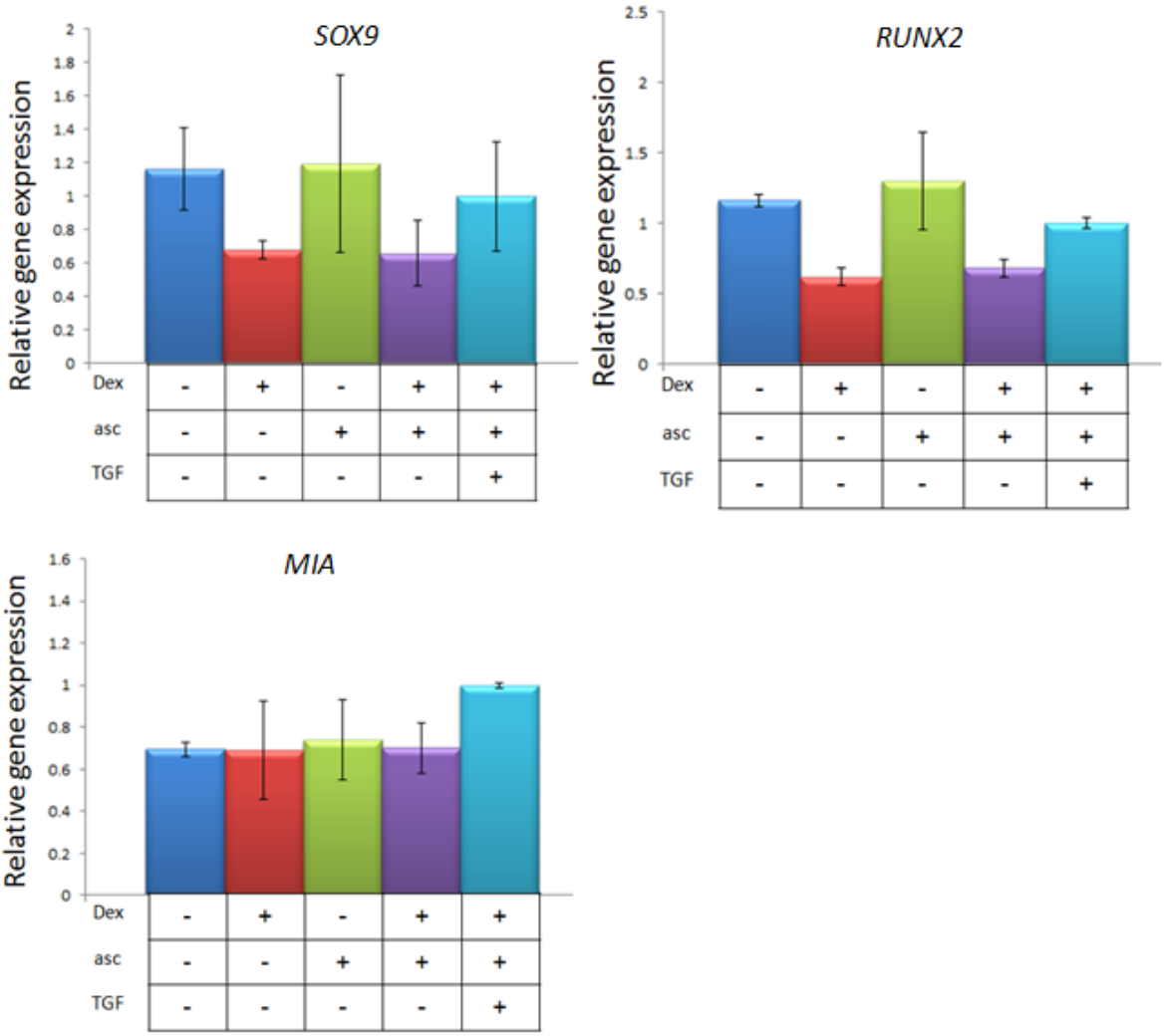


Figure 5-23 Relative mRNA levels of chondrocyte markers in hMSC pellets cultured with different supplements. (Dex: dexamethasone, asc: sodium ascorbate, TGF: TGF-β1) (relative to *GAPDH* and the sample group treated with Dex, asc and TGF; mean ± SD, biological duplicates).

5.4.9 Hypoxia

Hypoxia was suggested to promote chondrogenesis in rat MSCs [194] and human MSCs [195]. Thus we investigated the effect of hypoxia on hMSC chondrogensis in our system with pathway inhibitors. Similar to pellet culture in normoxia, pellets were formed from human bone marrow MSCs for all treatment groups under study for hypoxia (**Figure 5-24**). However, there was no significant difference in *ACAN*, *SOX9*, *MIA* and *RUNX1* expression between the pellets cultured in hypoxia and the pellets cultured in normoxia except that MIA expression was higher for normoxia when the pellets were cultured with TGF-β1 and p38 inhibitor (**Figure 5-25**).

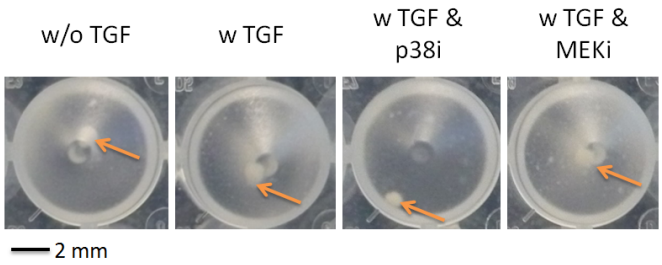


Figure 5-24 Photos of pellets in 96-well polypropylene plates cultured after 14 days in hypoxia condition. (arrows indicate the pellets formed, scale bar = 2 mm).

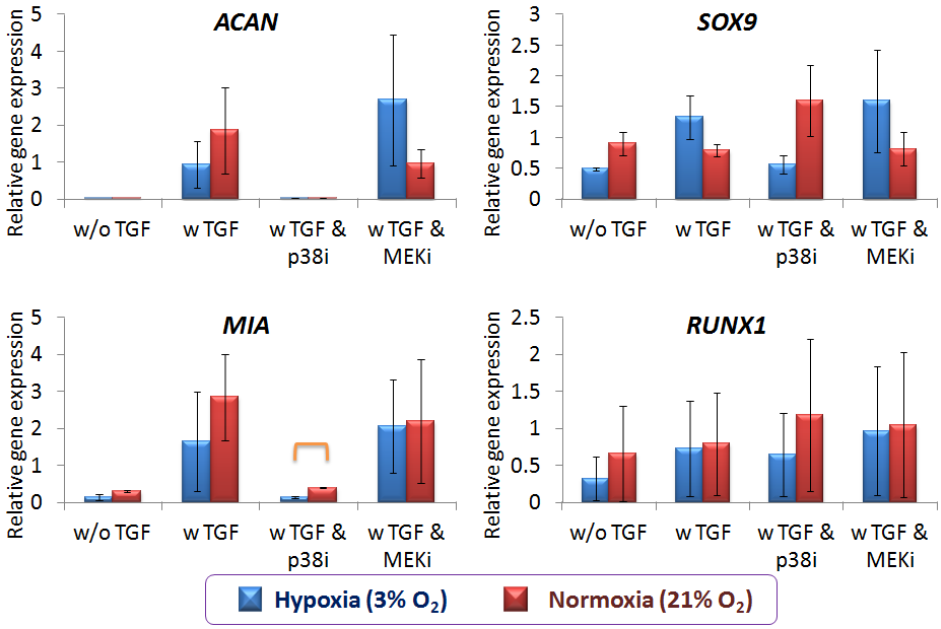


Figure 5-25 Comparison of hMSC pellets cultured in hypoxia (3% O_2) and normoxia (21% O_2) at day 14. (Relative to *GAPDH* and the average gene expression of the samples of hypoxia; mean ± SD, biological triplicates, $p < 0.05$ for the orange bracket).

5.5 Discussion

5.5.1 Chondrogenic potential of rat MSCs

There were limited studies about the gene expression using rat MSC pellet culture. A large number of chondrogenic differentiation studies using pellet culture was performed with human MSCs [207-211]. Risbud *et al.* have used rat MSCs in studying differentiation towards NP-like phenotype but they used 3-dimensional alginate hydrogel [169]. The effects of plating density and culture time of rat MSCs were studied by Neuhuber *et al.* using Fischer rats and they demonstrated the heterogeneous MSCs plated at all densities sustained the chondrogenic,

osteogenic and adipogenic potential through at least passage 5 [204]. There are over 200 different rat strains [212] and at least 7 rat stocks/ strains for experiments in laboratory. These include two outbred rat stocks (Sprague–Dawley, Wistar) and five inbred rat strains (Lewis, Fischer 344, ACI, Wistar-Kyoto, Brown Norway) [213]. Different strains have different responses to repeated electrical stimulation of a limbic brain region [213] and drugs [212]. It may be possible that the MSCs from different rat strains may have differences in ability in chondrogenesis. Peister*et al.* showed that the MSCs from five different strains of inbred mice have variations in surface epitopes, proliferation rates and differentiation potential [214] while Barzilay *et al.* showed that MSCs from different rat strains (Fisher, Lewis, Sprague-Dawley and Wistar) shared similar characteristics [215]. However, with regard to differentiation potential, only adipogenesis and osteogenesis were assessed for the rat MSCs in Barzilay's study [215]. Cells may have retained adipogenic and osteogenic potential but lost the chondrogenic potential. For example, 9 out of 10 clones of TIE2/ GD2 double positive cells isolated from human NP had adipogenic and osteogenic potentials but only 5 out of 10 clones had chondrogenic potential [58]. Thus whether MSCs from different rat strains differ in chondrogenic potential in Barzilay's study was unknown. In this study, we also did not rule out the possibility that the conditions of supplements used for chondrogenesis may cause the difference. Contamination with cells other than stem cells may be another reason for the observed loss of chondrogenic potential.

5.5.2 Genetic background of MSCs might affect the phenotype of MSCs harvested

In this study, we used immunodeficient mice for MSC harvest as they were available in our group. These mice were used in our lab for a human cell injection study as they had inhibited immune systems and mounted no rejection response when human cells were injected to them. They are also called "nude" mice since they do not have body hair. In these nude mice, the gene, forkhead transcription factor, *Foxn1* (*Whn*) was mutated [216] and the mice are athymic [217]. CD44 is a widely-expressed adhesion receptor that is associated with diverse biological processes involving migrating cells, including inflammation, angiogenesis, bone metabolism

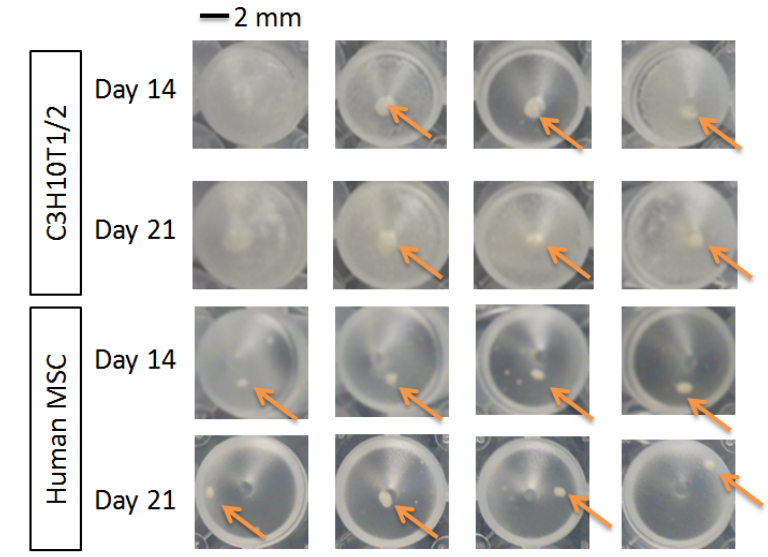
and wound healing [218]. In a normal immune system during the responses of naive T lymphocytes against invading microbes, CD44 is upregulated after the activation of the T lymphocytes. Once an infection is cleared, the levels of CD44 remain elevated on the surface of memory T cells which mediate protection against re-infection [218]. The expression of CD44 in cells of nude mice was not studied before and it may be possible that the mutation of the *Foxn1* gene also affects the expression of CD44 in the cells in the bone marrow of nude mice.

The special characteristics of MSCs from some strains may be employed to study specific protein function. In addition to its role in immune system, CD44 is a type I transmembrane glycoproteins that binds the ligand, hyaluronic acid (HA), a major glycosaminoglycan component of the extracellular matrix (ECM) involved in maintaining tissue integrity [219]. HA binding to CD44 was shown to activate Rac1 in an immortalized mouse mammary epithelial cell line [220]. In breast and ovarian tumor cells, the HA-CD44 interaction activates stem cell marker *Nanog* (an embryonic stem cell transcription factor) and the expression of pluripotent stem cell regulators *Rex1* and *Sox2* [221]. These imply the immunodeficient mice may have special characteristics other than impaired immune system and MSCs from these mice may be used to study CD44 along with MSCs from wild type mice without immunodeficiency.

5.5.3 Exogenous TGF- β1 is required in pellet formation in mouse C3H10T1/2 cells but not in human bone marrow MSCs

From **Table 5-4** in **Section 5.4.3** in the Results Section, it was shown that MSCs from different species and different sources may have different surface markers. And pellets could not be formed well from the rat MSCs I harvested but could be easily formed from the human MSCs. Thus I investigated whether cells from different species had different requirements in forming pellets and performed pellet culture with mouse C3H10T1/2 cells. The C3H10T1/2 cell line was established from C3H mouse embryos in 1973 [222]. These cells have

fibroblastic morphology and are functionally similar to mesenchymal stem cells. Inhibiting methylation with 5-azacytidine in C3H10T1/2 cells produces cells that exhibit stable morphological and biochemical features of muscle, adipose or cartilage cells [223]. It was considered as pluripotent stem cells [224-229] or multipotent cells [230] in a number of studies and used in studying chondrogenic differentiation in alginate culture [231]. Unlike human bone marrow MSCs, the C3H10T1/2 cells only form pellets when TGF-β1 was added (**Figure 5-26**). For both human bone marrow MSCs and the mouse C3H10T1/2 cells, p38 inhibition by SKF86002 and MEK inhibition by PD98059 did not affect pellet formation. This experiment confirmed the pellet forming ability of C3H10T1/2 cells and may indicate that this cell line may be used for chondrogenesis study using pellet culture. Compared to primary cells isolated from bone marrow, this cell line may have the advantage of less variability in results when different passages were used and for easier comparison with results from other groups.



Dex, asc	+	+	+	+
TGF	-	+	+	+
p38i	-	-	+	-
MEKi	-	-	-	+

Figure 5-26 Photos of pellets in 96-well polypropylene plates cultured after 14 or 21 days in normoxia condition. (Arrows indicate the pellets formed, scale bar = 2 mm).

5.6 Summary and Conclusions

In this study, the pellet forming ability of mouse pluripotent stem cell line, C3H10T1/2, was confirmed in this study, indicating that this cell line may be used in preliminary chondrogenic study. It has the advantage of less variability in results when different passages were used and for easier comparison with results from other groups. Besides, primary cells could be harvested from the cortical bones of deficient mice and they showed negative expression of CD44, suggesting animals of different genetic backgrounds may have different MSC marker expression. These differences may be employed to study the effect of certain genes when appropriate controls are used.

The MSCs from Lewis rats isolated from bone marrow and cortical bones in our study showed flattened morphology within three passages with loss of chondrogenic potential. The use of cell culture medium for human MSCs (α-MEM with 15% FBS and 0.5 ng/ml hFGF-2) did not rescue the change in cell morphology upon culturing on monolayer. It was unknown that whether MSCs from Lewis rats have high chondrogenic potential due to limited related systematic studies available in literatures. In contrast, human MSCs were used extensively in chondrogenesis and spindle-like cells were obtained from all eight human bone marrow samples used in our study without much difficulty.

Exogenous TGF- β1 is required in pellet formation in mouse C3H10T1/2 cells but not in human bone marrow MSCs, indicating there may be difference in requirements for chondrogenesis between mouse and human. The study of human umbilical cord MSCs and bone marrow MSCs implied the age of the donors or source of MSCs may have influence on the chondrogenic potential of the isolated MSCs. The MSCs from bone marrow clot and transferred medium have showed adipogenic and osteogenic potential, suggesting they may be used as well. Contrary to what was expected, culturing human MSC pellets in hypoxia (3% oxygen) did not show significant differences in gene expression compared to normoxia (21% oxygen). This may be due to the intrinsic hypoxic conditions developed by the high density

cell culture when the cells reduce the oxygen level during respiration. Yet further experiments may be required for more concrete evidence.

In short, different aspects of mouse, rat and human MSCs were studied and summarized in this Chapter, which help in the understanding of researches related to MSCs. Practically, the following were decided/ will affect our decisions in the experimental design.

- With the availability of human bone marrow in our department, we will focus on using human bone marrow MSCs.
- MSCs from other species may be considered for studying the effect of specific mutation such as in the NOD/SCID mice.
- The difference in requirements of chondrogenic supplements between mouse 10T1/2 cells and human bone marrow MSCs alerts us that cautions should be taken when deciding the experiment conditions based on studies using other species as cells from different species may behave differently.
- The pellet culture system may generate a hypoxic state in cells at the centre of the pellets which reduces the difference between the culturing at normoxic (21% O_2) and the culturing at hypoxic conditions (3% O_2). However, this study did not rule out the possibility of difference between normoxia and even lower oxygen concentrations such as 1% O_2.

5.7 Appendix

5.7.1 Hypoxia

5.7.1.1 Effect of oxygen tension on IVD

NP in the adult IVD is avascular [232, 233] and the oxygen tension is low within the IVD [234]. The disc cells were suggested to be highly adapted to the local environment by having limited need for oxygen [235]. HIF-1β was present in NP, AF and CEP but at lower levels in AF and CEP, while HIF-1α was only expressed in NP but not in AF or CEP. The immunostaining of HIF-1α in NP was light and diffuse [236]. Risbud *et al.* showed that HIF-2 protein was expressed *in vivo*. The protein and messenger RNA (mRNA) expression were similar under both normoxic and hypoxic conditions but a significant increase in HIF-2 transactivation was observed under hypoxic conditions. *VEGF* is a common target gene for HIF-1 and HIF-2 in NP cells and forced expression or suppression of *cited2* caused corresponding changes of *VEGF* expression, suggesting some mechanisms in the inhibition of blood vessel formation in the healthy disc [237]. Risbud *et al.* also showed that rat NP and AF cells expressed components of the Notch signaling pathway. *Notch1* and *Notch4* mRNA expression was increased in hypoxia and inhibition of Notch signaling blocked disc cell proliferation. The expression of Notch signaling proteins was found to be higher in degenerated discs [238]. In normoxia, HIF-1α subunit is constantly expressed in rat, sheep and human NP cells. Unlike other skeletal cells, when maintained under hypoxia, the NP cells had a minimal induction in HIF-1α protein levels. The HIF-1α in NP cells had increased transcriptional activity under hypoxia compared to normoxic level but this induction was small when compared to other cell types. These results indicate that normoxic stabilization of HIF-1α is a metabolic adaptation of NP cells to a unique oxygen-limited microenvironment. The study confirmed that HIF-1α can be used as a phenotypic marker of NP cells [88]. Regarding polymorphism, Lin *et al.* suggested that HIF-1α 1790 A > G polymorphisms may be used as a molecular marker to determine the susceptibility and severity of lumbar disc degeneration [239].

5.7.1.2 Effect of oxygen tension on cartilage

Compared to IVD, there are more studies of hypoxia in cartilage. NP cells in adult animals such as human, monkey and cow are chondrocyte-like and thus the understanding of the effects of hypoxia in cartilage is highly relevant to IVD. In cartilage of large animals, the cells are under hypoxia due to lack of blood supply. They are highly adapted to this hypoxic condition and use it to promote tissue-specific function [240]. Lafont *et al.* found that the matrix synthesis and SOX9 expression was enhanced by hypoxia for human articular chondrocytes [241]. In explant culture, spontaneous and induced destruction of human cartilage was suppressed by hypoxia [240]. They showed that HIF-2α, but not HIF-1α, is essential for hypoxic induction of the human articular chondrocyte phenotype. Depleting SOX9 prevented hypoxic induction of matrix genes, suggesting that HIF did not directly target matrix genes but up-regulated their expression via SOX9 [241]. HIF-2α was later found to promote SOX9-independent factors as well [242]. Under hypoxia, HIF-2α can directly bind to SOX9 and affects matrix synthesis. And HIF-1α mediates anticatabolic responses. Depleting HIF-targeting prolyl hydroxylase-containing protein 2 (PHD-2) further enhanced cartilage responses as compared to hypoxia alone. Similar hypoxic regulation of tissue-specific metabolism were found in cartilage of human and pig but not of mouse [240].

5.7.1.3 Different approaches of achieving hypoxia

As shown in **Figure 5-27**, there are different approaches of achieving hypoxic response in cells which are further explained in the following sections.

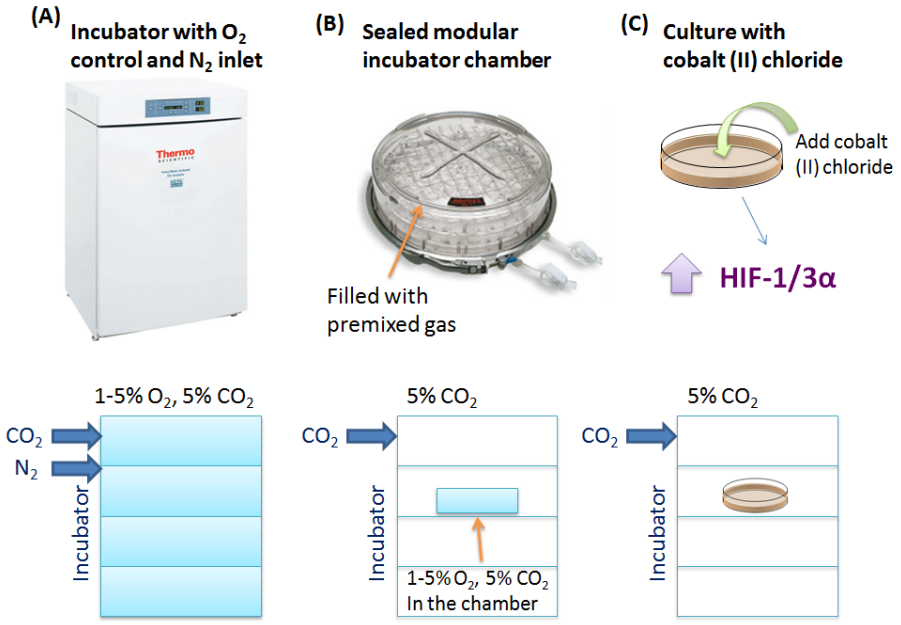


Figure 5-27 Some common approaches of achieving hypoxia. (A) Using a hypoxic incubator with oxygen control by nitrogen influx, (B) a sealed modular incubator chamber which can be filled with premixed gas of defined compositions and (C) the mimicking of hypoxic responses using cobalt (II) chloride.

5.7.1.4 Hypoxia using hypoxic incubator with nitrogen (Figure 5-27A)

In normal cell culture incubator, the carbon dioxide (CO_2) content is maintained at 5-10% to provide suitable CO_2 content in equilibrium with the bicarbonate buffered cell culture medium. This CO_2 concentration was maintained by the supply of CO_2 into the incubator in a controlled manner through a sensor and a regulator. Similarly, hypoxia can be achieved by using nitrogen to replace oxygen in the incubator, thus lowering the oxygen (O_2) content. In a hypoxic incubator (**Figure 5-27A**), there are both O_2 and CO_2 sensors and controls. The desired CO_2 content is regulated by the CO_2 sensor and control to supply appropriate quantity of CO_2 into the incubator while the desired O_2 content is regulated by the O_2 sensor and control to supply appropriate quantity of nitrogen (N_2) into the incubator. The more nitrogen is injected into the incubator, the lower the oxygen content is in it.

5.7.1.5 Hypoxia using a modular incubator chamber (Figure 5-27B)

Another method of achieving desired oxygen concentration is by filling a sealed modular incubator chamber with premixed gas of the desired gas compositions (**Figure 5-27B**). As the chamber is sealed, there is no gas exchange with the surroundings, thus the cells are cultured in an environment with the compositions similar to the premixed gas. The compositions of the premixed gas can be tailored by mixing different gases in particular ratios in the gas cylinder and this is done by the gas supply company (for HKU, Linde HKO Limited). The compositions of gases may be slightly different from the premixed gas compositions as water is normally excluded in the premixed gas but supplied in the chamber by placing a dish of sterile water without a lid covering it.

5.7.1.6 Hypoxia by Cobalt (II) chloride (Figure 5-27C)

When cells are cultured under hypoxia, the HIF1A expression is elevated. During hypoxia, hypoxia inducible factor alpha (HIF) is stabilized and regulates various genes such as those involved in angiogenesis [243]. Cobalt (II) chloride can mimic hypoxia by inducing HIF-1/3α (**Figure 5-27C**) and this method is comparatively inexpensive and fast. However, it can also regulate other genes, thus it may be necessary to check whether other non-hypoxia related effects are also induced by the chemical. The use of cobalt (II) chloride allows researchers to open the culture containers many times without affecting the "hypoxic condition" [244].

5.7.1.7 Calculations of gas compositions

In this study, we set up the hypoxia for studying MSCs. For *in vitro* cell culture, hypoxic/ normoxic conditions were maintained by controlling the air composition. In this section, we calculate the gas composition in order to understand the hypoxic system better. The percentage of water vapor in the incubator is not given directly by the manufacturer but it can be calculated based on relative humidity. In order to maintain a humid environment in the

incubator to avoid drying of cell culture, it is suggested that the relative humidity of the incubator should reach 95%. The following equation defines relative humidity:

$$RH = \frac{\text{vapor pressure of a sample}}{\text{SVP of the sample at same temperature}} \times 100\%$$

where RH is the relative humidity and SVP is the saturated vapor pressure of water at a given temperature [245]. The saturated vapor pressure of water at 37 ˚C can be calculated by the following Antoine equation:

$$\ln P^{sat} = 16.262 - \frac{3799.89}{T^{sat} + 226.35}$$

where T^{sat} is the temperature in ˚C and P^{sat} is the vapour pressure in kPa [246]. Thus the calculated saturated water vapor pressure was 6.25 kPa and 95% relative humidity corresponds to 6.25 × 95% kPa = 5.94 kPa.

At normal ambient atmosphere, the total air pressure is 101.325 kPa. Thus the percentage of water in air at 37˚C with 95% relative humidity = 5.94 kPa / 101.325 kPa × 100% = 6%.

Table 5-6 Percentages of some major gases in atmosphere and hypoxic conditions used in cell culture

	Atmosphere	Normoxia	Hypoxia
Nitrogen	78%	68%	84-88%
Oxygen	21%	21%	1-5%
Carbon dioxide	0.04%	5%	5%
Water	1%	6%	6%

5.7.2 Influence of ERK on NP cells/ MSCs

There is increasing evidence suggesting the association of obesity and aberrant proliferation of NP cells with IVD degeneration. Leptin, a hormone with increased circulating level in obesity, has been shown to induce human NP cell cyclin D1 expression and proliferation through the activation of JAK/STAT3, PI3K/Akt or MEK/ERK signaling [247]. Rat NP cells are adapted for survival in hypoxic condition through the activation of the PI3K/Akt and MAPK survival pathways [248]. On the other hand, NP cells were suggested to be optimally

adapted to a hyperosmotic state and the adaptation of the NP cells to their hyperosmotic milieu is dependent on activation of the ERK and p38-MAPK pathways acting through TonEBP and its target genes [249]. Expressions of collagen II and aggrecan were elevated when rat MSCs were inhibited by PD98059, an ERK inhibitor, during stimulation with TGF-β1 [201].

5.7.3 Influence of p38 on IVD cells/ MSCs/ spine

In a study of obesity in ECM degradation using rats, Cheng *et al.* concluded that p38 MAPK activation seemed to be an intermediate mechanism inducing ECM degradation in the IVD of diabetic rats by affecting MMPs/ TIMPs balance [250]. Studer *et al.* suggested that production of factors associated with inflammation, pain, and disc matrix catabolism can be reduced by inhibiting the p38 MAPK in cytokine-activated NP cells [99]. Besides, inhibiting p38 MAPK in rabbit NP cells increased mRNA for matrix proteins (aggrecan, collagen II, versican and collagen I) and anabolic factors (IGF-1, TGF and SOX-9) while decreased basal PGE-2 accumulation, but had no effect on message for TIMP-1, MMP-3 or COX-2 [200].

Activated p38 may be involved in the pathophysiology of pain following lumbar disc herniation [251]. It was also suggested that the p38 MAPK pathway signals are responsible for much of IL-6 and proteoglycan secretion from AF cells with macrophage-like cells, which suggest blocking this signal may be a therapeutic approach to discogenic pain [252]. The results of a study by Niu *et al.* supported that the p38 MAPK signal may be responsible for many of the inflammatory and catabolic changes seen in the human disc degeneration, and hyperbaric oxygen treatment may provide a therapeutic approach to slow the course of IVD degeneration [253]. The effect of asialo-erythropoietin, a neuroprotective agent, may be related to the inhibitory action of p-p38 and TNF-α in the dorsal root ganglion [254]. With the study using RAW 264.7 cells, Xiao *et al.* suggested that TGF-β1 inhibits inflammatory cytokine production selectively through cross-talk between MAPKs [255].

5.7.4 Gene expression markers

5.7.4.1 Matrix genes and typical chondrocyte markers

ACAN and COL2A1

Aggrecan (ACAN) and collagen II are two major extracellular matrix in NP [10, 22, 256] and they are commonly used as molecular markers for IVD cell studies [34, 169, 257, 258]. Collagen II is a fibril-forming collagen and three collagen type II alpha 1 chains (coded from *COL2A1*) form a triple helix. It is expressed in cartilage, vitreous body and NP [256, 259]. In transgenic mouse embryos, a 48bp sequence in the first intron of *Col2a1* drove gene expression specifically in cartilage [260].

COL1A1 and COL3A1

Collagen I and collagen III are two other fibril-forming collagens [256, 259]. Each triple helix of collagen I was formed by two collagen type I alpha 1 (COL1A1) chains and one collagen type I alpha 2 (COL1A2) chain. Collagen I is abundant and widespread. For example, it is present in dermis, bone, tendon, ligament and cornea. Collagen III is made of three collagen type III alpha 1 chains and it is present in skin, vessel wall and reticular fibers of most tissues [256, 259].

COMP

Cartilage oligomeric matrix protein (*COMP*) was shown to be a primary response gene of TGF-β1 and it was upregulated earlier than *COL2A1* during chondrogenic differentiation of human bone marrow MSCs [261]. *Comp* relative mRNA expression is lower in rat NP compared to AF and AC [262].

SOX9, SOX5 and SOX6

Lefebvre *et al.* showed that *Col2a1* expression correlated with SOX9 mRNA and protein in chondrocytes and SOX9 is involved in the control of the cell-specific activation of COL2A1 in chondrocytes [263]. L-Sox5, Sox6, and Sox9 are transcription factors that bind and

cooperatively activate the enhancer of *Col2a1 in vitro*. They were co-expressed in all pre-cartilaginous condensations in mouse embryos and continued to be expressed in chondrocytes until final hypertrophy of the cells [260]. When *Sox9* cDNA was stably overexpressed in rat chondrocytic cells like CFK2, there was a larger proportion of SOX9-transfected cells accumulated in the G0/ G1 phase [264]. SOX9 changes the rate of chondrocyte cell cycle progression and their differentiation by enhancing or inhibiting the expression of p21cip1 and ERK1, and N-cadherin is an additional direct target of SOX9 [264].

MIA

Melanoma inhibitory activity (MIA) is a protein isolated from human melanoma cell lines while the same protein isolated from primary bovine chondrocytes and cartilaginous tissues is called cartilage-derived retinoic acid-sensitive protein (CD-RAP). The expression of MIA was limited to cartilaginous tissues and was initiated with the advent of chondrogenesis, remaining abundant throughout development [265]. The nuclear RNA-binding protein 54-kDa ($p54^{nrb}$), a recently described modulator of Sox9 activity was shown to be downregulated in the cartilage tissue MIA deficient mice [266]. When human MSCs were cultured in the presence of MIA and BMP-2, osteopontin and osteocalcin expression was downregulated compared with BMP-2 treated MSCs cultured in the absence of MIA. Besides, MIA stimulates extracellular matrix deposition and increased the glycosaminoglycan content of human primary chondrocytes [267].

RUNX1

Runx1 and Runx2 were co-expressed in undifferentiated mesenchyme during embryonic development and Runx1 is highly expressed compared to Runx2 during chondrogenesis [268]. It was suggested that Runx1 may have a role in mediating early events in endochondral and intramembranous bone formation [269]. From *in situ* hybridization study in mouse embryo, Runx1 and Sox9 were specifically expressed in the osteogenic cell compartments and

downregulated when the osteoblasts were terminally differentiated [270]. Runx1 was required for the commitment and differentiation of chondroprogenitors into the chondrogenic lineage [271].

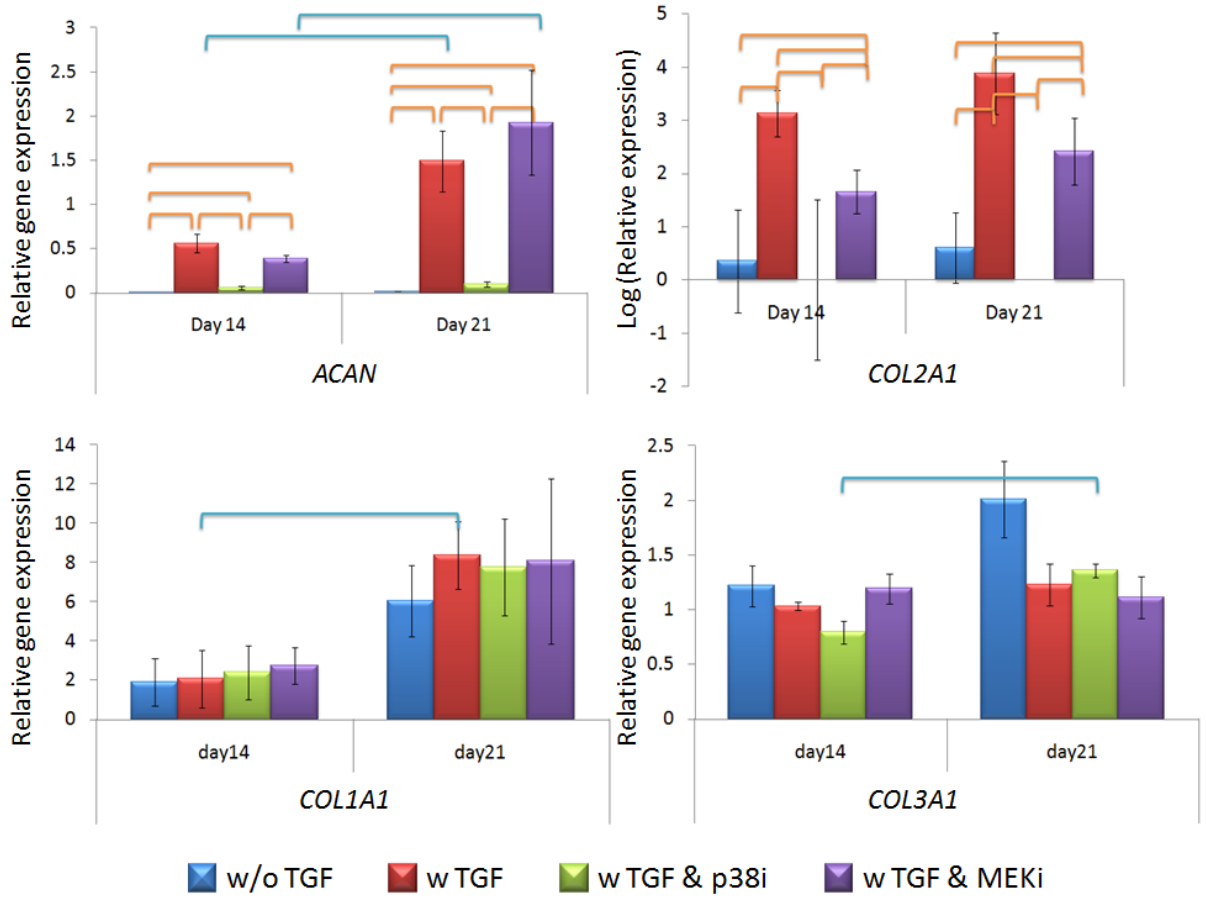


Figure 5-28 Relative mRNA levels of matrix genes in hMSC pellets cultured with different conditions (without TGF-β1, with TGF-β1 with and without p38/ MEK inhibitors) under normoxia. (relative to *GAPDH* and one of the samples with TGF-β1 at day 14 without inhibitors added; mean ± SEM for *ACAN*; mean ± SD for *COL2A1*, *COL1A1* and *COL3A1*; for *ACAN* and *COL2A1*, two independent experiments, biological triplicates and technical duplicates; for *COL1A1* and *COL3A1*, biological triplicates; $p < 0.05$, orange brackets for comparison between sample groups and blue brackets for comparison between day 14 and day 21).

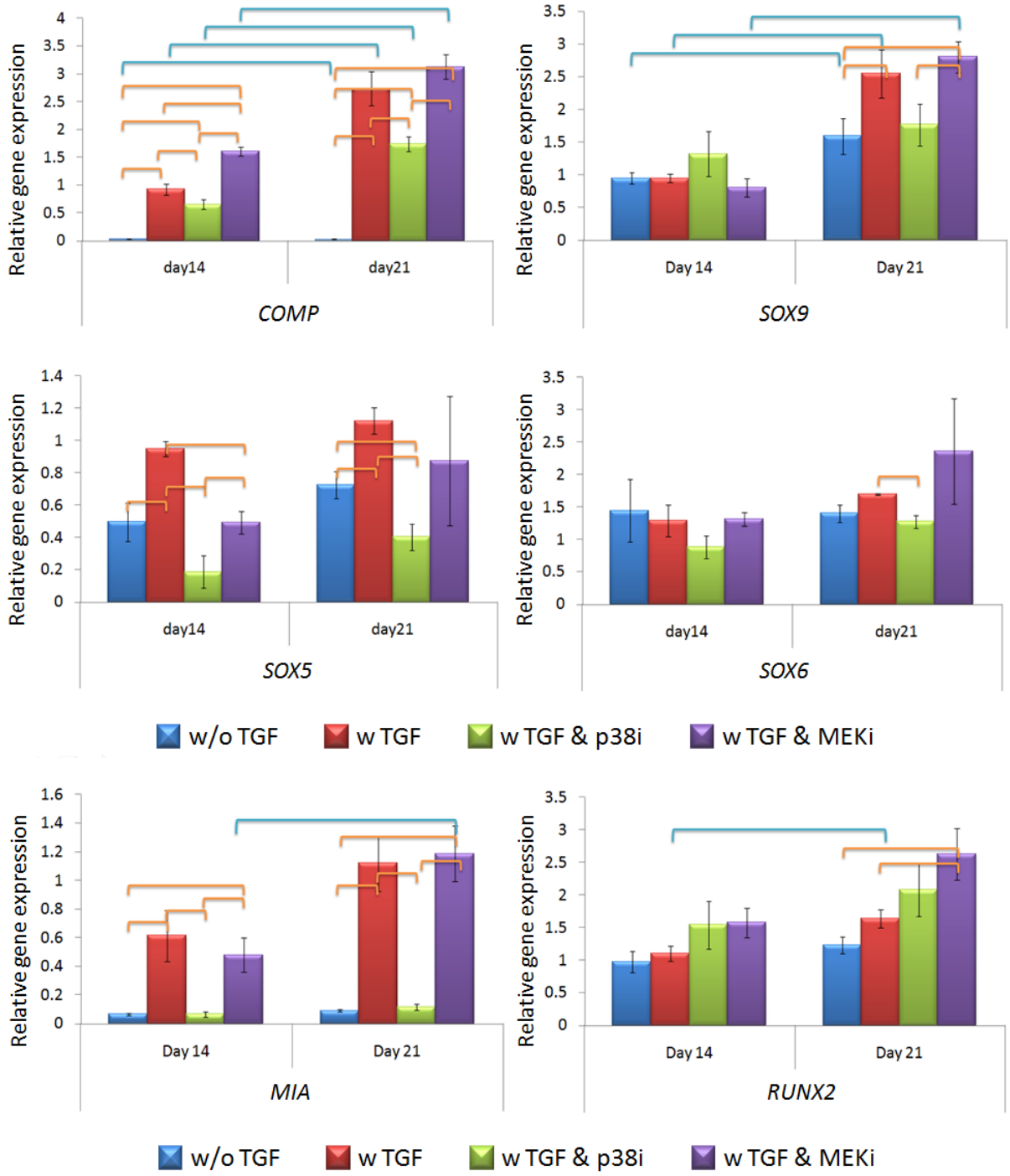


Figure 5-29 Relative mRNA levels of chondrogenic genes in hMSC pellets cultured with different conditions (without TGF-β1, with TGF-β1 with and without p38/ MEK inhibitors) under normoxia. (relative to *GAPDH* and one of the samples with TGF-β1 at day 14 without inhibitors added; mean ± SEM for *SOX9*, *MIA*, *RUNX1* and *COMP*; mean ± SD for *SOX5* and *SOX6*; for *SOX9*, *COMP*, *MIA*, *RUNX1*, two independent experiments, biological triplicates; for *SOX5* and *SOX6*, biological triplicates; $p < 0.05$, orange brackets for comparison between sample groups and blue brackets for comparison between day 14 and day 21).

5.7.5 FAST staining

The following protocol is provided by Dr. Victor Leung.

5.7.5.1 Principle

This protocol is designed for multi-color labeling of histological structure of IVD using a combination of Alcian blue, Safranin O, Tartrazine, and Fast green stain. The rationale of the technique is that, by first staining the acidic glycoproteins with Alcian blue, they are chemically blocked and will not react further with Safranin O. The neutral glycoproteins are subsequently demonstrated in a contrasting manner with Safranin O staining. Where there is a mixture of acidic and neutral glycoproteins, the resultant colour will reflect the dominant moiety. The Safranin O staining of the disc, mainly in the AF, is differentiated from the growth plate cartilage by a subsequent alcohol treatment. The remaining mucin and collagen moieties in bone and fibrous structures are finally stained by Tartrazine and Fast green. An extended staining in Alcian blue can further help defining the AF into discrete layers and visualization of the CEP in the expense of contrast between NP/ AF [203].

5.7.5.2 Reagents

1% (w/v) Alcian blue, pH 1.0

Alcian blue 8GX	5 g
Distilled water	450 ml
Hydrochloric acid 1M	50 ml (915 ml H_2O + 85 ml concentrated HCl)

(Dissolve the dye in the distilled water first, then add acid.)

0.1% (w/v) Safranin O Solution

Safranin O	0.5 g
Distilled water	500 ml

0.25% (w/v) Tartrazine Solution

Tartrazine	1.25 g
Distilled water	500 ml
Acetic acid	1.25 ml

0.01% (w/v) Fast Green (FCF) Solution

Fast green, FCF	0.05 g
Distilled water	500 ml

All materials can be obtained from Sigma.

5.7.5.3 Methods

FAST staining pattern largely depends on the proteoglycan content. Decalcification process has a strong impact on the staining pattern and intensity because inappropriate decalcifying agents may lead to a loss of proteoglycans from the tissue. Ethylenediaminetetraacetic acid (EDTA) is commonly used but is known to give inconsistent results due to this reason. Morse's solution (10% w/v sodium citrate, 20% v/v formic acid) has been tested and suggested to be a better choice of decalcifying agent for FAST staining. Bad quality sections might also result in altered behavior of the stains.

Procedures

Dewaxing and rehydration of paraffin sections

Step 1: Place in the oven at 60 ^{o}C for 2 h and leave it to cool down for 20-30 min

Step 2: Dewax in xylene for 10 min for 2 times

Step 3: Rehydrate the sections in 100% ethanol (5 min for 2 times), 70% (v/v) ethanol (5 min), 30% ethanol (5 min), tap water (5 min for 2 times)

FAST staining

Go through the following steps non-stop until sections are air-dried.

Step 1: Stain in Alcian blue solution for 2.5 min (10 min for extended protocol) [a]

Step 2: Rinse 3 times with tap water, briefly and gently

Step 3: Stain in Safranin O solution for 3 min

Step 4: Rinse 3 times with tap water, briefly and gently

Step 5: Differentiate in 50% ethanol for 1 min

Step 6: Rinse 3 times with tap water, briefly and gently

Step 7: Stain in Tartrazine solution (2.5X dilution) for 10 s [b]

Step 8: Rinse 3 times with tap water, briefly and gently

Step 9: Stain in Fast green solution for 5 min

Step 10: Rinse 3 times with tap water, briefly and gently

Step 11: Dry the sections using a hairdryer [c]

Step 12: Put into xylene and mount with Depex

Technical notes of FAST staining

a. Prolonged staining in Alcian blue will result in a domination of blue stain over red/ orange stain in the outcome. In practice, as IVD from different species will have slightly different GAG compositions and hence preference to Alcian blue interaction, researcher may wish to slightly adjust (usually reduce) the length of incubation time for a particular species to optimize the contrast. Increase the staining to 10 min for study of additional features (see Principle in **Section 5.7.5.1** described previously).

b. Overtime in tartrazine will result in loss of Safranin O stain.

c. The use of ethanol for dehydration should be avoided as it will result in loss of Safranin O stain.

Chapter 6 Optimization and Development of Cell Micropattern Preparation

6.1 Background

6.1.1 Effect of cell shape or geometry

It has been shown by different groups that cell shape can affect biological responses such as DNA synthesis, apoptosis and differentiation. In 1978, Folkman and Moscona studied the role of cell shape using different concentrations of poly(2-hydroxyethyl methacrylate) (pHEMA) [272]. In their study, the polymer solutions were applied on plastic culture surface to form a thin, hard, sterile and optically clear film that was tightly bonded to the plastic surface after the alcohol evaporated. Endothelial cells cultured on thicker layers of polymer were more spherical while the cells cultured on thinner layers were flatter. With this system, Folkman and Moscona observed a decrease in DNA synthesis when the endothelial cells were more spherical in shape. In 1997, Chen *et al.* has shown that endothelial cell shape could govern the growth and death of individual cells, independent of the type of matrix protein used to mediate the adhesion [273]. Consistently higher apoptosis rates were observed for endothelial cells cultured on 20 μm circles compared to non-patterned substrates prepared using different matrix proteins [273].

For chondrocytes, the relationship between cell shape and chondrogenesis has also been studied extensively for more than two decades [274]. Chondrogenesis in single cells was promoted when cultured in suspension, agarose, collagen gels or non-adhesive substrata which supported a round cell shape [274-277]. When isolated chondrocytes were cultured in monolayer, de-differentiation is observed which may be contributed by at least two possible mechanisms: (i) the de-differentiation of the differentiated chondrocytes and (ii) the proliferation of the less differentiated progenitor population which increases in its ratio in the cultured cells along passaging due to its potentially higher proliferation rate. Chondrocyte

de-differentiation may be partially reversed by restoring the round shape of cells [43]. This may be through the "re-differentiation" of the de-differentiated chondrocytes and the differentiation of the progenitor cells into chondrocytes.

Cell shape changes are mediated by proteins of cytoskeleton, cell surface receptors and molecules of extracellular matrix [278]. Cell shape and cytoskeleton were co-studied in some studies [278-282]. An alteration of mechanotransduction by blockage of integrin binding or disruption of actin filament organization has been shown to promote chondrogenesis [283, 284]. Actin organization can be affected by other cytoskeletal components or growth factors. It has notably been shown that the configuration of the actin cytoskeleton in bovine articular chondrocytes (AC) is indirectly altered when the intermediate filament structure is disrupted [285]. Actin organization can also be affected by exogeneous growth factors or cytokine. With GFP-actin expressed in human chondrocytes, Haudenschild *et al.* showed that TGF-β enhanced actin extensions and lamellar ruffling, while IL-1β resulted in cellular contraction [286].

NP cells in adult human are generally accepted as chondrocyte-like as they also constitutively express collagen II and proteoglycans [287, 288]. The cytoskeletal organization in bovine NP and AF cells has previously been studied. A differential distribution and expression of β-actin, tubulin and vimentin was observed between bovine NP and outer AF tissues [289]. A significantly higher expression of β-actin mRNA and protein levels was observed in the outer AF compared with NP in discs from both young and skeletally mature animals [289]. To date, however, little is known about how disc cells respond to cell shape in *in vitro* culture. It has been suggested that NP cells cultured in monolayer might revert to their native characteristics when returning to a 3D environment [44]. In our study, we optimized a platform for creating NP cell micropatterns.

6.1.2 Micropatterning

Micropatterning is the creation of patterns in micron scale, often in an array in a controlled fashion. It has been used to study different biological phenomenon such as apoptosis [273], traction force generation [290], cell internal organization [291] and division axis [292]. When the cells are cultured on small micropatterns, they are rounder in shape. When they are cultured on large micropatterns or flat culture surface of large cell adhesive area, they are more spread. Using micropatterns, it has been demonstrated that cell shape/ spreading plays an important role in the differentiation of MSCs to specific lineages or maintenance of the phenotypes in differentiated cells. For example, the expression of chondrogenic markers was higher when cells were round in shape compared to cells spread on planar surfaces. Gao *et al.* showed that the stimulation of well-spread hMSCs on 10000 μm^2 square micropatterns with TGF-β3 upregulated the expression of smooth muscle cell-specific genes, whereas cells allowed to spread on small square micropatterns of 1024 μm^2 upregulated chondrogenic genes [293]. Microcontact printing has also been used to study chondrocytes [294, 295] but has not been utilized to study NP cells to date.

Similar to chondrocytes, NP cells are spherical in shape when they are in the NP tissue *in vivo*. However, when the cells are isolated from the tissue and cultured on planar plastic surface using standard cell culture practice, the cells become flattened (**Figure 6-1A**). In order to maintain the native spherical shape of NP cells, several strategies have been used in the field. Cells can be seeded in a conical tube or polypropylene plates with V-shape bottoms to form dense pellet culture. The cells are in close contact with each other and maintain their spherical shape (**Figure 6-1B**). Alternatively, cells can be cultured in 3-dimensional biomaterials such as hydrogels where the cells remain spherical in shape (**Figure 6-1C**). These two methods have been commonly used in chondrogenic study but are often associated with nutrient and metabolite diffusion issues. The cells in the center of the pellets or 3-dimensional materials may have less access to nutrients or oxygen compared to cells near the pellet/ biomaterial surfaces. In this project, we impose defined cell shape by culturing cells on protein

micropatterns of defined shapes created by microcontact printing on plastic surfaces (**Figure 6-1**D).

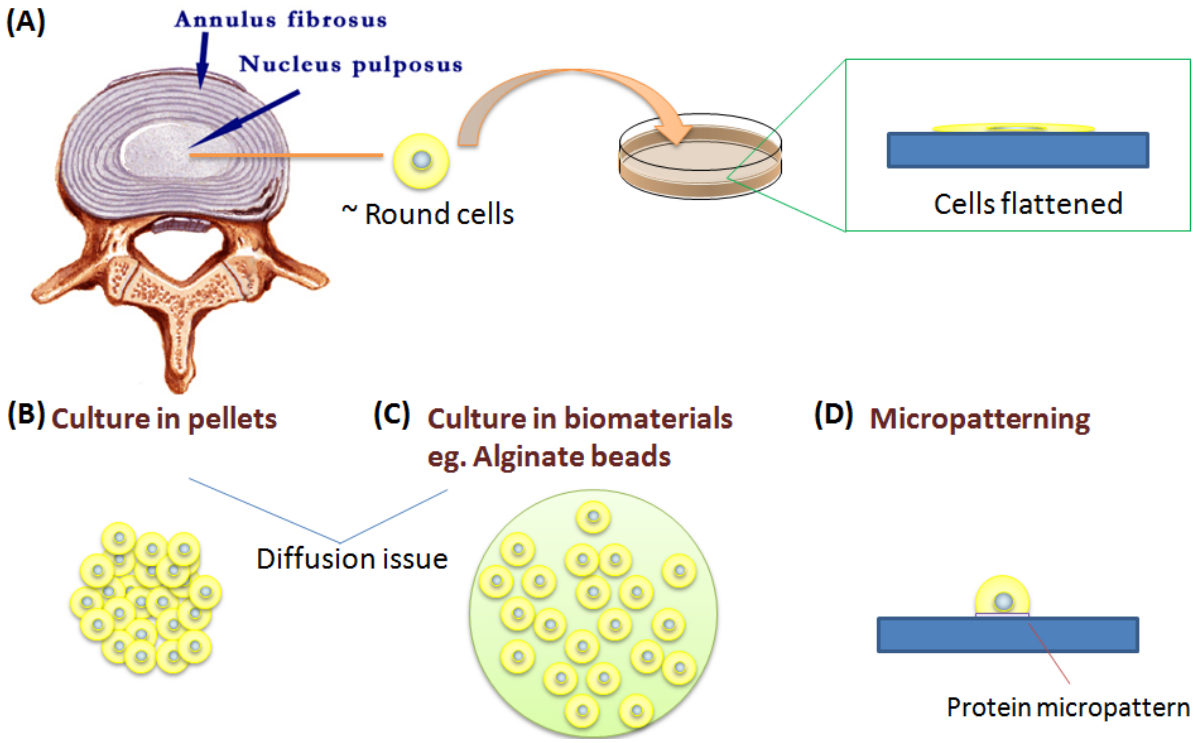


Figure 6-1 Schematic showing how cells are maintained in round shape using different methods. (A) Cells became flattened when cultured on a planar plastic surface, (B) cells cultured in pellets, (C) cells cultured in biomaterials and (D) cells cultured on a protein micropattern. Cells can be maintained in near-round shape when they are cultured in pellets or in biomaterials such as alginate beads but the cells at the centre of the pellets/ beads will have less access to nutrients and oxygen compared to those near the surface. With the use of micropatterns, the cells can be maintained in near-round shape at single cell level and surrounded by medium of concentrations the same as the bulk medium.

6.1.3 Micropatterning methods

A number of techniques have been developed to generate protein micropatterns, including photolithography, stencil-assisted patterning, laser/ electron beam etching, micro/ nano printing, microcontact printing, UV-based patterning, *etc.* [296-299]. Each method has its advantages and drawbacks. Although photolithography and stencil-assisted patterning give good spatial resolution, the requirement of specialized microfabrication facility with the involvement of highly toxic chemicals limits their use in biology studies [299]. Laser/

electron beam etching and micro/ nano printing are quite versatile but require special equipments and may be slow for generating a satisfactory spatial resolution [299]. UV-based methods can be more available to biologists but often require special surface chemistry and photomasks [299].

Microcontact printing technique was originally developed for the production of patterns in microelectronics application [300] but was later adapted to the creation of substrates for cellular patterning [301]. In microcontact printing, an elastomeric stamp is formed by casting the liquid-phase polymer over a microstructured master. The stamp is removed from the master after hardening and the surface with patterns is inked with protein solution. Excess protein solution is blown away and the stamp surface with proteins is brought into contact with the surface of a selected culture material, to which the proteins get transferred (**Figure 6-2**). Subsequently, the non-patterned area is backfilled with non-fouling molecules after which cells can be seeded and attached exclusively (or predominantly) on the area with "ink" [296]. Microcontact printing requires no special equipment and no special chemistry once the mold (silicon wafer with micropatterned photoresist) for stamp fabrication is available [299] (See **Section 6.1.4** for the details of the fabrication process). Thus this microcontact printing method may have great potential for use in most biology laboratories and it is cost-effective.

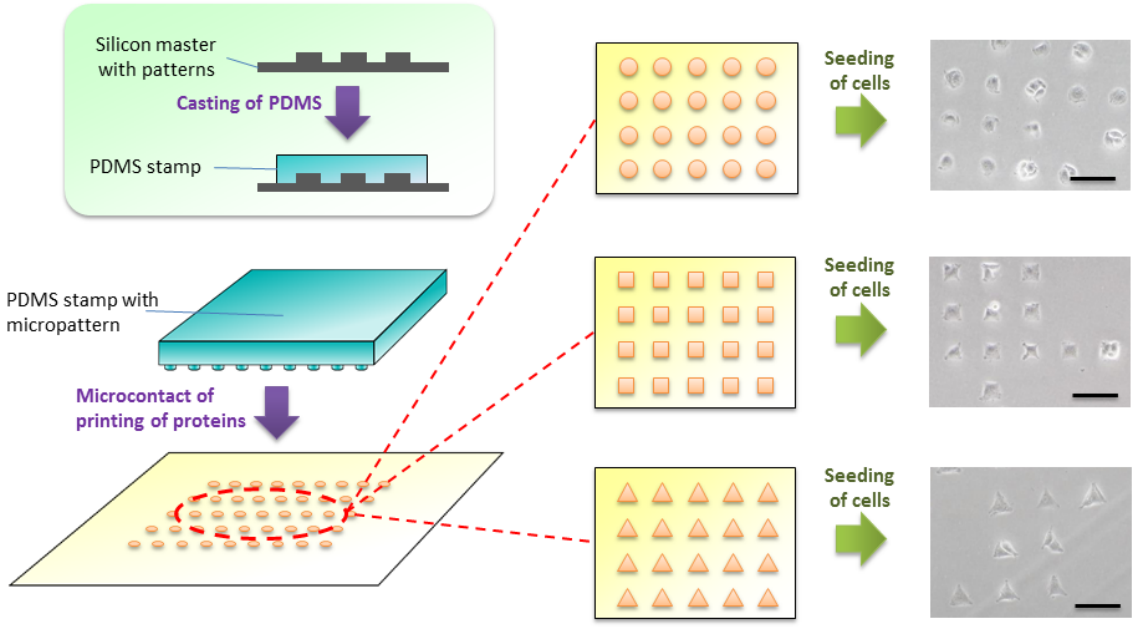


Figure 6-2 Simplified schematic showing cell patterning through microcontact printing of proteins. PDMS stamps with different patterns can be molded from the silicon master patterned with photolithography technique. Then these PDMS stamps can be used to print proteins on plastic surfaces. The cells take up the shapes of the patterns. Representative phase contrast photos of chondrocytes on different shapes of patterns after 1 day seeded on the protein micropatterns are shown on the right (scale bar = 100 μm).

6.1.4 General procedures involved in patterning with microcontact printing

Figure 6-3 shows the fabrication of silicon master with defined micropatterns and preparation of polydimethylsiloxane (PDMS) stamps. First, the silicon wafer is cleaned to remove any contaminant on it. A thin layer of photoresist is then spin-coated on the wafer (**Figure 6-3A**). The thickness of the photoresist will determine the height of the micropattern features in the PDMS stamps and can be controlled by choosing appropriate photoresits and tuning the spin coating speed. Then the silicon wafer with photoresist is covered with a photo mask containing the desired patterns and exposed to UV light (**Figure 6-3B**). Light can pass through the transparent area of the photomask and cause chemical change in the photoresist while the opaque part of the photo mask obstructs the UV, protecting the photoresist underneath. Afterwards, the photomask is removed and the photoresist is developed in a developer solution, followed by rinsing with water and drying with a flow of filtered air. The zones of photoresist that have been exposed to UV are removed by this development process,

leaving patterns on the silicon wafer that replicate as the opaque area of the photomask. This silicon master can then be used to fabricate PDMS stamps (**Figure 6-3C**). PDMS with micropatterns can be formed from the silicon master by pouring PDMS polymer mixed with curing agent on to the silicon master (**Figure 6-3D**). The PDMS gets into the cavities of the master and takes up the shape of the micropatterns. Then the PDMS is cured into a solid polymer block by heating at an elevated temperature (60 °C) overnight. The cured polymer block can be detached from the silicon master by careful cutting and peeling. PDMS stamps with appropriate sizes (eg. 1 cm × 1 cm) are cut from this polymer block.

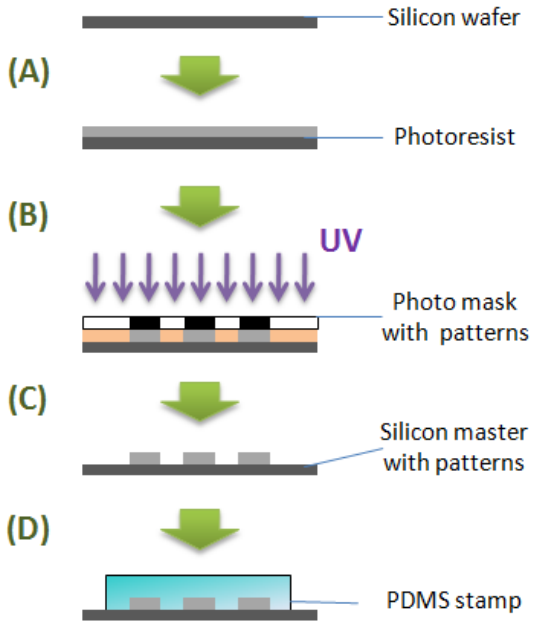


Figure 6-3 Fabrication of silicon master with micropatterns and preparation of PDMS stamps. (A) Coating of silicon wafer with photoresist by spin coating; (B) Changing the solubility of photoresist in a developer solution using UV radiation (the solubility of the area underneath the opaque area of the photo mask was not changed); (C) Removing the photoresist which has been irradiated by the developer solution; and (D) Preparation of a PDMS block on the patterned silicon wafer. The PDMS polymer will take up the patterns of the patterns on the silicon master.

The preparation procedures to produce protein patterns and eventually cell patterns are slightly different for different laboratories and **Figure 6-4** shows a simplified flow of the procedures used in our lab. To prepare cell micropatterns, the PDMS stamps are plasma treated in air to make the surfaces more hydrophilic which facilitate the uniform spreading of

protein solution on the stamp surface. This may also facilitate the transfer of proteins from the PDMS to the culture substrate surface when the proteins have weaker adhesion on hydrophilic surface [302, 303]. The stamps are then covered with a drop of protein solution (eg. fibronectin solution) and incubated at room temperature to allow time for the adsorption of proteins to the PDMS surfaces (**Figure 6-4A**). After the incubation, excess protein solution is blown away by compressed air, resulting in a thin film of protein on the PDMS stamps (**Figure 6-4B**). Immediately after this, the stamps are put into contact with the culture substrate surfaces such as untreated cell culture plates with the patterns facing down (**Figure 6-4C**). Gentle force is applied to ensure good transfer of proteins from the PDMS stamps to the culture surfaces. Insufficient force may result in incomplete pattern transfer and excessive force may result in non-specific transfer of proteins. The PDMS stamps are removed after several minutes of contact with the culture surfaces, leaving protein micropatterns on them (**Figure 6-4D**). The surfaces without protein patterns are passivated (made cell non-adhesive) by a passivating agent such as a 1% (w/v) pluronic solution (**Figure 6-4E**). After 30 to 60 min incubation at room temperature, the pluronic solution is removed and the culture surfaces are washed with PBS three times (**Figure 6-4F**). Cells in medium without serum are then seeded on the culture surface with protein micropatterns (**Figure 6-4G**). When cells have attached to a sufficient number of patterns (eg. 2 h after cell seeding), the cell suspension is removed and replaced by medium with serum. The attached cells remain on the culture surface while unattached cells are removed (**Figure 6-4H**). Longer time may be required for the cells to spread on the patterns.

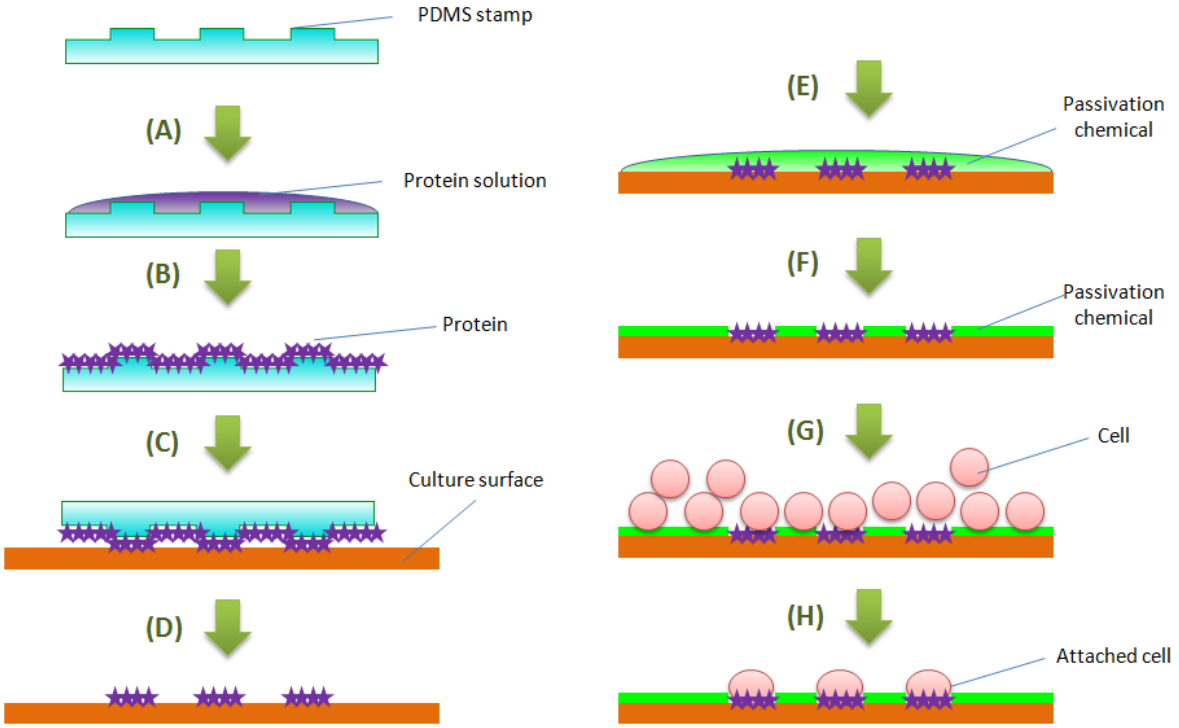


Figure 6-4 Preparation of protein micropatterns and cell micropatterns. (A) A drop of protein solution is put onto a PDMS stamp treated with plasma treatment; (B) Excess protein solution is blown away; (C) The PDMS stamp with protein on it is put into contact with a culture surface; (D) The PDMS stamp is removed from the culture surface leaving the protein behind as protein micropatterns; (E) The passivation chemical is put on top of the protein micropatterns; (F) The excess passivation chemical is removed and the culture surface is washed with PBS, leaving a thin layer of passivation chemical behind in area without protein patterns; (G) Cells are seeded on top of the protein patterns with non-specific area passivated; and (H) Unattached cells are removed by washing with PBS and replaced with fresh cell culture medium.

6.1.5 Cell type specific requirements of micropatterning

Table 6-1 summarized some studies of IVD cells, chondrocytes and hMSCs undergoing chondrogenesis that involve cell micropatterning. A variety of micropatterning methods were used in these studies and there were more studies using chondrocytes than IVD cells. In the study by Mwale *et al.* involving NP and AF cells, the authors created square micropatterns with the use of metal grids as masks and plasma treatments [304]. This method may be a feasible approach for creating square micropatterns of NP or AF cells but patterns of other shapes have not been reported for this method.

Table 6-1 Studies of IVD cells, chondrocytes and hMSCs in chondrogenesis which involved cell micropatterning (AFM: atomic force microscopy, DMMB: 1,9-dimethylmethylene blue, HUVEC: human umbilical vein endothelial cell, LbL: layer by layer, PDMS: polydimethylsiloxane, PEG: polyethylene glycol, RT-qPCR: reverse transcription-quantitative polymerase chain reaction, SAMs: self-assembled monolayers, SEM: scanning electron microscopy)

Group and year	*Cells*	*Micropattern method*	*Materials*	*Patterns*	*Readout*
Mwale *et al.* 2008 [304]	bovine AC, growth plate chondrocytes, NP and AF cells	nitrogen and ammonia plasma treatment with the use of metal grids as masks	polypropylene film	30 µm and 200 µm squares	microscopy
Shaik *et al.* 2013 [294]	canine chondrocytes	photolithography and LbL	microscope cover slips	strips of 80 µm and 100 µm	phase contrast microscopy
Darling *et al.* 2009 [43]	porcine chondrocytes	microcontact printing, with SAMs	glass cover slips	8 µm circles	AFM, SEM, RT-qPCR
Otsuka *et al.* 2012 [295]	bovine AC	photolithography	gold electrode coated with PEG hydrogel	100 µm circles	microscopy, DMMB assay, interfacial potential measurements
Yuan *et al.* 2014 [305]	juvenile bovine meniscus cells and HUVECs	printing using PDMS, with hydrogel	plastic slides	1000 µm wide, 200 µm high	microscopy, RT-qPCR, DNA assay, DMMB assay, hydroxyproline assay, ELISA
Gao *et al.* 2010 [293]	hMSCs	microcontact printing	flat PDMS	100 µm and 32 µm squares	microscopy, RT-qPCR, western blot, Rho GTPase assay, Rac GTPase assay

Different cell types display different behavior on micropatterns [306]. Fink *et al.* observed two challenges with cell micropatterns. They found that some cells can escape from the micropatterns and spread over the passivated area more easily. They also observed that some cells can round up and detach from the micropatterns after long incubation periods. Three cell types were tested to produce the findings in their study: HeLa cells, human retinal pigment epithelial (RPE1) cells and mouse embryonic fibroblasts. The mouse fibroblasts had the highest potential to escape and tear off the protein patterns, followed by RPE1 cells, while

HeLa cells gave patterns of higher stability [306]. Hence in our study, the micropatterning procedures were tested with different cell types related to IVD research.

6.1.6 Requirement of thin substrate for high resolution microscopy using an inverted microscope

In our study, we investigated methods in preparing cell micropatterns compatible with high resolution microscopy. The resolution of a microscope is defined as the minimum distance between two Airy disks that can be distinguished as shown in **Figure 6-5A**. It can be represented by the following equation:

$$R = \frac{d}{2} = \frac{0.61\lambda}{n \sin \alpha} = \frac{0.61\lambda}{NA} \quad (1)$$

where R is the resolution of a microscope, d is the minimum distance between the centers of two Airy disks, n is the refractive index of the medium between the object and objective lens, α is the half-angle of the cone of light entering the objective lens (**Figure 6-5B**), λ is the wavelength of the light and NA is the numerical aperture [307]. The larger the NA, the smaller the resolution in terms of the minimum distance between two Airy disks which means higher resolution.

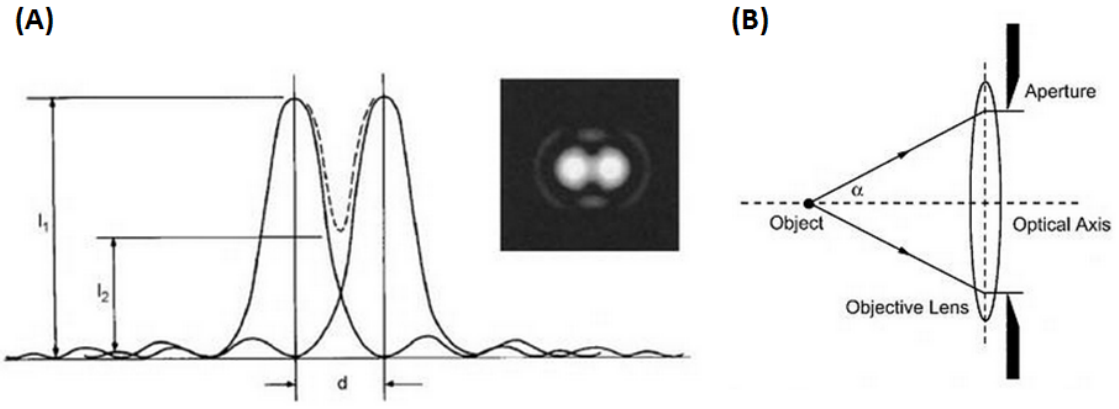


Figure 6-5 Resolution of microscope. (A) Intensity distribution of two Airy disks with a distance of d/2. I_1 indicates the maximum intensity of each point and I_2 represents overlap intensity. (B) The cone of light entering an objective lens showing α is the half angle. (Reproduced with permission of John Wiley and Sons from [307] © 2013 John Wiley and Sons).

Phase contrast microscopy and fluorescent microscopy have been used extensively to assess the behavior of cells on micropatterns. With the use of computer software, many important parameters can be extracted from the images. Confocal fluorescent microscopy has the advantage over ordinary fluorescent microscopy in terms of resolution and 3-dimensional reconstruction. However, for high resolution microscopy, microscope objectives of high NA are needed and generally only a short working distance is allowed for these objective lens.

Free working distance of a microscope objective is defined as the distance from the front lens element of the objective to the closest surface of the cover slip when the specimen is in sharp focus [308] (**Figure 6-6**). In general, an objective lens with high resolution has a short working distance.

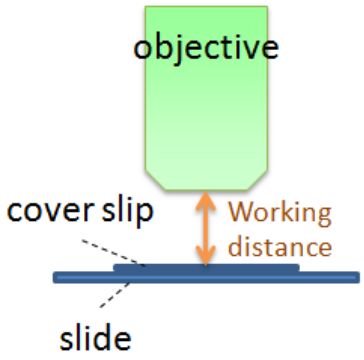


Figure 6-6 Schematic showing the working distance of a typical microscope objective. For an objective lens with a short working distance, the lens needs to be close to the sample. Thus only a thin material such as a glass cover slip can be placed in between the sample and the lens. Thicker materials will prevent the focus of sample using a lens of a short working distance, which is usually the case for higher resolution objective lens.

There can be two configurations of viewing cells at high resolution as shown in **Figure 6-7**. Cells can be cultured in ordinary culture containers and viewed using dipping objective lens which the lens is used in the solution. In another configuration, the cells are cultured in a thin bottomed container and viewed with an immersion objective lens from below through the thin bottom. In general, the objectives in the latter configuration give higher resolution. For

example, the 63× water immersion objective has a higher resolution (greater NA) than the water dipping objective of the same magnification power (**Table 6-2**).

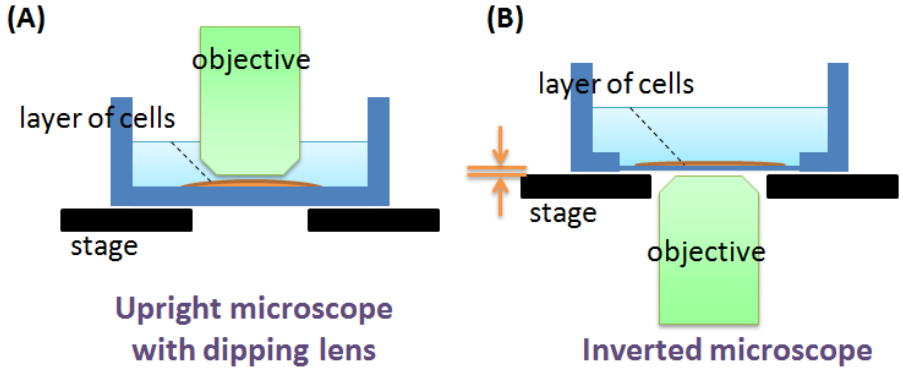


Figure 6-7 Schematic showing (A) a dipping lens in an upright microscope and (B) an immersion lens in an inverted microscope. Thin substrate is required for microscopy using an inverted microscope with objectives of a short working distance. Though the dipping lens configuration allows the imaging of cells cultured on ordinary culture plastic of about 1 mm thick, the resolution of dipping lens is generally lower than that of immersion lens and it is more difficult to keep the cells in sterile conditions for live cell imaging when dipping lens is used.

Table 6-2 Comparison of water dipping objective and water immersion objective for confocal microscopy that are available in Facility for Imaging by Light Microscopy (FILM) of Imperial College London (ICL)

	Water Dipping Objective	Water Immersion Objective
Serial number	506148	506279
Magnification	63×	63×
NA	0.9	1.2

The use of objective lens with large NA requires transparent substrates of small thickness but the preparation of cell micropatterns for high resolution confocal microscopy was not well documented in literature. Therefore, the preparation of cell micropatterns for confocal microscopy with minimal changes to cells was developed in my study. The technical details were explained in Section 6.5.7 in the Results and Discussion Section.

6.2 Introduction

Micropatterning is a useful approach to study the effect of cell shape, the role of cell-cell contact, as well as the impact of specific cell-matrix interactions on phenotype. Microcontact printing is one of the micropatterning techniques that has high potential for applications in biological studies as it does not require special equipment or chemicals once the mold is available. When the mold is available by in-house fabrication or from other laboratories, PDMS stamps can be prepared using the same mold repeatedly. The requirement of micropattern design is cell type specific but there was no reported study involving micropatterning bovine NP cells by microcontact printing. This necessitates the determination of the micropattern conditions optimal for bovine chondrocytes and NP cells. Besides, the micropatterning procedures used in different studies were slightly different (eg. the sterilization method, the choice of passivation reagent, the use of serum and the substrate used) without explanation about the principles. Hence different parameters involved in cell micropatterning using microcontact printing were investigated.

High-resolution microscopy that allows the cells on micropatterns to be studied in details requires the use of a thin substrate. Thus, we also explored different approaches to create cell micropatterns suitable for high resolution microscopy.

We hypothesize that micropatterning can be compatible with high resolution microscopy through surface modification or selection of suitable surfaces.

6.3 Objectives

The objectives of experiments described in this Chapter are:

- to optimize the micropatterning technique with bovine cells
    - the pattern size and the gap size
- to study and identify the critical parameters in the micropatterning procedures
    - sterilization by UV

- requirement of pluronic and serum
- glass substrate vs polystyrene substrate

- to develop a method for cell micropatterning compatible with high resolution microscopy
  - different approaches to micropattern cells on thin substrates

6.4 Materials and Methods

The experimental procedures involved in this Chapter are given in **Figure 6-8**.

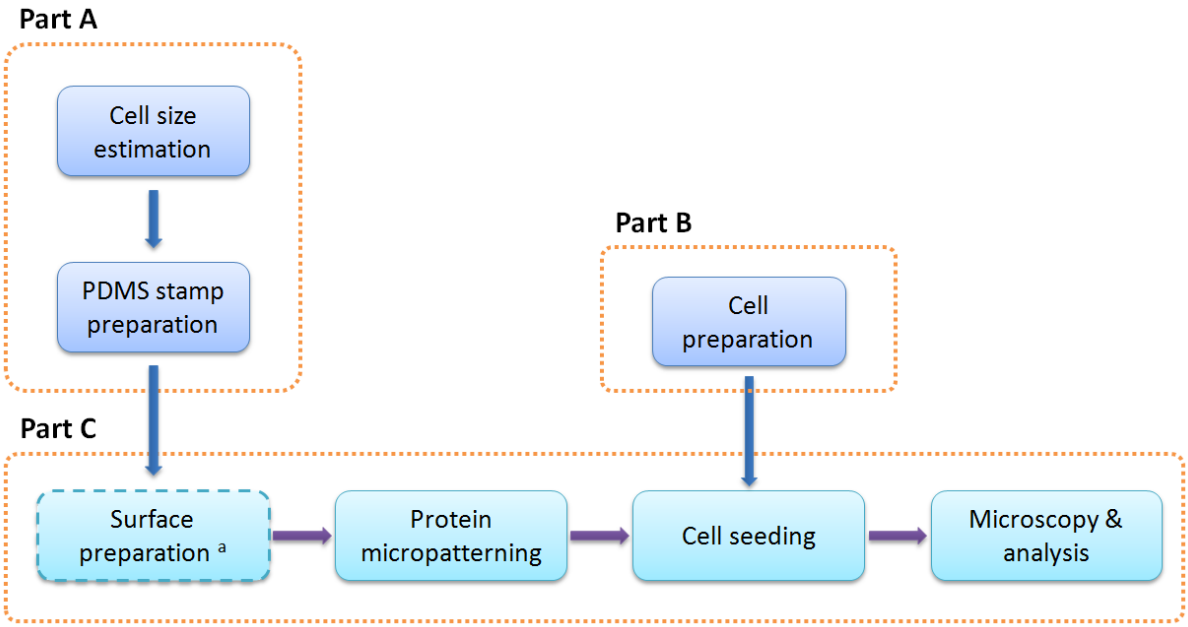


Figure 6-8 Experimental procedures involved in this Chapter. Part A represents some preparative work for micropatterning which does not need to be done for each experiment. The sizes of different cell types were determined and the patterns for the mold fabrication were designed. Silicon mold was fabricated to prepare the PDMS stamps. The stamps could be re-used in different experiments after washing and drying. Part B represents preparative work which involves cell isolation for primary cells which does not need to be done for each experiment. Some primary cells/ cell lines were also obtained from other group members. Part C represents procedures involved in each experiment in this Chapter. Surface preparation is an optional step which can be skipped for sterile untreated plates and Ibidi untreated dishes/ µ-slides. (Different surface preparation procedures are given in **Section 6.4.4** of this Chapter.) Then the protein micropatterns were prepared using microcontact printing, followed by cell seeding on the micropatterns. At last, the images of cells were taken using widefield/ confocal microscopy and the images were analysed using Fiji (software). [a.] optional/ dependent on substrate used.

6.4.1 Cell isolation

Bovine NP and AF cells were harvested from adult cow tails purchased from a local butcher in Brixton of London, United Kingdom. The surfaces of the tail were cleaned with 2% (w/v) Virkon and 70% (v/v) ethanol. The tails were dissected and the NP and AF tissues were collected in a biosafety cabinet. The tissues were cut into approximately 2 mm × 2 mm pieces and digested with 0.05% (w/v) collagenase Type II in DMEM (Invitrogen, catalog # 17101015) with 1% (v/v) antibiotic-antimycotic (Invitrogen, catalog # 15240-062) and 10% (v/v) fetal bovine serum (FBS) overnight at 37 °C with shaking. The subsequent cell isolation steps were the same as described in Chapter 2 of this thesis.

Bovine AC cells were obtained from Dr. Jean-Philippe St-Pierre of the Stevens group. Human umbilical vein endothelial cells (HUVECs) were obtained from Dr. Paola Campagnolo and Ms. Katie Hansel of the Stevens group in ICL. Human AC cells were obtained from Mr. Li Teng of the Orthopaedics and Traumatology Department in HKU. Human NP cells were obtained from Ms. Peng Yan in the spine research group in HKU.

6.4.2 Cell size estimation of different cell types

6.4.2.1 Cell diameter estimation of cells in suspension

Photos of human MSCs, human AC cells, human NP cells and bovine NP cells in suspension were taken and the diameters of cells were measured using the measurement tool in Adobe Photoshop.

6.4.2.2 Measurement of areas, aspect ratios and roundnesses of cells on culture surfaces

Bovine NP cells and AC cells were stained with CellTracker™ Green (Invitrogen, catalog # C2925) at room temperature in dark for about 20-30 min, washed three times with serum free medium and then seeded in a 12 well culture plate. Photos of the cells were taken at 4 h after cell seeding. The areas, aspect ratios and roundnesses of bovine NP cells and AC cells were

measured from images captured by fluorescent microscopy using Fiji (ImageJ) using the particle analysis function with the detailed procedures given in the following:

First, the photos were converted to 8-bit grayscale images (Image > Type > 8-bit). Second, the brightness and contrast were adjusted so that the edges of the cells were clear (Image > Type > Adjust > Brightness / Contrast). Third, the cells were "detected" by setting the threshold (Image > Type > Adjust > Threshold…). Fourth, the check boxes for "Area" and "Shape descriptors" were checked (Analyze > Set measurements…). Fifth, the area and other parameters of the cells were measured (Analyze > Analyze particles...).

The descriptions of the aspect ratio and roundness are given in the guide of the software ImageJ (http://rsbweb.nih.gov/ij/docs/guide/146-30.html) and in the following.

Aspect ratio refers to the aspect ratio $\left(\frac{\text{Major axis}}{\text{Minor axis}}\right)$ of the particle's fitted ellipse

Roundness refers to $4 \times \frac{\text{Area}}{(\text{Major axis})^2}$

6.4.3 PDMS stamp preparation

6.4.3.1 Silicon master design and fabrication

Patterns to be fabricated on silicon master were designed using LayoutEditor™ (available from http://www.layouteditor.net/) and film masks of the desired patterns were ordered from JD Photo - Tools (http://www.jdphoto.co.uk/). Fabrication of the silicon master with patterned photoresist was done by Dr. Ciro Chiappini of the Stevens group. Silicon masters for this project were also obtained from Dr. Mark Steedman or borrowed from Dr. Thomas Von Erlach of the Stevens group.

6.4.3.2 Preparation of PDMS stamps

PDMS and the curing agent (Sylgard 184) were mixed in 10:1 ratio in a wide mouth plastic bottle and mixed thoroughly. The PDMS mixture was then degassed under vacuum to remove

the air bubbles generated during mixing. A layer of degassed PDMS mixture (2 to 3 mm thick) was cast onto the photoresist master and cured at 60 °C overnight. The PDMS layer was gently peeled from the photoresist master and cut into stamps of approximately 1 cm x 1 cm. The PDMS stamps were washed with isopropanol, distilled water and 70% (v/v) ethanol sequentially for 5 to 10 min for each wash.

6.4.4 Preparation of surfaces for micropatterning

Different surfaces used for micropatterning in this Chapter and the next Chapter are summarized in **Table 6-3**.

Table 6-3 Surfaces used for micropatterning studies in Chapter 6 and Chapter 7.

Materials/ surfaces	*Application(s)*	*Passivation*	*Remarks*
Untreated polystyrene plates (6 well, Nunc, catalog # 150239; 12 well, Nunc, catalog # 150200)	Widefield microscopy, RT-qPCR	Pluronic	Supplied sterile
Glass cover slip (VWR, catalog # 631-1571)	Widefield/ confocal microscopy	PLL-g-PEG	UV sterilization required
Polystyrene coated glass cover slip (prepared from VWR, catalog # 631-1571, with coating using polystyrene)	Widefield/ confocal microscopy	Pluronic	UV sterilization required
1st generation tailor-made container for confocal microscopy (**Figure 6-9**A)	Widefield/ confocal microscopy	Pluronic	UV sterilization required; allow more accurate cell height measurement compared to the glass cover slip method; hole punching not required; allow other surface modification
2nd generation tailor-made container for confocal microscopy (**Figure 6-9**B)	Widefield/ confocal microscopy	Pluronic	UV sterilization required; hole punching required; allow other surface modification
Ibidi untreated dish (Ibidi, catalog # 81151)/ μ-slide 2 well (Ibidi, catalog # 80281)	Widefield/ confocal microscopy	Pluronic	Supplied sterile

Materials/ surfaces	*Application(s)*	*Passivation*	*Remarks*
Polystyrene-coated PEN (Life Technologies, catalog # LCM0531) or PET (Zeiss, catalog # 415190-9101-000) membrane frame slides	Laser capture microdissection (LCM)	Pluronic	UV sterilization required; the membranes have high absorbance at 355 nm which assists cutting using laser

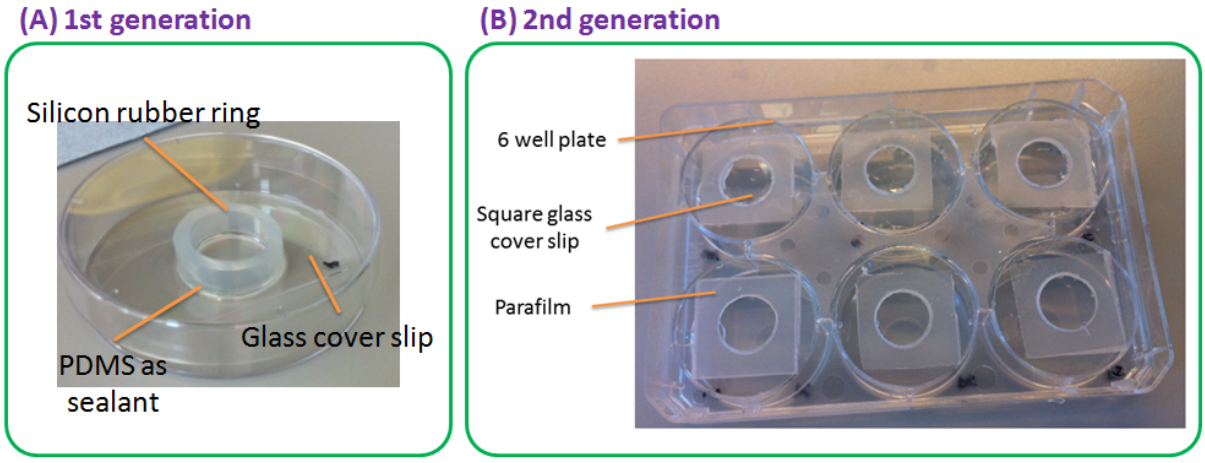


Figure 6-9 Approaches for preparing substrates for confocal microscopy of cell micropatterns. (A) 1st generation container made from a rubber ring sealed on a glass cover slip and (B) 2nd generation container made by attaching a glass cover slip to a punched untreated cell culture plate. The 1st generation container does not require the punching of holes on the brittle plastic but it is more difficult to handle during cell culturing compared with the 2nd generation one. For both prototypes, the glass cover slip may also be modified by different means (eg. spinning coating with PDMS of different stiffness) and still retains its thin thickness required for high resolution confocal microscopy.

6.4.4.1 Preparation of polystyrene coated glass cover slips

To prepare polystyrene solution for coating, the cover of an untreated polystyrene cell culture plastic was broken into pieces and weighted. The pieces of polystyrene were then dissolved in toluene to a final concentration of 25% (w/v) by rotating the glass vial overnight. Polystyrene in toluene (0.5% w/v) was prepared by diluting the 25% (w/v) solution with toluene. Glass cover slips were cleaned with 70% (v/v) ethanol and dried with KimWipe. A thin layer of polystyrene was coated on the glass cover slip using 200 µl pipet tips (without graduation mark so as not to leave scratches on the coating, as shown in **Figure 6-10**) inside a chemical fume hood.

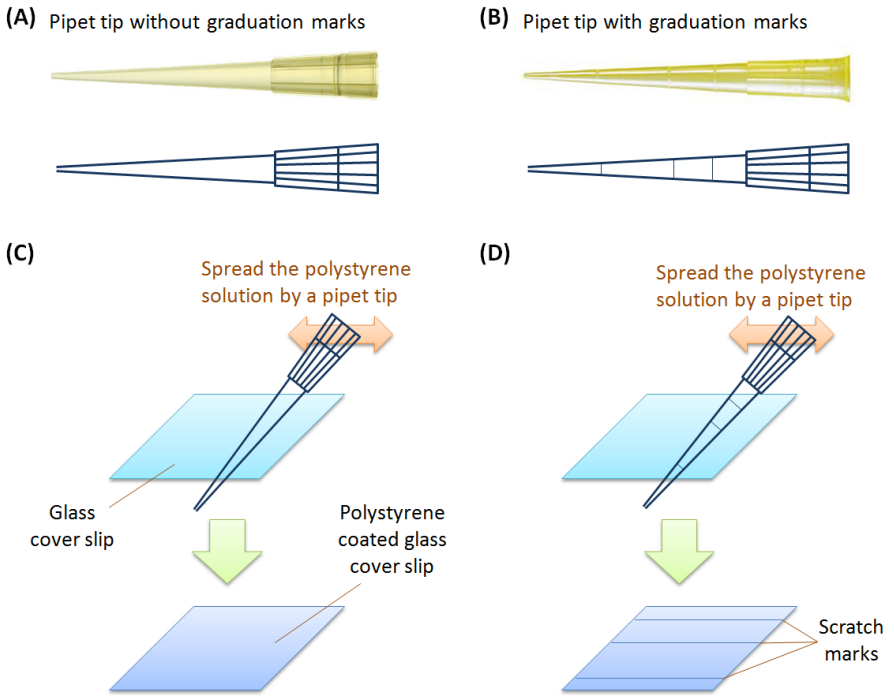


Figure 6-10 Schematic showing the preparation of polystryene coated cover slips. (A) A pipet tip without graduation marks; (B) A pipet tip without graduation marks; (C) A thin film of polystyrene was coated on a glass cover slip by adding a drop on polystyrene solution in toluene on the cover slip and spread it by using a pipet tip. The solution will form a thin film upon the evaporation of toluene. Using a pipet tip for solution spreading, a smooth coating can be formed but scratch marks will be formed when a pipet tip with graduation marks is used (D). Thus it is important to use a pipet tip without graduation marks to spread the polystyrene solution to avoid scratch marks left behind.

6.4.4.2 Preparation of thin bottom containers for confocal microscopy (1st generation)

Silicone tubing was cut to form rings of 3-5 mm thickness and washed with isopropanol, distilled water and 70% (v/v) ethanol sequentially. The rings of tubing were placed at the centres of the cover slips (**Figure 6-11A**) and sealed with PDMS 184 mixture (the same preparation method as the mixture used for PDMS stamp preparation). The sealant of the containers was cured at 65 °C overnight (**Figure 6-11B**). The containers were sterilized using UV in a biosafety cabinet for cell culture. When used in cell culturing, the containers were put in 60 mm dishes as shown in **Figure 6-9A**.

Ordinary untreated culture plates with bottom of approximately 1 mm thickness were not compatible with high resolution microscopy. For viewing under confocal microscopy,

different methods of preparing containers with thin bottom were devised and **Figure 6-9** shows two of the successful setups during the process. At first, we tried to punch holes in untreated plastic culture dishes with a metal puncher or an electric drill but the plastic cracked without forming intact holes due to its brittleness. Hence we attached a silicone tubing ring to the polystyrene coated glass cover slip with PDMS as a sealant (shown in **Figure 6-9A** with schematic of preparation in **Figure 6-11**). The silicone ring kept the cells with cell culture medium at the centre of the cover slip.

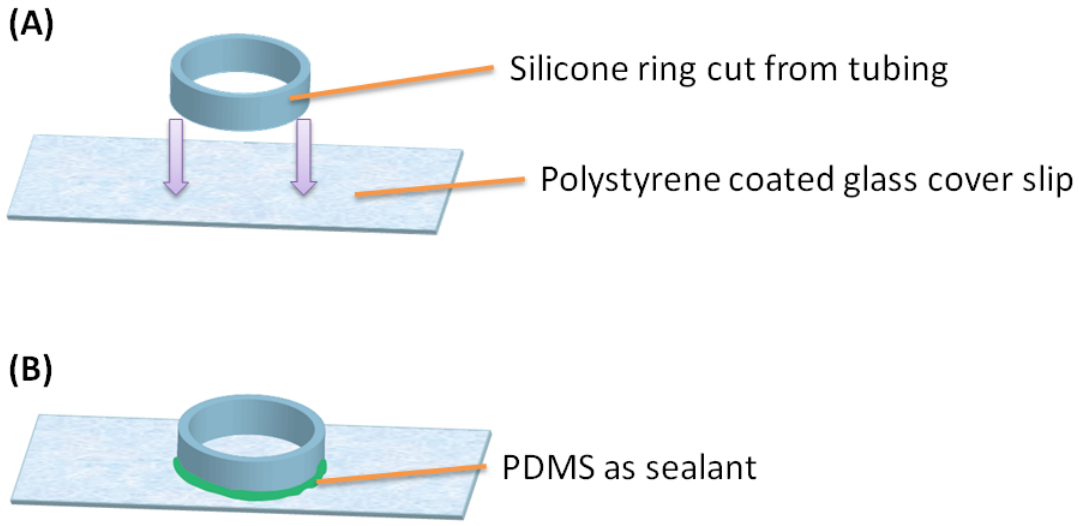


Figure 6-11 Preparation of a thin bottom container with a silicone ring. (A) A silicone ring was cut from a silicone tubing and placed on top of a polystyrene coated cover slip; (B) PDMS mixed with the curing agent was applied around the edge of the silicone ring-cover slip interface and the polymer was cross-linked by putting the whole setup in a 65 °C oven overnight.

6.4.4.3 Preparation of 6 well plates with thin bottom glass cover slips for confocal microscopy (2nd generation)

We continued to explore different methods of creating holes on the plastic culture plates with the equipments we had. With special equipments and technical support from the mechanical workshop, holes can be drilled in plastic culture plates without creating large cracks. Originally, we attached the coated glass slips to bottom with PDMS as sealant but this method

was quite time-consuming and required overnight curing of the PDMS in oven. Besides, there was leakage of the solution when cold PBS was put in the plates which may be due to the thermal shrinkage effect. Therefore other sealing methods were explored. We decided to use Parafilm® to attach the cover slips to plates with holes.

In this preparation method, holes of 15 mm in diameter were drilled in 6 well untreated culture plates by Mr. Russell Stracey. Special machine and techniques were required for the hole drilling of these plates as they were brittle and easy to break upon drilling. The 6 well plates were cleaned with 70% (v/v) ethanol, dried with KimWipes and sterilized with UV in a biosafety cabinet for cell culture. Parafilm® was cut into 1 in. × 1 in. (2.54 cm × 2.54 cm) and holes of 16 mm diameter were punched at the centre of the film in a stack. The paper attached to the Parafilm® was removed and the Parafilm® was placed on the 6 well plates with holes and cover slips prepared as in **Section 6.4.4.1** were put underneath. The cover slips were mounted to the 6 well plates by melting the Parafilm® in between the cover slips and the plastic plates using a heat block set at around 100 °C. Light pressure was applied using the wide opening side of a 200 μl pipet tip to ensure good attachment of the slips to the culture plates. A finished plate with cover slips mounted was shown in **Figure 6-9B** with schematic of preparation in **Figure 6-12**. The plastic plates with mounted cover slips were sterilized using UV in a biosafety cabinet for cell culture.

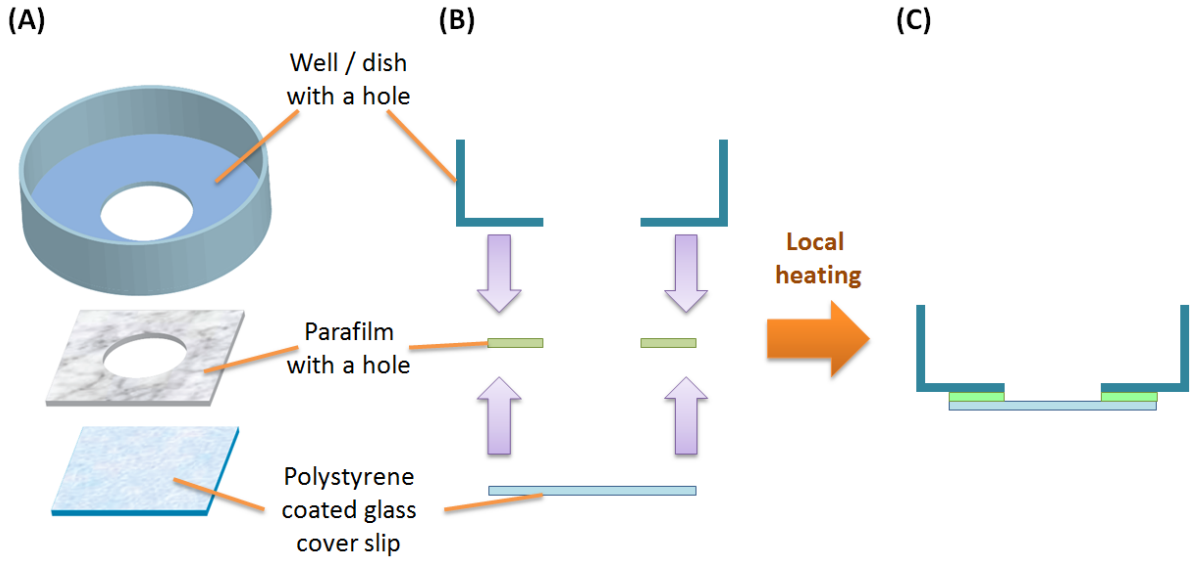


Figure 6-12 Preparation of a thin bottom container with a hole drilled at the centre of the culture plate well / dish (only one of the wells was shown for simplicity). (A) The three main components in the setup: the well/ dish with a hole drilled in the mechanical workshop, a Parafilm® sheet with a hole punched by a metal puncher and a square polystyrene coated cover slip. (B) The cross sectional view of the three components. They were placed together with alignments between the hole of the well and the Parafilm® sheet and also between the square Parafilm® and the square cover slip. (C) The Parafilm® in between the culture well and the cover slip was melted with a heat block heated to approximately 100 °C, forming the water leakage-free assembled setup.

6.4.4.4 UV sterilization of surfaces for micropatterns

Glass cover slip, polystyrene coated glass cover slips, the 1st generation container and the 2nd generation container were sterilized by UV in a biosafety cabinet for cell culture. Both sides of the cover slips were irradiated in turn (15 - 30 min for each side). The untreated polystyrene plates and Ibidi untreated dishes/ µ-slides were supplied sterile and required no sterilization before micropatterning.

6.4.5 Preparation of protein micropatterns by microcontact printing

The PDMS stamps were plasma treated in air for 3 min at room temperature to make the surfaces more hydrophilic. Fibronectin solution (Sigma, catalog # F1141) in PBS (DPBS, Gibco, catalog # D-PBS14190-169) at 20 µg/ml was added on top of the stamps with spreading using a pipet tip. Around 50 µl of fibronectin solution was used for each PDMS

stamp with 1 cm × 1 cm surface on the top side with micropatterns. Too little solution can result in drying of the stamps before stamping and too much solution results in overflowing of the solution to the side of the PDMS stamps as well as the surface underneath which reduces the volume of solution on the surface with patterns and may also result in drying of stamps. The stamps were incubated with the fibronectin solution for an hour at room temperature. Excess solution was blown away and the stamps were placed on the surfaces described in **Table 6-3** in **Section 6.4.4** of this Chapter. The PDMS stamps were pressed gently using the plastic forceps and the surfaces were left in contact for 3 - 15 min. Afterwards, the stamps were removed and 1 ml of 1% (w/v) pluronic in PBS was added to each well of the 6 well plates (0.5 ml per well for 12 well plates) and incubated at room temperature for at least 30 min. The pluronic solution was prepared by dissolving pluronic powder (Pluronic® F-127, Sigma, catalog # P2443) in PBS and vortexing after letting the solution stand with undissolved power at room temperature for 30 to 60 min. After all the powder was dissolved, the solution was sterilized by filtering with a 0.2 μm syringe filter. The solution was stored at 4 °C and was stable for at least a month. Prior to cell seeding, the pluronic solution was removed and the wells of the plates were washed 3 times with PBS with 1% (v/v) Antibiotic-Antimycotic (Gibco, catalog # 15240-062).

6.4.6 Seeding of cells on the micropatterns

Cells were seeded in serum-free DMEM (Invitrogen, catalog # 17101015) with 1% (v/v) Antibiotic-Antimycotic (Invitrogen, catalog # 15240-062) at a cell density of 10^4 cells per cm^2 (10^5 cells and 4×10^4 cells per well of 6 well plate and 12 well plate respectively). At 2 h after cell seeding, the plates were washed with PBS to remove unattached cells and the cells were cultured in DMEM with 1% (v/v) Antibiotic-Antimycotic and 10% (v/v) FBS.

6.4.7 Phase contrast microscopy and fluorescent microscopy of cells on micropatterns

Phase contrast photos were taken using an Olympus IX51 inverted microscope. For actin and nuclei staining, the cells were washed with PBS three times and then fixed with 4% (w/v)

paraformaldehyde (PFA) for 10 min. The cells were then washed three times with PBS and permeabilized with 0.2% (v/v) Triton X-100 (Sigma, catalog # X100) in PBS for 5 min. The cells were then washed with PBS twice and the surface was blocked with 1% (w/v) bovine serum albumin (BSA) in PBS for 20 min. The blocking solution was removed and replaced with the staining solution. The staining solution consisted of 1U/ml Alexa Fluor® 568 phalloidin (red, catalog # A12380, Life Technologies) or Alexa Fluor® 488 phalloidin (green, catalog # A12379, Life Technologies) and 300 nM 4',6-Diamidino-2-phenylindole dihydrochloride (DAPI, catalog # 32670, Sigma) in 0.1% (w/v) BSA in PBS. The cells were stained for 20 min to 2 h and then washed twice with PBS. The stained cells were imaged under a fluorescent microscope. Fluorescent microscopy photos were taken using an Olympus IX51 inverted microscope or a confocal microscope Leica SP5 MP. The areas, aspect ratios and roundnesses of bovine NP cell nuclei were estimated using the method described in **Section 6.4.2.2** of this Chapter.

6.4.8 Statistical analysis

P-values were calculated using Student's two-tailed t-test of unequal variance.

6.5 Results and Discussion

6.5.1 Different cell types exhibit different sizes and morphologies

The optimal size of micropatterns required will change depending on the cell types. In our study, we aimed to maintain the round shape of cells by constraining the area of substrates that the cells can attach to. As bovine NP cells have smaller diameters than human MSCs, AC cells and NP cells (**Table 6-4**, $p < 0.05$), patterns designed for human cells may not be applicable to bovine cells. More specifically, the pattern size that allows one human cell to attach may be too large for a bovine cell and more than one cell may attach to each protein pattern. There were a number of studies using human MSCs but limited characterization of patterns for bovine cells was available (**Table 6-5**).

Table 6-4 The cell diameters of cells in cell suspension (mean ± SD, 20 cells per cell type)

	human MSC	human AC	human NP	bovine NP
Cell diameter (μm)	16.9 ± 4.0	22.1 ± 5.4	22.5 ± 4.4	13.8 ± 2.2

Table 6-5 Summary of some single cell micropattern studies [a] measured from photos: ~50-60 μm.

Group	*Year*	*Shape*	*Pattern size*	*Gap size*	*Cell type*
Gadhari *et al.* [309]	2013	circle, square and rectangle	2000 μm^2	not given [a]	mouse embryonic kidney fibroblast cell line
Chen *et al.* [310]	2013	rectangle	900, 1600, 2500 μm^2	not given	mouse NIH 3T3 fibroblast
Wang *et al.* [311]	2013	circle with and without protrusion lines	diameters of 30, 50 and 70 μm (~700-3850 μm^2)	not given	hMSCs
Lee *et al.* [312]	2013	circle, ellipse, star	1000, 3000 and 5000 μm^2	not given	hMSCs
Song *et al.* [313]	2011	circle	diameters of 40, 60 and 80 μm (~1250-5000 μm^2)	not given	hMSCs
Song *et al.* [314]	2011	triangle, square, pentagon, hexagon, circle	~1150 μm^2	not given	hMSCs
Kilian *et al.* [315]	2010	square, rectangle, flower, pentagon, star	1000, 2500 and 5000 μm^2	not given	hMSCs
Gao *et al.* [293]	2010	square	1024 and 10000 μm^2	not given	hMSCs
McBeath *et al.* [279]	2004	square	1024 and 10000 μm^2	not given	hMSCs
Chen *et al.* [273]	1997	square	width of 5, 10, 20, 30, 40 μm (~25-1600 μm^2)	not given	Human and bovine capillary endothelial cells

Figure 6-13 shows that different cells have different sizes and morphologies when they are allowed to spread on culture surfaces to reach confluence. A rough estimation of the cell spread area was given in **Table 6-10** in **Section 6.7.2** of the Appendix. The areas occupied by bovine NP cells and mouse 10T1/2 cells were smaller than HUVECs and hMSCs when the cells were allowed to spread on culture surfaces. This observation further supports that a

micropattern that can be fully filled by a single cell of a specific type may be too large for another type. From the literature (**Table 6-5**), a number of studies used patterns of more than 1000 μm^2. These patterns are probably too large for bovine NP cells which have area smaller than 700 μm^2 when well spread on culture surfaces based on our analysis. This indicates the necessity to fine tune the micropattern design for studying bovine NP cells.

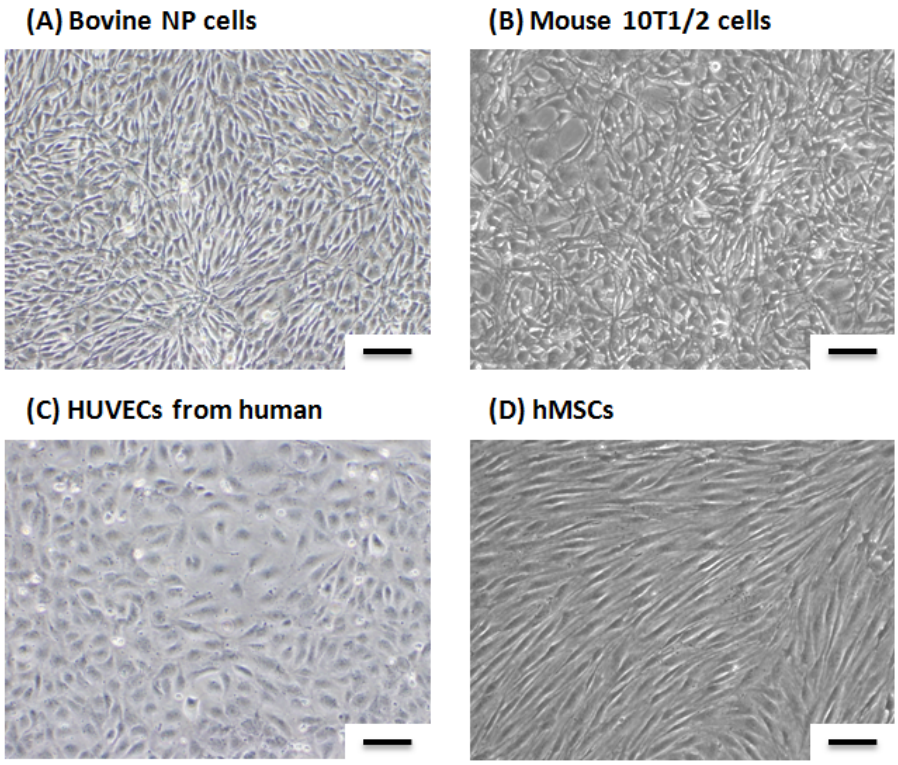


Figure 6-13 Phase contrast photos of (A) bovine NP cells, (B) mouse 10T1/2 cells, (C) HUVECs (human cells) and (D) hMSCs at confluence. (Scale bar = 100 μm). Different cells have different morphologies and cell areas at confluence.

In order to estimate the individual cell area of bovine NP and AC cells more accurately, the cells were pre-stained with fluorescent dye CellTracker green and photos were captured after the cells have attached to the culture surface (**Figure 6-14A**). The cell areas, aspect ratios and roundnesses were estimated from the photos through a particle analysis function in Fiji (ImageJ) and a sample of the outline of cells in the particle analysis was shown in **Figure 6-14B**. As shown in **Table 6-6**, bovine NP and AC cells had roughly the same areas of 368 μm^2 and 396 μm^2 respectively at 4 h after cell seeding. Hence micropatterns of area smaller

than 368 μm^2 were designed for bovine NP cells in order to restrict the spreading of cells. These two cell types had no significant differences in aspect ratios and roundnesses. Bovine NP cells from adult animals are regarded as chondrocyte-like cells and this may explain the similarity of the cell areas, aspect ratios and roundnesses of bovine NP cells and AC cells. In our study, circle miropatterns of 20 μm in diameter were included as this is equivalent to an area of about 314 μm^2 which is smaller than the spread cell area of bovine NP and AC cells.

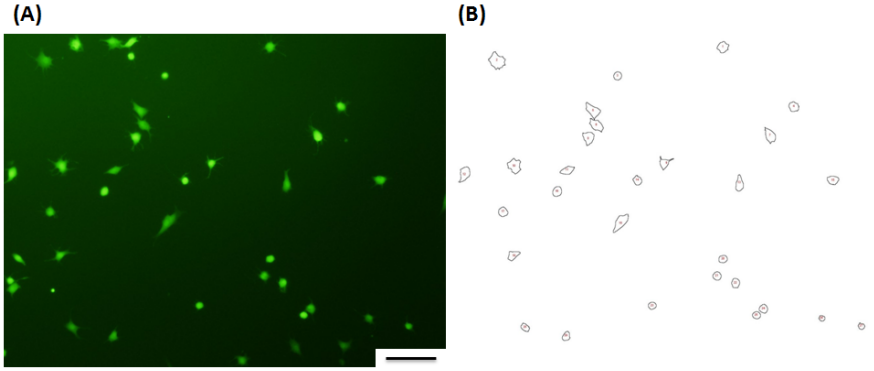


Figure 6-14 (A) Sample fluorescent photo of bovine NP cells at 4 h after cell plating used for cell area and shape analysis using Fiji; (B) Outline of cells in the particle analysis of Fiji. (Scale bar = 100 μm).

Table 6-6 Areas, aspect ratios and roundnesses of bovine NP and AC cells at 4 h after cell plating. (Mean ± SD, 125 cells for NP and 96 cells for AC). Bovine NP and AC cells have similar area of around 368 – 396 μm^2.

	Bovine NP	Bovine AC
Area (μm^2)	368 ± 144	396 ± 197
Aspect Ratio	1.50 ± 0.55	1.53 ± 0.61
Roundness	0.72 ± 0.17	0.72 ± 0.18

6.5.2 Pattern and gap size affect the success of single cell micropatterns

The differences in spreading areas of different cell types at confluence (**Table 6-10** in **Section 6.7.2** of the Appendix) and the lack of information from literature about the gap sizes between patterns (**Table 6-5** in the previous section) necessitates the optimization of pattern design. When bovine cells were seeded on 50 μm circle patterns, most patterns were occupied by more than one cell (**Figure 6-15A**). As bovine NP cells are smaller than human MSCs, the

pattern sizes need to be adjusted to obtain single cell patterns that retain the round shape of cells. As indicated in Chapter 2, the diameter of bovine NP/ AF cells isolated from tissues was determined to be approximately 13 µm, thus patterns of 10 µm, 15 µm and 20 µm were also tested. Cells could specifically attach to patterns with 20 µm or 50 µm diameters (**Figure 6-15A** and **B**) but not to those with 10 µm and 15 µm diameters (**Figure 6-15C** and **D**). Non-specific cell attachment was seen for 15 µm patterns separated by 85 µm gaps and 10 µm patterns separated by 90 µm gaps.

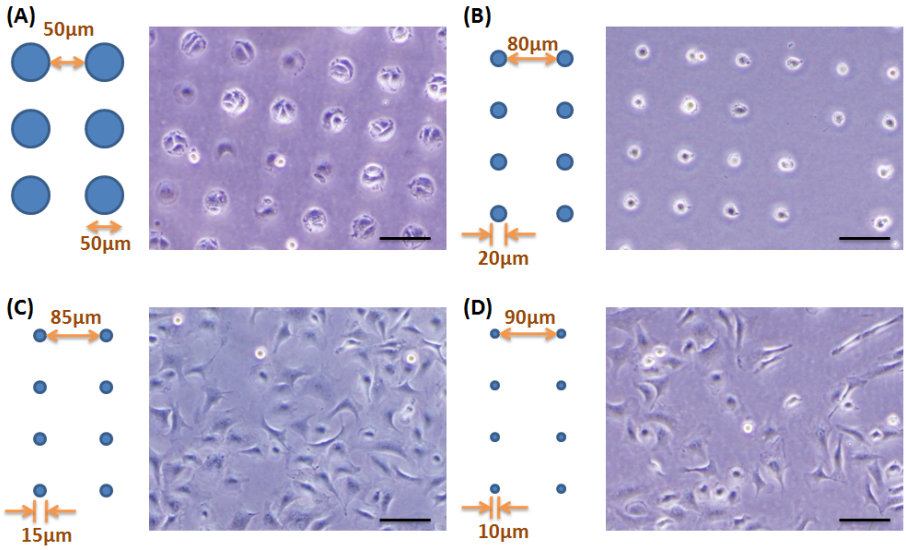


Figure 6-15 Phase contrast photos of bovine chondrocytes on fibronectin patterns of different circle sizes at 4 h after cell seeding. (Scale bar = 100 µm). (A) 50 µm circle patterns separated by 50 µm gaps, (B) 20 µm circle patterns separated by 80 µm gaps, (C) 15 µm circle patterns separated by 85 µm gaps, and (D) 10 µm circle patterns separated by 90 µm gaps. Non-specific patterns were observed for 15 µm micropatterns separated by 85 µm gaps and 10 µm patterns separated by 90 µm gaps.

Possible causes of these non-specific patterns are illustrated in **Figure 6-16**. One of the possible causes is that the gap is too wide causing the trench region of the PDMS stamps to come in contact with the culture surface when force is applied (**Figure 6-16A** and **B**). Thus gap size of not more than 50 µm was used in my study. Another cause is the deformation of the pillar part of the stamp when force is applied (**Figure 6-16C** and **D**). The smaller the patterns, the greater deformation results for a same force applied (**Figure 6-17**) and this can also make the trench part of the stamp get into contact with the culture surface, creating

non-specific cell patterns. Hence pattern sizes of no smaller than 20 μm were used in my study. The effects of gap size and pattern size illustrated in **Figure 6-16** may co-exist and it is not possible to evaluate the extent of each parameter independently based on these data but it was not deemed worthwhile to carry out extensive experiments to further investigate the effects of gap size and pattern size because desired protein patterns were achieved to elicit appropriate single cell attachment. As a rule of thumb, we used patterns no smaller than 20 μm and gap sizes not greater than 50 μm and one of our designs was shown in **Figure 6-31** in the Appendix. This is based on stamps created from the silicon master fabricated in our group, for which the thickness of photoresist is around 10 to 15 μm (**Figure 6-18**). For photoresists of different thicknesses, the parameters may need to be adjusted. In our study, the compression was applied by hands through forceps and the force required was decided based on experience. Deformation of the PDMS stamps was observed during the stamping and it was used as a guide to decide whether stronger or weaker force was required.

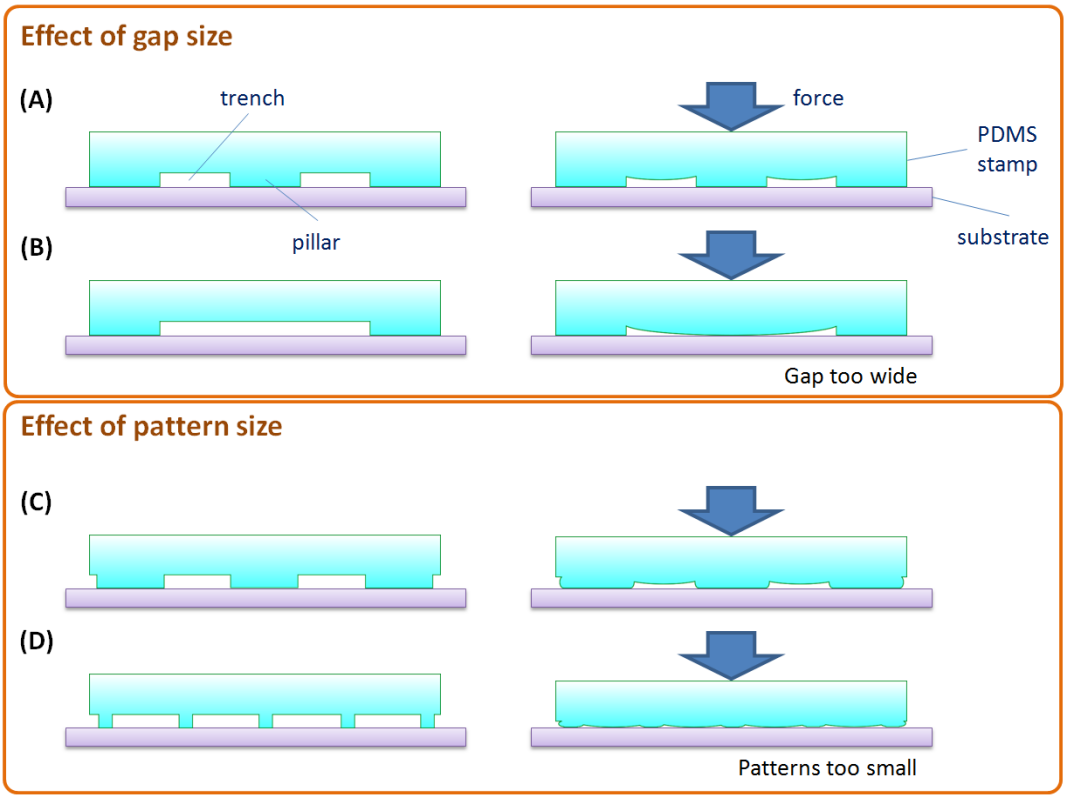


Figure 6-16 Schematic of possible explanation for the non-specific patterns. Non-specific patterns may be resulted due to the deformation of the PDMS stamp. (A) When the gap is narrow enough, the

deformation of the trench part will not cause touching of the stamp with the substrate but when the gap size is too large as in (B), the deformation of the PDMS may allow the trench part touch the substrate, causing the non-specific transfer of proteins to the substrate. (C) When the pattern size is large enough, the pillar part of patterns will prevent the trench part from touching the substrate but when the pattern size is too small as in (D), the pillars of the stamps may be deformed more readily for the same applied force and may cause non-specific transfer of proteins.

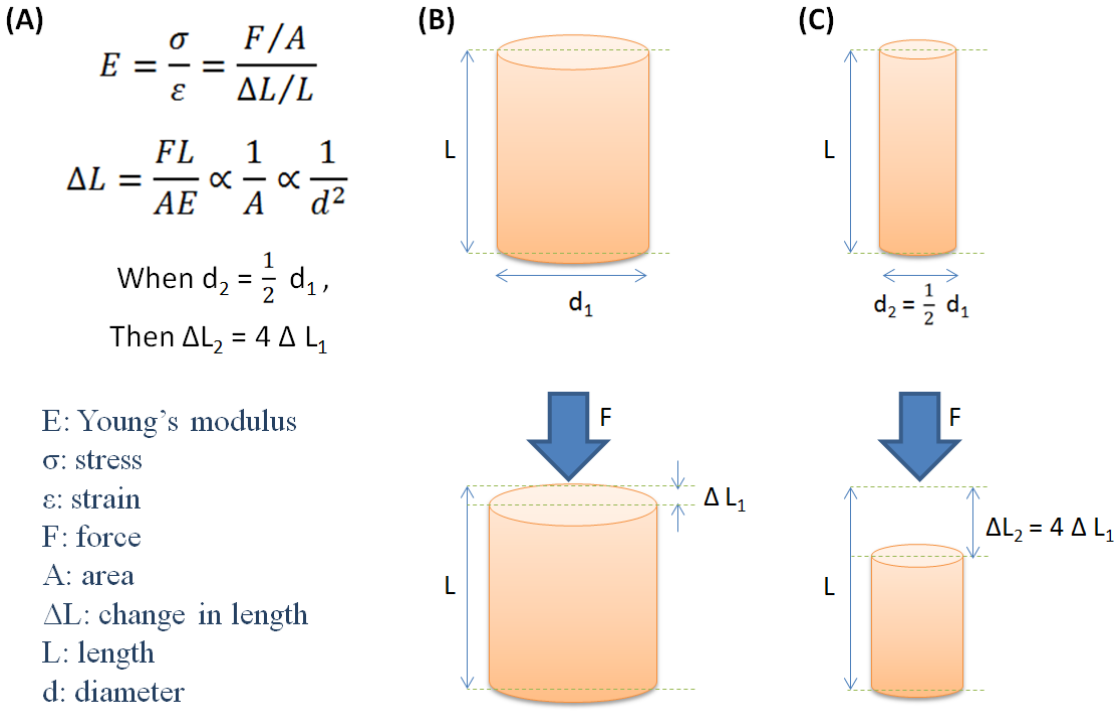


Figure 6-17 The relationship between the change in length and the cross-sectional area. (A) The Young's modulus is defined as the ratio of stress σ over strain ε where stress is the force F per area A and strain is the ratio of change in length ΔL to the length L. The Young's modulus is a property of material and independent of the shape of the material. For constant F, L and E, the change in length ΔL is inversely proportional to the area A. For cylindrical material, ΔL is inversely proportional to the square of diameter, d. When the diameter is halved, the change in length will be 4 times (as shown in B and C). The figure is not exactly drawn to scale.

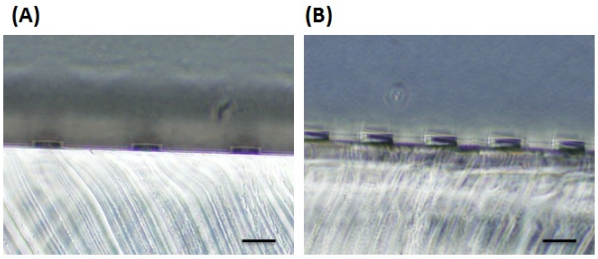


Figure 6-18 Photos of cross-sections of PDMS stamps captured under phase contrast microscopy. PDMS stamps fabricated from silicon masters from (A) Dr. Mark Steedman and (B) Dr. Thomas Von Erlach (scale bar = 50 μm). The thickness of the patterns is around 10 to 15 μm.

With the PDMS stamps fabricated from the design in **Figure 6-31** (in the Appendix of this Chapter), NP cells could be patterned in different arrangements, a selection of which is shown in **Figure 6-19**. For 20 μm circles, most patterns were occupied by single cells while 50 μm patterns were occupied by several cells on each pattern. The cells on 20 μm strips were highly elongated, forming strips of cells of 1-2 cells in width. The cells on 50 μm strips were elongated but less compared to 20 μm strips. Compared to strip patterns, the cells on circle patterns were rounder in shape. The cells on fibronectin without micropatterns were spread and had a morphology that resembled that on 50 μm strips more than on circle patterns. Besides the overall shapes, the nuclear areas and shapes were also different for cells on different patterns as shown in the next Section. Using the PDMS stamps designed, bovine NP cells can be patterned into round shape, elongated shape and spread shape.

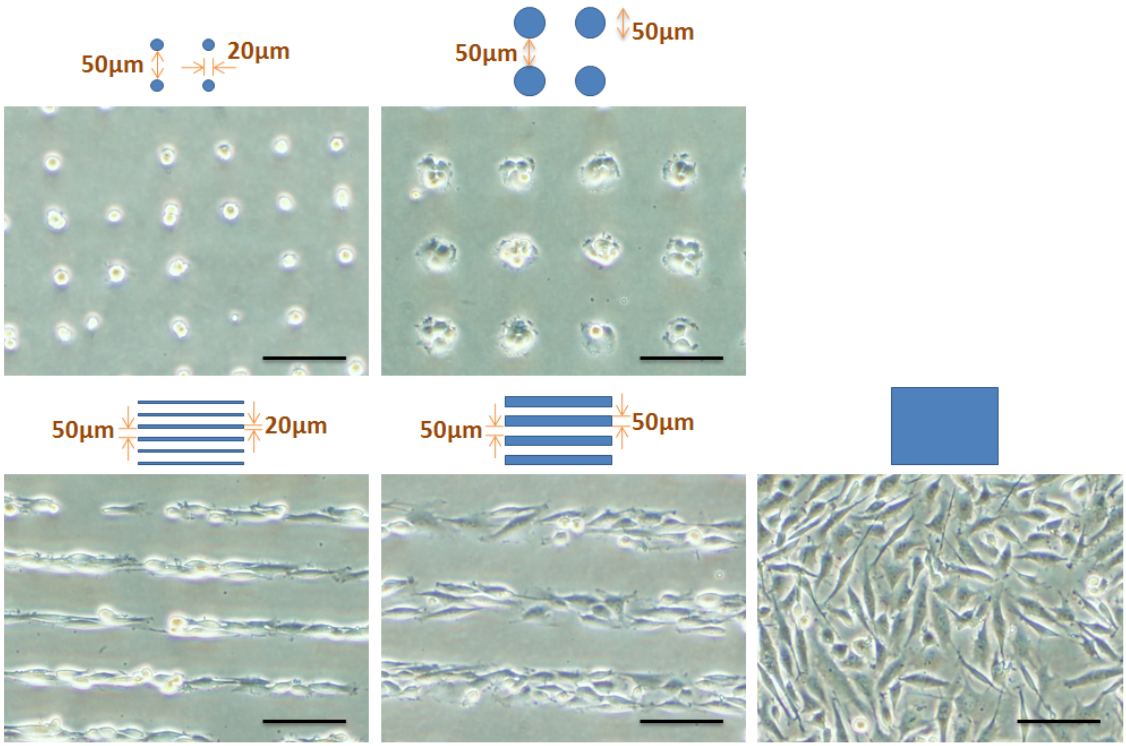


Figure 6-19 Phase contrast photos of bovine NP cells on fibronectin patterns of 20 μm circles, 50 μm circles, 20 μm strips, 50 μm strips and fibronectin coating at day 1. (Scale bar = 100 μm). With gap size not more than 50 μm and pattern size not less than 20 μm, micropatterns of bovine NP cells could be successfully formed.

6.5.3 Quantification of nuclear areas and shapes

In **Figure 6-19** in the last Section, it was shown that the shape of NP cells can be changed using micropatterns. The shape of nuclei has been suggested to affect many cellular processes but no study to date was done with IVD cells. Thus we investigated whether using the micropatterns can change the shape of NP cell nuclei through the use of DAPI staining and fluorescence microscopy. From **Figure 6-20**, the cell nuclei were round in shape when the cells were cultured on 20 µm circles but were more elongated with a larger aspect ratio and a lower roundness when cultured on 20 µm strips. The nuclei of cells cultured on 20 µm circle or strip patterns had smaller areas compared to those of cells cultured on fibronectin without micropatterns.

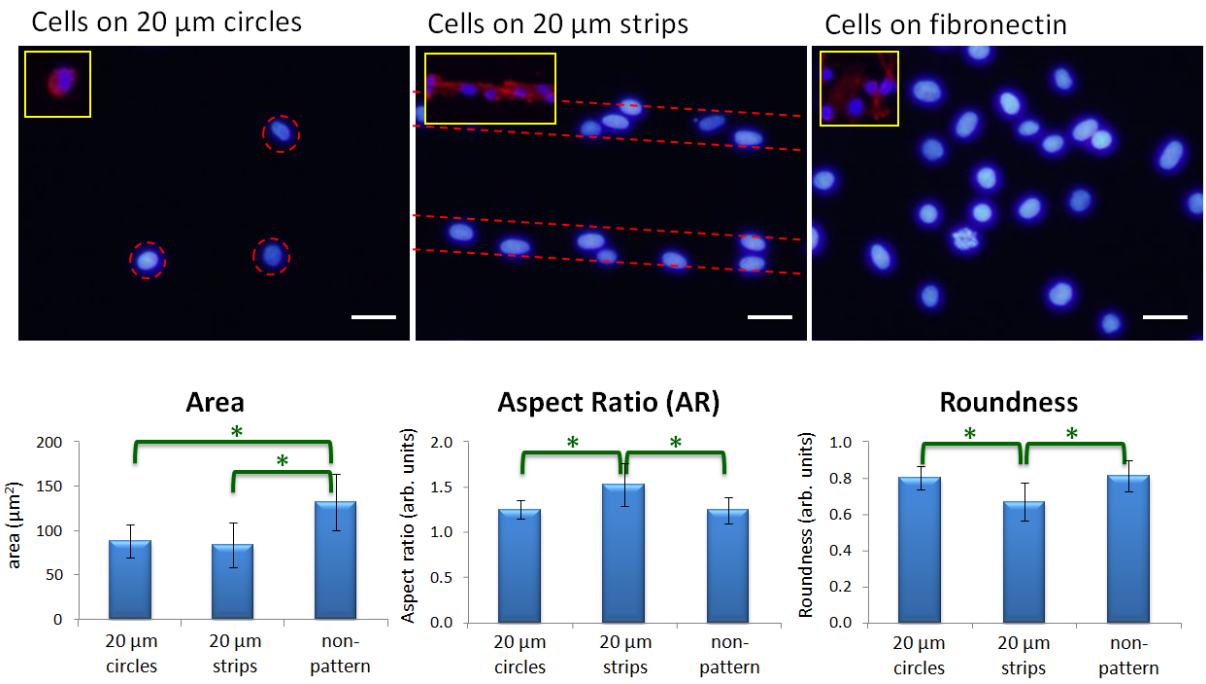


Figure 6-20 Fluorescent photos of nuclei of bovine NP cells stained with DAPI at day 1 (scale bar = 25 µm) and the quantification of areas, aspect ratios and roundness descriptors using Fiji. (Mean ± SD, n = 19 cells for 20 µm circles, 55 for 20 µm strips and 80 for non-pattern; for 20 µm circles, only patterns with only one cell per pattern were taken into account; * $p < 0.001$). The cells on non-patterns had larger projected nuclear area than the cells on 20 µm circles or strips. The cells on 20 µm strips were elongated as in the photo and reflected by the higher aspect ratio and lower roundness.

An analysis of the nucleus orientation showed that the nuclei of cells on 20 µm strips aligned with the patterns as shown by the preferential orientation of nuclei at 0-30° and 150-180° (**Figure 6-21**). There is no such preferential orientation for 20 µm circles or fibronectin without micropatterns.

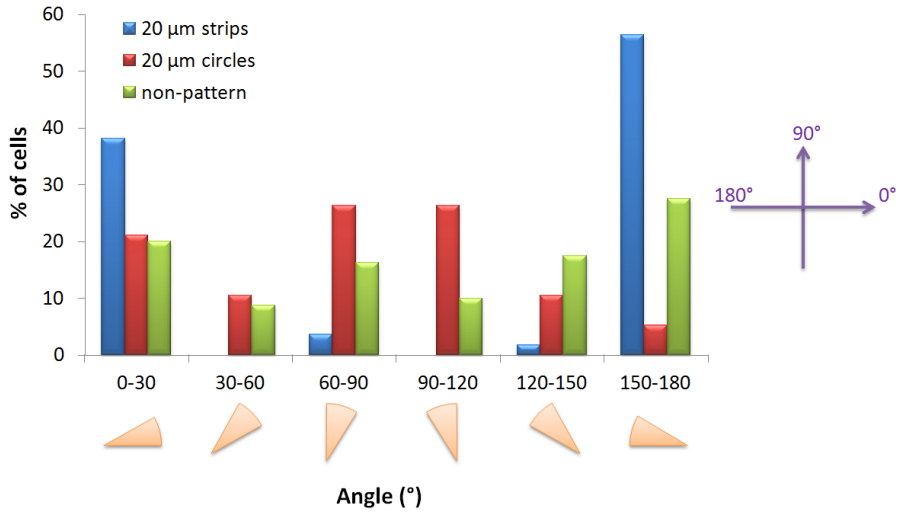


Figure 6-21 The alignment of cells on 20 µm strips compared to 20 µm circles and non-patterns. (n = 55 cells for 20 µm strips, 19 cells for 20 µm circles and 80 cells for non-pattern). The nuclei of cells on 20 µm strips had their long axes in the elliptical fit aligned with the strips.

6.5.4 Fewer cells were observed on protein patterns irradiated with UV

UV irradiation is a common method to sterilize materials for cell culture. When micropatterning was performed on a polystyrene coated glass cover slip without sterilization using UV, contamination with bacteria was often observed (little dots in **Figure 6-22A**). Therefore UV sterilization using a biosafety cabinet was used to sterilize surfaces before micropatterning if they were not supplied sterile or when there might be potential contamination during additional surface processing. Besides, as there may be a chance of contamination during protein micropatterning procedures, the use of UV sterilization on the protein patterns was investigated. Cells bind to fibronectin via specific binding sequences on the protein as listed in **Table 6-7** through integrin receptors on the cell membrane [316]. When the culture surface was UV sterilized without further sterilization after protein patterning, cell micropatterns could be obtained without noticeable contamination (**Figure**

6-22B). However, UV irradiation after protein patterning reduced the number of cells attached on patterns (**Figure 6-22C**). This may be due to the fact that UV may induce covalent modifications of proteins by oxidation. This may change the binding sites or affect the conformation of the protein, which may affect the binding of the cells to this protein. Some fibronectin-binding integrins are given in **Table 6-7**.

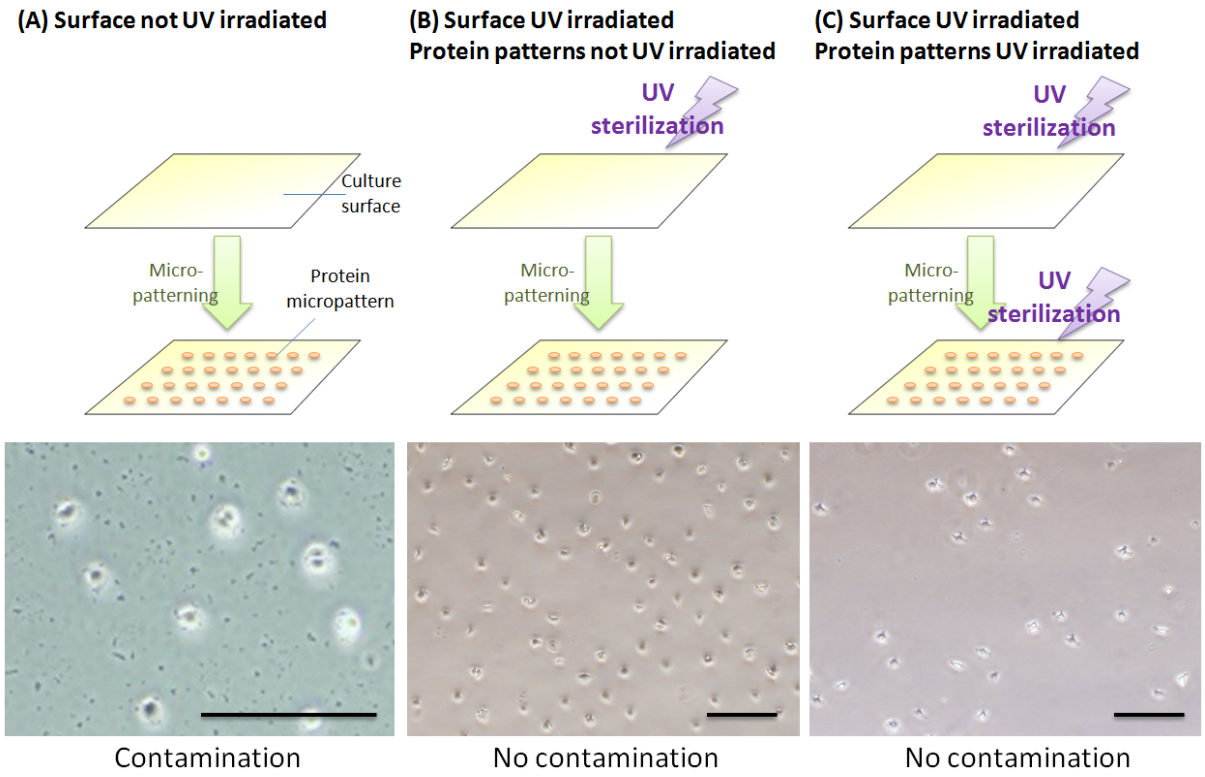


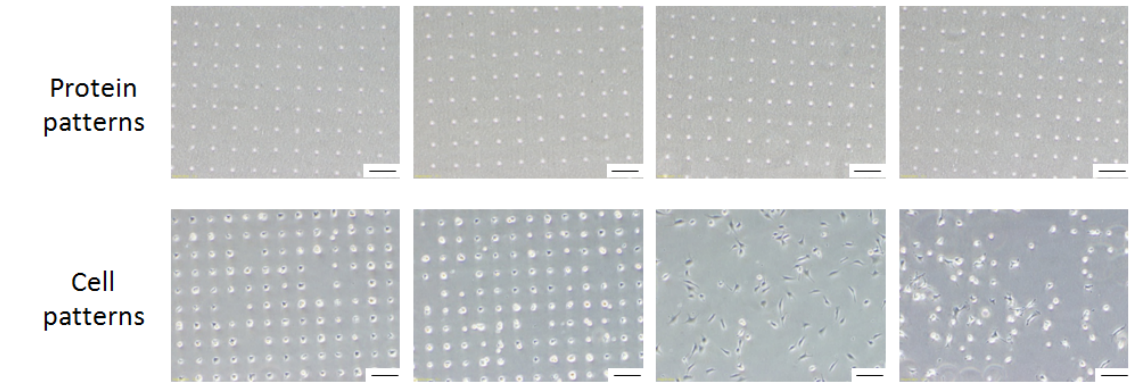
Figure 6-22 Schematics and phase contrast photos of (A) bovine NP cells on fibronectin patterns on surfaces without UV sterilization, (B) bovine AF cells on fibronectin patterns on UV sterilized surfaces without UV irradiated protein patterns and (C) with UV irradiated protein patterns. Photos were taken at 3 h after cell seeding (scale bar = 200 μm). When the cover slip was not sterilized before micropatterning, contamination was often observed as shown in (A). When the surface was sterilized by UV without further sterilization by UV after micropatterning, cells micropatterns could be observed as shown in (B). When the cover slip was sterilized by UV both before and after micropatterning, cell patterns could be formed but the density was lower (as shown in C) than the one without UV irradiation after micropatterning. The UV treatment on proteins may have damaged the proteins, causing fewer cells being able to attach on the protein micropatterns.

Table 6-7 Fibronectin-binding integrins (Reproduced with permission of Frontiers in Bioscience from [316] for reproduction of educational nature) (FN: fibronectin, FG: fibrinogen, LN: laminin, MAdCAM: mucosal addressin cell adhesion molecule, OP: osteopontin, TN: tenascin; TSP: thrombospondin, VCAM: vascular cell adhesion molecule, VN: vitronectin, vWF: von Willebrand factor)

Receptor	Main binding site in FN	Additional binding sites in FN	Other protein ligands
α3β1	RGD		LN5
α4β1	LDV in CS1	H1, CS5, (RGD)	VCAM-1
α5β1	RGD	PHSRN	
α8β1	RGD		VN, TN
αVβ1	RGD		
αVβ3	RGD		VN, OP, vWF, FG, TSP
αIIbβ3	RGD	PHSRN	FG, vWF, VN
αVβ6	RGD		TN
α4β7	LDV in CS1		MAdCAM-1, VCAM-1
α?β8	CS1		

6.5.5 Pluronic is required for micropatterning

We investigated the need for pluronic and serum for cell micropatterning. Before cell seeding, protein patterns were clearly seen on the culture surface (**Figure 6-23**). As the fibronectin was dissolved in PBS, the protein patterns seen were probably fibronectin together with crystals of salts from PBS. The confirmation of protein patterns ensured that the success or failure of cell patterns was due to the effect of pluronic or serum but not incomplete transfer of protein patterns from the stamps to the culture surfaces. From **Figure 6-23**, cell micropatterns could be formed only on surfaces treated by pluronic no matter in the presence of serum or not. This demonstrated that the use of pluronic was critical for the success of cell micropatterns while whether serum was used during cell seeding was not critical. Using untreated polystyrene culture plates as the substrate and with a pluronic passivation step, cells micropatterns could be formed using different cell types as shown in **Section 6.7.3** of the Appendix.



Pluronic	+	+	-	-
Serum	+	-	+	-

Figure 6-23 Phase contrast photos of bovine NP cells with and without surface passivation by pluronic and with and without serum (10% FBS) used during cell seeding. Photos are taken at 2 h after cell seeding. (Scale bar = 100 μm). Cell micropatterns could be formed only on surfaces treated by pluronic no matter in the presence of serum or not. This demonstrated that the use of pluronic was critical for the success of cell micropatterns while whether serum was used during cell seeding was not critical.

6.5.6 Stability of cell patterns

In this work, polystyrene untreated culture plates were used in combination with pluronic passivation. In other studies, glass or plasma treated culture plates were also used in combination with poly(l-lysine)-graft-poly(ethylene glycol) (PLL-g-PEG). This is probably due to the difference in hydrophilicity of the surfaces and hence the requirement of different passivation reagents. Pluronic adsorption occurred on surfaces of intermediate to low wettability but glass or plastma treated culture plates have hydrophilic surfaces [317]. A more detailed study of surface hydrophilicity is given in Chapter 7. For bovine AC cells, cell patterns were obtained for both polystryene surface and glass surface at 2 h after cell seeding but the bovine AC cells spread to non-pattern area for micropatterns formed on glass passivated by PLL-g-PEG at day 3.

Cells could be patterned on glass substrate directly by microcontact printing but the patterns were not as stable as on polystyrene (**Figure 6-24**). This may be due to the shelf-life of the reagent used in passivation. PLL-g-PEG is used for the passivation for patterns on glass slide

and it is usually available commercially in solution form. The stability may be lower than the pluronic F127 used for polystyrene substrate which can be readily purchased in powder form. Stable patterns could be obtained on glass coated with polystyrene.

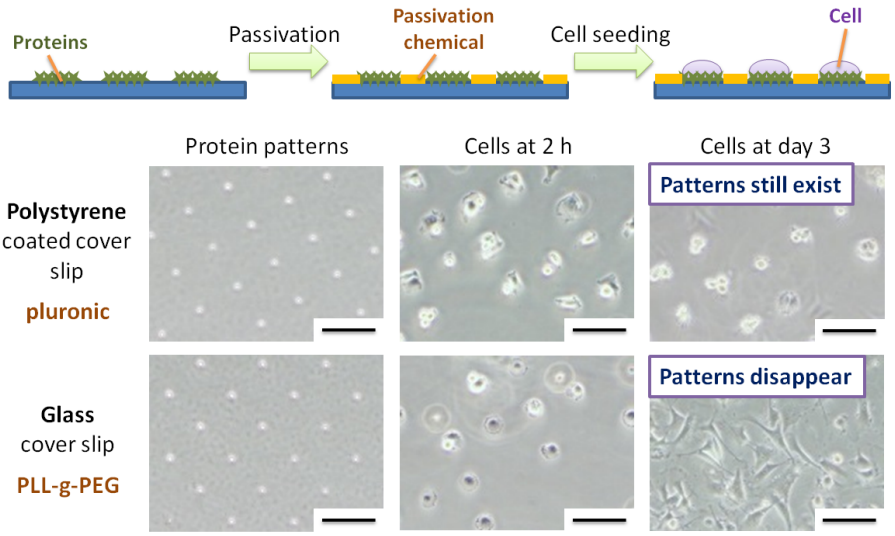


Figure 6-24 Schematic showing the covering of area without proteins with passivation chemicals to prevent cell attachment. Phase contrast photos of fibronectin patterns before passivation and bovine AC cells on fibronectin patterns at 2 h and day 3 after cell seeding. Pluronic solution was used as the passivation reagent for the polystyrene coated cover slip and PLL-g-PEG solution for the glass cover slip (scale bar = 100 μm). Both polystyrene together with pluronic and glass together with PLL-g-PEG gave cell micropatterns at 2 h after cell seeding but the bovine chondrocytes spread to non-pattern area for micropatterns formed on glass passivated by PLL-g-PEG at day 3.

6.5.7 Preparing cell micropatterns for confocal microscopy

As mentioned in Section 6.1.6 in the Background Section, confocal fluorescent microscopy has the advantage over ordinary fluorescent microscopy as it allows increased resolution and 3-dimensional reconstruction. Objectives with larger numerical apertures can give higher resolution images but have shorter working distances, requiring the cell micropatterns to be prepared on thin substrates. One common substrate used to visualize cells for confocal microscopy is glass cover slips but as shown in **Figure 6-24** in the previous section, cells spread to non-pattern area after only 3 days of culture, which is short for studies on

chondrogenesis. To address this issue, the use of polystyrene coated glass cover slip for confocal microscopy was explored.

Glass cover slips have been widely used in confocal microscopy but if cell heights are to be measured, the cells need to be in a hydrated state throughout the staining and viewing process but without extra weight (eg. weight of cover slip) on them as explained in **Figure 6-25**. Thin bottom containers are ideal choices but typical thin bottom culture dishes with glass cover slip bottom are not good for micropatterning when pluronic is used as a passivation agent. Hence, we attempted to create containers with polystyrene coated glass cover slips. First, we tried to punch holes in untreated plastic culture dishes with a metal puncher or an electric drill but the plastic cracked without forming intact holes. Hence we attached a silicone tubing ring to the polystyrene coated glass cover slip with PDMS as a sealant (shown in **Figure 6-9A** in the Materials and Methods Section). This set up allows cells to be cultured on the polystyrene coated glass cover slip which is compatible with cell micropatterning. Meanwhile, we continued to try different hole preparation approaches. With special equipments from the mechanical workshop, holes can be drilled in plastic culture plates without creating large cracks. Originally, we attached the coated glass slips to the bottom of plates with PDMS as sealant but this method was quite time-consuming and required overnight curing of the PDMS in an oven. Besides, there was leakage of the solution when cold PDMS was put in the plates which may be due to the thermal shrinkage effect. Therefore other sealing methods were explored. We decided to use Parafilm® to attach the cover slip to plates with holes. The detailed procedure was described in **Section 6.4.4.3** of the Materials and Methods. The biocompatibility of Parafilm® was previously shown in a study where Parafilm® was used as a microopatterning method [318].

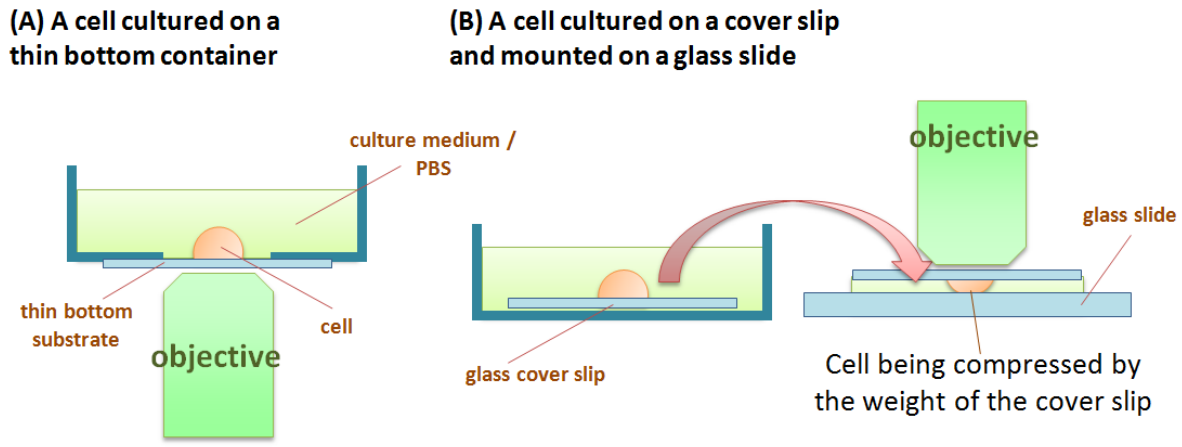


Figure 6-25 The requirement of thin bottom substrate for high resolution confocal microscopy with immersion lens for reliable cell shape or height estimation. (A) The cells can be viewed directly when they are cultured on thin bottom container, (B) the cells cultured on glass cover slip can be mounted on another glass slide to image the cell morphology but the cell will be compressed by the pressure exerted by the cover slip placed on top. Thus it is not advisable to measure cell heights using this setup.

Using Ibidi untreated dishes, cells could be micropatterned on a thin substrate which enabled the use of immersion objective with a working distance smaller than the thickness of typical culture dishes or plates which is around 1 mm. **Figure 6-26** shows the micropatterned NP cells with nuclei stained blue and actin stained red captured using a 20× objective in a confocal microscope Leica SP5 MP. The working distance of this 20× air objective is 0.59 mm. It was not possible to use this objective with cell culture plate directly when the objective was placed underneath the plate as the bottom thickness exceeded the working distance. But this objective is compatible with the Ibidi untreated plastic dish with bottom thickness of 0.18 mm. The Ibidi untreated plastic contains cyclic olefin but the exact composition was not disclosed by the company. The surface hydrophilicity and optical absorbance of this plastic were further characterized and are discussed in the next Chapter.

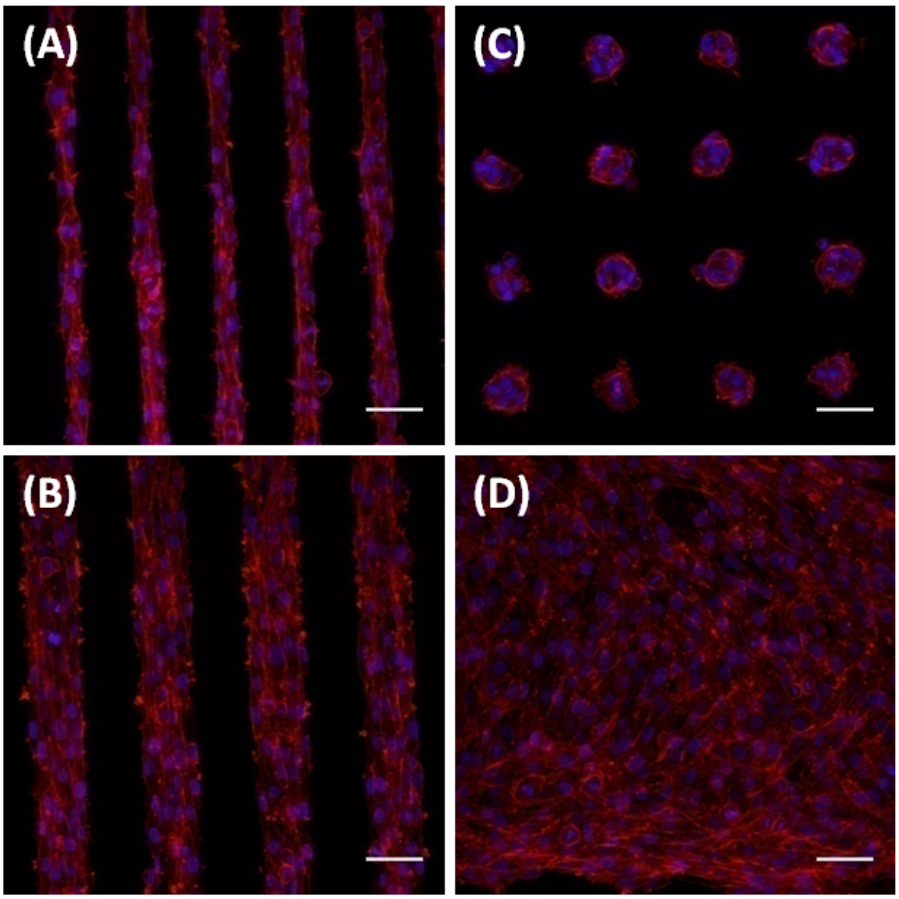


Figure 6-26 Fluorescent photos of bovine NP cells on (A) 20 µm strips, (B) 50 µm strips, (C) small circles and (D) large area of fibronectin. The cells were seeded in Ibidi untreated dishes at 1×10^5 cells per dish, fixed at 2 h and stained blue with DAPI for cell nuclei and red with Phalloidin Alexafluor 568 for actin. The density of cells was higher than the cells seeded at the same density in 6 well plates with wells of similar diameter as there was higher tendency of the cells to concentrate at the centre of the Ibidi dish compared to the culture plate or flat bottom culture dish. Note: There is a shallow well at the centre of the Ibidi dish. (Scale bar = 50 µm, photos captured using a 20× air objective using a confocal microscope Leica SP5 MP).

Stress fibers of cells were one of the subcellular features that can be studied with high resolution confocal microscopy but difficult to be studied with widefield microscopy. Thus we stained the cells with phalloidin stain and viewed the cells using a confocal microscope. However, the stress fibers were not conspicuous for the bovine NP cells (**Figure 6-27**).

On small round patterns, the NP cells have smaller areas to spread, resulting in less stress-fibers. *In vivo*, F-actin is predominantly punctate in NP cells but extends into the

processes of the outer AF cells [289]. When the NP cells are cultured on planar surfaces without micropatterns, the cells tend to spread much and more conspicuous stress fibers were observed. Thus the small circular fibronectin patterns which resulted in fewer stress-fibers in NP cells simulate the *in vivo* conditions better than planar surfaces without micropatterns.

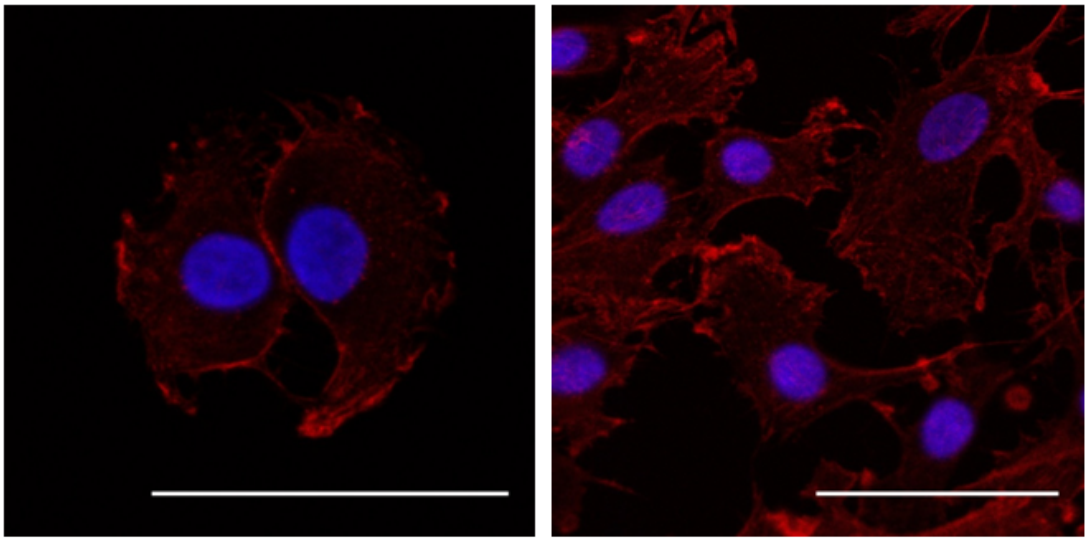


Figure 6-27 Fluorescent photos of bovine NP cells on a circle fibronectin pattern (left) and non-pattern fibronectin (right). The cells were seeded in an Ibidi untreated 35 mm dish, fixed at day 1, stained blue with DAPI for cell nuclei and red with Phalloidin Alexafluor 568 for actin (scale bar = 50 μm, photos captured using a 63× water objective using a confocal microscope Leica SP5 MP). The morphology of the bovine NP cells on micropatterns could be viewed using confocal microscopy but the stress fibers were not conspicuous.

From the equation given in Section 6.1.6 in the Background Section of this Chapter, the resolution is also dependent on wavelength. The shorter the wavelength is, the better is the resolution. In my study, two main Alexa Fluor dyes were used (green Alexa Fluor 488 and red Alexa Fluor 568). They have emission wavelengths of 519 nm and 603 nm respectively (**Table 6-8**). The calculated resolutions of different objectives based on this information and the numerical apertures (NA) are given in **Table 6-9**. The resolution obtained using Alexa Fluor 488 is 12-16% smaller than when Alexa Fluor 568 is used. Using a 63× water immersion objective, resolution of 0.26 μm can be obtained (**Table 6-9**).

Table 6-8 Excitation (Ex) and emission (Em) wavelengths of the fluorescent probes used in this study. Alexa Fluor 488 has a slightly shorter emission wavelength and will give slightly better resolution based on the equation given in the **Section 6.1.6** in the Background Section in this Chapter.

Probe	Ex (nm)	Em (nm)
DAPI	345	455
Alexa Fluor 488	499	519
Alexa Fluor 568	579	603

Table 6-9 Estimated resolutions of objectives for confocal microscopy available in Facility for Imaging by Light Microscopy (FILM) of Imperial College London (ICL). The highest resolution achievable using the water immersion objective is 0.26 μm when Alexa Fluor 488 dye is used.

	Air (dry) Objective	Water Dipping Objective	Water Immersion Objective	Oil Immersion Objective	Oil Immersion Objective
Serial number	506513	506148	506279	506188	506042
Magnification	20×	63×	63×	63×	100×
NA [a]	0.7	0.9	1.2	1.4	1.4
Free working distance (mm)	0.59	2.2	0.22	0.1	0.09
Resolution (Alexa Fluor 488) (μm)	0.45	0.35	0.26	0.23	0.23
Resolution (Alexa Fluor 568) (μm)	0.53	0.41	0.31	0.26	0.26

[a.] NA: numerical aperture

From literature, no high resolution image of cultured bovine cells was found while HUVECs was previously reported to have stress fibers [319]. Hence we prepared micropatterns with HUVECs and stained it with phalloidin Alexa Fluor 488 instead of Alexa Fluor 568, which may give a slightly better resolution compared to Alexa Fluor 568 as explained earlier. As shown in **Figure 6-28**, cells in different shapes had different amounts of stress fibers. The cells which were free to spread on the surface had conspicuous stress fibers in different orientations while the elongated cells had stress fibers aligned to the long axis of the pattern. The cell on the 20 μm circle was round in shape with less clear stress fibers and the cell on a triangle pattern had stress fibers pointing towards the vertices of the triangle.

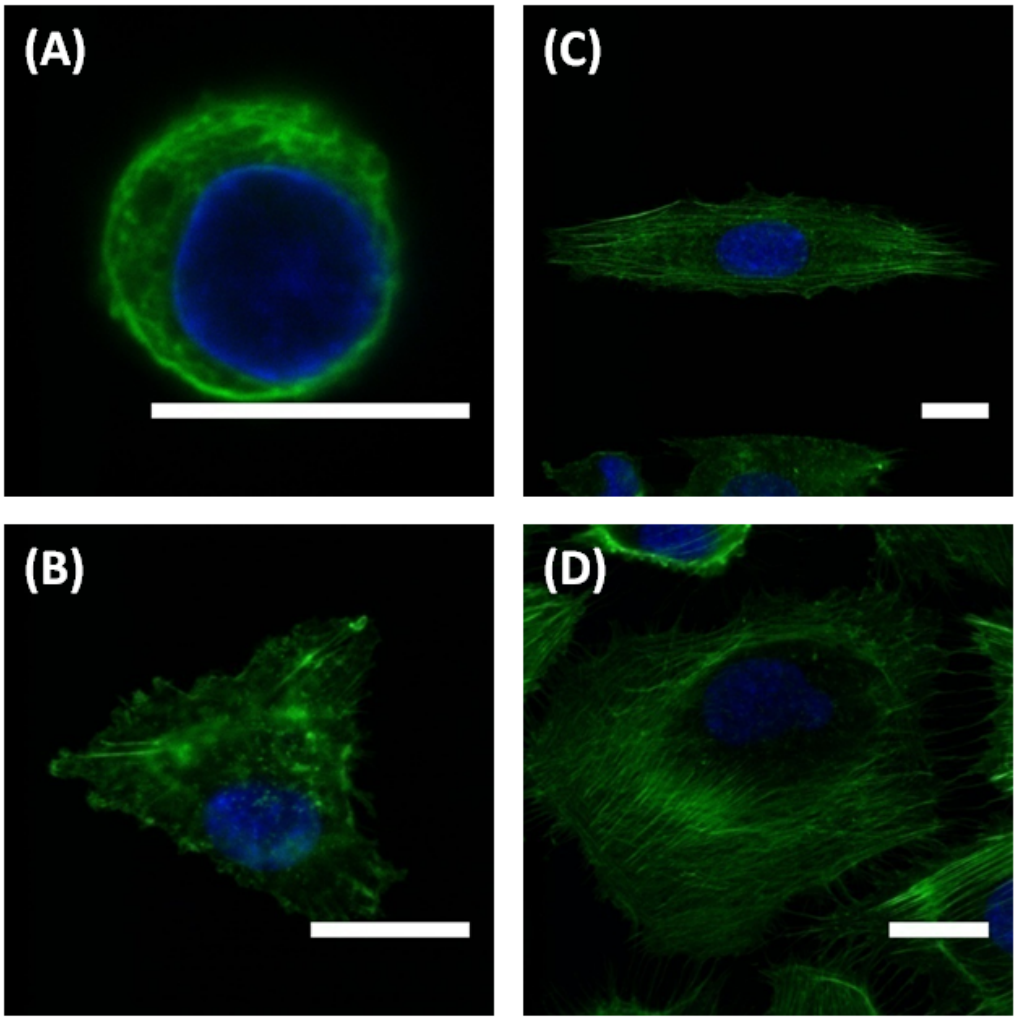


Figure 6-28 Fluorescent photos of HUVECs on (A) circle pattern, (B) triangle pattern, (C) rhombus pattern and (D) large area of fibronectin. The cells were seeded in an Ibidi untreated 2 well µ-slide, fixed at day 1, stained blue with DAPI for cell nuclei and green with Phalloidin Alexafluor 488 for actin (scale bar = 20 µm, photos captured using a 63× water objective using a confocal microscope Leica SP5 MP). Stress fibers were not conspicuous for the cell in round shape but conspicuous for the cells extensively spread on the culture surface.

When stacks of images along z-direction were captured, orthogonal views of the cells could be generated using image processing software such as Fiji (**Figure 6-29** and **Figure 6-30**). They gave a better idea about the shape of the cells cultured on micropatterns along the plane orthogonal to the cell culture surface. With this view, the height of cells at different points can be measured using the tools in Fiji. For instance, the cell heights at the centers of the cells

were estimated to be 2-4 μm and 28-29 μm for the cells in **Figure 6-29** and **Figure 6-30** respectively.

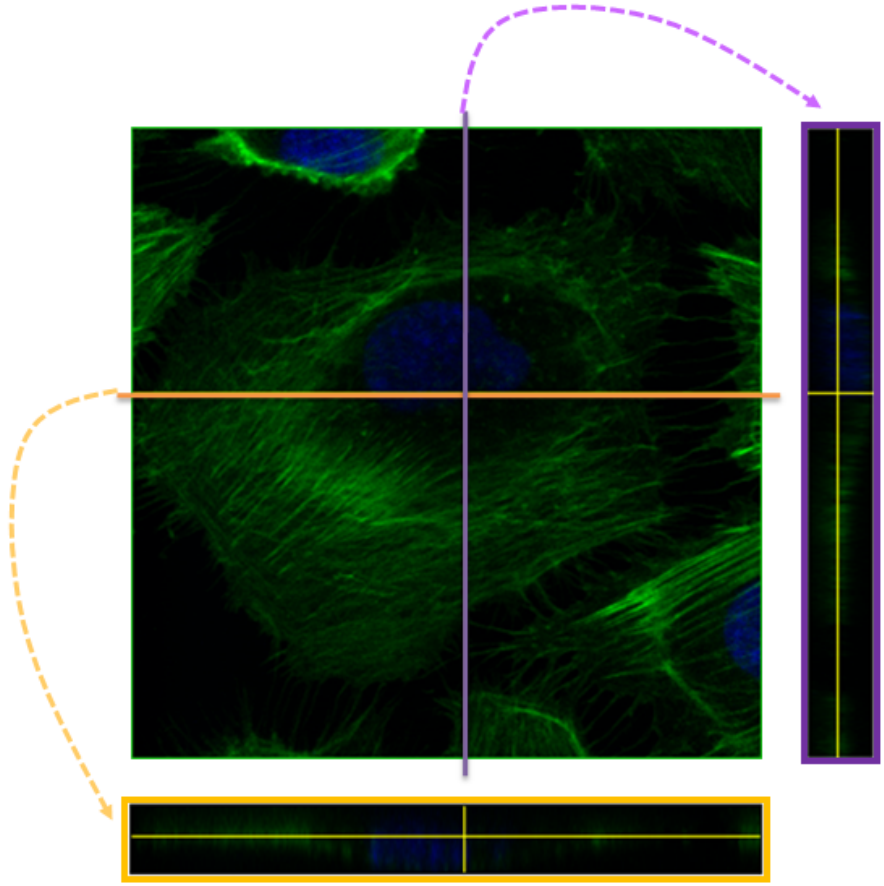


Figure 6-29 Orthogonal view of a HUVEC in spread morphology stained blue with DAPI for cell nuclei and green with Phalloidin Alexafluor 488 for actin. (Stacks of photos captured using a 63× water objective using a confocal microscope Leica SP5 MP and processed using Fiji.) The window on the right indicates the cross-sectional view of the cell along the purple line in the vertical direction of the cell in the main window in the top left corner and the window in the bottom indicates the cross-sectional view of the cell along the orange line in the horizontal direction of the cell in the main window. The resolution in the x- or y- direction is higher than the z-direction for confocal microscopy. The cell height at the center of this cell was estimated to be 2 - 4 μm.

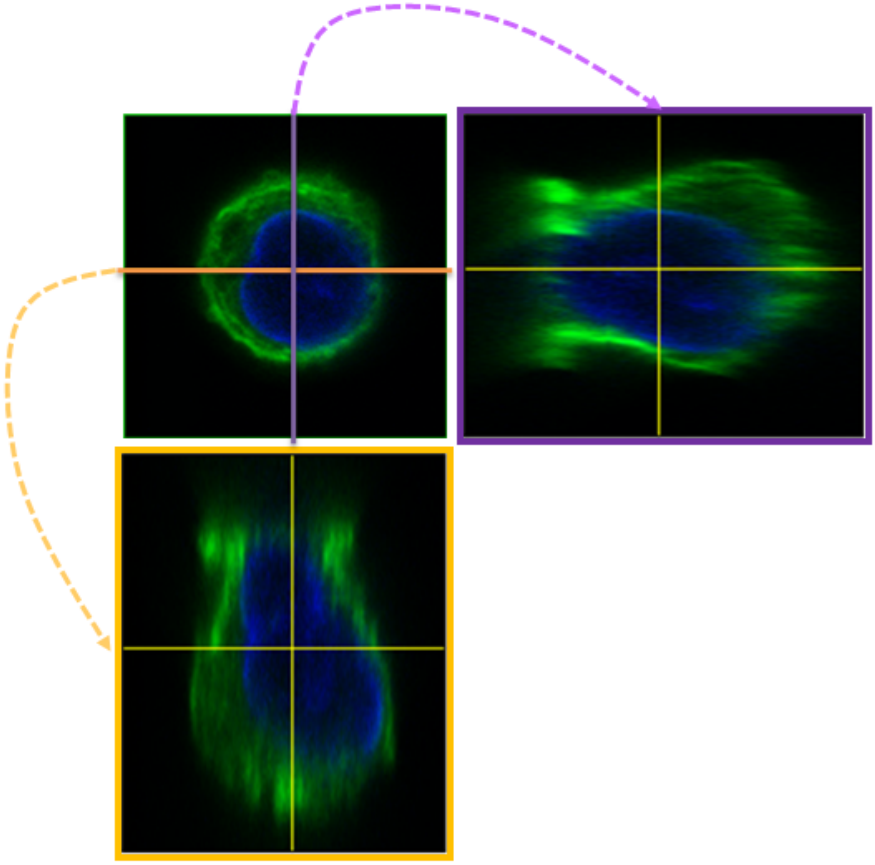


Figure 6-30 Orthogonal view of a HUVEC in round morphology stained blue with DAPI for cell nuclei and green with Phalloidin Alexafluor 488 for actin. (Stacks of photos were captured using a 63× water objective using a confocal microscope Leica SP5 MP and processed using Fiji.) The window on the right indicates the cross-sectional view of the cell along the purple line in the vertical direction of the cell in the main window in the top left corner and the window in the bottom indicates the cross-sectional view of the cell along the orange line in the horizontal direction of the cell in the main window. The resolution in the x- or y- direction is higher than the z-direction for confocal microscopy. The cell height at the center of this cell was estimated to be 28 - 29 μm.

In addition to the orthogonal view, the cells could be viewed from different angles with 3D reconstruction from stacks of images taken in the z-direction (orthogonal to the culture surface). Examples were created using a round cell, an elongated cell, a triangle cell and a cell allowed to spread freely from micropatterns of HUVECs. With 3D reconstruction, we can have a better idea about the spatial conformation of the cells.

6.6 Conclusions

Micropatterning of bovine NP cells has been optimized. Cells can be constrained into round shape when they are cultured on 20 μm circular protein patterns while they become elongated on 20 μm strips. Passivation of the non-patterned zones by pluronic is essential while the presence of serum during cell seeding does not affect the success of cell micropatterns. The cell patterns formed on polystyrene surfaces passivated with pluronic solution are more stable than the patterns on glass surfaces passivated with PLL-g-PEG.

With DAPI staining, the area and shape of the nuclei of NP cells on micropatterns can also be analyzed. Cells cultured on 20 μm circles or strips have smaller nucleus area compared to cells allowed to spread freely. Nuclei of cells on 20 μm strips had the highest aspect ratio and the lowest roundness. The ability to assess the nucleus shape and monitor gene expression quantitatively as described in the next Chapter will allow more systematic studies of the effects of cell shape, cell-cell contact and cell-matrix interactions on NP cell phenotype.

Different methods to prepare cell micropatterns compatible with high resolution confocal microscopy were explored and the use of Ibidi untreated dishes was found to be applicable to cell micropatterning. With this, high resolution photos were taken using confocal microscopy and enabled the estimations of cell heights, the creation of orthogonal views to visualize the cells from the sideway and the construction of 3D view of the cells. These allow the study of cellular features down to a small scale that was not possible with ordinary widefield microscopy.

6.7 Appendix

6.7.1 Patterns of cells could be successfully formed when gap size was not larger than 50 µm while pattern size not smaller than 20 µm

Based on the design criteria in **Section 6.5.2** in the Results and Discussion Section, circle and strip patterns were designed as shown in **Figure 6-31** using LayoutEditor. This software allows drawing with high precision and creating repeating patterns using the "Cell" function. After the design has been made, the film with patterns was ordered from JD Photo-Tools. The photographic film used is a polyester-based film with a dense photographic emulsion. The smallest feature that can be imaged on this photographic film is 8 µm at super-high resolution option. Film mask was chosen in this study as it was inexpensive and gave circle and strip patterns of reasonable quality with patterns without great deviation from the design. For Film mask, patterns for four silicon wafers can be put in the same film mask which saved cost. However, when more complicated patterns (eg. star shape) with small pattern sizes (eg. each pattern of area < 500 μm^2), glass/ chrome mask should be used. It allows the fabrication of higher resolution patterns but it is more expensive and one chrome mask is required for each silicon wafer.

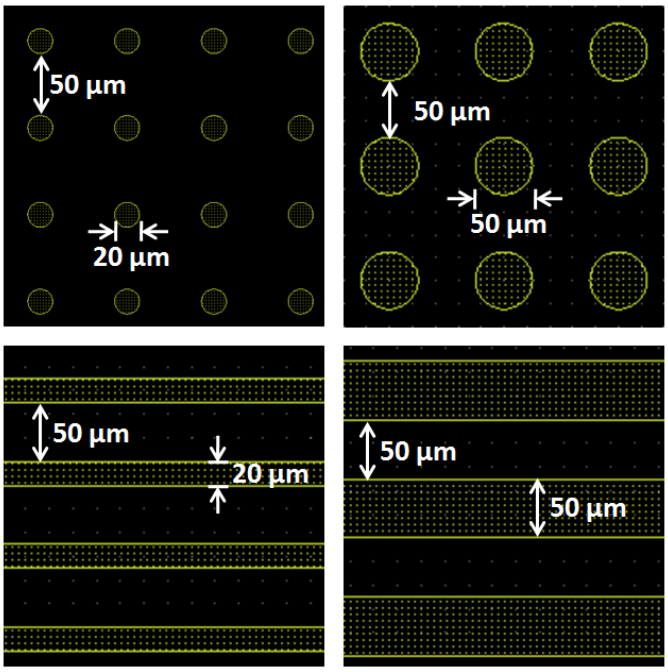


Figure 6-31 Design of patterns in the software LayoutEditor to mimic the round shape of NP cells and the elongated shape of tendon cells.

6.7.2 Cell area evaluation at cell confluence

Estimates of the average cell areas of bovine NP cells, mouse C3H10T1/2 cells, HUVECs and hMSCs at confluence were estimated from phase contrast photos captured using a 10× objective and evaluated using the software Adobe Photoshop. Squares of 200 μm × 200 μm were drawn on the photos and the numbers of cells within the squares were counted. Cells with > 90% of area lying within the square were counted as one cell while cells with 10-90% area lying within the square were counted as half a cell. Three regions on each photo were counted for each cell type. The areas of cells were calculated based on the estimated number of cells in a known area.

Table 6-10 The approximate numbers of cells per mm² and areas of cells estimated from photos in Figure 6-13 in the Results and Discussion Section (mean ± SD, counted from 3 areas of 200 μm × 200 μm each for each cell type)

	bovine NP	mouse 10T1/2	HUVEC	hMSC
Number of cells per mm^2	1513 ± 172	1204 ± 104	479 ± 155	579 ± 26
Area (μm^2)	667 ± 79	835 ± 75	2283 ± 909	1729 ± 79

6.7.3 Study of spheroid formation by NP cells

Using untreated polystyrene culture plates as the substrate and with a pluronic passivation step, cell micropatterns could be formed using different cell types as shown in **Figure 6-32**.

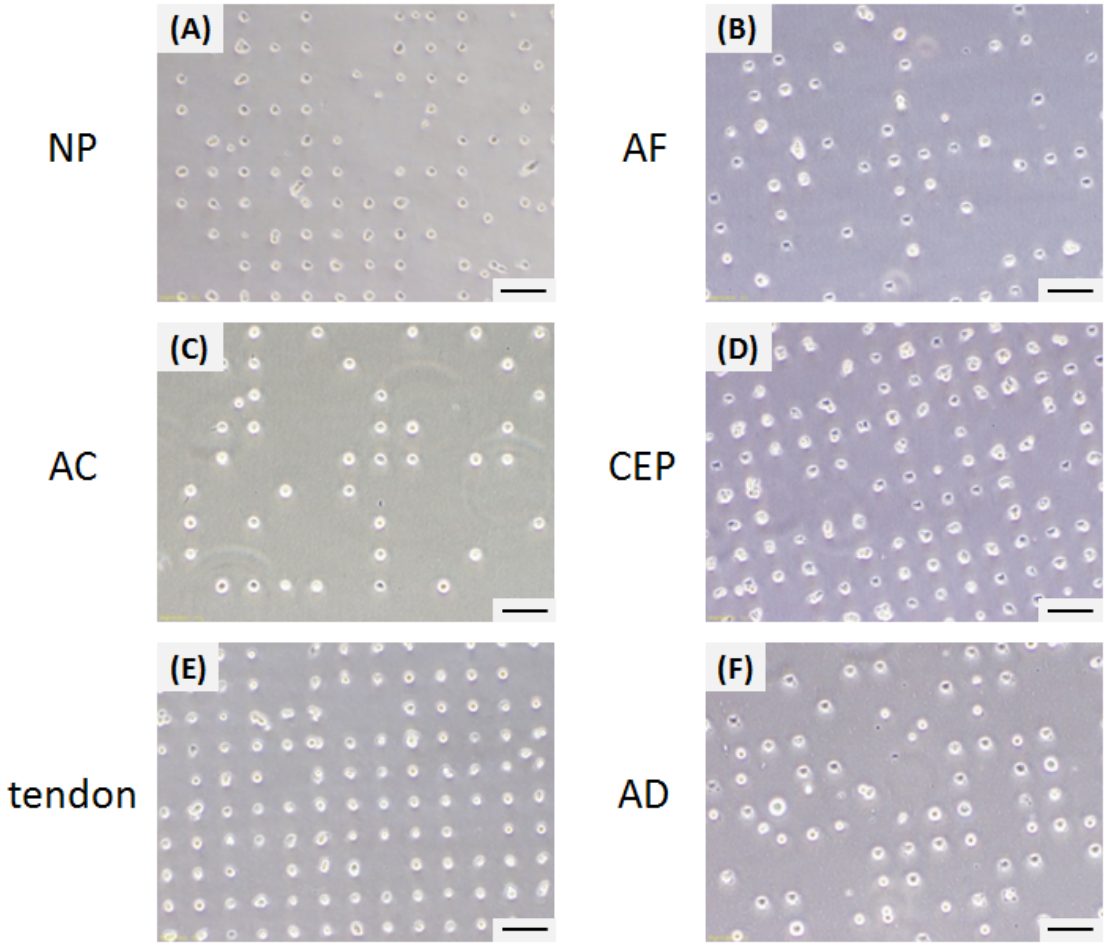


Figure 6-32 Phase contrast photos of micropatterns formed from cells of different sources. (NP: nucleus pulposus, AC: articular cartilage, tendon, AF: annulus fibrosus, CEP: cartilaginous endplate, AD: adipose tissue). Photos were taken at 2-6 h after cell seeding (scale bar = 100 μm).

Interestingly, our preliminary experiments showed that different cells have different ability to proliferate on patterns. NP cells could proliferate on the patterns and form spheres which eventually detached from the surface (**Figure 6-33A**). AC cells could proliferate on the patterns and formed a dense mass without detaching from the patterns (**Figure 6-33B**). Tenocytes did not appear to proliferate and form micromass on the patterns (**Figure 6-33C**). The ability of NP cells to form microspheres spontaneously will allow NP cells to be studied in 3D conformation but without the diffusion limitation that are characteristic of pellet cultures formed from about 2×10^5 cells. It was reported that in 2% oxygen conditions, micropellets formed by approximately 167 MSCs have higher aggrecan and collagen II

expression compared with pellets from 2×10^5 MSCs [320]. Using methylcellulose culture, Sakai *et al.* found that spheroid-forming cells have higher NP matrix gene expression compared with fibroblast-like cells in the primary cell population [58]. In this study, the NP spheroid formation can be monitored by phase contrast microscopy and the relative gene expression levels estimated by RT-qPCR.

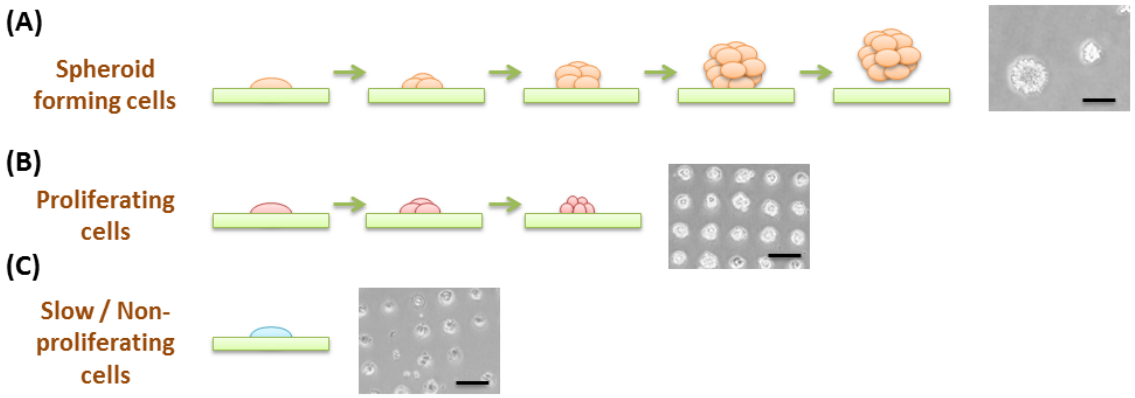


Figure 6-33 Different behavior of cells on micropatterns. (A) Spheroid – forming cells eg. NP cells; (B) Proliferating cells eg. AC cells; and (C) Slow/ non-proliferating cells eg. cells from tendon (all photos shown were cells at day 7 after cell seeding, scale bar = 100 μm).

Chapter 7 Quantitative Gene Expression Analysis of Micropatterned Cells

7.1 Introduction

7.1.1 Background about laser capture microdissection (LCM)

7.1.1.1 LCM and its advantages

Before the introduction of laser capture microdissection (LCM), regions of interest from tissue sections on glass slides were isolated manually [321] using a scalpel or a razor blade [322] or using a needle with higher precision [323]. However, it is difficult to achieve high precision without contamination with manual microdissection [324]. In 1976, Meier-Ruge *et al.* developed a novel method using a laser for microdissection and this enabled microdissection with greater speed, higher precision and higher reproducibility compared to manual methods [325, 326]. To date, LCM has been applied in diverse applications such as RT-PCR, proteomic and genomic profiling, forensic analysis of mixed cell samples and hair follicles, evaluation of tumor microenvironment, studies in developmental biology and embryology, animal models and xenografts as well as infectious disease biology [327].

The most widely used sample types for LCM are tissue sections, in particular cryosections. Tissue sections often consist of a mixture of different cell types, which may affect the interpretation of the studies and LCM can provide great insight on specific cell subpopulations [328]. RT-qPCR of the whole tissue results in averaging of gene expression of different cell types, which may mask the expression profile of specific cell populations. Hence the ability to isolate cells into different categories from a tissue sample is beneficial to specific molecular analysis. LCM is one of the methods to achieve this on tissue sections while flow cytometry and glass capillaries are other methods to collect single cells from cells isolated from tissues [329]. With micropatterning techniques, cells can be manipulated into different shapes and spatial arrangement. Variations within the cell population can be observed and the

use of LCM on cell micropatterns allows the selection of cells of interest from the micropatterns.

7.1.1.2 Two types of LCM

There are a variety of instruments with different system configurations and intended applications but LCM is the standard terminology used regardless of laser method type [330]. Two different laser capture microdissection platforms were developed almost concurrently in the late 1990s [326, 327]. They are the infrared (IR) capture systems [331, 332] and the ultraviolet (UV) cutting systems [333-338]. All commercially available LCM systems are based on one of these two platforms [326].

The first platform using IR laser capture microdissection system was built by Emmert-Buck *et al.* at the National Institutes of Health in 1996 [331]. This system was commercialized as the PixCell system by Arcturus Engineering a year later. As shown in **Figure 7-1** (from [326]), a thin transparent thermoplastic film is placed over a tissue section and cells of interest are selectively adhered to the film with a fixed-position, short-duration, focused pulse from an IR laser [331]. The selective removal of the cells of interest was attained when the adherence of the cells to the film is stronger than the adhesion to the glass slide [339]. Then the film is lifted and the cells together with the film are transferred to a micro-centrifuge tube containing buffer solutions for the isolation of DNA or RNA [328].

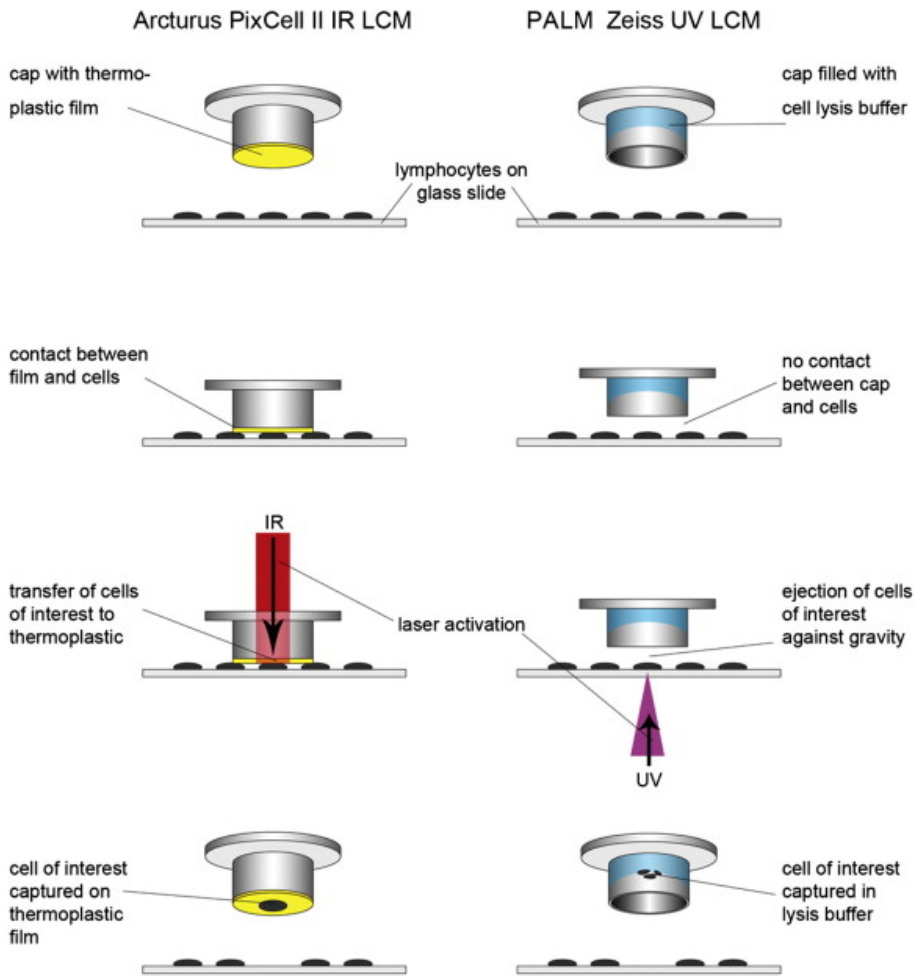


Figure 7-1 Schematic representation of the two main LCM systems: the Arcturus PixCell II IR laser system and the PALM Zeiss UV laser system. (Reproduced with permission of Elsevier from [326] © 2013 Elsevier).

In 1996, Schütze *et al.* developed the second platform with the UV laser microbeam microdissection system [333]. In this system, the cells or regions of interest are cut by a highly focused laser beam. They are then catapulted against gravity into a collection device by increasing the power of the laser as shown in **Figure 7-1** (from [326]). This system was subsequently made commercially available by PALM Zeiss Microlaser Technologies.

In 2013, Vandewoestyne *et al.* compared the IR and UV laser systems using bovine peripheral blood mononuclear cells cytocentrifuged on a glass slide as well as sections of bovine blastocysts [326]. They compared the speed, precision, user-friendliness, sample preparation

necessities, and effect on DNA and RNA quality of these two systems and concluded that the UV system allows faster and more precise sample collection and permits the collection of single cell samples for DNA extraction and downstream PCR applications. In this study, a UV laser system from Zeiss was used.

7.1.1.3 Laser cutting and catapulting in PALM MicroBeam from Carl Zeiss

PALM MicroBeam is an equipment for laser capture microdisssection from Carl Zeiss. There are two types of laser uses associated with it: the laser cutting function and the catapulting function (**Figure 7-2**). In laser cutting, the movement of the sample is controlled by a computer so that specific shape can be cut. In catapulting, the laser generates an upward force that pushes the area of interest to the cap of the collection tube.

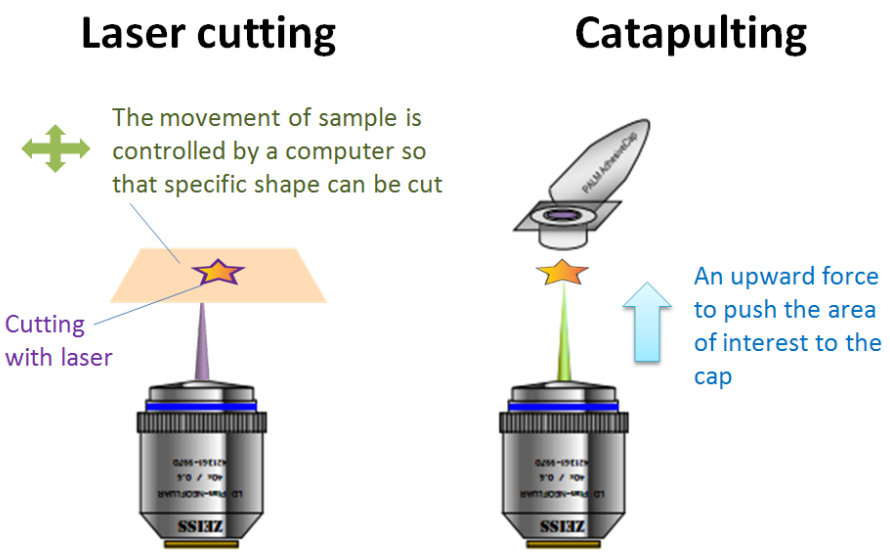


Figure 7-2 The laser cutting function and the catapulting function in PALM MicroBeam from Carl Zeiss.

7.1.2 Motivation for developing methods for preparing micropatterns compatible with LCM

Phase contrast microscopy and fluorescence microscopy have been widely used in studying cell micropatterns but they provide limited quantitative information on the cell phenotype. A

number of studies have been performed using immunostaining of cells on micropatterns. With this method, only a limited number of proteins (typically one or two) can be monitored for each sample. Besides, the protein expression of some genes such as extracellular matrix and growth factors which are secreted out of the cells can be difficult to be assessed using immunostaining and subject to the availability and quality of antibodies. Furthermore, the quantification of protein expression levels through immunostaining is affected by the photobleaching effect of the fluorescent dyes involved, making quantification difficult. *In situ* PCR has been used in assessing micropatterned cells [340] but it requires the synthesis of a probe for each gene under study and it is not quantitative. In contrast, RT-qPCR allows multiple genes to be monitored from the same sample, including genes that code for proteins that are secretory. The quantification using RT-qPCR is not affected by photobleaching. One of the challenges associated with RT-qPCR of micropatterned cells is the small number of cells available from micropatterned surfaces compared with culture surfaces of the same area where cells can spread throughout. Commercially available kits such as Ambion® Cell-to-Ct™ kit from Life Technologies now allow RT-qPCR to be performed with cells without a RNA extraction step. Therefore, in this study, the Cell-to-Ct™ kit was adapted for micropatterned cells.

Cells attached on micropatterns are not a uniform population (eg. some patterns may contain single cells while others may contain more than one cell on the same micropattern) and RT-qPCR using the cell lysate from the whole micropattern surface will result in averaging of the individual differences. To study specific cell population within a mixed population, LCM has been applied to frozen sections in genomic and proteomic studies in both clinical and research laboratories [327, 331, 341-343] and to sections of chemically fixed tissues [344]. LCM has also been used to study cells on micropatterns created by microarray techniques [345, 346]. However, only circular patterns of around 150-500 μm diameter could be made using this microarray technique. In contrast, a wide range of pattern shapes and sizes can be obtained using microcontact printing without sophisticated instruments in every run of

experiments. Nevertheless, there is no study using LCM for micropatterned cells prepared by microcontact printing. The microcontact printing technique is dependent on the substrate used. Hence a micropatterning procedure compatible with LCM was developed and optimized. We hypothesize that micropatterning can be compatible with LCM through surface modification.

7.2 Objectives

The objectives of experiments described in this Chapter are:

- to adapt a commercial kit for RT-qPCR of micropatterned cells
- to develop a method for gene expression analysis of selected cells using laser capture microdissection (LCM)

7.3 Materials and Methods

There are three main parts in this Chapter and the Materials and Methods Section is organized as shown in **Figure 7-3**.

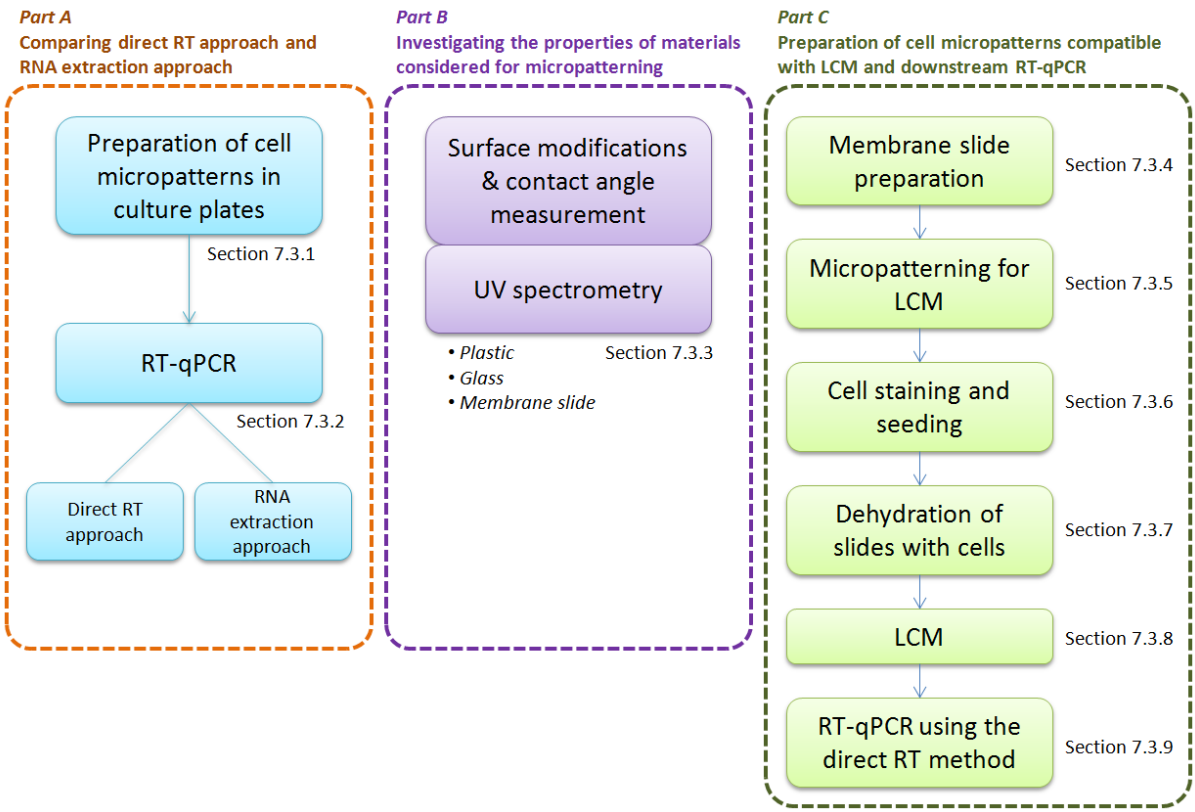


Figure 7-3 Experimental procedures involved in this Chapter. There are three main parts in Chapter 7. Part A is comparing the direct RT approach and the RNA extraction approach of RT-qPCR of

micropatterned cells. Part B is the investigation of the properties of materials considered for micropatterning. Three main types of materials were used and they are plastic, glass and membrane surfaces. The wettability and UV absorbance properties were assessed by contact angle measurement and UV spectrometry. Part C is the preparation of cell micropatterns that are compatible with LCM and downstream RT-qPCR.

7.3.1 Preparation of micropatterned surfaces in cell culture plates

The preparation of micropatterned surfaces for RT-qPCR in untreated cell culture plates and the cell seeding protocol were described in Chapter 6.

7.3.2 RT-qPCR of micropatterned cells in cell culture plates

Reverse transcription (RT) was performed on cell lysate prepared with the Cell-to-Ct kit directly without RNA extraction or on purified RNA using QuantiTect Rev Transcription Kit with RNA extracted with RNeasy kit. qPCR was performed using QuantiTect SYBR Green PCR Kit as depicted in the two approaches in **Figure 7-4**.

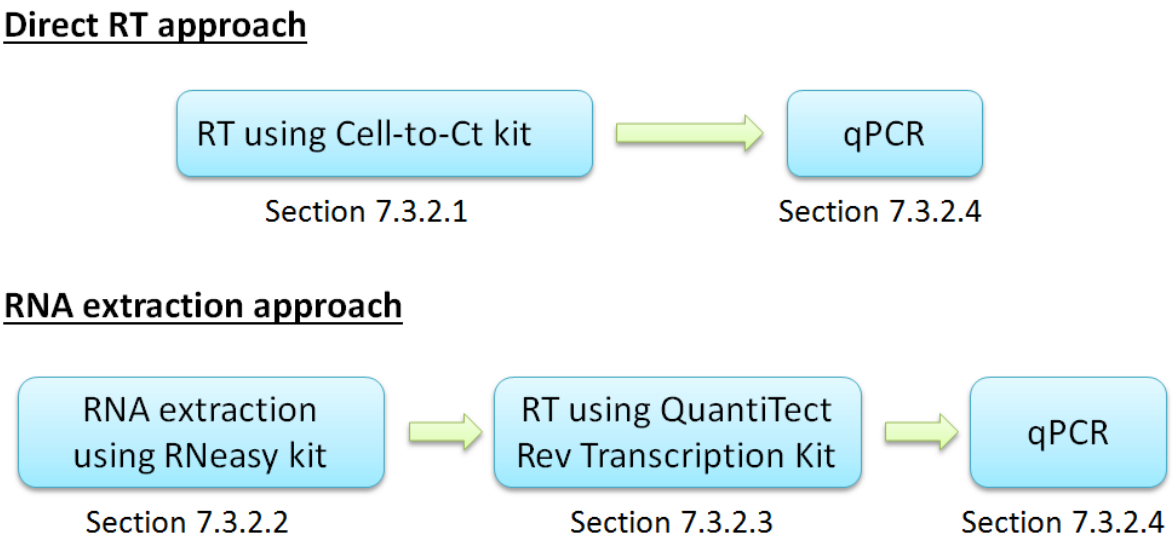


Figure 7-4 Two approaches of RT-qPCR used for micropatterned cells in this study.

7.3.2.1 RT using Cell-to-Ct kit

The reagents in this section were supplied in the Cell-to-Ct kit (Power SYBR® Green Cells-to-CT™ Kit, catalog # 4402953, Life Technologies). Cells seeded on micropatterns in 6

well or 12 well plates were washed with PBS (DPBS, Gibco, catalog # D-PBS14190-169). Cell lysis solution with DNase1 was freshly prepared before each experiment by mixing the cell lysis solution and the DNase1 in 100:1 v/v ratio. Immediately after removing the PBS, 10 µl of cell lysis solution with DNase1 was added to the well and the cell lysis was aided by pipetting the solution up and down. The cell lysate was then transferred to a sterile 0.2 ml PCR tube and incubated at room temperature for 10 min. After this incubation, 1 µl of stop solution was added to the lysate, mixed and incubated at room temperature for 2-5 min. The lysate was put on ice before further steps when several samples were handled in a single experiment. For each RT reaction, 5 µl of 2× SYBR® RT Buffer was mixed with 0.5 µl of 20× RT Enzyme Mix and 4.5 µl of lysate. RT reactions were performed at 37 °C for 60 min followed by 95 °C for 5 min using a thermocycler. The samples were cooled to 4 °C and then put on ice. The cDNA was diluted 5× by adding 40 µl of autoclaved water. No RT controls were prepared by the same RT reactions except that the RT Enzyme Mix was replaced by DEPC-treated water. The cDNA was used immediately for qPCR or stored at -20 °C.

7.3.2.2 RNA extraction using RNeasy kit

RNA extraction using the Qiagen RNeasy Mini Kit (catalog # 74106, Qiagen) was performed according to the manufacturer's instruction (RLT buffer, RW1 buffer and RPE buffer mentioned below were provided in the RNeasy Mini Kit). In brief, the cells were washed with PBS and lysed with 350 µl of RLT buffer per well of cell micropatterns. The lysate in RLT buffer was proceeded with RNA extraction or stored at -80 °C before extraction. For RNA extraction, 1 volume of 70% (v/v) ethanol was added to the lysate, and mixed well by pipetting. Around 700 µl of the sample, including any precipitate, was transferred to an RNeasy Mini spin column placed in a supplied 2 ml collection tube. The tube was centrifuged for 15 s at 8000 × g. The flow-through was discarded. 700 µl of Buffer RW1 was added to the RNeasy spin column and centrifuged for 15 s at 8000 × g. The flow-through was discarded. 500 µl of Buffer RPE was added to the RNeasy spin column and centrifuged for 15 s at 8000 × g. The flow-through was discarded. 500 µl of Buffer RPE was added again to the RNeasy

spin column and centrifuged for 2 min at ≥ 8000 × g. The RNeasy spin column was then placed in a new 1.5 ml collection tube and 30 µl of RNase-free water was added directly to the spin column membrane. The tube was centrifuged for 1 min at ≥ 8000 × g to elute the RNA.

7.3.2.3 RT using QuantiTect Rev Transcription Kit

Genomic DNA elimination reactions were performed with 100 ng of total RNA per sample with the gDNA Wipeout Buffer provided in the QuantiTect Rev Transcription Kit (Qiagen, catalog # 205314 in a reaction volume of 7 µl). The samples were incubated at 42 °C for 2 min using a thermocycler for good heat transfer and temperature control. The samples were then placed on ice immediately. Reverse transcription was performed to generate cDNA in a 10 µl reaction volume with 1 µl of Quantiscript reverse transcriptase, 4 µl of 5X Quantiscript RT buffer, 1 µl of RT primer mix and 3 µl of genomic DNA elimination reaction with RNA in it. The samples were incubated at 42 °C for 15 min followed by 95 °C for 3 min using a thermocycler. Afterwards, the samples were put on ice (or stored at -20 °C before further experiments). The cDNA was diluted five times by adding 40 µl of autoclaved water.

7.3.2.4 qPCR

qPCR was performed with a total reaction volume of 10 µl, containing 1 µl of single stranded cDNA, 5 µl of QuantiTect SYBR Green PCR Kit (Qiagen, catalog # 204145) and 500 nM each of forward primer and reverse primer (*GAPDH*, *ACAN*, *COL2A1*, *CDH2*, *KRT18* and *KRT19* from [113] with sequences given in Chapter 2), in 0.1 ml strip tubes and caps (catalog # 981103, Qiagen) using a standard PCR protocol for SYBR green reactions (Rotor-Gene Q, Qiagen) with a melt curve analysis. The primers were ordered from Invitrogen. Autoclaved water was used as a negative control when necessary and no RT control was used to estimate the level of residual genomic DNA contamination. The relative gene expression was calculated based on comparative Ct method. The qPCR program was as follows:

Table 7-1 Conditions used in qPCR using Rotor Gene Q (Qiagen)

	Temperature	*Time*
DNA polymerase heat activation	95 °C	15 min
Thermocycling (40 cycles)	94 °C	15 s
	60 °C	15 s
	72 °C	15 s
Melt curve	70 to 95 °C (step of 1 °C)	/

7.3.3 Surface modifications, contact angle measurement and UV spectrometry

Contact angles of different materials were analyzed in this study as shown in **Figure 7-5** with details of modifications given in **Table 7-2** and explained in the next paragraph.

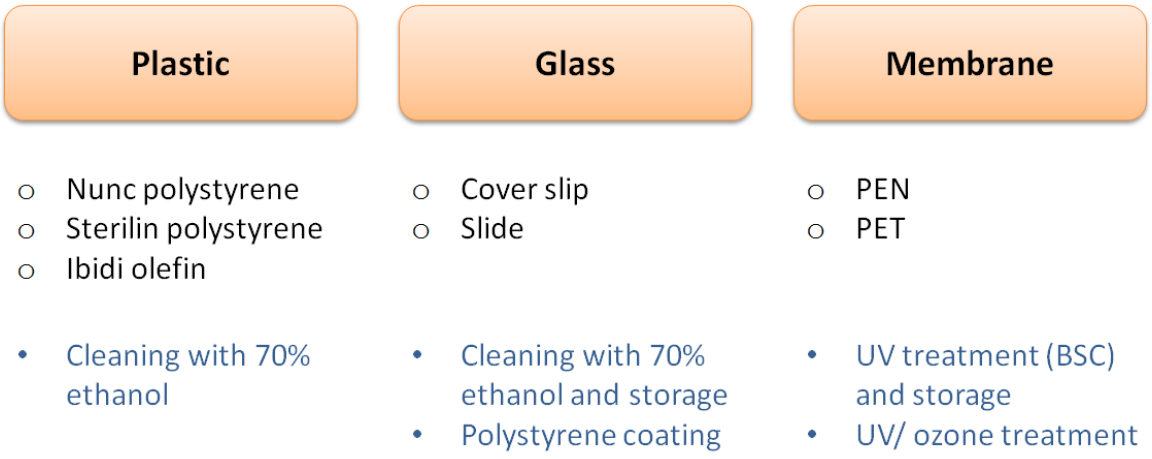


Figure 7-5 Materials and types of modifications involved in this study.

The contact angles of different surfaces were measured using Krüss Easydrop. Nunc untreated polystyrene plastic (catalog # 150200) and Ibidi plastic untreated dish (catalog # 81151) were studied as cell micropatterns could be formed on these materials (involved in experiments in Chapter 6). Untreated culture dish from Sterilin (catalog # PDS-140-180P) was also studied as an untreated polystyrene from another company. In Chapter 6, the polystyrene untreated plates used for the 2nd generation containers were cleaned with 70% (v/v) ethanol after hole punching in the mechanical workshop. Thus the effect of cleaning with 70% (v/v) ethanol was assessed.

In Chapter 6, cell micropatterns could be prepared with glass cover slip with PLL-g-PEG passiviation and polystyrene-coated glass cover slip with pluronic passivation. The patterns formed on polystyrene-coated glass cover slip with pluronic passivation was more stable for the bovine AC cells compared to the glass cover slip treated with PLL-g-PEG. In the polystyrene-coated cover slip preparation, the cover slip was cleaned with 70% (v/v) ethanol and coated with polystyrene. Hence the contact angles of glass cover slip, cover slip after 70% (v/v) ethanol cleaning and after polystyrene coating were measured. The contact angle of the ethanol cleaned cover slip was re-measured at day 1 after cleaning to assess whether the change of wettability resulted from cleaning was reversed upon storage. For the Zeiss Microbeam LCM machine, there was a holder for glass or metal slide but not cover slip. Thus we measured the contact angles of a glass slide before and after cleaning as well as storage and after polystyrene coating similarly.

Although cell micropatterns could be formed with polystyrene coated glass cover slips, our study in this Chapter demonstrated that the cutting and catapulting did not work well with polystyrene coated glass slide (see **Figure 7-9** in **Section 7.4.2** of the Results and Discussion Section). This urged us to study the PEN (Life Technologies, catalog # LCM0531) or PET (Zeiss, catalog # 415190-9101-000) membrane slides specially designed for LCM application. In the product information provided by Zeiss about the membrane slides, it is recommended to irradiate the membrane with UV light at 254 nm for 30 min, which makes the membrane becomes more hydrophilic for tissue section adherence. This step can sterilize and destroy potentially contaminating nucleic acids. Therefore we examined the effect of UV treatment using the UV light in a biosafety cabinet (BSC). In the membrane slide product information, it is also suggested that this UV treatment is preferably performed shortly before use (up to some days before), which implies the treatment may not be stable. Hence the contact angles were re-measured at day 3 and day 8 after the UV irradiation for the PEN membrane slide irradiated with UV overnight. On the other hand, UV/ ozone treatment is also a method of surface sterilization. Thus the contact angles were also measured after this treatment.

UV-vis spectrometry measurements were performed with six different materials using a Perkin Elmer Lambda 25, UV-Vis spectrophotometer. The materials measured were the polystyrene (PS) in the untreated culture plates from Nunc (catalog # 150200), the PS of untreated culture dish from Sterilin (catalog # PDS-140-180P), the plastic bottom material of Ibidi plastic untreated dish (catalog # 81151), plain glass slide from VWR (catalog # 631-0113), PEN membrane of PEN membrane frame slide from Life Technologies (catalog # LCM0531) and PET membrane of PET membrane frame slide from Zeiss (catalog # 415190-9101-000). The scans of UV-visible light absorbances were from 300 nm to 500 nm to include the 355 nm data point, which is the wavelength of laser used in cutting in LCM.

Table 7-2 Different types of surface treatments used in samples for contact angle measurements

Treatments	*Descriptions*
Cleaning with 70% ethanol	The surfaces were sprayed with 70% (v/v) ethanol, wiped with KimWipe and dried at room temperature. *Reason for testing this treatment:* Cleaning with 70% ethanol is a method to sterilize surface
Cleaned surface, stored at ambient conditions	After cleaning with 70% ethanol, the samples were put at ambient atmosphere and temperature for a particular length of time. Then the contact angles were re-measured. This is to assess the changes in surface due to interaction with the ambient. *Reason for testing this treatment:* Cleaning with 70% ethanol may change the surface properties of materials and re-measurement of the contact angles after storage at ambient conditions was done to assess the stability of the modification induced by the 70% ethanol treatment.
UV (in BSC)	The samples were put inside a BSC right under the UV lamp so that the distance between the sample and the UV lamp is the shortest possible distance. *Reason for testing this treatment:* Irradiation under UV is a method to sterilize surface.
UV, stored at ambient conditions	After UV irradiation in BSC, the samples were put at ambient atmosphere and temperature for a particular length of time. Then the contact angles were re-measured. *Reason for testing this treatment:* Irradiation in UV may change the surface properties of materials and re-measurement of the contact angles after storage at ambient conditions was done to assess the stability of the modification induced by the UV treatment.
UV/ ozone	The samples were put inside the drawer of the UV/ ozone machine (UV Ozone Cleaner-ProCleaner™ Plus) and UV radiated for the desired length of time. *Reason for testing this treatment:* One of the applications of ProCleaner™ Plus is surface sterilization.
PS coating	The surfaces were coated with PS solution in toluene as described in Chapter 6. *Reason for testing this treatment:* Coating with PS is a method demonstrated in Chapter 6 to be effective for cell micropatterning when pluronic solution was used as the passivation reagent.

7.3.4 Preparation of slides for cell micropatterns for LCM

Polystyrene in toluene (0.5% w/v) was prepared as described in Chapter 6. PEN membrane slides from Life Technologies (catalog # LCM0531) and PET membrane slides from Zeiss (catalog # 415190-9101-000) were used. To prepare polystyrene coated membrane slides, the membranes were coated with polystyrene by spreading the 0.5% (w/v) polystyrene in toluene with a 200 µl pipet tip on the membranes. The slides were placed in vacuum to remove residual solvent when they were used immediately or prepared 3-5 days before use in cell culture so as to ensure complete evaporation of residual solvent. The membrane slides were sterilized by UV prior to cell culture for 10-30 min for each side. Glass slides to be put underneath the membrane frame slides were cleaned with 70% (v/v) ethanol and also sterilized under UV in a BSC.

7.3.5 Preparation of protein micropatterns on membrane slides

Protein micropatterns were stamped on the polystyrene-coated membrane slides with procedures similar to those described in Chapter 6 with the difference that a glass slide was put underneath the membrane frame slide for more uniform pattern transfer (explained in **Figure 7-15** in **Section 7.4.5** the Results and Discussion Section). Prior to cell seeding, the surface without protein patterns was passivated by pluronic. This was done by adding about 1 ml of 1% (w/v) pluronic solution in PBS to the well of a frame slide. The slides were washed three times with PBS before cell seeding.

Technical note: It is important to avoid spreading of the pluronic solution to the metal frames of the membrane frame slides. Otherwise, the solution may leak out to the containers holding the slides, causing the membrane to dry more easily. When the metal frame surface has been wetted by the pluronic solution, the cell suspension will probably leak out even if the frame slide is completely dried before cell seeding. This could be due to a modification of the hydrophilicity of the metal surface by the pluronic. In such case, a larger volume of cell

suspension should be used to ensure the cells in the well of the frame slide are not dried before the replacement of cell suspension by cell culture medium.

7.3.6 Seeding of cells on membrane slides

In order to visualize the cells more clearly during the LCM, they were stained with fluorescent dye(s). Cells in suspension were stained with CellTracker Green or CellTracker Red. Cells were trypsinized from the culture flasks, centrifuged and resuspended in serum free medium. Stock solutions (10 mM) of CellTracker™ Green CMFDA (Life Technologies, catalog # C2925) and CellTracker™ Red CMTPX (Life Technologies, catalog # C34552) were prepared by adding dimethyl sulfoxide (DMSO, Sigma, catalog # D2650) to the chemicals. The stock solution of dye was added to the cell suspension in serum free medium to a final concentration of 1 μM (10, 000× dilution). The cells were stained at room temperature for 20-30 min in dark. The cells were then washed three times with serum free medium. 1 ml of cell suspension was seeded in the well of the membrane slide with protein micropatterns placed in a petri dish (Fisher Scientific, catalog # PDS-140-045V) or a QuadriPerm cell culture plate (Greiner Bio-One, catalog # 96077307). The cells were incubated at 37 °C with 5% CO_2 for 2 h. Then the membrane slide was washed with PBS and DMEM (Invitrogen, catalog # 17101015) with 10% (v/v) FBS and 1% (v/v) Antibiotic-Antimycotic (Invitrogen, catalog # 15240-062) was added to the dish or plate so that the whole membrane slide was covered with medium.

7.3.7 Dehydration of slides for LCM

At 4 h after cell seeding, the membrane slides for LCM were removed from the cell culture medium, washed with PBS and immersed in 100% ethanol for about 5 min. The slides were then dried at room temperature (and kept in the dark if the cells have been stained with a fluorescent dye). After the slides have been completely dried, they were transferred to a 50 ml centrifuge tube and stored at -80 °C or used immediately for LCM. The use of air tight centrifuge tubes reduces the condensation of water vapor on the slide when they are taken out

from the freezer. This reduces the chance of RNA degradation by keeping any potential RNase present in an inactive dry state.

7.3.8 LCM

The procedures of LCM were performed according to the protocol from Zeiss with the adaptations for using Cell-to-Ct kit. In brief, capped 0.6 ml tubes were pre-cooled on ice. The frame slide with cell micropatterns was mounted to the stage holder of the LCM machine. The cells of interest were selected using the Zeiss LCM software. Then 5 µl of Cell-to-Ct lysis buffer was added to the centre of the cap of a 0.6 ml tube pre-cooled in ice and cells were catapulted into the lysis buffer with the following settings in the Zeiss MicroBeam software (positioning speed: 100%, LPC energy: 90 and focus: 86). The tube with catapulted cells was removed from the tube holder and kept on ice before DNase1 treatment.

7.3.9 RT-qPCR of laser captured cells using Cell-to-Ct kit

RT-qPCR was performed on laser-captured cells with procedures similar to **Sections 7.3.2.1** and **7.3.2.4** with the following modifications for the step before adding the stop solution of the Cell-to-Ct kit. To adjust the volume of solution due to evaporation, the volume of the lysis solution remained in the cap was approximately estimated using a pipet and DEPC-treated water was added so that the total volume was 5 µl. The 5 µl of cell lysates in 0.6 ml tubes were then mixed with another 5 µl of lysis buffer with 2× DNase1. The mixtures were centrifuged and transferred to 0.2 ml tubes.

7.3.10 Statistical analysis

P-values were calculated using Student's two-tailed t-test of unequal variance. P-values of smaller than 0.05 was considered as statistically significant.

7.4 Results and Discussion

7.4.1 The use of Cell-to-Ct kit for micropatterned cells

With the use of RNeasy mini kit for RNA extraction, gene expression could be studied for micropatterned bovine NP cells cultured for 3 days. As shown in **Figure 7-6**, the *ACAN* and *COL2A1* expression of cells on 20 µm circles was higher than those on 20 µm strips. For RNA extracted from cells on these micropatterns, the RNA concentrations were rather low with an average concentration of 22.9 ng/µl for RNA from 20 µm circles (**Table 7-3**). The number of cells available from micropatterns at day 1 may even be smaller than that of day 3 (**Figure 7-7A&B** compared to **Figure 7-7C&D**). Hence, we explored other methods to perform RT-qPCR with cells on micropatterns. Cell-to-Ct kit was designed for studying gene expression in a small number of cells (eg. cells from a well in a 96 well plate). It incorporates a breakthrough cell lysis and RNA stabilization technology that eliminates the laborious and time-consuming RNA purification process completely. These features suggest that this kit can be a potential less laborious option for studying gene expression on cells cultured on micropatterns.

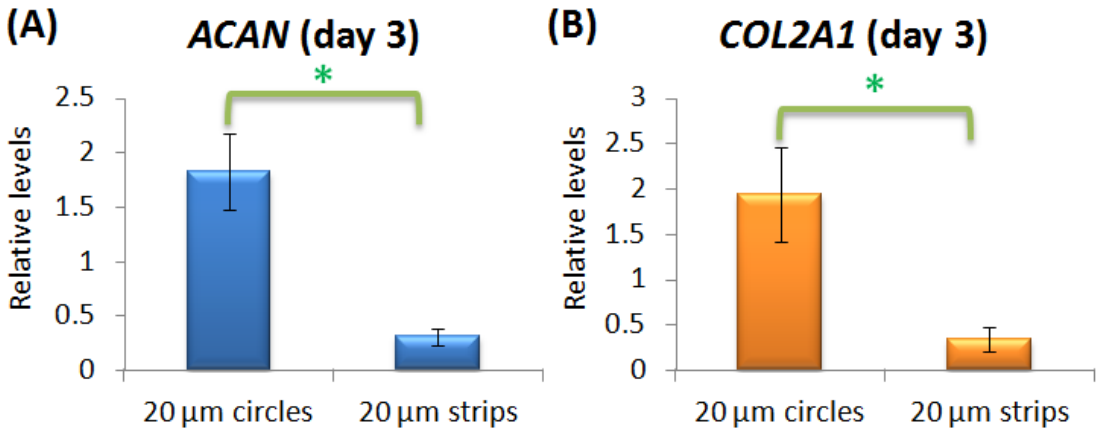


Figure 7-6 Relative mRNA levels in bovine NP cells on fibronectin micropatterns of 20 µm circles and 20 µm strips at day 3 with RNA extracted using a RNeasy kit and reverse transcribed using a QuantiTect Rev Transcription Kit. (Relative to *GAPDH* and the average gene expression of the two groups; mean ± SD; 1 sample from batch 1 and 2 samples from batch 2; technical duplicates in qPCR; * $p < 0.05$). *ACAN* and *COL2A1* expression of cells on 20 µm circles was higher than those on 20 µm strips.

Table 7-3 Concentrations, A_{260}/A_{280} and A_{260}/A_{230} of RNA extracted with a RNeasy kit from bovine NP cells on fibronectin micropatterns at day 3. (Mean ± SD, 1 sample form batch 1 and 2 samples from batch 2)

	Conc. (ng/µl)	A_{260}/A_{280}	A_{260}/A_{230}
20 µm circles	22.9 ± 2.9	2.25 ± 0.05	1.10 ± 0.12
20 µm strips	156.1 ± 79.5	2.07 ± 0.02	1.68 ± 0.77

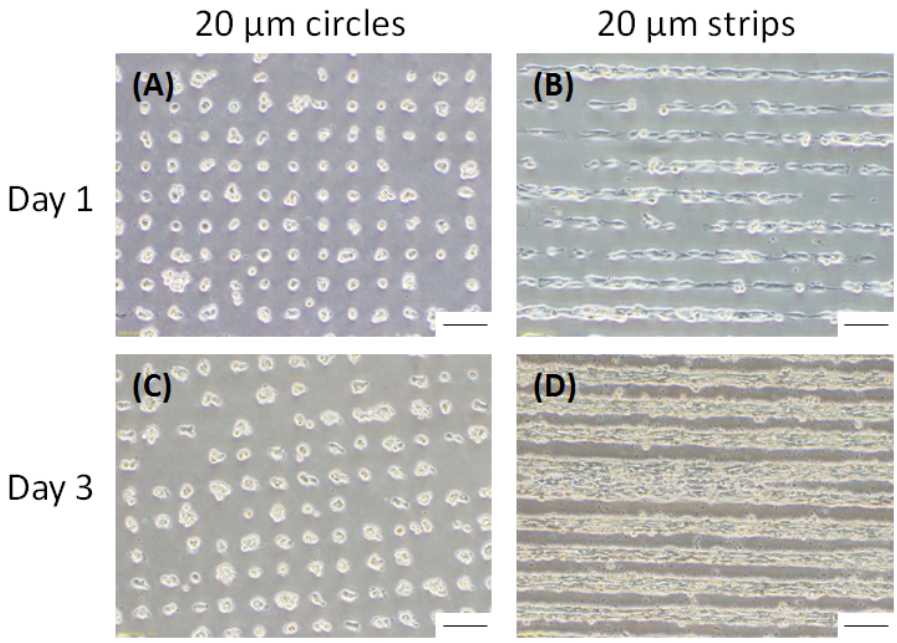


Figure 7-7 Phase contrast photos of NP cells on micropatterns. NP cells on (A) 20 µm circles at day 1, (B) 20 µm strips at day 1, (C) 20 µm circles at day 3 and (E) 20 µm strips at day 3. (Scale bar = 100 µm). The numbers of bovine NP cells on micropatterns increased at day 3 compared to day 1 after cell seeding.

The Cell-to-Ct kit was designed for cells cultured in 96 well plates but the cells on micropatterns were cultured in 12 well plates or 6 well plates. Therefore, the lysis buffer was added to the 12 or 6 well plates and transferred to 0.2 ml tubes for subsequent steps instead of carrying out the reactions in the plates. This could slow down the drying of the lysate resulted from the larger area in each well of the 12 or 6 well plates compared to that of 96 well plates. By adapting this Cell-to-Ct kit to the micropatterned cells, RT-qPCR analysis can be performed on day 1 and day 3 cells (**Figure 7-8**). Higher expression of *ACAN* and *COL2A1*

was consistently observed in cells on 20 µm circles compared to 20 µm strips for samples assayed using both the RNeasy kit (**Figure 7-6A&B**) and the Cell-to-Ct kit (**Figure 7-8C&D**).

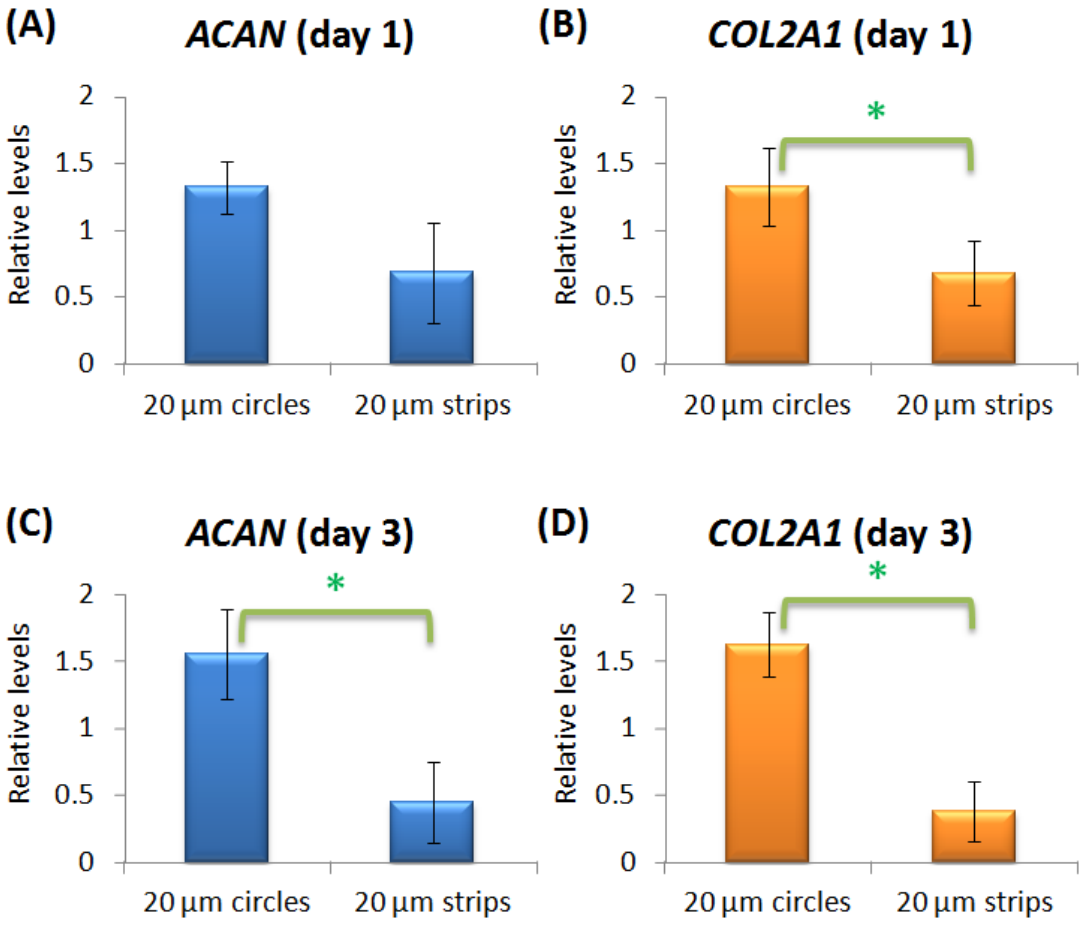


Figure 7-8 Relative mRNA levels in bovine NP cells on fibronectin micropatterns of 20 µm circles and 20 µm strips detected using a Cell-to-Ct Kit. (Relative to *GAPDH* and the average gene expression of the two groups; mean ± SD; 4 samples from 3 independent experiments for *ACAN* and 5 samples from 4 independent experiments for *COL2A1*; technical duplicates in qPCR; * $p < 0.05$).

7.4.2 Laser cutting and catapult of polystyrene (PS) coated glass slide

According to the protocols available from the LCM company Zeiss, plain glass slides may also be used for LCM. The use of plain glass slide with LCM of cryosections was demonstrated in some literature [327, 347-352]. Thus the use of glass slide was tested in this study. In order to make the glass surface compatible with the procedures of cell micropatterning using pluronic as the passivation agent, plain glass slide was coated with

polystyrene (PS) after cleaning with 70% ethanol and dried. Laser cutting and catapult was done on PS coated glass slide. As shown in **Figure 7-9A**, the PS coating could not be cut by the laser at the three laser energy settings tested (50%, 70% and 90%). 70% or 90% laser energy damaged the glass slides without giving sharp cutting. Catapult with the PS coated glass slide created a hole on the slide and the surrounding PS coating being cracked and deformed (**Figure 7-9B**). This is in contrast to the catapult in the PEN membrane slide, which is specially designed for LCM. The catapult on this PEN membrane created a hole with a sharp edge (**Figure 7-9C**). Hence we studied the properties of different categories of materials (plastic, glass and LCM compatible membrane) to obtain information for developing a method to study the gene expression of micropatterned cells using LCM.

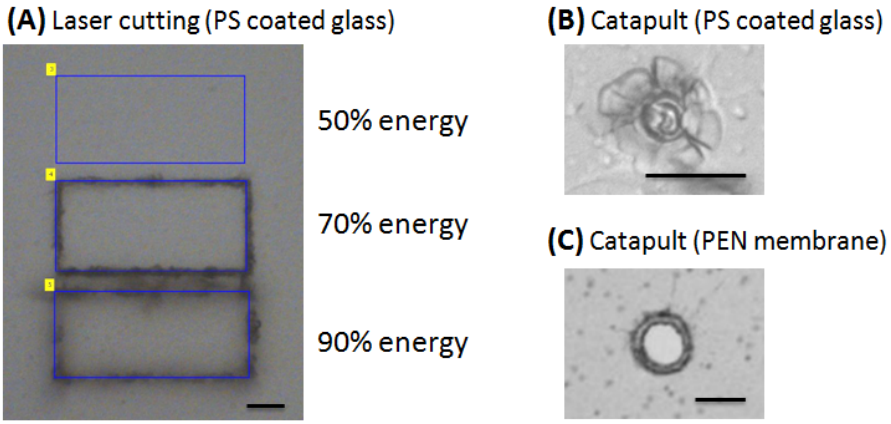


Figure 7-9 Laser cutting and catapult using Zeiss LCM on PS coated glass slide. (A) Laser cutting and (B) catapult on PS coated glass slide, and (C) catapult on PEN membrane slide (scale bar = 50 µm for A and scale bar = 25 µm for B and C).

7.4.3 Identifying materials for micropatterning compatible with LCM through understanding the material wettability and UV absorbance

In order to create cell micropatterns compatible with LCM, the wettability and the UV absorption of different materials were studied. Contact angles (as indicators of wettability) were measured as the success of micropatterning depends on the wettability of substrates [317]. UV absorption properties were assessed as the cutting and catapulting of the Zeiss

Microbeam LCM system uses a laser at 355 nm, which is in the UV range. Three main categories of materials were measured and they were plastic, glass, and membrane slides. In Chapter 6, micropatterning could be performed with polystyrene plastic and Ibidi plastic dishes using pluronic as the passivation agent. The use of plain glass slide with LCM of cryosections was demonstrated in some literature [327, 347-352] and membrane slides were specially designed for LCM applications. The details of the materials and the associated surface modifications were given in **Section 7.3.3** in the Materials and Methods Section.

7.4.3.1 Contact angles of plastic

Contact angles were measured for the plastic surfaces that were used in the micropattern study. Cells were successfully patterned on these surfaces using pluronic as the passivation agent. The water drops on the surfaces were dome shaped (**Figure 7-10**). As shown in **Table 7-4**, all the untreated plastic surfaces being used have hydrophobic surfaces with average contact angles greater than 70°. Cleaning the Sterilin polystyrene surface with 70% ethanol did not change the wettability of it.

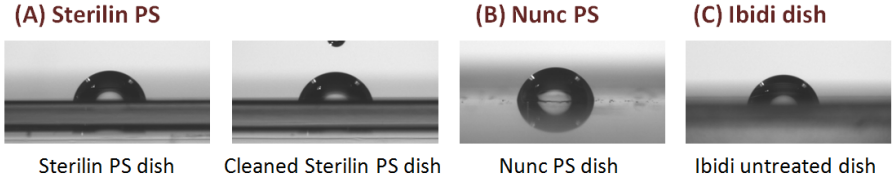


Figure 7-10 Photos of water droplets on plastic substrates in contact angle measurements.

Table 7-4 Contact angles of plastic substrates without and with cleaning with 70% ethanol (n = 4 measurements)

Substrate	Substrate and treatment	Contact angles
dish	60 mm dish	82.0 ± 2.0
	cleaned 60 mm dish	79.6 ± 6.4
plate	12 well plate	78.3 ± 3.9
Ibidi	Ibidi untreated dish	70.5 ± 6.8

7.4.3.2 Contact angles of glass

The water drop on untreated glass cover slip was dome shaped but the water contact angle decreased from 65.9° to 43.3° after the glass cover slip was cleaned with 70% ethanol and dried (**Figure 7-11** and **Table 7-5**). Unlike polystyrene, the cleaning of glass using 70% ethanol changed its wettability. Compared to glass cover slip, the glass slide before cleaning with 70% ethanol was highly hydrophilic with contact angles of around 5.2° (**Table 7-5**) and became more hydrophobic with a contact angle of 27.8° after cleaning with 70% ethanol.

It was reported that PDMS has hydrophobic recovery properties i.e. the PDMS surface that has been made hydrophilic by surface treatments such as plasma treatment will regain its hydrophobicity after some time when it is left in air [353]. Thus the contact angles of cleaned glass cover slip were also measured one day after cleaning with 70% ethanol. There was no significant difference in contact angles for the glass substrate at day 1 after cleaning (**Table 7-5**).

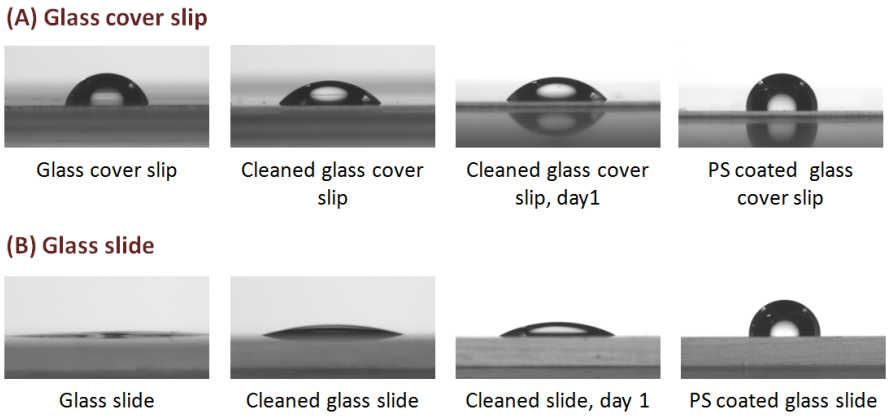


Figure 7-11 Photos of water droplets on glass substrates in contact angle measurements.

Table 7-5 Contact angles of glass substrates without and with different treatments (n = 4 measurements)

Substrate	Substrate and treatment	Contact angles
Cover slip	glass cover slip	65.9 ± 3.7
	cleaned glass cover slip	43.3 ± 5.7
	cleaned glass cover slip day 1	49.4 ± 2.5
	PS coated glass cover slip	96.8 ± 1.6
Slide	glass slide	5.2 ± 6.8
	cleaned glass slide	27.8 ± 8.4
	cleaned slide day 1	23.8 ± 1.7
	PS coated glass slide	96.0 ± 1.3

In Chapter 6, cells were successfully cultured on micropatterns prepared on Nunc untreated culture plates, thus we used the polystyrene from the untreated culture plate to coat glass cover slips. The polystyrene coating rendered the glass cover slip or glass slide more hydrophobic (**Table 7-5**). Cell patterns were performed on polystyrene coated glass cover slip and polystyrene coated glass slides with attempts to prepare cell patterns for LCM. Coating detachment was always observed for glass slide but not for glass cover slip. The lower hydrophobicity of glass slides compared to glass cover slip (**Table 7-5**) may be the cause of the difference in coating adhesion strength.

7.4.3.3 PEN and PET membrane slides have higher absorbance at 355 nm

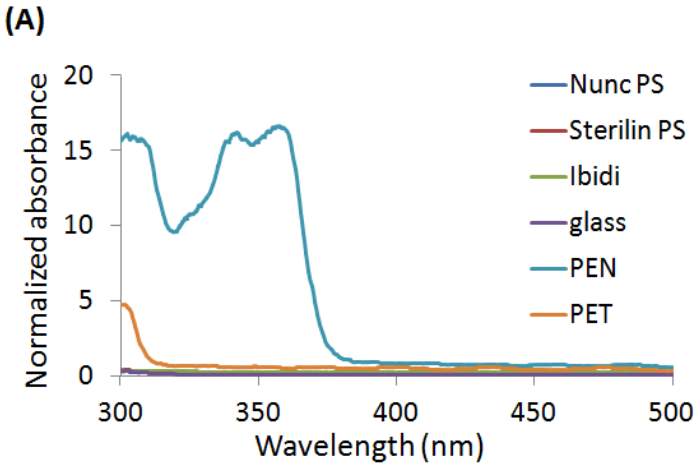
Although cell micropatterns could be formed on polystyrene-coated glass cover slip, the polystyrene-coated glass was not compatible with LCM (as shown previously in **Figure 7-9**). In the Zeiss Microbeam LCM system, a laser of 355 nm is used. Hence, we measured the UV-vis spectra of six different materials listed in **Table 7-6** to further understand the material requirements for LCM with the reasons for choosing these materials given earlier in **Section 7.3.3** in the Materials and Method Section. As the absorbance of light is dependent on the thickness of materials, the thickness was either measured by a caliper, obtained from manufacturer's data or by assumption when thickness values from the prior two sources were not available. The thickness of the Ibidi untreated dish was available from the Ibidi company

website and was 0.18 mm. The thickness of Nunc PS, the Sterilin PS and the VWR glass slide were measured by a caliper and were 1.12 mm, 0.8 mm and 1.08 mm respectively. The PEN membrane and PET membrane were too thin to be measured by a caliper and was assumed to be less than 0.18 mm thick as it was definitely thinner than the bottom plastic of the Ibidi dishes. The absorbances in UV-vis spectrometry were normalized by the thickness. 0.18 mm was used for the normalization of the absorbances of PEN membrane and PET membrane as the exact thickness was not known. This will cause under-estimations of the normalized absorbances of these two materials.

Table 7-6 Materials used for UV-vis spectrometry measurements and contact angle measurements

	Brand	Catalog #	Thickness (mm)	Source
Nunc PS	Nunc	150200	1.12	Caliper
Sterilin PS	Sterilin	PDS-140-180P	0.8	Caliper
Ibidi	Ibidi	81151	0.18	Manufacturer's data
Glass slide	VWR	631-0113	1.08	Caliper
PEN	Life Technologies	LCM0531	< 0.18	By assumption
PET	Zeiss	415190-9101-000	< 0.18	By assumption

Figure 7-12A shows the UV-vis spectra of materials listed in **Table 7-6**. PEN membrane and PET membrane have higher absorbances than other materials. However, the absorbances measured were underestimated due to the uncertainty of the membrane thickness. At 355 nm, which is the wavelength of laser used in LCM for cutting, PEN membrane had the highest absorbance followed by PET membrane (**Figure 7-12B**). Compared to PET membrane, PEN membrane has nearly 30 times higher absorbance at 355 nm. Even with under-estimation, the normalized absorbance of PET was still more than double that of Ibidi plastic, PS or glass. This is possibly one of the reasons for using PET membrane and PEN membrane in LCM as the membrane can be cut more easily using a laser at 355 nm.



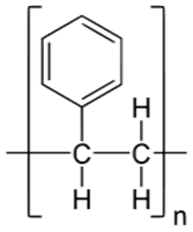
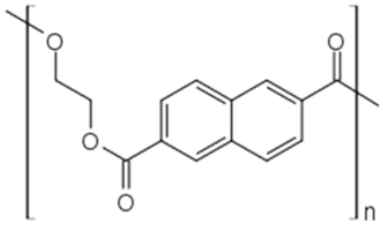
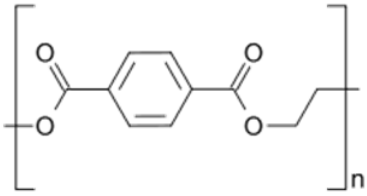
(B)

Material	Normalized abs. at 355nm
Nunc PS	0.115
Sterilin PS	0.191
Ibidi	0.246
Glass slide	0.038
PEN *	16.513
PET *	0.554

Figure 7-12 (A) UV-vis spectra of materials listed in Table 7-6 normalized with material thickness and (B) the corresponding normalized absorbances at 355 nm. (* The absorbances for PEN and PET were under-estimated due to the assumption of thickness of 0.18 mm which is an overestimated value).

Table 7-7 shows the chemical structures of polystyrene (PS), polyethylene naphthalate (PEN) and polyethylene terephthalate (PET). The peak wavelengths tend to be shifted towards the long wavelength as the conjugated systems (connected *p*-orbitals with delocalized electrons from the benzene ring) get larger (**Figure 7-13**). Among the three molecules, PEN has the largest conjugated system due to the naphthalene, thus the largest shift of absorbance to longer wavelength. The benzene ring in the PET can form delocalized electron clouds with the neighbouring *p*-orbitals of the double bonds, which also shifts the peak to longer wavelength compared to polystyrene without extended delocalized electrons outside the benzene ring. Thus the peak absorbance wavelengths are: PS < PET < PEN as observed in **Figure 7-12** (the absorbance peak of PS was out of the detection range measured).

Table 7-7 Chemical structures of polystyrene (PS), polyethylene naphthalate (PEN) and polyethylene terephthalate (PET)

Polystyrene (PS)	*Polyethylene naphthalate (PEN)*	*Polyethylene terephthalate (PET)*
		

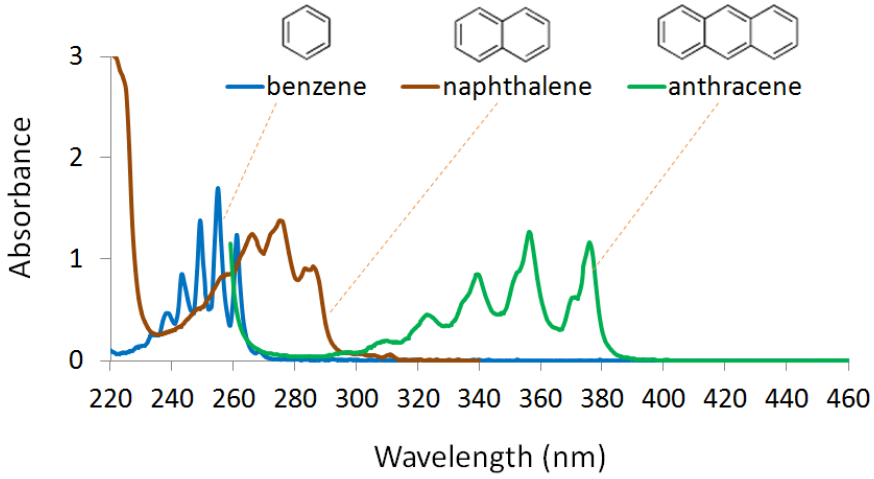


Figure 7-13 Absorption spectra of benzene, naphthalene and anthracene in cyclohexane. The spectra were plotted from the database in the software PhotochemCAD, which is downloadable from http://www.photochemcad.com. The data of absorption spectra of benzene, naphthalene and anthracene in the database were provided by Ruchun A. Fuh and plotted using Microsoft Excel.

7.4.3.4 Contact angles of membrane slides

As explained in the previous Section, PEN membranes and PET membranes facilitate cutting by laser in LCM due to their high absorbances at 355 nm. It was suggested that wettability is an important factor that affects the success of micropatterning [317] but little information is available. Therefore the contact angles of the PEN and PET membranes were measured with results shown in **Figure 7-14** and **Table 7-8**. The contact angles were approximately 90.5° for PEN and 79.7° for PET but the difference was not statistically significant due to the large standard deviations for the measurements for the PEN membrane.

Since the membrane slides were supplied non-sterile, the effects of UV on surface hydrophobicity were also assessed. According to the product information of the membrane slides of Zeiss, UV treatment for membrane-covered slides is an optional procedure. It is recommended to irradiate the membrane with UV light at 254 nm for 30 min, which makes the slides more hydrophilic. This treatment is preferably performed shortly before use (up to some days before), which implies there may be changes during storage after UV treatment. Hence the contact angles were measured again at day 3 and day 8 after the UV treatment of PEN membrane.

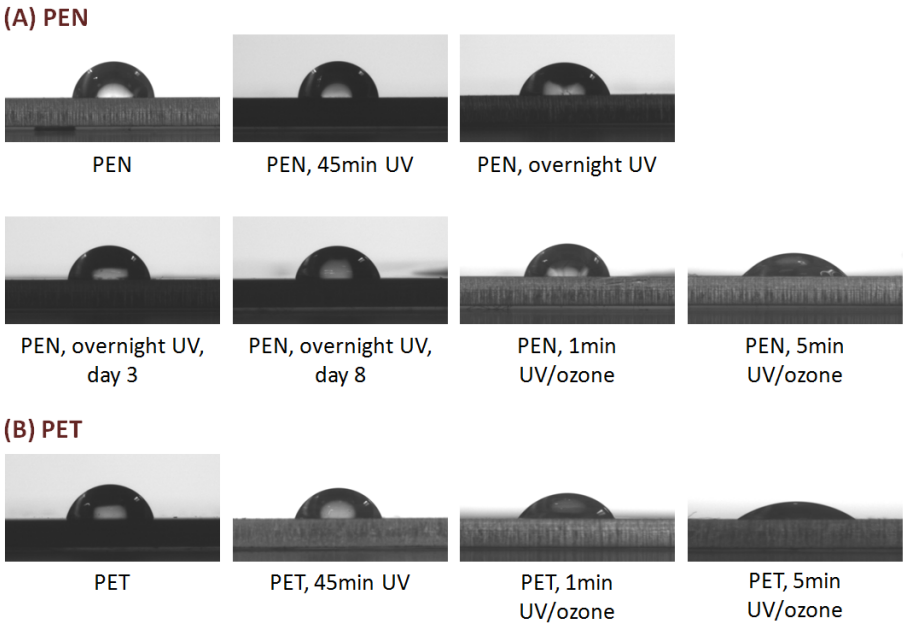


Figure 7-14 Photos of water droplets on glass substrates in contact angle measurements.

Table 7-8 Contact angles of membrane slides without and with different treatments (n = 4-5 measurements)

Substrate	Substrate and treatment	Contact angles
PEN	PEN	90.5 ± 9.4
	45min UV PEN	88.8 ± 3.0
	overnight UV PEN	72.4 ± 6.2
	overnight UV PEN day 3	78.4 ± 8.0
	overnight UV PEN day 8	75.6 ± 14.7
	PEN 1min UV/ozone	77.1 ± 3.3
	PEN 5min UV/ozone	52.2 ± 9.6
PET	PET	79.7 ± 0.8
	45min UV PET	83.3 ± 11.5
	PET 1min UV/ozone	59.1 ± 14.4
	PET 5min UV/ozone	38.2 ± 4.9

As shown in **Table 7-8**, the contact angles were 88.8° and 83.3° for PEN membrane and PET respectively after 45 min of UV treatment using the UV light in a biosafety cabinet (BSC) for cell culture. With overnight UV treatment using BSC UV light, the surface seemed to become more hydrophilic with contact angle decreased from 90.5° to 72.4° compared to without UV treatment but the difference was not statistically significant. No obvious hydrophobic recovery was observed at day 3 and day 8. With UV/ ozone treatment, the water drops spread more with 5 min treatment for PEN membrane and with 1 min treatment for PET membrane. For PEN membrane, the contact angles reduced to 77.1° and 52.2° for 1 min and 5 min UV/ ozone treatment respectively and for PET membrane, 59.1° and 38.2° respectively. Compared to BSC UV light, the UV/ ozone was much stronger in changing the hydrophobicity of the membrane surfaces of PEN and PET.

7.4.4 Summary of findings of contact angle measurements and UV spectrometry

Based on the findings in **Sections 7.4.3.1 - 7.4.3.4** presented earlier, the following information was used in developing a method to prepare cell micropatterns compatible with LCM.

- ✧ PEN membrane and PET membrane have high absorbance at 355 nm and PEN has higher absorbance than PET

- ✧ Cleaning with 70% ethanol may induce changes to glass surfaces but not to polystyrene
- ✧ Coating with polystyrene can increase the contact angles of the glass surface
- ✧ UV/ ozone treatment makes the surface of PEN/ PET membrane more hydrophilic

Therefore, in our study, we used PEN/ PET membrane slides and attempted to coat them with polystyrene. UV treatment using BSC was used instead of UV/ ozone to avoid making the surface hydrophilic.

7.4.5 Critical precautions in successful cell micropatterning on membrane slides

Initially, micropatterning of cells on PEN membrane glass slides were attempted but protein patterns could not be formed reproducibly. Hence we explored different types of membrane slides and also tried coating the membrane with polystyrene. There are two types of membrane slides available commercially: the PEN membrane glass slide and the PEN membrane frame slide. For membrane glass slide, a thin membrane is mounted on a glass slide with a thin layer of air in between to facilitate catapulting in LCM. For membrane frame slide, a thin membrane is mounted on a regular metal frame with the outer dimension same as an ordinary microscopy glass slide. We compared the cell patterns formed on PEN membrane glass slides and PEN membrane frame slides with and without polystyrene coating. Patterns were not formed for PEN glass slide for the area observed (**Figure 7-15B&C**). Occasionally cell patterns were found for PEN glass slide but this was not reproducible. The schematic of the structure of a membrane glass slide in **Figure 7-15** illustrates this. During micropatterning of proteins, the PDMS stamps coated with proteins were pressed against the membrane. As there was a thin layer of air between the membrane and the glass underneath (**Figure 7-15A**), the "non-pattern" part of the PDMS stamp could touch the membrane due to its flexible nature, resulting in protein transferred to the "non-patterned" area. In contrast, only a very thin layer of air exists in between the membrane and substrate underneath for membrane frame slide (**Figure 7-15D**). In my study, a glass slide was put underneath the membrane frame slide for better contact of the PDMS stamps and the membrane, which resulted in higher reproducibility of patterns. Without PS coating, cells attached non-specifically (**Figure**

7-15E). With PS coating on frame slides, cell micropatterns could be obtained as shown in **Figure 7-15F**.

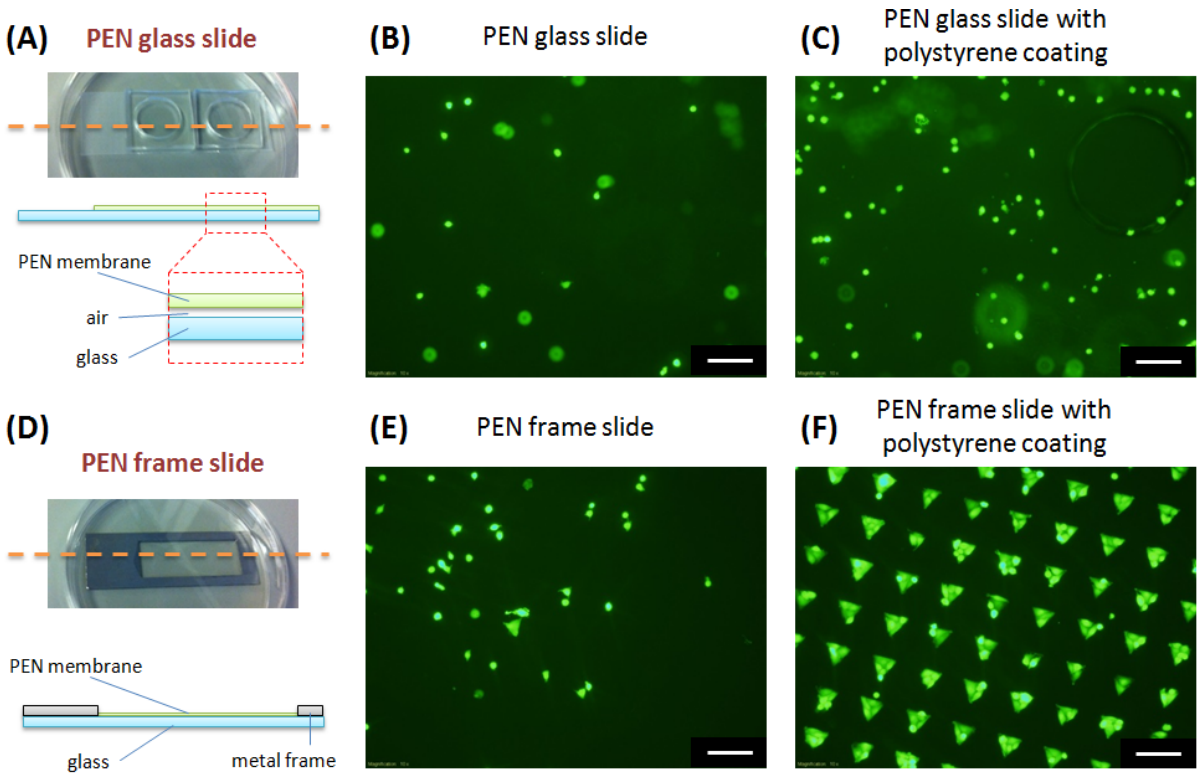


Figure 7-15 Fluorescence images of bovine NP cells cultured on fibronectin patterns on a PEN membrane glass slide and a PEN membrane frame slide with and without polystyrene coating. (Scale bar = 100 μm). (A) A PEN membrane slide and the schematic showing an air layer between the membrane and the substrate underneath; (B) cells on a PEN membrane glass slide without polystyrene coating and (C) with polystyrene coating; (D) a PEN membrane frame slide and the schematic showing a negligible air layer between the membrane and the substrate underneath; (E) cells on a PEN frame membrane slide without polystyrene coating and (F) with polystyrene coating. Photos were captured at 2 h after cell seeding. For the membrane glass slide, punched PDMS blocks were put on the slide for cell seeding to create reservoirs for holding the cell suspension on the slide.

It was suggested that a hydrophobic surface is required for micropatterning when pluronic passivation is used. PEN membranes are hydrophobic even after 45 min of UV treatment in a BSC but cell patterns were not stable on this membrane. Taken together, hydrophobic surface seems to be an essential but inadequate requirement for micropatterning when pluronic is used as a passivation agent.

7.4.6 Specific area of cells on membrane slide could be cut or catapulted precisely

As shown in **Figure 7-16**, precise cutting and catapulting of the selected area was made possible by LCM. With control using computer, different patterns and shapes can be drawn using the software for the LCM and patterns can be cut exactly the same as the patterns drawn (**Figure 7-16A**). After cutting the membrane with cells (**Figure 7-16B**), the specific area of membrane could be catapulted to the cap for collection (**Figure 7-16C**). Cells of interest from the micropatterns could also be selected precisely (**Figure 7-16D-G**).

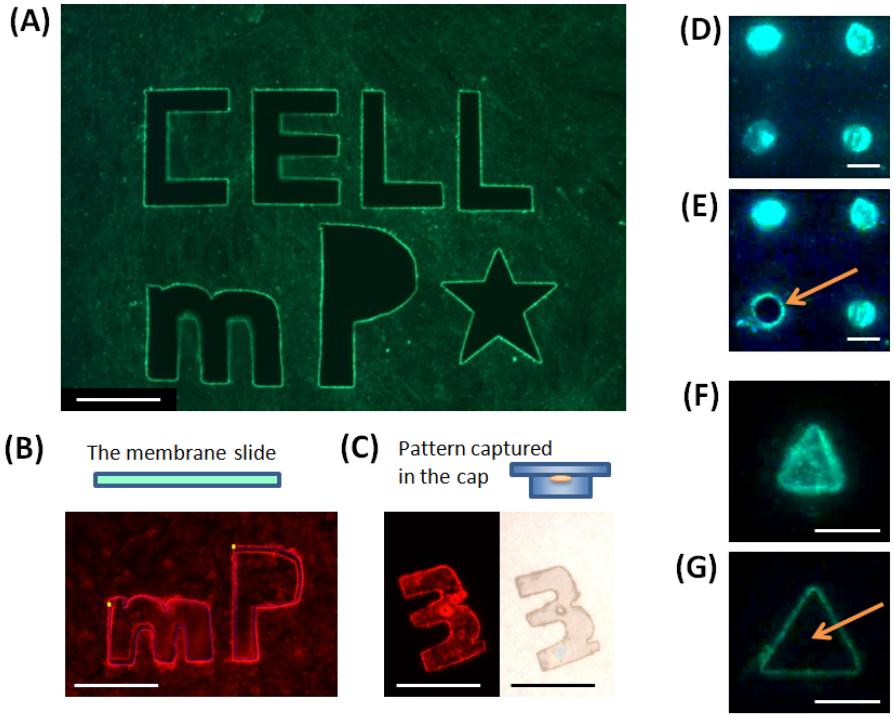


Figure 7-16 Precise cutting and catapulting. (A) Photo of patterns "CELL mP ☆" cut by the laser in Zeiss Microbeam on a polystyrene-coated PEN membrane frame slide with bovine NP cells pre-stained with CellTracker green. The photo was taken after catapult. (B) Photo of pattern "mP" cut by the laser in Zeiss Microbeam on a polystyrene-coated PEN membrane frame slide with bovine NP cells pre-stained with CellTracker red. The photo was taken before catapult. (C) The corresponding membrane with cells of the pattern "m" in (B) which was catapulted to the adhesive cap for sample collection. (D-G) Photos of HUVECs on fibronectin micropatterns on a polystyrene-coated PET membrane frame slide post-stained with Alexafluor 488 - phalloidin. (D) and (E) show cells on circle micropatterns before and after catapult repetitively. (F) and (G) show cells on a triangle pattern before and after catapult respectively with prior laser cutting. The arrows show the holes that were left behind on the membranes when the cells were catapulted to the collection caps. (Scale bar = 150 µm for A - C and scale bar = 25 µm for D - G).

7.4.7 Minimum cell number required to perform RT-qPCR

To evaluate gene expression from LCM samples, Vandewoestyne *et al.* used the Arcturus PicoPure RNA Isolation Kit, an extraction kit specifically designed for a small number of cells, and has demonstrated sufficient RNA can be extracted from as few as 10 cells for RT-qPCR analysis [326]. Now, direct cDNA synthesis with crude cell lysates is possible and Van Peer *et al.* have demonstrated this approach has good accuracy and superior sensitivity [354]. In this study, we directly lyse the cells in Cell-to-Ct lysis buffer and perform subsequent RT-qPCR without column based RNA extraction. This avoided the potential loss of RNA during extraction. Other modifications were made to adapt the use of this kit for micropatterned cells.

To assess the number of cells required for qPCR analysis, we catapulted different numbers of cells from small circle patterns of fibronectin on polystyrene-coated PEN membrane frame slide at 4 h after cell seeding. *GAPDH* and *18S rRNA* expression were detected in all samples of 5 to 40 cells and the relative levels were in good correlation with the number of catapulted cells with R^2 of 0.975 and 0.976 respectively (**Figure 7-17A** and **B**). To assess whether this method allows the detection of the expression levels of gene encoding proteins that are secreted out of the cells and may not be best assessed reliably by immunostaining in cell culture, we assessed the mRNA level of *ACAN* and *COL2A1*. These two genes can be detected in all samples (**Figure 7-17C-F**). The *ACAN* and *COL2A1* expression relative to *GAPDH* and *18S rRNA* were similar for samples of different numbers of cells, indicating that the detected relative expression level is cell number independent after normalization with the housekeeping genes *GAPDH* or *18S rRNA*.

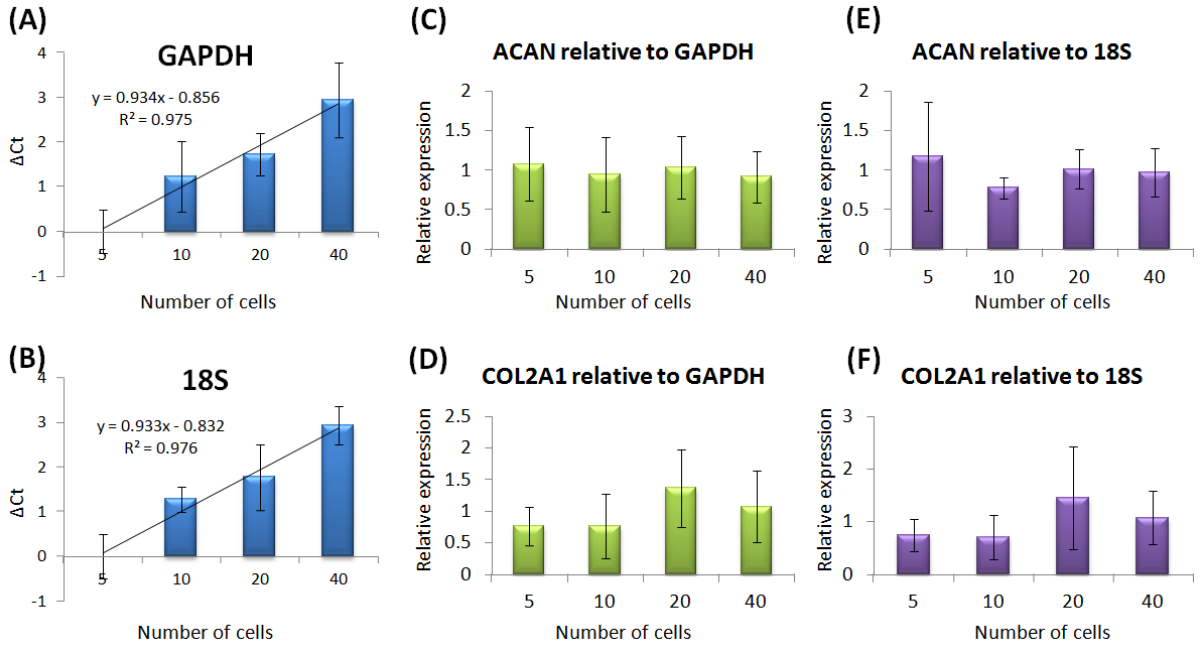


Figure 7-17 Titration of bovine NP cells. Cells were stained with CellTracker green and seeded on polystyrene-coated PEN membrane frame slides. The cells were fixed at 4 h after cell seeding. Different numbers of cells (5, 10, 20, 40) were collected using the Zeiss Microbeam by catapult. ΔCt of the house keeping genes (A) *GAPDH* and (B) *18S rRNA* relative to the Ct of the sample of 5 cells. The ΔCt defined here is (Ct of the sample of 5 cells - Ct of the sample of 5/ 10/ 20/ 40 cells). (C-F) *ACAN* and *COL2A1* expression of cells relative to *GAPDH* or *18S rRNA*. (2 batches of experiments, biological duplicates and technical duplicates; mean ± SD). *GAPDH* and *18S rRNA* expression were detected in all samples of 5 to 40 cells and the relative levels were in good correlation with the number of catapulted cells with R^2 of 0.975 and 0.976 respectively. Besides, the *ACAN* and *COL2A1* expression relative to *GAPDH* and *18S rRNA* were similar for samples of different numbers of cells, indicating that the detected relative expression level is cell number independent after normalization with the housekeeping gene *GAPDH* or *18S rRNA*.

Keays *et al.* have performed direct RT with laser captured single cells without RNA purification [355]. They used SuperScript III first-strand RT buffer containing 1% NP40 to lyse the collected cell and performed RT on the cap surface. Amplications of heavy chain IgG were detected in four out of six samples using nested PCR. In our study, we modified the protocol of a commercial kit designed for cells in 96 well plates and detected *GAPDH* and *18S rRNA* expression in all of our samples with 5 cells or more. This may suggest the adaption of the Cell-to-Ct kit to laser captured cells may provide an easier way of RT-qPCR with higher chances of successful amplification.

We further tested the RT-qPCR of smaller numbers of cells (1 cell, 3, cells and 5 cells) collected from cell micropatterns. As shown in **Table 7-9**, amplifications were detected in all reactions for *18S rRNA*, which was highly expressed in cells (reflected by the smaller Ct values compared to other genes). However, amplifications of *GAPDH*, *COL2A1* and *ACTB* were not always detected for 1 cell. This indicates the minimum number of cells required depends on the genes to be studied. A smaller number of cells was required for highly expressed genes.

Table 7-9 The Ct values and frequency of amplification detected for *GAPDH*, *COL2A1*, *ACTB*, *18S rRNA* in samples of 1 cell, 3 cells and 5 cells. The specified number of cells was catapulted into a 0.6 ml tube with 5 µl of lysis solution placed at the center of the cap. To adjust the volume of solution due to evaporation, the volume of the lysis solution remained in the cap was approximately estimated using a pipet and DEPC-treated water was added so that the total volume was 5 µl. The lysis solution with catapulted cells was transferred to a 0.2 ml tube and DNase1 treatment was performed by adding 0.5 µl of 10× DNase solution. The following RT-qPCR was performed using the Ambion Cell-to-Ct kit and the Qiagen QuantiTect SYBR Green PCR Kit. (Ct values were represented as mean ± SD for groups with more than one amplification detected; the ratio in bracket represents the frequency of amplification detected. For example, 3/4 denotes amplifications were detected in 3 out of 4 reactions.) Amplifications were detected in all reactions for *18S rRNA*, which was highly expressed in cells (reflected by the smaller Ct values compared to other genes).

	1 cell	3 cells	5 cells
GAPDH	32.93 (1/4)	31.4 ± 1.3 (3/4)	31.9 ± 1.1 (4/4)
COL2A1	/ (0/4)	32.5 ± 2.6 (4/4)	33.0 ± 1.3 (4/4)
ACTB	35.5 ± 0.8 (2/4)	32.1 ± 1.0 (4/4)	32.9 ± 1.9 (4/4)
18S rRNA	26.1 ± 2.5 (16/16)	23.1 ± 2.6 (16/16)	21.5 ± 1.7 (16/16)

7.4.8 Gene expression profile in single-cell patterns versus two-cell patterns

In **Section 7.6.1** in the Appendix of this Chapter, it was shown that it was unlikely to obtain cell micropatterns with only one cell per pattern throughout the whole pattern area as the expected number of cells per micropattern followed a distribution similar to a Poisson distribution. There was a higher chance of getting single cells when the patterns were smaller but might not be exclusive. Even for small 20 µm circles, patterns with two cells attached were observed. The use of LCM on cell micropatterns enabled the study of the gene

expression difference between single round cells versus double round cells which was difficult with ordinary RNA extraction methods which the whole area of cells were lysed to form a single sample. **Figure 7-18** shows the *ACAN* and *COL2A1* expression of single round cells and two cells from the same slide. There was no significant difference for the *COL2A1* expression between the two but the *ACAN* expression was slightly lower on patterns with 2 cells compared to patterns with single cells. Yet the difference was small and with a p-value of around 0.06. A large number of samples was required to confirm the slight difference. Nevertheless, this experiment demonstrated that different cells could be sampled from the same slide to answer different biological questions with fewer limitations associated with changes in the medium as all the cells on the same slide shared the same cell culture medium.

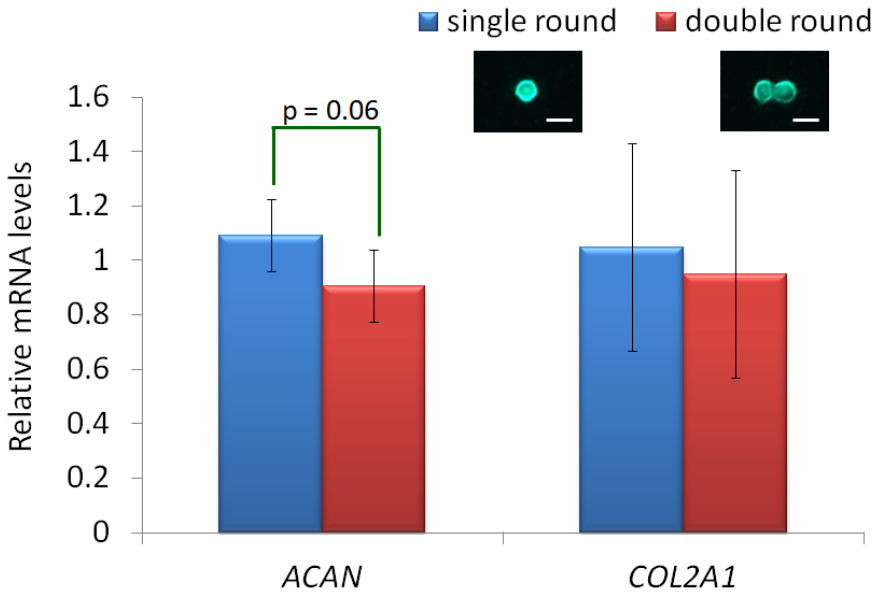


Figure 7-18 *ACAN* and *COL2A1* gene expression of single round cells and double round cells of bovine NP at 4 h after cell seeding. (Relative to *GAPDH* and the average gene expression level of both sample groups; 6 samples from 3 independent experiments; technical duplicates in qPCR; mean ± SD). The cells were stained with CellTracker green and seeded in a polystyrene-coated PEN membrane frame slide. Photos of the fluorescent cells were taken using the Zeiss MicroBeam (scale bar = 20 µm). Cells were selected using the catapult function in the MicroBeam and RT-qPCR was performed with the Cell-to-Ct kit. There was no significant difference for the *COL2A1* expression between the two but the *ACAN* expression was slightly lower on patterns with 2 cells compared to patterns with single cells (p = 0.06).

7.4.9 LCM to select different cell populations on micropatterns

To assess whether different cells can be selected from the same slide using LCM, we pre-stained cells from bovine articular cartilage (AC) and cells from bovine adipose tissue (AD) in different colors and seeded them on the same membrane slides with polystyrene coating and fibronectin micropatterns. LCM was used to select AC cells and AD cells separately into different tubes. Higher *ACAN* and *COL2A1* expression was detected for the AC cells compared to the AD cells (**Figure 7-19**), which is consistent with the literature.

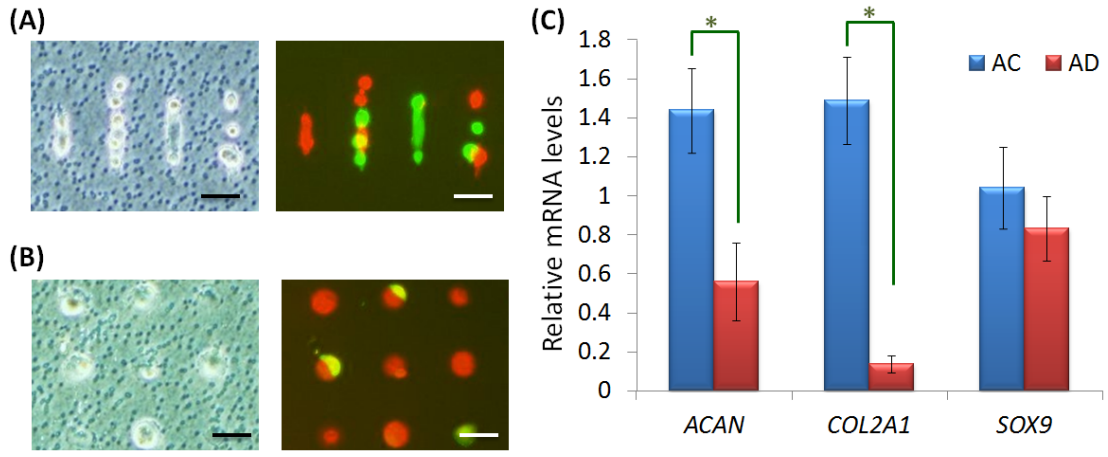


Figure 7-19 Study of two cell types from the same membrane slide. (A) Phase contrast and fluorescent photos of AC cells stained with CellTracker green and AD cells stained with Vybrant Dil (red) on rhombus patterns. (B) Phase contrast and fluorescent photos of AC cells stained with CellTracker green and AD cells stained with CellTracker red on circle patterns. Cells were seeded on fibronectin micropatterns prepared on polystyrene-coated PEN membrane frame slides and photos were taken using a widefield fluorescent microscope at 4 h after cell seeding (scale bar = 50µm). (C) *ACAN*, *COL2A1* and *SOX9* expression of AC cells and AD cells cultured on fibronectin micropatterns on PEN membrane frame slides. The membrane slides were fixed in ethanol and dried at 4 h after cell seeding. The cells of a particular type were selected using the catapult function in the MicroBeam and RT-qPCR was performed with the Cell-to-Ct kit (8 samples from 4 independent experiments; mean ± SEM; * $p < 0.05$). On average, higher *ACAN* and *COL2A1* expression was observed for AC cells than AD cells, which is consistent with the literature. This shows that the Zeiss Microbeam can be used to select cells of different types co-cultured on micropatterns on the same membrane slide.

7.5 Conclusions

In summary, modifications have been made to the protocol of the Cell-to-Ct kit to allow the study of cells cultured on micropatterns with RT-qPCR. Furthermore, we developed a method to selectively study the gene expression of cells of interests on micropatterns, which was impossible with existing methods. This method only requires simple coating of the membrane slides and a modified protocol for direct RT-qPCR for laser captured cells on micropatterns. This qPCR analysis combined with laser capture microdissection can be used to study gene expression quantitatively for the selected cells on micropatterns. This will enable the investigation of the effect of cell shape, cell spreading and cell-cell interaction at mRNA level in a particular group of selected cells. With the simplicity of the modifications required, we anticipate this can be incorporated into a variety of projects when LCM equipment is available.

7.6 Appendix

7.6.1 Relationship between cell seeding density and number of cells per micropattern

Although gene expression could be studied using the Cell-to-Ct kit, the gene expression detected was the average of the whole populations of cells on the micropatterns. There are some occasions when the study of subpopulations of cells on micropatterns is beneficial eg. studying single isolated cells or cells in contact with each other. When cells were seeded on micropatterns, more than one cell per micropattern could be observed occasionally. Thus we tested the cell micropatterning with different numbers of seeded cells with an attempt to find a cell seeding density that yields only one cell per micropattern. However, as shown in **Figure 7-20**, none of the cell seeding density gave micropatterns of one cell per pattern only throughout the whole area. The higher the cell seeding density, the more cells attached to the patterns on average and the more patterns with more than one cell meanwhile. There was a trade-off between percentage of micropatterns with single cell and percentage of occupancy of the micropatterns.

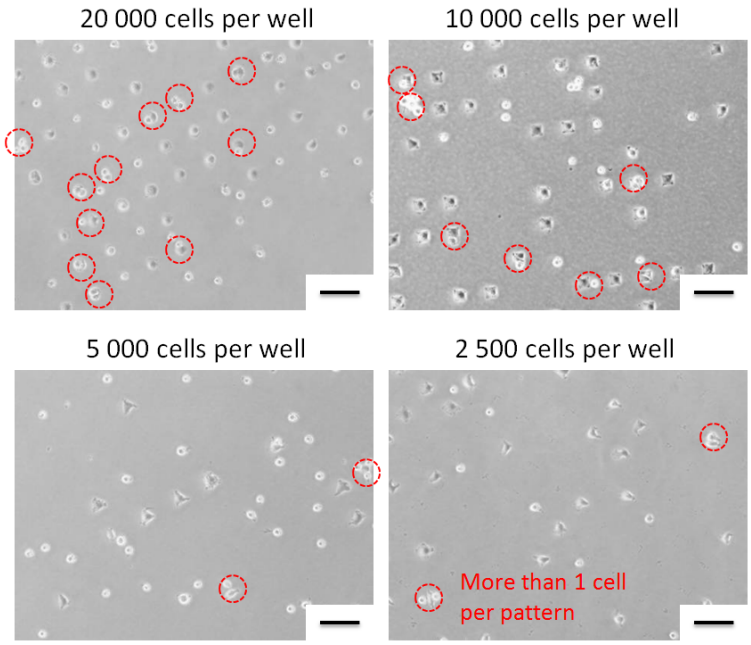


Figure 7-20 Trade off between obtaining single cells and percentage occupancy. Bovine AC cells were seeded at different cell densities (20,000 cells, 10,000 cells, 5,000 cells and 2,500 cells per well of a 12 well plates). The red broken line circles indicate the micropatterns that have more than one cell per pattern.

The number of cells per pattern is a probability function, which can be estimated by a binomial distribution model. The probability of getting exactly k successes in n trials is given by the probability mass function:

$$f(k;n,p) = \Pr(X = k) = \frac{n!}{k!(n-k)!}p^k(1-p)^{n-k} \quad (1)$$

where X is the random variable that follows the binomial distribution.

This distribution can be approximated by Poisson distribution due to the large n (>> 20) and small p (<< 0.05) [356]. For Poisson distribution, with a discrete random variable X' with parameter $\lambda > 0$ for k = 0, 1, 2, …, the probability mass function of X' is given by the following formula [357]:

$$f(k';\lambda) = \Pr(X' = k') = \frac{\lambda^k e^{-\lambda}}{k'!} \quad (2)$$

where *e* is Euler's number which is equal to 2.71828, k'! is the factorial of k' and λ is a positive real number that is equal to the expected value and also the variance of X' as shown in the relationship below:

$$\lambda = \mathrm{E}(\mathrm{X}') = \mathrm{Var}(\mathrm{X}') \quad (3)$$

Note: The symbol (') was used in the probability function of the Poisson distribution here in order to distinguish from the symbols used in Binomial distribution in this section.

Gobaa *et al.* observed distinct Poisson distributions of cells in their microwell study [358]. They tested 3 different seeding densities (5×10^4, 7.5×10^4 and 10^5 cells) and obtained λ of 0.86, 1.90 and 4.58 respectively for the number of cells per microwell. It was noted that seeding 10^5 cells resulted in a number of cells per microwell five times more than that of seeding 5×10^4 cells, which indicated the expected number of cells per microwell was not exactly proportional to the cell seeding density (as shown in **Figure 7-21** by the deviations from the trend line assuming perfect proportionality between the number of cells seeded and λ). The deviation from the perfect proportionality may be due to the events that are not taken into account in the simplified probability model, eg. the spreading of cells, the difference in time

that cells sank to micropattern surface, *etc.* Nevertheless, the λ increased with cell seeding density which indicated that we could tune the expected number of cells by changing the cell seeding density.

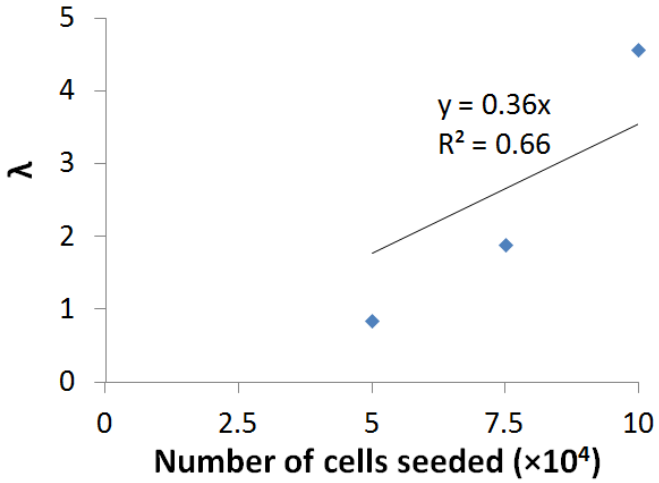


Figure 7-21 Relationship between the number of cells seeded and λ. (Plotted from values in figures in [358]). The expected number of cells per microwell was not exactly proportional to the cell seeding density as shown by the deviations from the trend line assuming perfect proportionality between the number of cells seeded and λ.

Figure 7-22 shows a plot of Poisson distribution with different λs and **Table 7-10** shows the percentage of single/ double cells and the percentage of single/ double cells over other cells. In the 5 tested values of λ, the highest percentage (37%) of single cells was obtained for λ = 1 but only 58% of micropatterns occupied by cells had one cell per pattern in such case (i.e. 42% of occupied micropatterns had more than one cell). With smaller λ, a higher percentage of single cells over other cells (88% for λ = 0.25) was obtained but only 19% of micropatterns were occupied by single cells.

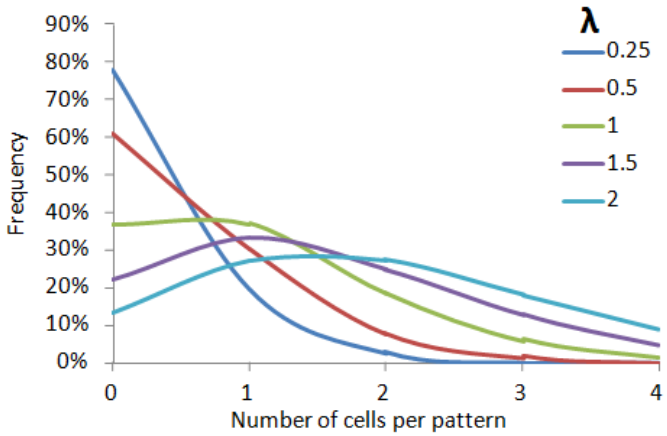


Figure 7-22 Plot of Poisson distribution with different λs.

Table 7-10 Poisson distribution of numbers of cells per micropattern for different values of λ.

λ	0.25	0.5	1	1.5	2
% of single cells	19%	30%	37%	33%	27%
% of single cells over other cells	88%	77%	58%	43%	31%
% of double cells	2%	8%	18%	25%	27%
% of double cells over other cells	11%	19%	29%	32%	31%

Taken together, these results show that it can be difficult to obtain micropatterns of only one cell per pattern with a high percentage of pattern occupancy. In the method described in this study, the use of LCM in cell micropatterns enables the study of patterns containing one cell versus two cells from the same membrane slide as described in **Section 7.4.8** of the Results and Discussion Section.

Chapter 8 Overall Conclusion and Perspective

In my study, different aspects of IVD researches were involved and this thesis focuses the optimization and development of methods along the way which can accelerate scientific discovery, reduce the sacrifice of animals and enable more effective use of funding.

Some of the aspects studied are summarized in the following:

8.1 Optimization of NP cell isolation from tissues

In summary, the cell yield from bovine NP tissue can be increased by using a high collagenase concentration, long digestion time or with pronase pre-treatment in general. Depending on different purposes, the procedures should be fine tuned with a good understanding of the various factors involved in the isolation. For cell culturing, we can obtain a reasonably good yield with a wide range of protocols. In other words, either using a higher collagenase concentration for shorter time or a lower collagenase concentration for longer time may achieve a similar yield. The use of pronase prior to collagenase treatment may facilitate the isolation but not absolutely necessary for bovine NP tissue. For RNA extraction, shorter isolation duration is preferable. And for flow cytometry characterization, cautions are required for cells with pronase treatment for reliable interpretation. Based on this information, researchers can devise their own cell isolation protocols for their applications based on a clear rationale and enhance the efficiency and reliability of the associated experiments. With a better understanding of the isolation procedures, the cell yield can be increased without sacrifice of the quality of cells obtained.

8.2 RNA extraction from IVD tissues

RT-qPCR gene expression analysis of cells in bovine IVD tissues was made possible without the requirement of cell isolation before RNA extraction. This method does not require a

specialized homogenizer and cryosections can be prepared simultaneously. The introduction of second phase separation in the TRIzol isolation protocol also enables RNA to be extracted from tissue with high proteoglycan content with low cellularity such as bovine or human NP tissue. The protocol avoids the futile attempts of RNA extraction from bovine NP tissue which is particularly difficult.

8.3 Concentration correction for RNA contaminated with TRIzol

We developed a computational method based on subtraction to correct the concentrations of RNA contaminated with TRIzol. The accuracy of the RNA concentration with phenol contamination was improved after using the correction. The findings that low level of contamination (< 0.1% TRIzol) did not show detectable inhibition in the reaction systems used in this study also suggest RNA with a low level of contamination may provide meaningful results if used appropriately.

8.4 Isolation and culturing of MSCs for chondrogenic / discogenic studies

MSCs have been implicated in tissue engineering and regenerative medicine for disc degeneration therapy in the future. Different aspects of MSCs were investigated for the set up of study for MSC differentiation into NP-like cells through signaling pathway inhibition. In our group, it is easier to obtain MSCs with chondrogenic potential from human compared to from Lewis rat. There may be possibility that the MSCs from different rat strains differs in properties. Unlike MSCs from other sources, MSCs from immunodeficient NOD/SCID mice did not display CD44 surface marker expression. Though hypoxia was suggested to enhance chondrogenic phenotype for human MSCs cultured in alginate beads or on 3D materials, this enhancement was not observed for human MSCs cultured in pellets. Exogenous TGF- β1 is required in pellet formation in mouse C3H10T1/2 cells but not in human bone marrow MSCs, suggesting the difference in requirement of culture conditions for MSCs from different sources.

8.5 Study of micropatterning methods and imaging

Micropatterning of bovine NP cells has been optimized in this study. Preparation of micropatterns compatible with high resolution microscopy was also investigated. We developed two prototypes of cell culture containers for micropattern study using high resolution microscopy. After testing with different commercially available materials, we successfully obtained micropatterns on untreated culture dishes from Ibidi® with pluronic passivation. High resolution images and 3D models can be obtained using confocal microscopy for the cell micropatterns.

8.6 Methods for gene expression study at mRNA levels

The use of Cell-to-Ct kit has been explored and adapted for the micropatterned cells. With modified procedures, it has been shown that RT-qPCR can be successfully performed as demonstrated in the gene expression of the NP cells on 20 μm circles compared to 20 μm strips. It has been demonstrated that cell micropatterns can be formed on PEN membrane frame slides with polystyrene coating and cells of interest can be selected precisely using LCM.

8.7 Significance

Chapter	*Significance*
Chapter 2 (NP cell isolation)	A guide to NP cell isolation was provided based on theoretical analysis and experimental study. This may increase the cell yield obtained which reduces the number of animals that need to be sacrificed. It can lead to better utilization of clinical samples, allowing more studies to be performed with limited samples.
Chapter 3 (RNA isolation from NP tissue)	The isolation of RNA from bovine NP tissue was made possible with an extra phase separation step together with other modifications to the TRIzol extraction protocol. This allows the study of gene expression of cells in NP tissue directly, assisting the understanding of the changes that may be introduced during the cell isolation process.

Chapter	*Significance*
Chapter 4 (RNA concentration correction)	A mathematical model was developed to correct the concentrations estimated from UV spectrometry for samples with low levels of TRIzol. With the correction, the concentration of RNA of low concentration such as from NP tissue can be estimated more accurately. The method can also be applied to other RNA samples with phenol contamination.
Chapter 5 (Isolation and culturing of MSCs for chondrogenic/ discogenic studies)	Different aspects of MSCs were studied and provided information in the setting up and understanding of the experiments. This avoids futile experiments which were due to lack of associated information in the field and hence enables more effective experimental design to answer specific biological questions.
Chapter 6 (Optimization and development of cell micropattern preparation)	Various aspects of micropatterning IVD cells were studied and the maintenance of roughly round shape of cells was achieved through the use of small circular micropatterns. This allows studies about cell shape without the bulk diffusion issues that are present in pellet or alginate bead cultures. It was also first reported about the high resolution imaging of the micropatterned cells that the cells are not being compressed by the weights of cover slips. This enables the spatial arrangement of cellular structures to be examined in more details.
Chapter 7 (Quantitative gene expression analysis of micropatterned cells)	A commercial kit without the need of RNA isolation was adapted to micropatterned cells. This facilitates the study of gene expression using RT-qPCR for a relatively small number of micropatterned cells, increasing the practicality and feasibility of such studies. The novel method to produce cell micropatterns compatible with laser capture microdissection (LCM) allows the selection of cells of interest in micropatterns for RT-qPCR. This permits the setting of more precise questions about different cells cultured on the same micropattern surface.

In this thesis, different methods related to IVD research were developed and optimized. We have developed methods in cell isolation, RNA extraction and RNA concentration correction. Different aspects of MSC isolation, characterization and culturing were also studied. Besides, micropatterning was optimized and the novel method of performing qPCR with selected cells from the micropatterns with the use of laser capture microdissection was developed. With improved methods together with a better understanding of the underlying rationale, researchers can save time and cost in their experiments and reduce experiment failure rate. This will help to accelerate researches. New methods also enable studies which were not feasible in the past.

References

[1] Clouet J, Vinatier C, Merceron C, Pot-Vaucel M, Hamel O, Weiss P, et al. The intervertebral disc: from pathophysiology to tissue engineering. Joint, bone, spine : revue du rhumatisme. 2009;76:614-8.

[2] Juniper M, Le TK, Mladsi D. The epidemiology, economic burden, and pharmacological treatment of chronic low back pain in France, Germany, Italy, Spain and the UK: a literature-based review. Expert opinion on pharmacotherapy. 2009;10:2581-92.

[3] O'Halloran DM, Pandit AS. Tissue-engineering approach to regenerating the intervertebral disc. Tissue engineering. 2007;13:1927-54.

[4] Maniadakis N, Gray A. The economic burden of back pain in the UK. Pain. 2000;84:95-103.

[5] Richardson SM, Hoyland JA, Mobasheri R, Csaki C, Shakibaei M, Mobasheri A. Mesenchymal stem cells in regenerative medicine: Opportunities and challenges for articular cartilage and intervertebral disc tissue engineering. Journal of cellular physiology. 2010;222:23-32.

[6] Katz JN. Lumbar disc disorders and low-back pain: socioeconomic factors and consequences. The Journal of bone and joint surgery American volume. 2006;88 Suppl 2:21-4.

[7] Cheung KM, Karppinen J, Chan D, Ho DW, Song YQ, Sham P, et al. Prevalence and pattern of lumbar magnetic resonance imaging changes in a population study of one thousand forty-three individuals. Spine. 2009;34:934-40.

[8] Kjaer P, Leboeuf-Yde C, Korsholm L, Sorensen JS, Bendix T. Magnetic resonance imaging and low back pain in adults: a diagnostic imaging study of 40-year-old men and women. Spine. 2005;30:1173-80.

[9] Samartzis D, Karppinen J, Mok F, Fong DY, Luk KD, Cheung KM. A population-based study of juvenile disc degeneration and its association with overweight and obesity, low back pain, and diminished functional status. The Journal of bone and joint surgery American volume. 2011;93:662-70.

[10] Raj PP. Intervertebral disc: anatomy-physiology-pathophysiology-treatment. Pain practice : the official journal of World Institute of Pain. 2008;8:18-44.

[11] McCann MR, Tamplin OJ, Rossant J, Seguin CA. Tracing notochord-derived cells using a Noto-cre mouse: implications for intervertebral disc development. Dis Model Mech. 2012;5:73-82.

[12] Marchand F, Ahmed AM. Investigation of the laminate structure of lumbar disc anulus fibrosus. Spine. 1990;15:402-10.

[13] Yu J, Winlove PC, Roberts S, Urban JP. Elastic fibre organization in the intervertebral discs of the bovine tail. Journal of anatomy. 2002;201:465-75.

[14] Roberts S, Menage J, Urban JPG. Biochemical and Structural-Properties of the Cartilage Endplate and Its Relation to the Intervertebral-Disk. Spine. 1989;14:166-74.

[15] Donohue PJ, Jahnke MR, Blaha JD, Caterson B. Characterization of link protein(s) from human intervertebral-disc tissues. The Biochemical journal. 1988;251:739-47.

[16] Errington RJ, Puustjarvi K, White IRF, Roberts S, Urban JPG. Characterisation of cytoplasm-filled processes in cells of the intervertebral disc. Journal of anatomy. 1998;192:369-78.

[17] Bruehlmann SB, Rattner JB, Matyas JR, Duncan NA. Regional variations in the cellular matrix of the annulus fibrosus of the intervertebral disc. Journal of anatomy. 2002;201:159-71.

[18] Roberts S. Disc morphology in health and disease. Biochem Soc Trans. 2002;30:864-9.

[19] Boos N, Weissbach S, Rohrbach H, Weiler C, Spratt KF, Nerlich AG. Classification of age-related changes in lumbar intervertebral discs: 2002 Volvo Award in basic science. Spine. 2002;27:2631-44.

[20] Aguiar DJ, Johnson SL, Oegema TR. Notochordal cells interact with nucleus pulposus cells: regulation of proteoglycan synthesis. Experimental cell research. 1999;246:129-37.

[21] Hunter CJ, Matyas JR, Duncan NA. The notochordal cell in the nucleus pulposus: A review in the context of tissue engineering. Tissue engineering. 2003;9:667-77.

[22] Pattappa G, Li Z, Peroglio M, Wismer N, Alini M, Grad S. Diversity of intervertebral disc cells: phenotype and function. Journal of anatomy. 2012;221:480-96.

[23] Beddington RS, Robertson EJ. Axis development and early asymmetry in mammals. Cell. 1999;96:195-209.

[24] Purves D, Augustine GJ, Fitzpatrick D, Katz LC, LaMantia A-S, McNamara JO, et al. Neuroscience. Sunderland, Mass.: Sunderland, Mass. : Sinauer Associates; 2001.

[25] Yamanaka Y, Tamplin OJ, Beckers A, Gossler A, Rossant J. Live imaging and genetic analysis of mouse notochord formation reveals regional morphogenetic mechanisms. Developmental cell. 2007;13:884-96.

[26] Urban JPG, Roberts S, Ralphs JR. The nucleus of the intervertebral disc from development to degeneration. Am Zool. 2000;40:53-61.

[27] Stemple DL. Structure and function of the notochord: an essential organ for chordate development. Development. 2005;132:2503-12.

[28] Eloy-Trinquet S, Nicolas JF. Clonal separation and regionalisation during formation of the medial and lateral myotomes in the mouse embryo. Development. 2002;129:111-22.

[29] Risbud MV, Schaer TP, Shapiro IM. Toward an understanding of the role of notochordal cells in the adult intervertebral disc: from discord to accord. Developmental dynamics : an official publication of the American Association of Anatomists. 2010;239:2141-8.

[30] Zhao CQ, Wang LM, Jiang LS, Dai LY. The cell biology of intervertebral disc aging and degeneration. Ageing Research Reviews. 2007;6:247-61.

[31] Colombini A, Lombardi G, Corsi MM, Banfi G. Pathophysiology of the human intervertebral disc. The international journal of biochemistry & cell biology. 2008;40:837-42.

[32] Hardingham TE, Fosang AJ. Proteoglycans: many forms and many functions. FASEB journal : official publication of the Federation of American Societies for Experimental Biology. 1992;6:861-70.

[33] Bowles RD, Gebhard HH, Hartl R, Bonassar LJ. Tissue-engineered intervertebral discs produce new matrix, maintain disc height, and restore biomechanical function to the rodent spine. Proceedings of the National Academy of Sciences of the United States of America. 2011;108:13106-11.

[34] Bron JL, Vonk LA, Smit TH, Koenderink GH. Engineering alginate for intervertebral disc repair. Journal of the mechanical behavior of biomedical materials. 2011;4:1196-205.

[35] Ruan D, He Q, Ding Y, Hou L, Li J, Luk KD. Intervertebral disc transplantation in the treatment of degenerative spine disease: a preliminary study. Lancet. 2007;369:993-9.

[36] Taksali S, Grauer JN, Vaccaro AR. Material considerations for intervertebral disc replacement implants. The spine journal : official journal of the North American Spine Society. 2004;4:231S-8S.

[37] Kandel R, Roberts S, Urban JP. Tissue engineering and the intervertebral disc: the challenges. European spine journal : official publication of the European Spine Society, the European Spinal Deformity Society, and the European Section of the Cervical Spine Research Society. 2008;17 Suppl 4:480-91.

[38] Nerurkar NL, Elliott DM, Mauck RL. Mechanical design criteria for intervertebral disc tissue engineering. Journal of biomechanics. 2010;43:1017-30.

[39] Richardson SM, Mobasheri A, Freemont AJ, Hoyland JA. Intervertebral disc biology, degeneration and novel tissue engineering and regenerative medicine therapies. Histology and histopathology. 2007;22:1033-41.

[40] Langer R, Vacanti JP. Tissue engineering. Science. 1993;260:920-6.

[41] Mason C, Dunnill P. A brief definition of regenerative medicine. Regenerative medicine. 2008;3:1-5.

[42] Alini M, Eisenstein SM, Ito K, Little C, Kettler AA, Masuda K, et al. Are animal models useful for studying human disc disorders/degeneration? European Spine Journal. 2008;17:2-19.

[43] Darling EM, Pritchett PE, Evans BA, Superfine R, Zauscher S, Guilak F. Mechanical Properties and Gene Expression of Chondrocytes on Micropatterned Substrates Following Dedifferentiation in Monolayer. Cellular and molecular bioengineering. 2009;2:395-404.

[44] Gan JC, Ducheyne P, Vresilovic EJ, Shapiro IM. Intervertebral disc tissue engineering II: Cultures of nucleus pulposus cells. Clinical orthopaedics and related research. 2003:315-24.

[45] Illien-Junger S, Gantenbein-Ritter B, Grad S, Lezuo P, Ferguson SJ, Alini M, et al. The combined effects of limited nutrition and high-frequency loading on intervertebral discs with endplates. Spine. 2010;35:1744-52.

[46] Wang DL, Jiang SD, Dai LY. Biologic response of the intervertebral disc to static and dynamic compression in vitro. Spine. 2007;32:2521-8.

[47] Dai J, Wang H, Liu G, Xu Z, Li F, Fang H. Dynamic compression and co-culture with nucleus pulposus cells promotes proliferation and differentiation of adipose-derived mesenchymal stem cells. Journal of biomechanics. 2014;47:966-72.

[48] Feng G, Li L, Hong Y, Liu H, Song Y, Pei F, et al. Hypoxia promotes nucleus pulposus phenotype in 3D scaffolds in vitro and in vivo. Journal of neurosurgery Spine. 2014;21:303-9.

[49] Foss BL, Maxwell TW, Deng Y. Chondroprotective supplementation promotes the mechanical properties of injectable scaffold for human nucleus pulposus tissue engineering. Journal of the mechanical behavior of biomedical materials. 2014;29:56-67.

[50] Gupta MS, Nicoll SB. Functional nucleus pulposus-like matrix assembly by human mesenchymal stromal cells is directed by macromer concentration in photocrosslinked carboxymethylcellulose hydrogels. Cell and tissue research. 2014.

[51] Kim HY, Kim HN, Lee SJ, Song JE, Kwon SY, Chung JW, et al. Effect of pore sizes of PLGA scaffolds on mechanical properties and cell behaviour for nucleus pulposus regeneration in vivo. Journal of tissue engineering and regenerative medicine. 2014.

[52] Naqvi SM, Buckley CT. Differential Response of Encapsulated Nucleus Pulposus Cells and Bone Marrow Derived MSCs in Isolation and Co-culture in Alginate and Chitosan Hydrogels. Tissue engineering Part A. 2014.

[53] Tam V, Rogers I, Chan D, Leung VY, Cheung KM. A comparison of intravenous and intradiscal delivery of multipotential stem cells on the healing of injured intervertebral disk. Journal of orthopaedic research : official publication of the Orthopaedic Research Society. 2014;32:819-25.

[54] Bridgen DT, Gilchrist CL, Richardson WJ, Isaacs RE, Brown CR, Yang KL, et al. Integrin-mediated interactions with extracellular matrix proteins for nucleus pulposus cells of the human intervertebral disc. Journal of orthopaedic research : official publication of the Orthopaedic Research Society. 2013;31:1661-7.

[55] Chen J, Lee EJ, Jing L, Christoforou N, Leong KW, Setton LA. Differentiation of mouse induced pluripotent stem cells (iPSCs) into nucleus pulposus-like cells in vitro. PloS one. 2013;8:e75548.

[56] Feng G, Li L, Liu H, Song Y, Huang F, Tu C, et al. Hypoxia differentially regulates human nucleus pulposus and annulus fibrosus cell extracellular matrix production in 3D scaffolds. Osteoarthritis and cartilage / OARS, Osteoarthritis Research Society. 2013;21:582-8.

[57] Ning B, Liu H, Gong W, Jiang J, Hu Y, Yang SY. Biological characteristics of adult degenerative nucleus pulposus cells in a three-dimensional microcarrier stirring culture system. Journal of orthopaedic research : official publication of the Orthopaedic Research Society. 2013;31:858-63.

[58] Sakai D, Nakamura Y, Nakai T, Mishima T, Kato S, Grad S, et al. Exhaustion of nucleus pulposus progenitor cells with ageing and degeneration of the intervertebral disc. Nature communications. 2012;3:1264.

[59] Tang X, Jing L, Chen J. Changes in the molecular phenotype of nucleus pulposus cells with intervertebral disc aging. PloS one. 2012;7:e52020.

[60] Minogue BM, Richardson SM, Zeef LA, Freemont AJ, Hoyland JA. Characterization of the human nucleus pulposus cell phenotype and evaluation of novel marker gene expression to define adult stem cell differentiation. Arthritis and rheumatism. 2010;62:3695-705.

[61] Minogue BM, Richardson SM, Zeef LA, Freemont AJ, Hoyland JA. Transcriptional profiling of bovine intervertebral disc cells: implications for identification of normal and degenerate human intervertebral disc cell phenotypes. Arthritis research & therapy. 2010;12:R22.

[62] Fujita N, Miyamoto T, Imai JI, Hosogane N, Suzuki T, Yagi M, et al. CD24 is expressed specifically in the nucleus pulposus of intervertebral discs. Biochemical and biophysical research communications. 2005;338:1890-6.

[63] Stimler NP. High-performance liquid chromatographic quantitation of collagen biosynthesis in explant cultures. Analytical biochemistry. 1984;142:103-8.

[64] Levine RS. A nanogram method for hydroxyproline. Mikrochimica acta. 1973:797-800.

[65] Jamall IS, Finelli VN, Que Hee SS. A simple method to determine nanogram levels of 4-hydroxyproline in biological tissues. Analytical biochemistry. 1981;112:70-5.

[66] Lareu RR, Zeugolis DI, Abu-Rub M, Pandit A, Raghunath M. Essential modification of the Sircol Collagen Assay for the accurate quantification of collagen content in complex protein solutions. Acta biomaterialia. 2010;6:3146-51.

[67] Barbosa I, Garcia S, Barbier-Chassefiere V, Caruelle JP, Martelly I, Papy-Garcia D. Improved and simple micro assay for sulfated glycosaminoglycans quantification in

biological extracts and its use in skin and muscle tissue studies. Glycobiology. 2003;13:647-53.

[68] Renart J, Reiser J, Stark GR. Transfer of proteins from gels to diazobenzyloxymethyl-paper and detection with antisera: a method for studying antibody specificity and antigen structure. Proceedings of the National Academy of Sciences of the United States of America. 1979;76:3116-20.

[69] Towbin H, Staehelin T, Gordon J. Electrophoretic transfer of proteins from polyacrylamide gels to nitrocellulose sheets: procedure and some applications. 1979. Biotechnology. 1979;24:145-9.

[70] Boenisch T, Farmild AJ, Stead RH, Key M, Welcher R, Harvey R, et al. Immunochemical Staining Methods Handbook. Third Edition ed2001.

[71] Taylor CR, Rudbeck L, Sjorup AH. Immunohistochemical Staining Methods Education Guide. Sixth Edition ed2013.

[72] Hnasko R, Lin A, McGarvey JA, Stanker LH. A rapid method to improve protein detection by indirect ELISA. Biochemical and biophysical research communications. 2011;410:726-31.

[73] Freeman WM, Walker SJ, Vrana KE. Quantitative RT-PCR: pitfalls and potential. BioTechniques. 1999;26:112-22, 24-5.

[74] Schmittgen TD, Zakrajsek BA, Mills AG, Gorn V, Singer MJ, Reed MW. Quantitative reverse transcription-polymerase chain reaction to study mRNA decay: comparison of endpoint and real-time methods. Analytical biochemistry. 2000;285:194-204.

[75] Ziegler CA. Technology and the Process of Scientific Discovery - the Case of Cosmic-Rays. Technol Cult. 1989;30:939-63.

[76] Gershon D. Technology: pushing the boundaries of scientific discovery. Nat Med. 2003;9:97-.

[77] Yuan M, Yeung CW, Li YY, Diao H, Cheung KM, Chan D, et al. Effects of nucleus pulposus cell-derived acellular matrix on the differentiation of mesenchymal stem cells. Biomaterials. 2013;34:3948-61.

[78] Hunter CJ, Matyas JR, Duncan NA. Cytomorphology of notochordal and chondrocytic cells from the nucleus pulposus: a species comparison. Journal of anatomy. 2004;205:357-62.

[79] Alini M, Eisenstein SM, Ito K, Little C, Kettler AA, Masuda K, et al. Are animal models useful for studying human disc disorders/degeneration? European spine journal : official publication of the European Spine Society, the European Spinal Deformity Society, and the European Section of the Cervical Spine Research Society. 2008;17:2-19.

[80] Oshima H, Ishihara H, Urban JP, Tsuji H. The use of coccygeal discs to study intervertebral disc metabolism. Journal of orthopaedic research : official publication of the Orthopaedic Research Society. 1993;11:332-8.

[81] Neufeld JH, Machado T, Margolin L. Variables affecting disc size in the lumbar spine of rabbits: anesthesia, paralysis, and disc injury. Journal of orthopaedic research : official publication of the Orthopaedic Research Society. 1991;9:104-12.

[82] Stokes IA, Aronsson DD, Spence H, Iatridis JC. Mechanical modulation of intervertebral disc thickness in growing rat tails. Journal of spinal disorders. 1998;11:261-5.

[83] Gilchrist CL, Darling EM, Chen J, Setton LA. Extracellular matrix ligand and stiffness modulate immature nucleus pulposus cell-cell interactions. PloS one. 2011;6:e27170.

[84] Kakutani K, Nishida K, Uno K, Takada T, Shimomura T, Maeno K, et al. Prolonged down regulation of specific gene expression in nucleus pulposus cell mediated by RNA interference in vitro. Journal of orthopaedic research : official publication of the Orthopaedic Research Society. 2006;24:1271-8.

[85] Yang SH, Lin CC, Hu MH, Shih TT, Sun YH, Lin FH. Influence of age-related degeneration on regenerative potential of human nucleus pulposus cells. Journal of orthopaedic research : official publication of the Orthopaedic Research Society. 2010;28:379-83.

[86] Lee JTY, Cheung KMC, Leung VYL. Systematic Study of Cell Isolation from Bovine Nucleus Pulposus: Improving Cell Yield and Experiment Reliability. Journal of orthopaedic research : official publication of the Orthopaedic Research Society. 2015.

[87] Gilbertson L, Ahn SH, Teng PN, Studer RK, Niyibizi C, Kang JD. The effects of recombinant human bone morphogenetic protein-2, recombinant human bone morphogenetic protein-12, and adenoviral bone morphogenetic protein-12 on matrix synthesis in human annulus fibrosis and nucleus pulposus cells. The spine journal : official journal of the North American Spine Society. 2008;8:449-56.

[88] Risbud MV, Guttapalli A, Stokes DG, Hawkins D, Danielson KG, Schaer TP, et al. Nucleus pulposus cells express HIF-1 alpha under normoxic culture conditions: a metabolic adaptation to the intervertebral disc microenvironment. Journal of cellular biochemistry. 2006;98:152-9.

[89] Gantenbein-Ritter B, Chan SC. The evolutionary importance of cell ratio between notochordal and nucleus pulposus cells: an experimental 3-D co-culture study. European spine journal : official publication of the European Spine Society, the European Spinal Deformity Society, and the European Section of the Cervical Spine Research Society. 2012;21 Suppl 6:S819-25.

[90] Gantenbein-Ritter B, Benneker LM, Alini M, Grad S. Differential response of human bone marrow stromal cells to either TGF-beta(1) or rhGDF-5. European Spine Journal. 2011;20:962-71.

[91] Arana CJ, Diamandis EP, Kandel RA. Cartilage tissue enhances proteoglycan retention by nucleus pulposus cells in vitro. Arthritis and rheumatism. 2010;62:3395-403.

[92] Gilson A, Dreger M, Urban JP. Differential expression level of cytokeratin 8 in cells of the bovine nucleus pulposus complicates the search for specific intervertebral disc cell markers. Arthritis research & therapy. 2010;12:R24.

[93] Halloran DO, Grad S, Stoddart M, Dockery P, Alini M, Pandit AS. An injectable cross-linked scaffold for nucleus pulposus regeneration. Biomaterials. 2008;29:438-47.

[94] Jones P, Gardner L, Menage J, Williams GT, Roberts S. Intervertebral disc cells as competent phagocytes in vitro: implications for cell death in disc degeneration. Arthritis research & therapy. 2008;10.

[95] Korecki CL, Kuo CK, Tuan RS, Iatridis JC. Intervertebral disc cell response to dynamic compression is age and frequency dependent. Journal of orthopaedic research : official publication of the Orthopaedic Research Society. 2009;27:800-6.

[96] Zeiter S, der Werf M, Ito K. The fate of bovine bone marrow stromal cells in hydrogels: a comparison to nucleus pulposus cells and articular chondrocytes. Journal of tissue engineering and regenerative medicine. 2009;3:310-20.

[97] Watanabe T, Sakai D, Yamamoto Y, Iwashina T, Serigano K, Tamura F, et al. Human Nucleus Pulposus Cells Significantly Enhanced Biological Properties in a Coculture System with Direct Cell-to-Cell Contact with Autologous Mesenchymal Stem Cells. Journal of Orthopaedic Research. 2010;28:623-30.

[98] Purmessur D, Freemont AJ, Hoyland JA. Expression and regulation of neurotrophins in the nondegenerate and degenerate human intervertebral disc. Arthritis research & therapy. 2008;10:R99.

[99] Studer RK, Aboka AM, Gilbertson LG, Georgescu H, Sowa G, Vo N, et al. p38 MAPK inhibition in nucleus pulposus cells: a potential target for treating intervertebral disc degeneration. Spine. 2007;32:2827-33.

[100] Le Maitre CL, Freemont AJ, Hoyland JA. The role of interleukin-1 in the pathogenesis of human intervertebral disc degeneration. Arthritis research & therapy. 2005;7:R732-45.

[101] Fernando HN, Czamanski J, Yuan TY, Gu WY, Salahadin A, Huang CYC. Mechanical Loading Affects the Energy Metabolism of Intervertebral Disc Cells. Journal of Orthopaedic Research. 2011;29:1634-41.

[102] Guehring T, Wilde G, Sumner M, Grunhagen T, Karney GB, Tirlapur UK, et al. Notochordal intervertebral disc cells: sensitivity to nutrient deprivation. Arthritis and rheumatism. 2009;60:1026-34.

[103] Cheng YH, Yang SH, Yang KC, Chen MP, Lin FH. The effects of ferulic acid on nucleus pulposus cells under hydrogen peroxide-induced oxidative stress. Process Biochem. 2011;46:1670-7.

[104] Yuan M, Leong KW, Chan BP. Three-dimensional culture of rabbit nucleus pulposus cells in collagen microspheres. The spine journal : official journal of the North American Spine Society. 2011;11:947-60.

[105] Su WY, Chen YC, Lin FH. Injectable oxidized hyaluronic acid/adipic acid dihydrazide hydrogel for nucleus pulposus regeneration. Acta biomaterialia. 2010;6:3044-55.

[106] Hiyama A, Sakai D, Arai F, Nakajima D, Yokoyama K, Mochida J. Effects of a glycogen synthase kinase-3beta inhibitor (LiCl) on c-myc protein in intervertebral disc cells. Journal of cellular biochemistry. 2011;112:2974-86.

[107] Hiyama A, Sakai D, Risbud MV, Tanaka M, Arai F, Abe K, et al. Enhancement of intervertebral disc cell senescence by WNT/beta-catenin signaling-induced matrix metalloproteinase expression. Arthritis and rheumatism. 2010;62:3036-47.

[108] Gilbert HT, Hoyland JA, Millward-Sadler SJ. The response of human anulus fibrosus cells to cyclic tensile strain is frequency-dependent and altered with disc degeneration. Arthritis and rheumatism. 2010;62:3385-94.

[109] Wan Y, Feng G, Shen FH, Balian G, Laurencin CT, Li X. Novel biodegradable poly(1,8-octanediol malate) for annulus fibrosus regeneration. Macromolecular bioscience. 2007;7:1217-24.

[110] Demers CN, Antoniou J, Mwale F. Value and limitations of using the bovine tail as a model for the human lumbar spine. Spine. 2004;29:2793-9.

[111] Oshima H, Ishihara H, Urban JPG, Tsuji H. The Use of Coccygeal Disks to Study Intervertebral Disc Metabolism. J Orthop Res. 1993;11:332-8.

[112] Chomczynski P, Mackey K. Substitution of chloroform by bromo-chloropropane in the single-step method of RNA isolation. Analytical biochemistry. 1995;225:163-4.

[113] Minogue BM, Richardson SM, Zeef LAH, Freemont AJ, Hoyland JA. Transcriptional profiling of bovine intervertebral disc cells: implications for identification of normal and degenerate human intervertebral disc cell phenotypes. Arthritis Res Ther. 2010;12.

[114] Hermann PM, Lukowiak K, Wildering WC, Bulloch AG. Pronase acutely modifies high voltage-activated calcium currents and cell properties of Lymnaea neurons. The European journal of neuroscience. 1997;9:2624-33.

[115] Lee GM, Poole CA, Kelley SS, Chang J, Caterson B. Isolated chondrons: a viable alternative for studies of chondrocyte metabolism in vitro. Osteoarthritis and cartilage / OARS, Osteoarthritis Research Society. 1997;5:261-74.

[116] Ikejima K, Enomoto N, Seabra V, Ikejima A, Brenner DA, Thurman RG. Pronase destroys the lipopolysaccharide receptor CD14 on Kupffer cells. The American journal of physiology. 1999;276:G591-8.

[117] Lobo PI, Spencer CE, Stevenson WC, McCullough C, Pruett TL. The use of pronase-digested human leukocytes to improve specificity of the flow cytometric crossmatch.

Transplant international : official journal of the European Society for Organ Transplantation. 1995;8:472-80.

[118] Lee JTY, Cheung KMC, Leung VYL. Correction for concentration overestimation of nucleic acids with phenol. Analytical biochemistry. 2014;465:179-86.

[119] Sharova LV, Sharov AA, Nedorezov T, Piao Y, Shaik N, Ko MSH. Database for mRNA Half-Life of 19 977 Genes Obtained by DNA Microarray Analysis of Pluripotent and Differentiating Mouse Embryonic Stem Cells. DNA Res. 2009;16:45-58.

[120] Hermann PM, Lukowiak K, Wildering WC, Bulloch AGM. Pronase acutely modifies high voltage-activated calcium currents and cell properties of Lymnaea neurons. Eur J Neurosci. 1997;9:2624-33.

[121] Lee GM, Poole CA, Kelley SS, Chang J, Caterson B. Isolated chondrons: A viable alternative for studies of chondrocyte metabolism in vitro. Osteoarthr Cartilage. 1997;5:261-74.

[122] Ikejima K, Enomoto N, Seabra V, Ikejima A, Brenner DA, Thurman RG. Pronase destroys the lipopolysaccharide receptor CD14 on Kupffer cells. Am J Physiol-Gastr L. 1999;276:G591-G8.

[123] Lobo PI, Isaacs RB, Spencer CE, Pruett TL, Sanfey HA, Sawyer RG, et al. Improved specificity and sensitivity when using pronase-digested lymphocytes to perform flow-cytometric crossmatch prior to renal transplantation. Transplant international : official journal of the European Society for Organ Transplantation. 2002;15:563-9.

[124] Shuler ML. Bioprocess engineering : basic concepts Upper Saddle River, NJ : Prentice Hall; 2002.

[125] Lee JTY, Cheung KMC, Leung VYL. Extraction of RNA from tough tissues with high proteoglycan content by cryosection, second phase separation and high salt precipitation. Journal of Biological Methods; Vol 2, No 2 (2015). 2015.

[126] Mason PE, Neilson GW, Dempsey CE, Barnes AC, Cruickshank JM. The hydration structure of guanidinium and thiocyanate ions: implications for protein stability in aqueous solution. Proceedings of the National Academy of Sciences of the United States of America. 2003;100:4557-61.

[127] Grad S, Gawri R, Haglund L, Ouellet J, Mwale F, Creemers LB, et al. New insight into human disc degeneration by gene expression profiling. Global Spine Journal: Global Spine Journal; 2014. p. 37.

[128] Lee C, Grad S, Sakai D, Mochida J, Alini M. Comparison of gene expression profiles of nucleus pulposus, annulus fibrosus and articular cartilage cells. 52nd Annual Meeting of the Orthopaedic Research Society. 52nd Annual Meeting of the Orthopaedic Research Society2006. p. 1199.

[129] Das PJ, Paria N, Gustafson-Seabury A, Vishnoi M, Chaki SP, Love CC, et al. Total RNA isolation from stallion sperm and testis biopsies. Theriogenology. 2010;74:1099-106, 106e1-2.

[130] Deng MY, Wang H, Ward GB, Beckham TR, McKenna TS. Comparison of six RNA extraction methods for the detection of classical swine fever virus by real-time and conventional reverse transcription-PCR. Journal of veterinary diagnostic investigation : official publication of the American Association of Veterinary Laboratory Diagnosticians, Inc. 2005;17:574-8.

[131] Santiago-Vazquez LZ, Ranzer LK, Kerr RG. Comparison of two total RNA extraction protocols using the marine gorgonian coral Pseudopterogorgia elisabethae and its symbiont Symbiodinium sp. Electron J Biotechn. 2006;9:598-603.

[132] Xiang XY, Qiu DW, Hegele RD, Tan WC. Comparison of different methods of total RNA extraction for viral detection in sputum. J Virol Methods. 2001;94:129-35.

[133] Reno C, Marchuk L, Sciore P, Frank CB, Hart DA. Rapid isolation of total RNA from small samples of hypocellular, dense connective tissues. BioTechniques. 1997;22:1082-6.

[134] Wang L, Stegemann JP. Extraction of high quality RNA from polysaccharide matrices using cetyltrimethylammonium bromide. Biomaterials. 2010;31:1612-8.

[135] Hwang NS, Varghese S, Theprungsirikul P, Canver A, Elisseeff J. Enhanced chondrogenic differentiation of murine embryonic stem cells in hydrogels with glucosamine. Biomaterials. 2006;27:6015-23.

[136] Brew CJ, Clegg PD, Boot-Handford RP, Andrew JG, Hardingham T. Gene expression in human chondrocytes in late osteoarthritis is changed in both fibrillated and intact cartilage without evidence of generalised chondrocyte hypertrophy. Annals of the rheumatic diseases. 2010;69:234-40.

[137] Brighton CT, Wang W, Clark CC. Up-regulation of matrix in bovine articular cartilage explants by electric fields. Biochemical and biophysical research communications. 2006;342:556-61.

[138] Davidson RK, Waters JG, Kevorkian L, Darrah C, Cooper A, Donell ST, et al. Expression profiling of metalloproteinases and their inhibitors in synovium and cartilage. Arthritis research & therapy. 2006;8:R124.

[139] Schoor O, Weinschenk T, Hennenlotter J, Corvin S, Stenzl A, Rammensee HG, et al. Moderate degradation does not preclude microarray analysis of small amounts of RNA. BioTechniques. 2003;35:1192-+.

[140] Fleige S, Pfaffl MW. RNA integrity and the effect on the real-time qRT-PCR performance. Molecular Aspects of Medicine. 2006;27:126-39.

[141] Wang J, Markova D, Anderson DG, Zheng Z, Shapiro IM, Risbud MV. TNF-alpha and IL-1beta promote a disintegrin-like and metalloprotease with thrombospondin type I

motif-5-mediated aggrecan degradation through syndecan-4 in intervertebral disc. The Journal of biological chemistry. 2011;286:39738-49.

[142] Capossela S, Schlafli P, Bertolo A, Janner T, Stadler BM, Potzel T, et al. Degenerated human intervertebral discs contain autoantibodies against extracellular matrix proteins. European cells & materials. 2014;27:251-63; discussion 63.

[143] Yurube T, Takada T, Suzuki T, Kakutani K, Maeno K, Doita M, et al. Rat tail static compression model mimics extracellular matrix metabolic imbalances of matrix metalloproteinases, aggrecanases, and tissue inhibitors of metalloproteinases in intervertebral disc degeneration. Arthritis research & therapy. 2012;14:R51.

[144] Mwale F, R. P, 2Epure L, Yoshikawa T, Hemmed A, Bokar M, et al. Stimulation of Aggrecan Synthesis and Suppression of Proteinase Synthesis by Link N Peptide ORS 2011 Annual Meeting: ORS 2011 Annual Meeting; 2011. p. 356.

[145] Chomczynski P, Mackey K. Short technical reports. Modification of the TRI reagent procedure for isolation of RNA from polysaccharide- and proteoglycan-rich sources. BioTechniques. 1995;19:942-5.

[146] Groppe JC, Morse DE. Isolation of full-length RNA templates for reverse transcription from tissues rich in RNase and proteoglycans. Analytical biochemistry. 1993;210:337-43.

[147] Re P, Valhmu WB, Vostrejs M, Howell DS, Fischer SG, Ratcliffe A. Quantitative polymerase chain reaction assay for aggrecan and link protein gene expression in cartilage. Analytical biochemistry. 1995;225:356-60.

[148] Schick BP, Eras J. Proteoglycans partially co-purify with RNA in TRI Reagent and can be transferred to filters by northern blotting. BioTechniques. 1995;18:574-6, 8.

[149] Raman T, O'Connor TP, Hackett NR, Wang W, Harvey BG, Attiyeh MA, et al. Quality control in microarray assessment of gene expression in human airway epithelium. BMC genomics. 2009;10:493.

[150] Thompson KL, Pine PS, Rosenzweig BA, Turpaz Y, Retief J. Characterization of the effect of sample quality on high density oligonucleotide microarray data using progressively degraded rat liver RNA. BMC biotechnology. 2007;7:57.

[151] Wankat PC. Equilibrium staged separations : separations in chemical engineering. Englewood Cliffs, N.J.: Prentice Hall; 1988.

[152] Krebs S, Fischaleck M, Blum H. A simple and loss-free method to remove TRIzol contaminations from minute RNA samples. Analytical biochemistry. 2009;387:136-8.

[153] Stockwell RA. The cell density of human articular and costal cartilage. Journal of anatomy. 1967;101:753-63.

[154] Chomczynski P. A reagent for the single-step simultaneous isolation of RNA, DNA and proteins from cell and tissue samples. BioTechniques. 1993;15:532-4, 6-7.

[155] Hembruff SL, Villeneuve DJ, Parissenti AM. The optimization of quantitative reverse transcription PCR for verification of cDNA microarray data. Analytical biochemistry. 2005;345:237-49.

[156] Brattelid T, Winer LH, Levy FO, Liestol K, Sejersted OM, Andersson KB. Reference gene alternatives to Gapdh in rodent and human heart failure gene expression studies. BMC molecular biology. 2010;11:22.

[157] Hernandez JL, Garces CM, Sumillera M, Fernandez-Aldasoro EV, Garcia-Ibarbia C, Ortiz-Gomez JA, et al. Aromatase expression in osteoarthritic and osteoporotic bone. Arthritis and rheumatism. 2008;58:1696-700.

[158] Kotorashvili A, Ramnauth A, Liu C, Lin J, Ye K, Kim R, et al. Effective DNA/RNA co-extraction for analysis of microRNAs, mRNAs, and genomic DNA from formalin-fixed paraffin-embedded specimens. PloS one. 2012;7:e34683.

[159] Arrizabalaga O, Lacerda HM, Zubiaga AM, Zugaza JL. Rac1 protein regulates glycogen phosphorylase activation and controls interleukin (IL)-2-dependent T cell proliferation. The Journal of biological chemistry. 2012;287:11878-90.

[160] Span PN, Thomas CM, Heuvel JJ, Bosch RR, Schalken JA, vd Locht L, et al. Analysis of expression of chorionic gonadotrophin transcripts in prostate cancer by quantitative Taqman and a modified molecular beacon RT-PCR. The Journal of endocrinology. 2002;172:489-95.

[161] Jung KM, Astarita G, Zhu C, Wallace M, Mackie K, Piomelli D. A key role for diacylglycerol lipase-alpha in metabotropic glutamate receptor-dependent endocannabinoid mobilization. Molecular pharmacology. 2007;72:612-21.

[162] Hughes GJ, Smith JS, Hanlon CA, Rupprecht CE. Evaluation of a TaqMan PCR assay to detect rabies virus RNA: influence of sequence variation and application to quantification of viral loads. Journal of clinical microbiology. 2004;42:299-306.

[163] Freimark D, Czermak P. Cell-based regeneration of intervertebral disc defects: review and concepts. The International journal of artificial organs. 2009;32:197-203.

[164] Ho G, Leung VY, Cheung KM, Chan D. Effect of severity of intervertebral disc injury on mesenchymal stem cell-based regeneration. Connective tissue research. 2008;49:15-21.

[165] Yang F, Leung VY, Luk KD, Chan D, Cheung KM. Mesenchymal stem cells arrest intervertebral disc degeneration through chondrocytic differentiation and stimulation of endogenous cells. Molecular therapy : the journal of the American Society of Gene Therapy. 2009;17:1959-66.

[166] Richardson SM, Walker RV, Parker S, Rhodes NP, Hunt JA, Freemont AJ, et al. Intervertebral disc cell-mediated mesenchymal stem cell differentiation. Stem Cells. 2006;24:707-16.

[167] Yang SH, Wu CC, Shih TTF, Sun YH, Lin FH. In vitro study on interaction between human nucleus pulposus cells and mesenchymal stem cells through paracrine stimulation. Spine. 2008;33:1951-7.

[168] Tao FH, Li F, Li GG, Pan F. Differentiation of mesenchymal stem cells into nucleus pulposus cells in vitro. J Huazhong U Sci-Med. 2008;28:156-8.

[169] Risbud MV, Albert TJ, Guttapalli A, Vresilovic EJ, Hillibrand AS, Vaccaro AR, et al. Differentiation of mesenchymal stem cells towards a nucleus pulposus-like phenotype in vitro: Implications for cell-based transplantation therapy. Spine. 2004;29:2627-32.

[170] Zhu H, Guo ZK, Jiang XX, Li H, Wang XY, Yao HY, et al. A protocol for isolation and culture of mesenchymal stem cells from mouse compact bone. Nature protocols. 2010;5:550-60.

[171] Soleimani M, Nadri S. A protocol for isolation and culture of mesenchymal stem cells from mouse bone marrow. Nature protocols. 2009;4:102-6.

[172] Minguell JJ, Erices A, Conget P. Mesenchymal stem cells. Exp Biol Med (Maywood). 2001;226:507-20.

[173] Williams JT, Southerland SS, Souza J, Calcutt AF, Cartledge RG. Cells isolated from adult human skeletal muscle capable of differentiating into multiple mesodermal phenotypes. The American surgeon. 1999;65:22-6.

[174] Sakaguchi Y, Sekiya I, Yagishita K, Ichinose S, Shinomiya K, Muneta T. Suspended cells from trabecular bone by collagenase digestion become virtually identical to mesenchymal stem cells obtained from marrow aspirates. Blood. 2004;104:2728-35.

[175] Tuli R, Seghatoleslami MR, Tuli S, Wang ML, Hozack WJ, Manner PA, et al. A simple, high-yield method for obtaining multipotential mesenchymal progenitor cells from trabecular bone. Molecular biotechnology. 2003;23:37-49.

[176] Tuli R, Tuli S, Nandi S, Wang ML, Alexander PG, Haleem-Smith H, et al. Characterization of multipotential mesenchymal progenitor cells derived from human trabecular bone. Stem Cells. 2003;21:681-93.

[177] Noth U, Osyczka AM, Tuli R, Hickok NJ, Danielson KG, Tuan RS. Multilineage mesenchymal differentiation potential of human trabecular bone-derived cells. Journal of orthopaedic research : official publication of the Orthopaedic Research Society. 2002;20:1060-9.

[178] Sottile V, Halleux C, Bassilana F, Keller H, Seuwen K. Stem cell characteristics of human trabecular bone-derived cells. Bone. 2002;30:699-704.

[179] Zhang JY, Wang JHC. Human Tendon Stem Cells Better Maintain Their Stemness in Hypoxic Culture Conditions. PloS one. 2013;8.

[180] Zhang J, Wang JH. Characterization of differential properties of rabbit tendon stem cells and tenocytes. BMC musculoskeletal disorders. 2010;11:10.

[181] Mizuno H, Tobita M, Uysal AC. Concise review: Adipose-derived stem cells as a novel tool for future regenerative medicine. Stem Cells. 2012;30:804-10.

[182] Konno M, Hamabe A, Hasegawa S, Ogawa H, Fukusumi T, Nishikawa S, et al. Adipose-derived mesenchymal stem cells and regenerative medicine. Development, growth & differentiation. 2013;55:309-18.

[183] Harasymiak-Krzyzanowska I, Niedojadlo A, Karwat J, Kotula L, Gil-Kulik P, Sawiuk M, et al. Adipose tissue-derived stem cells show considerable promise for regenerative medicine applications. Cellular & molecular biology letters. 2013.

[184] Gimble JM, Nuttall ME. Adipose-derived stromal/stem cells (ASC) in regenerative medicine: pharmaceutical applications. Current pharmaceutical design. 2011;17:332-9.

[185] Gimble JM, Katz AJ, Bunnell BA. Adipose-derived stem cells for regenerative medicine. Circulation research. 2007;100:1249-60.

[186] de Villiers JA, Houreld N, Abrahamse H. Adipose derived stem cells and smooth muscle cells: implications for regenerative medicine. Stem cell reviews. 2009;5:256-65.

[187] Pasquinelli G, Valente S. Ultrastructural assessment of the differentiation potential of human multipotent mesenchymal stromal cells. Ultrastructural pathology. 2013;37:318-27.

[188] Lu LL, Liu YJ, Yang SG, Zhao QJ, Wang X, Gong W, et al. Isolation and characterization of human umbilical cord mesenchymal stem cells with hematopoiesis-supportive function and other potentials. Haematologica. 2006;91:1017-26.

[189] Liu L, Yu Y, Hou Y, Chai J, Duan H, Chu W, et al. Human umbilical cord mesenchymal stem cells transplantation promotes cutaneous wound healing of severe burned rats. PloS one. 2014;9:e88348.

[190] Lee OK, Kuo TK, Chen WM, Lee KD, Hsieh SL, Chen TH. Isolation of multipotent mesenchymal stem cells from umbilical cord blood. Blood. 2004;103:1669-75.

[191] Can A, Balci D. Isolation, culture, and characterization of human umbilical cord stroma-derived mesenchymal stem cells. Methods Mol Biol. 2011;698:51-62.

[192] Csaki C, Matis U, Mobasheri A, Ye H, Shakibaei M. Chondrogenesis, osteogenesis and adipogenesis of canine mesenchymal stem cells: a biochemical, morphological and ultrastructural study. Histochemistry and cell biology. 2007;128:507-20.

[193] Gnecchi M, Melo LG. Bone marrow-derived mesenchymal stem cells: isolation, expansion, characterization, viral transduction, and production of conditioned medium. Methods Mol Biol. 2009;482:281-94.

[194] Kanichai M, Ferguson D, Prendergast PJ, Campbell VA. Hypoxia promotes chondrogenesis in rat mesenchymal stem cells: a role for AKT and hypoxia-inducible factor (HIF)-1alpha. Journal of cellular physiology. 2008;216:708-15.

[195] Lee HH, Chang CC, Shieh MJ, Wang JP, Chen YT, Young TH, et al. Hypoxia enhances chondrogenesis and prevents terminal differentiation through PI3K/Akt/FoxO dependent anti-apoptotic effect. Scientific reports. 2013;3:2683.

[196] Lai WT, Krishnappa V, Phinney DG. Fibroblast growth factor 2 (Fgf2) inhibits differentiation of mesenchymal stem cells by inducing Twist2 and Spry4, blocking extracellular regulated kinase activation, and altering Fgf receptor expression levels. Stem Cells. 2011;29:1102-11.

[197] Kähkönen T, Ivaska KK, Härkönen P. The effect of fibroblast growth factor 2 on mesenchymal stromal cell differentiation. Bone Abstracts. 2013.

[198] Hagmann S, Moradi B, Frank S, Dreher T, Kammerer PW, Richter W, et al. FGF-2 addition during expansion of human bone marrow-derived stromal cells alters MSC surface marker distribution and chondrogenic differentiation potential. Cell proliferation. 2013;46:396-407.

[199] Richter W, Bock R, Hennig T, Weiss S. Influence of FGF-2 and PTHRP on chondrogenic differentiation of human mesenchymal stem cells. The Journal of bone and joint surgery British volume. 2009;91:444.

[200] Studer RK, Gilbertson LG, Georgescu H, Sowa G, Vo N, Kang JD. p38 MAPK inhibition modulates rabbit nucleus pulposus cell response to IL-1. Journal of orthopaedic research : official publication of the Orthopaedic Research Society. 2008;26:991-8.

[201] Li J, Zhao Z, Liu J, Huang N, Long D, Wang J, et al. MEK/ERK and p38 MAPK regulate chondrogenesis of rat bone marrow mesenchymal stem cells through delicate interaction with TGF-beta1/Smads pathway. Cell proliferation. 2010;43:333-43.

[202] Penick KJ, Solchaga LA, Welter JF. High-throughput aggregate culture system to assess the chondrogenic potential of mesenchymal stem cells. BioTechniques. 2005;39:687-91.

[203] Leung VYL, Chan WCW, Hung SC, Cheung KMC, Chan D. Matrix Remodeling During Intervertebral Disc Growth and Degeneration Detected by Multichromatic FAST Staining. Journal of Histochemistry & Cytochemistry. 2009;57:249-56.

[204] Neuhuber B, Swanger SA, Howard L, Mackay A, Fischer I. Effects of plating density and culture time on bone marrow stromal cell characteristics. Experimental hematology. 2008;36:1176-85.

[205] Nadri S, Soleimani M, Hosseni RH, Massumi M, Atashi A, Izadpanah R. An efficient method for isolation of murine bone marrow mesenchymal stem cells. The International journal of developmental biology. 2007;51:723-9.

[206] Yang ZX, Han ZB, Ji YR, Wang YW, Liang L, Chi Y, et al. CD106 identifies a subpopulation of mesenchymal stem cells with unique immunomodulatory properties. PloS one. 2013;8:e59354.

[207] Zhang LM, Su PQ, Xu CX, Yang JL, Yu WH, Huang DS. Chondrogenic differentiation of human mesenchymal stem cells: a comparison between micromass and pellet culture systems. Biotechnology letters. 2010;32:1339-46.

[208] Solchaga LA, Penick KJ, Welter JF. Chondrogenic differentiation of bone marrow-derived mesenchymal stem cells: tips and tricks. Methods Mol Biol. 2011;698:253-78.

[209] Chen J, Li C, Wang S. Periodic heat shock accelerated the chondrogenic differentiation of human mesenchymal stem cells in pellet culture. PloS one. 2014;9:e91561.

[210] Ullah M, Eucker J, Sittinger M, Ringe J. Mesenchymal stem cells and their chondrogenic differentiated and dedifferentiated progeny express chemokine receptor CCR9 and chemotactically migrate toward CCL25 or serum. Stem cell research & therapy. 2013;4.

[211] Hagmann S, Moradi B, Frank S, Dreher T, Kammerer PW, Richter W, et al. Different culture media affect growth characteristics, surface marker distribution and chondrogenic differentiation of human bone marrow-derived mesenchymal stromal cells. BMC musculoskeletal disorders. 2013;14:223.

[212] Kacew S, Festing MF. Role of rat strain in the differential sensitivity to pharmaceutical agents and naturally occurring substances. Journal of toxicology and environmental health. 1996;47:1-30.

[213] Loscher W, Cramer S, Ebert U. Differences in kindling development in seven outbred and inbred rat strains. Experimental neurology. 1998;154:551-9.

[214] Peister A, Mellad JA, Larson BL, Hall BM, Gibson LF, Prockop DJ. Adult stem cells from bone marrow (MSCs) isolated from different strains of inbred mice vary in surface epitopes, rates of proliferation, and differentiation potential. Blood. 2004;103:1662-8.

[215] Barzilay R, Sadan O, Melamed E, Offen D. Comparative characterization of bone marrow-derived mesenchymal stromal cells from four different rat strains. Cytotherapy. 2009;11:435-42.

[216] Nehls M, Kyewski B, Messerle M, Waldschutz R, Schuddekopf K, Smith AJ, et al. Two genetically separable steps in the differentiation of thymic epithelium. Science. 1996;272:886-9.

[217] Pantelouris EM. Absence of thymus in a mouse mutant. Nature. 1968;217:370-1.

[218] Baaten BJ, Li CR, Bradley LM. Multifaceted regulation of T cells by CD44. Communicative & integrative biology. 2010;3:508-12.

[219] Ponta H, Sherman L, Herrlich PA. CD44: From adhesion molecules to signalling regulators. Nat Rev Mol Cell Bio. 2003;4:33-45.

[220] Oliferenko S, Kaverina I, Small JV, Huber LA. Hyaluronic acid (HA) binding to CD44 activates Rac1 and induces lamellipodia outgrowth. The Journal of cell biology. 2000;148:1159-64.

[221] Bourguignon LYW, Peyrollier K, Xia WL, Gilad E. Hyaluronan-CD44 interaction activates stem cell marker Nanog, Stat-3-mediated MDR1 gene expression, and ankyrin-regulated multidrug efflux in breast and ovarian tumor cells. Journal of Biological Chemistry. 2008;283:17635-51.

[222] Reznikoff CA, Brankow DW, Heidelberger C. Establishment and characterization of a cloned line of C3H mouse embryo cells sensitive to postconfluence inhibition of division. Cancer research. 1973;33:3231-8.

[223] Pinney DF, Emerson CP, Jr. 10T1/2 cells: an in vitro model for molecular genetic analysis of mesodermal determination and differentiation. Environmental health perspectives. 1989;80:221-7.

[224] Xue RD, Wan Y, Zhang S, Zhang QY, Ye HY, Li YM. Role of bone morphogenetic protein 4 in the differentiation of brown fat-like adipocytes. Am J Physiol-Endoc M. 2014;306:E363-E72.

[225] Zhang Y, Kong L, Carlson CS, Liu CJ. Cbfa1-dependent expression of an interferon-inducible p204 protein is required for chondrocyte differentiation. Cell Death Differ. 2008;15:1760-71.

[226] Huang HY, Hu LL, Song TJ, Li X, He Q, Sun X, et al. Involvement of cytoskeleton-associated proteins in the commitment of C3H10T1/2 pluripotent stem cells to adipocyte lineage induced by BMP2/4. Molecular & cellular proteomics : MCP. 2011;10:M110 002691.

[227] Wang SS, Huang HY, Chen SZ, Li X, Zhang WT, Tang QQ. Gdf6 induces commitment of pluripotent mesenchymal C3H10T1/2 cells to the adipocyte lineage. Febs J. 2013;280:2644-51.

[228] Liu Y, Zhang ZC, Qian SW, Zhang YY, Huang HY, Tang Y, et al. MicroRNA-140 promotes adipocyte lineage commitment of C3H10T1/2 pluripotent stem cells via targeting osteopetrosis-associated transmembrane protein 1. The Journal of biological chemistry. 2013;288:8222-30.

[229] Tang QQ, Otto TC, Lane MD. Commitment of C3H10T1/2 pluripotent stem cells to the adipocyte lineage. Proceedings of the National Academy of Sciences of the United States of America. 2004;101:9607-11.

[230] Miyawaki J, Kamei S, Sakayama K, Yamamoto H, Masuno H. 4-tert-octylphenol regulates the differentiation of C3H10T1/2 cells into osteoblast and adipocyte lineages. Toxicological sciences : an official journal of the Society of Toxicology. 2008;102:82-8.

[231] Steinert A, Weber M, Dimmler A, Julius C, Schutze N, Noth U, et al. Chondrogenic differentiation of mesenchymal progenitor cells encapsulated in ultrahigh-viscosity alginate. Journal of orthopaedic research : official publication of the Orthopaedic Research Society. 2003;21:1090-7.

[232] Rudert M, Tillmann B. Lymph and blood supply of the human intervertebral disc. Cadaver study of correlations to discitis. Acta orthopaedica Scandinavica. 1993;64:37-40.

[233] Gruber HE, Ashraf N, Kilburn J, Williams C, Norton HJ, Gordon BE, et al. Vertebral endplate architecture and vascularization: application of micro-computerized tomography, a vascular tracer, and immunocytochemistry in analyses of disc degeneration in the aging sand rat. Spine. 2005;30:2593-600.

[234] Bartels EM, Fairbank JC, Winlove CP, Urban JP. Oxygen and lactate concentrations measured in vivo in the intervertebral discs of patients with scoliosis and back pain. Spine. 1998;23:1-7; discussion 8.

[235] Lee DC, Adams CS, Albert TJ, Shapiro IM, Evans SM, Koch CJ. In situ oxygen utilization in the rat intervertebral disc. Journal of anatomy. 2007;210:294-303.

[236] Rajpurohit R, Risbud MV, Ducheyne P, Vresilovic EJ, Shapiro IM. Phenotypic characteristics of the nucleus pulposus: expression of hypoxia inducing factor-1, glucose transporter-1 and MMP-2. Cell and tissue research. 2002;308:401-7.

[237] Agrawal A, Gajghate S, Smith H, Anderson DG, Albert TJ, Shapiro IM, et al. Cited2 modulates hypoxia-inducible factor-dependent expression of vascular endothelial growth factor in nucleus pulposus cells of the rat intervertebral disc. Arthritis and rheumatism. 2008;58:3798-808.

[238] Hiyama A, Skubutyte R, Markova D, Anderson DG, Yadla S, Sakai D, et al. Hypoxia activates the notch signaling pathway in cells of the intervertebral disc: implications in degenerative disc disease. Arthritis and rheumatism. 2011;63:1355-64.

[239] Lin WP, Wang XJ, Wang CR, Zhang LQ, Li N, Wang FS, et al. Polymorphism in the Hypoxia-Inducible Factor 1alpha Gene May Confer Susceptibility to LDD in Chinese Cohort. PloS one. 2013;8.

[240] Thoms BL, Dudek KA, Lafont JE, Murphy CL. Hypoxia promotes the production and inhibits the destruction of human articular cartilage. Arthritis and rheumatism. 2013;65:1302-12.

[241] Lafont JE, Talma S, Murphy CL. Hypoxia-inducible factor 2alpha is essential for hypoxic induction of the human articular chondrocyte phenotype. Arthritis and rheumatism. 2007;56:3297-306.

[242] Lafont JE, Talma S, Hopfgarten C, Murphy CL. Hypoxia promotes the differentiated human articular chondrocyte phenotype through SOX9-dependent and -independent pathways. The Journal of biological chemistry. 2008;283:4778-86.

[243] Semenza GL. HIF-1 and human disease: one highly involved factor. Genes & development. 2000;14:1983-91.

[244] Wu D, Yotnda P. Induction and testing of hypoxia in cell culture. Journal of visualized experiments : JoVE. 2011.

[245] Mason N. Introduction to environmental physics : planet Earth, life and climate. London: London : Taylor and Francis; 2001.

[246] Ahuja P. Chemical Engineering Thermodynamics2008.

[247] Li Z, Shen J, Wu WK, Yu X, Liang J, Qiu G, et al. Leptin Induces Cyclin D1 Expression and Proliferation of Human Nucleus Pulposus Cells via JAK/STAT, PI3K/Akt and MEK/ERK Pathways. PloS one. 2012;7:e53176.

[248] Risbud MV, Fertala J, Vresilovic EJ, Albert TJ, Shapiro IM. Nucleus pulposus cells upregulate PI3K/Akt and MEK/ERK signaling pathways under hypoxic conditions and resist apoptosis induced by serum withdrawal. Spine. 2005;30:882-9.

[249] Tsai TT, Guttapalli A, Agrawal A, Albert TJ, Shapiro IM, Risbud MV. MEK/ERK signaling controls osmoregulation of nucleus pulposus cells of the intervertebral disc by transactivation of TonEBP/OREBP. Journal of bone and mineral research : the official journal of the American Society for Bone and Mineral Research. 2007;22:965-74.

[250] Cheng X, Ni B, Zhang Z, Liu Q, Wang L, Ding Y, et al. Polyol pathway mediates enhanced degradation of extracellular matrix via p38 MAPK activation in intervertebral disc of diabetic rats. Connective tissue research. 2013;54:118-22.

[251] Ito T, Ohtori S, Inoue G, Koshi T, Doya H, Ozawa T, et al. Glial phosphorylated p38 MAP kinase mediates pain in a rat model of lumbar disc herniation and induces motor dysfunction in a rat model of lumbar spinal canal stenosis. Spine. 2007;32:159-67.

[252] Kim JH, Studer RK, Vo NV, Sowa GA, Kang JD. p38 MAPK inhibition selectively mitigates inflammatory mediators and VEGF production in AF cells co-cultured with activated macrophage-like THP-1 cells. Osteoarthritis and cartilage / OARS, Osteoarthritis Research Society. 2009;17:1662-9.

[253] Niu CC, Yuan LJ, Chen LH, Lin SS, Tsai TT, Liao JC, et al. Beneficial effects of hyperbaric oxygen on human degenerated intervertebral disk cells via suppression of IL-1beta and p38 MAPK signal. Journal of orthopaedic research : official publication of the Orthopaedic Research Society. 2011;29:14-9.

[254] Sasaki N, Sekiguchi M, Kikuchi S, Konno S. Effects of asialo-erythropoietin on pain-related behavior and expression of phosphorylated-p38 map kinase and tumor necrosis factor-alpha induced by application of autologous nucleus pulposus on nerve root in rat. Spine. 2011;36:E86-94.

[255] Xiao YQ, Malcolm K, Worthen GS, Gardai S, Schiemann WP, Fadok VA, et al. Cross-talk between ERK and p38 MAPK mediates selective suppression of pro-inflammatory cytokines by transforming growth factor-beta. The Journal of biological chemistry. 2002;277:14884-93.

[256] Gelse K, Poschl E, Aigner T. Collagens - structure, function, and biosynthesis. Advanced drug delivery reviews. 2003;55:1531-46.

[257] Gruber HE, Ingram JA, Leslie K, Norton HJ, Hanley EN, Jr. Cell shape and gene expression in human intervertebral disc cells: in vitro tissue engineering studies. Biotechnic & histochemistry : official publication of the Biological Stain Commission. 2003;78:109-17.

[258] Zhang YH, Zhao CQ, Jiang LS, Dai LY. Substrate stiffness regulates apoptosis and the mRNA expression of extracellular matrix regulatory genes in the rat annular cells. Matrix Biology. 2011;30:135-44.

[259] Shoulders MD, Raines RT. Collagen structure and stability. Annual review of biochemistry. 2009;78:929-58.

[260] Lefebvre V, Behringer RR, de Crombrugghe B. L-Sox5, Sox6 and Sox9 control essential steps of the chondrocyte differentiation pathway. Osteoarthritis and Cartilage. 2001;9:S69-S75.

[261] Li H, Haudenschild DR, Posey KL, Hecht JT, Di Cesare PE, Yik JHN. Comparative analysis with collagen type II distinguishes cartilage oligomeric matrix protein as a primary TGF beta-responsive gene. Osteoarthritis and Cartilage. 2011;19:1246-53.

[262] Lee CR, Sakai D, Nakai T, Toyama K, Mochida J, Alini M, et al. A phenotypic comparison of intervertebral disc and articular cartilage cells in the rat. European spine journal : official publication of the European Spine Society, the European Spinal Deformity Society, and the European Section of the Cervical Spine Research Society. 2007;16:2174-85.

[263] Lefebvre V, Huang WD, Harley VR, Goodfellow PN, deCrombrugghe B. SOX9 is a potent activator of the chondrocyte-specific enhancer of the pro alpha 1(II) collagen gene. Molecular and cellular biology. 1997;17:2336-46.

[264] Panda DK, Miao DS, Lefebvre V, Hendy GN, Goltzman D. The transcription factor SOX9 regulates cell cycle and differentiation genes in chondrocytic CFK2 cells. Journal of Biological Chemistry. 2001;276:41229-36.

[265] Bosserhoff AK, Kondo S, Moser M, Dietz UH, Copeland NG, Gilbert DJ, et al. Mouse CD-RAP/MIA gene: structure, chromosomal localization, and expression in cartilage and chondrosarcoma. Developmental dynamics : an official publication of the American Association of Anatomists. 1997;208:516-25.

[266] Schmid R, Schiffner S, Opolka A, Grassel S, Schubert T, Moser M, et al. Enhanced cartilage regeneration in MIA/CD-RAP deficient mice. Cell death & disease. 2010;1:e97.

[267] Tscheudschilsuren G, Bosserhoff AK, Schlegel J, Vollmer D, Anton A, Alt V, et al. Regulation of mesenchymal stem cell and chondrocyte differentiation by MIA. Experimental cell research. 2006;312:63-72.

[268] Wang Y, Belflower RM, Dong YF, Schwarz EM, O'Keefe RJ, Drissi H. Runx1/AML1/Cbfa2 mediates onset of mesenchymal cell differentiation toward chondrogenesis. Journal of bone and mineral research : the official journal of the American Society for Bone and Mineral Research. 2005;20:1624-36.

[269] Smith N, Dong Y, Lian JB, Pratap J, Kingsley PD, van Wijnen AJ, et al. Overlapping expression of Runx1(Cbfa2) and Runx2(Cbfa1) transcription factors supports cooperative induction of skeletal development. Journal of cellular physiology. 2005;203:133-43.

[270] Yamashiro T, Wang XP, Li Z, Oya S, Aberg T, Fukunaga T, et al. Possible roles of Runx1 and Sox9 in incipient intramembranous ossification. Journal of bone and mineral research : the official journal of the American Society for Bone and Mineral Research. 2004;19:1671-7.

[271] Soung do Y, Talebian L, Matheny CJ, Guzzo R, Speck ME, Lieberman JR, et al. Runx1 dose-dependently regulates endochondral ossification during skeletal development and fracture healing. Journal of bone and mineral research : the official journal of the American Society for Bone and Mineral Research. 2012;27:1585-97.

[272] Folkman J, Moscona A. Role of cell shape in growth control. Nature. 1978;273:345-9.

[273] Chen CS, Mrksich M, Huang S, Whitesides GM, Ingber DE. Geometric control of cell life and death. Science. 1997;276:1425-8.

[274] Daniels K, Solursh M. Modulation of chondrogenesis by the cytoskeleton and extracellular matrix. Journal of cell science. 1991;100 (Pt 2):249-54.

[275] Archer CW, Rooney P, Wolpert L. Cell shape and cartilage differentiation of early chick limb bud cells in culture. Cell differentiation. 1982;11:245-51.

[276] Solursh M, Linsenmayer TF, Jensen KL. Chondrogenesis from single limb mesenchyme cells. Developmental biology. 1982;94:259-64.

[277] Solursh M, Reiter RS. Determination of limb bud chondrocytes during a transient block of the cell cycle. Cell differentiation. 1975;4:131-7.

[278] Mermelstein CS, Rebello MI, Amaral LM, Costa ML. Changes in cell shape, cytoskeletal proteins and adhesion sites of cultured cells after extracellular Ca2+ chelation. Brazilian journal of medical and biological research = Revista brasileira de pesquisas medicas e biologicas / Sociedade Brasileira de Biofisica [et al]. 2003;36:1111-6.

[279] McBeath R, Pirone DM, Nelson CM, Bhadriraju K, Chen CS. Cell shape, cytoskeletal tension, and RhoA regulate stem cell lineage commitment. Developmental cell. 2004;6:483-95.

[280] Ingber DE, Prusty D, Sun Z, Betensky H, Wang N. Cell shape, cytoskeletal mechanics, and cell cycle control in angiogenesis. Journal of biomechanics. 1995;28:1471-84.

[281] Luxenburg C, Pasolli HA, Williams SE, Fuchs E. Developmental roles for Srf, cortical cytoskeleton and cell shape in epidermal spindle orientation. Nature cell biology. 2011;13:203-14.

[282] Wang N, Ingber DE. Control of cytoskeletal mechanics by extracellular matrix, cell shape, and mechanical tension. Biophysical journal. 1994;66:2181-9.

[283] Zanetti NC, Dress VM, Solursh M. Comparison between ectoderm-conditioned medium and fibronectin in their effects on chondrogenesis by limb bud mesenchymal cells. Developmental biology. 1990;139:383-95.

[284] Zanetti NC, Solursh M. Induction of chondrogenesis in limb mesenchymal cultures by disruption of the actin cytoskeleton. The Journal of cell biology. 1984;99:115-23.

[285] Chahine NO, Blanchette C, Thomas CB, Lu J, Haudenschild D, Loots GG. Effect of age and cytoskeletal elements on the indentation-dependent mechanical properties of chondrocytes. PloS one. 2013;8:e61651.

[286] Haudenschild DR, Chen J, Steklov N, Lotz MK, D'Lima DD. Characterization of the chondrocyte actin cytoskeleton in living three-dimensional culture: response to anabolic and catabolic stimuli. Molecular & cellular biomechanics : MCB. 2009;6:135-44.

[287] Wang F, Wu XT, Zhuang SY, Wang YT, Hong X, Zhu L, et al. Ex vivo observation of human nucleus pulposus chondrocytes isolated from degenerated intervertebral discs. Asian spine journal. 2011;5:73-81.

[288] Sakai D. Future perspectives of cell-based therapy for intervertebral disc disease. European spine journal : official publication of the European Spine Society, the European Spinal Deformity Society, and the European Section of the Cervical Spine Research Society. 2008;17 Suppl 4:452-8.

[289] Li S, Duance VC, Blain EJ. Zonal variations in cytoskeletal element organization, mRNA and protein expression in the intervertebral disc. Journal of anatomy. 2008;213:725-32.

[290] Thery M, Pepin A, Dressaire E, Chen Y, Bornens M. Cell distribution of stress fibres in response to the geometry of the adhesive environment. Cell motility and the cytoskeleton. 2006;63:341-55.

[291] Thery M, Racine V, Piel M, Pepin A, Dimitrov A, Chen Y, et al. Anisotropy of cell adhesive microenvironment governs cell internal organization and orientation of polarity. Proceedings of the National Academy of Sciences of the United States of America. 2006;103:19771-6.

[292] Thery M, Racine V, Pepin A, Piel M, Chen Y, Sibarita JB, et al. The extracellular matrix guides the orientation of the cell division axis. Nature cell biology. 2005;7:947-53.

[293] Gao L, McBeath R, Chen CS. Stem Cell Shape Regulates a Chondrogenic Versus Myogenic Fate Through Rac1 and N-Cadherin. Stem Cells. 2010;28:564-72.

[294] Shaik J, Shaikh Mohammed J, McShane MJ, Mills DK. Chondrocyte Behavior on Micropatterns Fabricated Using Layer-by-Layer Lift-Off: Morphological Analysis. Journal of Medical Engineering. 2013;2013:12.

[295] Otsuka H, Nagamura M, Kaneko A, Kutsuzawa K, Sakata T, Miyahara Y. Chondrocyte spheroids on microfabricated PEG hydrogel surface and their noninvasive functional monitoring. Sci Technol Adv Mat. 2012;13.

[296] Falconnet D, Csucs G, Grandin HM, Textor M. Surface engineering approaches to micropattern surfaces for cell-based assays. Biomaterials. 2006;27:3044-63.

[297] Whitesides GM, Ostuni E, Takayama S, Jiang XY, Ingber DE. Soft lithography in biology and biochemistry. Annu Rev Biomed Eng. 2001;3:335-73.

[298] Folch A, Toner M. Microengineering of cellular interactions. Annu Rev Biomed Eng. 2000;2:227-+.

[299] Thery M, Piel M. Adhesive micropatterns for cells: a microcontact printing protocol. Cold Spring Harbor protocols. 2009;2009:pdb prot5255.

[300] Kumar A, Whitesides GM. Features of Gold Having Micrometer to Centimeter Dimensions Can Be Formed through a Combination of Stamping with an Elastomeric Stamp and an Alkanethiol Ink Followed by Chemical Etching. Appl Phys Lett. 1993;63:2002-4.

[301] Singhvi R, Kumar A, Lopez GP, Stephanopoulos GN, Wang DIC, Whitesides GM, et al. Engineering Cell-Shape and Function. Science. 1994;264:696-8.

[302] Tang X, Ali MY, Saif MT. A Novel Technique for Micro-patterning Proteins and Cells on Polyacrylamide Gels. Soft matter. 2012;8:7197-206.

[303] Noh H, Vogler EA. Volumetric interpretation of protein adsorption: mass and energy balance for albumin adsorption to particulate adsorbents with incrementally increasing hydrophilicity. Biomaterials. 2006;27:5801-12.

[304] Mwale F, Bullett N, Petit A, Antoniou J, Lerouge S, Wertheimer MR. Micropatterning on Nitrogen and Ammonia Plasma-Treated Surfaces as a Means of Distinguishing Between the Nucleus Pulposus and Cartilage Phenotypes. 54th Annual Meeting of the Orthopaedic Research Society2008. p. 1496.

[305] Yuan X, Arkonac DE, Chao PH, Vunjak-Novakovic G. Electrical stimulation enhances cell migration and integrative repair in the meniscus. Scientific reports. 2014;4:3674.

[306] Fink J, Thery M, Azioune A, Dupont R, Chatelain F, Bornens M, et al. Comparative study and improvement of current cell micro-patterning techniques. Lab on a chip. 2007;7:672-80.

[307] Leng Y. Materials characterization : introduction to microscopic and spectroscopic methods. Hoboken, NJ: Hoboken, NJ : J. Wiley; 2008.

[308] MicroscopyU. Working Distance and Parfocal Length http://www.microscopyu.com/articles/formulas/formulasworkingparfocal.html.

[309] Gadhari N, Charnley M, Marelli M, Brugger J, Chiquet M. Cell shape-dependent early responses of fibroblasts to cyclic strain. Biochimica et biophysica acta. 2013;1833:3415-25.

[310] Chen B, Kumar G, Co CC, Ho CC. Geometric control of cell migration. Scientific reports. 2013;3:2827.

[311] Wang XL, Song W, Kawazoe N, Chen GP. Influence of cell protrusion and spreading on adipogenic differentiation of mesenchymal stem cells on micropatterned surfaces. Soft matter. 2013;9:4160-6.

[312] Lee J, Abdeen AA, Zhang D, Kilian KA. Directing stem cell fate on hydrogel substrates by controlling cell geometry, matrix mechanics and adhesion ligand composition. Biomaterials. 2013;34:8140-8.

[313] Song W, Kawazoe N, Chen GP. Dependence of Spreading and Differentiation of Mesenchymal Stem Cells on Micropatterned Surface Area. J Nanomater. 2011.

[314] Song W, Lu H, Kawazoe N, Chen G. Adipogenic differentiation of individual mesenchymal stem cell on different geometric micropatterns. Langmuir : the ACS journal of surfaces and colloids. 2011;27:6155-62.

[315] Kilian KA, Bugarija B, Lahn BT, Mrksich M. Geometric cues for directing the differentiation of mesenchymal stem cells. Proceedings of the National Academy of Sciences of the United States of America. 2010;107:4872-7.

[316] Johansson S, Svineng G, Wennerberg K, Armulik A, Lohikangas L. Fibronectin-integrin interactions. Frontiers in bioscience : a journal and virtual library. 1997;2:d126-46.

[317] Tan JL, Liu W, Nelson CM, Raghavan S, Chen CS. Simple approach to micropattern cells on common culture substrates by tuning substrate wettability. Tissue engineering. 2004;10:865-72.

[318] Paz AC, Javaherian S, McGuigan AP. Tools for micropatterning epithelial cells into microcolonies on transwell filter substrates. Lab on a chip. 2011;11:3440-8.

[319] Tojkander S, Gateva G, Lappalainen P. Actin stress fibers--assembly, dynamics and biological roles. Journal of cell science. 2012;125:1855-64.

[320] Markway BD, Tan GK, Brooke G, Hudson JE, Cooper-White JJ, Doran MR. Enhanced Chondrogenic Differentiation of Human Bone Marrow-Derived Mesenchymal Stem Cells in Low Oxygen Environment Micropellet Cultures. Cell Transplant. 2010;19:29-42.

[321] Murray GI. An overview of laser microdissection technologies. Acta Histochem. 2007;109:171-6.

[322] Eltoum IA, Siegal GP, Frost AR. Microdissection of histologic sections: past, present, and future. Advances in anatomic pathology. 2002;9:316-22.

[323] Going JJ, Lamb RF. Practical histological microdissection for PCR analysis. The Journal of pathology. 1996;179:121-4.

[324] Hernandez S, Lloreta J. Manual versus laser micro-dissection in molecular biology. Ultrastructural pathology. 2006;30:221-8.

[325] Meier-Ruge W, Bielser W, Remy E, Hillenkamp F, Nitsche R, Unsold R. The laser in the Lowry technique for microdissection of freeze-dried tissue slices. The Histochemical journal. 1976;8:387-401.

[326] Vandewoestyne M, Goossens K, Burvenich C, Van Soom A, Peelman L, Deforce D. Laser capture microdissection: should an ultraviolet or infrared laser be used? Analytical biochemistry. 2013;439:88-98.

[327] Espina V, Wulfkuhle JD, Calvert VS, VanMeter A, Zhou W, Coukos G, et al. Laser-capture microdissection. Nature protocols. 2006;1:586-603.

[328] Fend F, Raffeld M. Laser capture microdissection in pathology. Journal of clinical pathology. 2000;53:666-72.

[329] Stahlberg A, Bengtsson M. Single-cell gene expression profiling using reverse transcription quantitative real-time PCR. Methods. 2010;50:282-8.

[330] Espina V, Heiby M, Pierobon M, Liotta LA. Laser capture microdissection technology. Expert review of molecular diagnostics. 2007;7:647-57.

[331] Emmert-Buck MR, Bonner RF, Smith PD, Chuaqui RF, Zhuang Z, Goldstein SR, et al. Laser capture microdissection. Science. 1996;274:998-1001.

[332] Bonner RF, Emmert-Buck M, Cole K, Pohida T, Chuaqui R, Goldstein S, et al. Laser capture microdissection: molecular analysis of tissue. Science. 1997;278:1481,3.

[333] Schutze K, Becker I, Becker KF, Thalhammer S, Stark RW, Heckl WM, et al. Cut out or poke in - The key to the world of single genes: Laser micromanipulation as a valuable tool on the look-out for the origin of disease. Genet Anal-Biomol E. 1997;14:1-8.

[334] Schutze K, Lahr G. Identification of expressed genes by laser-mediated manipulation of single cells. Nature biotechnology. 1998;16:737-42.

[335] Schutze K, Posl H, Lahr G. Laser micromanipulation systems as universal tools in cellular and molecular biology and in medicine. Cell Mol Biol (Noisy-le-grand). 1998;44:735-46.

[336] Schermelleh L, Thalhammer S, Heckl W, Posl H, Cremer T, Schutze K, et al. Laser microdissection and laser pressure catapulting for the generation of chromosome-specific paint probes. BioTechniques. 1999;27:362-7.

[337] Kolble K. The LEICA microdissection system: design and applications. J Mol Med (Berl). 2000;78:B24-5.

[338] Micke P, Ostman A, Lundeberg J, Ponten F. Laser-assisted cell microdissection using the PALM system. Methods Mol Biol. 2005;293:151-66.

[339] von Eggeling F, Melle C, Ernst G. Microdissecting the proteome. Proteomics. 2007;7:2729-37.

[340] Thomas CH, Collier JH, Sfeir CS, Healy KE. Engineering gene expression and protein synthesis by modulation of nuclear shape. Proceedings of the National Academy of Sciences of the United States of America. 2002;99:1972-7.

[341] Golubeva YG, Smith RM, Sternberg LR. Optimizing Frozen Sample Preparation for Laser Microdissection: Assessment of CryoJane Tape-Transfer System(R). PloS one. 2013;8:e66854.

[342] Flake GP, Rivera MP, Funkhouser WK, Maygarden SJ, Meadows KL, Long EH, et al. Detection of pre-invasive lung cancer: technical aspects of the LIFE project. Toxicologic pathology. 2007;35:65-74.

[343] Lauridsen JB, Johansen JL, Rekling JC, Thirstrup K, Moerk A, Sager TN. Regulation of the Bcas1 and Baiap3 transcripts in the subthalamic nucleus in mice recovering from MPTP toxicity. Neuroscience research. 2011;70:269-76.

[344] Goossens K, De Spiegelaere W, Stevens M, Burvenich C, De Spiegeleer B, Cornillie P, et al. Differential microRNA expression analysis in blastocysts by whole mount in situ hybridization and reverse transcription quantitative polymerase chain reaction on laser capture microdissection samples. Analytical biochemistry. 2012;423:93-101.

[345] Stybayeva G, Zhu H, Ramanculov E, Dandekar S, George M, Revzin A. Micropatterned co-cultures of T-lymphocytes and epithelial cells as a model of mucosal immune system. Biochemical and biophysical research communications. 2009;380:575-80.

[346] Lee JY, Jones C, Zern MA, Revzin A. Analysis of local tissue-specific gene expression in cellular micropatterns. Analytical chemistry. 2006;78:8305-12.

[347] Torres MS, Ace CI, Okulicz WC. Assessment and application of laser microdissection for analysis of gene expression in the rhesus monkey endometrium. Biology of reproduction. 2002;67:1067-72.

[348] Adeyinka A, Emberley E, Niu Y, Snell L, Murphy LC, Sowter H, et al. Analysis of gene expression in ductal carcinoma in situ of the breast. Clinical cancer research : an official journal of the American Association for Cancer Research. 2002;8:3788-95.

[349] Espina V, Liotta L. Laser Capture Microdissection. Microdissection2006. p. 339-44.

[350] Ge H, Gong X, Tang CK. Evidence of high incidence of EGFRvIII expression and coexpression with EGFR in human invasive breast cancer by laser capture microdissection and immunohistochemical analysis. International journal of cancer Journal international du cancer. 2002;98:357-61.

[351] Morimoto M, Morimoto M, Whitmire J, Star RA, Urban JF, Jr., Gause WC. Laser Capture Microdissection (LCM): Preparation and Sectioning of Frozen Tissue Blocks and Purification of RNA from Isolated Cells. CSH protocols. 2006;2006.

[352] Curran S, McKay JA, McLeod HL, Murray GI. Laser capture microscopy. Molecular pathology : MP. 2000;53:64-8.

[353] Bodas D, Khan-Malek C. Hydrophilization and hydrophobic recovery of PDMS by oxygen plasma and chemical treatment - An SEM investigation. Sensor Actuat B-Chem. 2007;123:368-73.

[354] Van Peer G, Mestdagh P, Vandesompele J. Accurate RT-qPCR gene expression analysis on cell culture lysates. Scientific reports. 2012;2:222.

[355] Keays KM, Owens GP, Ritchie AM, Gilden DH, Burgoon MP. Laser capture microdissection and single-cell RT-PCR without RNA purification. Journal of immunological methods. 2005;302:90-8.

[356] NIST/SEMATECHNIST/SEMATECH. Counts Control Charts, e-Handbook of Statistical Methods http://www.itl.nist.gov/div898/handbook/pmc/section3/pmc331.htm. 2012.

[357] Yates RD. Probability and stochastic processes : a friendly introduction for electrical and computer engineers. 2nd ed. ed. Hoboken, NJ :: John Wiley & Sons; 2005.

[358] Gobaa S, Hoehnel S, Roccio M, Negro A, Kobel S, Lutolf MP. Artificial niche microarrays for probing single stem cell fate in high throughput. Nature methods. 2011;8:949-55.